

Studies on the Reverse Antibiotic Natural Products, the Nybomycins

A Thesis submitted by:
Oliver Bardell-Cox

In partial fulfilment of the requirements for the degree of:

Doctor of Philosophy

July 2021

Supervisors:

Professor Luis Aragón Alcaide

MRC London Institute of Medical Sciences (LMS), Du Cane Road,
London W12 0NN, UK

And

Professor Matthew J. Fuchter

Department of Chemistry Imperial College London Molecular
Sciences Research Hub Wood Lane London, W12 0BZ

Declaration of Originality

I, Oliver Bardell-Cox, can hereby confirm that the work presented in this thesis is my own and was undertaken with the supervision of Professor Matthew J. Fuchter, Department of Chemistry, Imperial College London and Luis A. Aragón, Cell Cycle Group, MRC London Institute of Medical Science. All work disclosed herein that has been completed by others has been acknowledged and referenced where appropriate.

O. A. Bardell-Cox

July 2021

Declaration of Contributions by Others

I would like to offer my sincere thanks to Dr Alison Howells from Inspiralis for running the enzymatic assays (DNA gyrase (WT and mutant) supercoiling, DNA gyrase cleavage and topological IV decatenation), shown in Section 3.1.5.

I would also like to show my appreciation to Adam Jarmuz for running the initial controls for the Kirby-Bauer Disc Diffusion Assay, shown in Appendix 7.2. These included the loading solvents (CHCl_3 MeOH and EtOH) and the commercial antibiotic Amoxicillin.

I would also like to thank Dr Andrew J. P. White for solving the X-ray crystal structures in Figure 26 and 28 in Section 3.1.2.

Copyright Declaration

The copyright of this thesis rests with the author. Unless otherwise indicated, its contents are licensed under a Creative Commons Attribution-Non Commercial 4.0 International Licence (CC BY-NC).

Under this licence, you may copy and redistribute the material in any medium or format. You may also create and distribute modified versions of the work. This is on the condition that: you credit the author and do not use it, or any derivative works, for a commercial purpose.

When reusing or sharing this work, ensure you make the licence terms clear to others by naming the licence and linking to the licence text. Where a work has been adapted, you should indicate that the work has been changed and describe those changes.

Please seek permission from the copyright holder for uses of this work that are not included in this licence or permitted under UK Copyright Law.

Abstract

Antimicrobial resistance (AMR) is likely to be one of the greatest challenges faced by humanity and if nothing changes it is projected to kill one person every 5 seconds by 2050.¹ Despite this, there are few new therapeutic options in development and so there is a need for new solutions to be identified. One new strategy is the reverse antibiotic approach originally published by Akamatsu and co-workers.² Here treatment with the first antibiotic leads to resistance so a new antibiotic is needed. Resistance to the second antibiotic can only be achieved by a back-mutation thus re-sensitising the bacteria to the first antibiotic. The bacteria will be trapped in an 'evolutionary loop' where it will always be sensitive to either the first or second antibiotic.

Work outlined in this thesis will look to investigate and develop one of the key series of antibiotics in the reverse antibiotic approach, the Nybomycin family of natural products. A new robust and scalable synthetic route that facilitated the synthesis of the best literature compound **DNM-2**, as well as novel analogues to probe the SAR, is reported. The whole cell inhibition of these compounds is reported as well as selected analogue's enzymatic inhibition of the key biological targets. The ability of the series to inhibit Gram-negative bacteria was also explored and led to the discovery that the series is a substrate for efflux *via* the AcrAB/TolC efflux channel. However, the compounds are active in *E. coli* if TolC or AcrB is removed. After initial profiling, aqueous solubility was found to be the major hurdle in the development of the series. This was addressed using medicinal chemistry techniques as well as computational chemistry to aid in the design of novel analogues. This led to the discovery of **6DNM-2-L1A**, the most potent and soluble analogue tested to date.

Acknowledgements

I would like to thank my supervisors, Professor Luis Aragón Alcaide and Professor Matthew J. Fuchter, for the opportunity to explore such an interesting series of molecules and allowing me the freedom to take the project in the direction I wanted. Thank you for your advice and encouragement, especially when it comes to Bonsai care!

Particular thanks to Professor Phil Parsons for the great food, wine and even better company throughout my time at Imperial.

Thank you to Pete Haycock for the NMR support and for putting up with my ramblings, Dr Lisa Haigh for running the MS service, Dr Andrew White for crystallography and Dr Trevor Ferris for running some NMR samples in the challenging COVID period.

I would also like to thank the Cell Cycle group at the LMS for taking in a stray chemist and showing me the ropes in microbiology, with a particular thanks to Adam Jarmuz. Thank you to past and present members of the Fuchter, Barrett, and Lewis groups, who have made my time at Imperial so enjoyable.

I would also like to give a special thanks to my beautiful wife Rose. Thank you for putting up with me and all your support throughout the years. Thank you for proof reading this thesis and always being willing to discuss this project and offer advice. Without your help this would never have been finished!

Finally, thank you to my wonderful daughter Roberta for making my time writing my thesis at home in lockdown a blessing not a curse.

Abbreviations

°C	Degrees Centigrade
<i>A. baumannii</i>	<i>Acinetobacter Baumannii</i>
AMR	Antimicrobial Resistance
APCI	Atmospheric Pressure Chemical Ionization
aq.	Aqueous Solution
ATP	Adenosine Triphosphate
<i>B. mycoides</i>	<i>Bacillus Mycoides</i>
<i>B. subtilis</i>	<i>Bacillus Subtilis</i>
B ₂ pin ₂	Bis(pinacolato)diboron
Boc ₂ O	Di- <i>tert</i> -butyl Dicarboxylate
Bpin	Boron Pinacol
br.	Broad
C	Carbon
calc'd	Calculated
CAP	Community-Acquired Pneumonia
CC ₅₀	Concentration Achieving 50% of Maximum Cleaved DNA
CDC	Centers for Disease Control and Prevention
CNS	Central Nervous System
CRO	Contract Research Organization
d	Doublet
<i>d</i> -TFA	Deuterated Trifluoroacetic Acid
<i>d</i> ₆ -DMSO	Deuterated Dimethyl Sulfoxide
DCE	1,2-Dichloroethane
DCGI	Drugs Controller General of India
DIPEA	<i>N,N</i> -Diisopropylethylamine
DMAP	4-Dimethylaminopyridine
DME	Dimethoxyethane
DMEDA	1,2-Dimethylethylenediamine
DMF	Dimethylformamide
DMP	Dess–Martin Periodinane
DMSO	Dimethyl Sulfoxide
DNM	Deoxyribomycin
DNP	2,4-Dinitrophenol
dppbz	1,2-Bis(diphenylphosphino)benzene
<i>E. coli</i>	<i>Escherichia Coli</i>
EDCI	1-Ethyl-3-(3-dimethylaminopropyl)carbodiimide
EI	Electron Ionization
ESI	Electrospray Ionization
ESBL	Extended Spectrum <i>Beta</i> -Lactamases
Et	Ethyl
EtB	Ethidium Bromide

FDA	Food and Drug Administration
FQ	Fluoroquinolone
FQR	Fluoroquinolone Resistant
FQS	Fluoroquinolone Sensitive
FTMS	Fourier Transform Mass Spectrometry
g	Gram
GDP	Gross Domestic Product
GI	Gastrointestinal
GSK	GlaxoSmithKline
h	Hour
H	Hydrogen
<i>H. influenzae</i>	<i>Haemophilus Influenzae</i>
H ₂ NPMB	4-Methoxybenzylamine
HBA	Hydrogen Bond Acceptor
HBD	Hydrogen Bond Donor
HBpin	Pinacolborane
HGT	Horizontal Gene Transfer
HTS	High Throughput Screen
Hz	Hertz
IPA	Isopropyl Alcohol
IC ₅₀	Half-Maximal Inhibitory Concentration
IP	Intellectual Property
/Pr.HCl	1,3-Bis-(2,6-diisopropylphenyl)imidazolinium Chloride
IV	Intravenous
J	Coupling Constant
K	Kelvin
L	Litre
LCMS	Liquid Chromatography Mass Spectrometry
LDA	Lithium Diisopropylamide
M	Molarity
m	Multiplet
m.p.	Melting Point
m/z	Mass to Charge Ratio
MGE	Mobile Genetic Elements
MIC	Minimum Inhibitory Concentration
min	Minute
mmol	Millimoles
MOE	Molecular Operating Environment
mol. sieve	Molecular Sieve
MRCT	Medical Research Council Technology
MRSA	Methicillin-Resistant <i>Staphylococcus Aureus</i>
MS	Mass Spectrometry
MsCl	Methanesulfonyl Chloride

MSSA	Methicillin-Susceptible <i>Staphylococcus Aureus</i>
MW	Molecular Weight
N	Nitrogen
<i>n</i>	Normal
N ₂	Nitrogen (elemental)
NBS	<i>N</i> -Bromosuccinimide
ⁿ BuLi	<i>n</i> -Butyllithium
NMR	Nuclear Magnetic Resonance
NOE	Nuclear Overhauser Effect
O	Oxygen
OMe	Methoxy
OmpF	Outer Membrane Porin F
P(<i>o</i> -tol) ₃	Tris(<i>o</i> -tolyl)phosphine
PBS	Phosphate-Buffered Saline
PCR	Polymerase Chain Reaction
Pd(dppf)Cl ₂	(1,1'-Bis(diphenylphosphino)ferrocene)palladium(II) dichloride
Pd(OH) ₂ /C	Palladium Hydroxide on Carbon
Pd/C	Palladium on Carbon
Pdb	Protein Data Bank
PK	Pharmacokinetics
PMA	Phosphomolybdic Acid
PMB	<i>para</i> -Methoxybenzyl
PMHS	Polymethylhydrosiloxane
ppm	Parts per Million
PSA	Polar Surface Area
q	Quartet
QRDR	Quinolone Resistance-Determining Regions
rt	Room Temperature
s	Singlet
<i>S. aureus</i>	<i>Staphylococcus Aureus</i>
<i>S. pneumoniae</i>	<i>Streptococcus Pneumoniae</i>
<i>S. typhi</i>	<i>Salmonella Typhi</i>
SAR	Structure–Activity Relationship
sat.	Saturated
SDS	Sodium Dodecyl Sulfate
S _N Ar	Nucleophilic Aromatic Substitution
STAB	Sodium Triacetoxyborohydride
t	Triplet
T3P	Propanephosphonic Acid Anhydride
TB	Tuberculosis
TBAF	Tetra- <i>n</i> -Butylammonium Fluoride
TBAH	Tetrabutylammonium Hydroxide
TBDPS	<i>tert</i> -Butyldiphenylsilyl

<i>tert, t</i>	Tertiary
TFA	Trifluoroacetic Acid
THF	Tetrahydrofuran
TLC	Thin Layer Chromatography
TMS	Trimethylsilyl
TMSCl	Trimethylsilyl Chloride
TMSOK	Potassium Trimethylsilanolate
TOF	Time of Flight
topo IV	Topoisomerase IV
UNODC	United Nations Office on Drugs and Crime
UTI	Urinary Tract Infection
UV	Ultraviolet
WHO	World Health Organization
WT	Wild Type
xantphos	4,5-Bis(diphenylphosphino)-9,9-dimethylxanthene
xphos	2-Dicyclohexylphosphino-2',4',6'-triisopropylbiphenyl
δ	Chemical Shift
α	<i>Alpha</i>
β	<i>Beta</i>

Table of Contents

Declaration of Originality	2
Declaration of Contributions by Others	3
Copyright Declaration	4
Abstract	5
Acknowledgements	6
Abbreviations	7
1. Introduction	15
1.1 Why is Antibiotic Resistance a Problem?	15
1.2 Antibiotics and Agriculture	18
1.3 Antibiotic Stewardship	19
1.4 De-novo Antibiotic Development	19
1.5 Bacteria Developing Resistance	20
1.5.1 Gram-Positive and Gram-Negative Bacteria	20
1.5.2 Developing Antibacterial Resistance	22
1.5.3 Establishment and Transfer of Antibacterial Resistance	23
1.5.4 Bacterial Resistance Mechanisms.....	25
1.5.5 Fitness Costs and Maintenance of a Resistance Phenotype	29
1.6 Economics – Lack of Investment	31
1.7 Scientific Challenges of Developing Antibiotics	33
1.8 Current Antibiotic Strategies – Fluoroquinolones	38
1.8.1 Development of Fluoroquinolones	38
1.8.2 Fluoroquinolones Currently in Development or Recently Released	40
1.8.3 Mode of Action of the Fluoroquinolones.....	41
1.8.3.1 Biological Target - Topoisomerases	41
1.8.4 Resistance Mechanism	43
1.8.5 General SAR of Fluoroquinolones.....	47
1.8.6 Fluoroquinolone Safety Profile	48
1.8.7 Non-Fluoroquinolone Gyrase Inhibitors in the Clinical Development	48
1.9 Reverse Antibiotic Approach	49
1.9.1 Introduction to the Reverse Antibiotic Approach.....	49
1.9.2 Nybomycin Family of Natural Products	52
1.9.3 Historical Context of Nybomycins.....	57
1.9.4 Why Synthesise the Nybomycin Family of Natural Products?	57
1.9.5 Why is the Nybomycin Series Currently Not a Drug?	58
2. Aims of the Project	59
3. Results and Discussion	61
3.1 Confirming the Mutant Selective Phenotype	61
3.1.2 Synthesis	62
3.1.2.1 Synthetic plan	62
3.1.2.2 Route 2 – Nussbaum	63
3.1.2.3 Route 3 – Hergenrother and Co-workers.....	69
3.1.3 Microbiology - Kirby-Bauer Disc Diffusion Assay	89

3.1.3.1 New DNM Analogues	89
3.1.4 Gene Editing in <i>E. coli</i>	93
3.1.5 Enzymatic inhibition of the Key Derivates Conducted in Collaboration with Inspiralis	106
3.1.6 Section Conclusion	114
3.2 Increasing Aqueous Solubility	117
3.2.1 Design of New Analogues	118
3.2.1.1 Designs of New Analogues Containing a Solubilising Handle.....	118
3.2.1.2 Designs of Cyclopropyl Analogues	123
3.2.1.3 Designs of Novel Core Alteration	125
3.2.2 Synthesis	126
3.2.2.1 Synthesis of Analogues Containing a Solubilising Handle	126
3.2.2.2 Synthesis of the Cyclopropyl Analogues	131
3.2.2.3 Synthesis of Novel Core Alterations.....	134
3.2.3 Predictors for Aqueous Solubility.	145
3.2.4 Kirby–Bauer Disc Diffusion Assay for New Analogues	149
3.2.5 Section Conclusion.....	156
4. Concluding Thoughts and Future Work	158
4.1 Conclusion	158
4.2 Future work	159
5. Experimental	162
5.1 General Experimental	162
5.1.1 LCMS Conditions	163
5.2 Synthetic Procedures	165
2-Methoxy-1,3-dinitrobenzene (7)	165
2-Methoxybenzene-1,3-diamine (1) - Method 1	166
1-Methoxy-2-nitrobenzene (8)	167
4-Bromo-1-methoxy-2-nitrobenzene (9)	168
5-Bromo-2-methoxy-1,3-dinitrobenzene (10)	169
2-Methoxybenzene-1,3-diamine (1) - Method 2	170
4,6-Dibromo-2-methoxybenzene-1,3-diamine (2).....	171
(4,6-Dichloro-5-methoxy-1,3-phenylene)bis(trimethylsilane) (20).	172
2,4-Dichloro-1,5-diiodo-3-methoxybenzene (21)	174
2,2'-(4,6-Dichloro-5-methoxy-1,3-phenylene)bis(4,4,5,5-tetramethyl-1,3,2-dioxaborolane) (22).....	175
(Z)-3-Iodobut-2-enoic acid (18).....	176
(Z)-3-Iodo-N-(4-methoxybenzyl)but-2-enamide (19).....	177
Ethyl (Z)-3-(4,4,5,5-tetramethyl-1,3,2-dioxaborolan-2-yl)but-2-enoate (27)	178
Diethyl 3,3'-(4,6-dichloro-5-methoxy-1,3-phenylene)(2 <i>E</i> ,2' <i>E</i>)-bis(but-2-enoate) (28)	179
N-(4-Methoxybenzyl)but-2-ynamide (32).....	180
(Z)-N-(4-Methoxybenzyl)-3-(4,4,5,5-tetramethyl-1,3,2-dioxaborolan-2-yl)but-2-enamide (33)	181
(2 <i>E</i> ,2' <i>E</i>)-3,3'-(4,6-Dichloro-5-methoxy-1,3-phenylene)bis(N-(4-methoxybenzyl)but-2-enamide) (30)	182
(E)-N-(4-Methoxybenzyl)but-2-enamide (36)	183
Potassium N-(4-methoxybenzyl)-3-(trifluoro- λ^4 -boraneryl)butanamide (37).....	184
Ethyl (Z)-3-(4,4,5,5-tetramethyl-1,3,2-dioxaborolan-2-yl)but-2-enoate (40)	185
Diethyl 3,3'-(4,6-dichloro-5-methoxy-1,3-phenylene)(2 <i>Z</i> ,2' <i>Z</i>)-bis(but-2-enoate) (41)	186
<i>tert</i> -Butyl but-2-ynoate (43)	187
<i>tert</i> -Butyl (E)-3-(4,4,5,5-tetramethyl-1,3,2-dioxaborolan-2-yl)but-2-enoate (44)	188
Di- <i>tert</i> -butyl 3,3'-(4,6-dichloro-5-methoxy-1,3-phenylene)(2 <i>Z</i> ,2' <i>Z</i>)-bis(but-2-enoate) (45).....	189
(2 <i>Z</i> ,2' <i>Z</i>)-3,3'-(4,6-Dichloro-5-methoxy-1,3-phenylene)bis(but-2-enoic acid) (42)	190
(2 <i>Z</i> ,2' <i>Z</i>)-3,3'-(4,6-Dichloro-5-methoxy-1,3-phenylene)bis(N-(4-methoxybenzyl)but-2-enamide) (26)	191
10-Methoxy-1,9-bis(4-methoxybenzyl)-4,6-dimethylpyrido[3,2- <i>g</i>]quinoline-2,8(1 <i>H</i> ,9 <i>H</i>)-dione (34)	193
10-Hydroxy-4,6-dimethylpyrido[3,2- <i>g</i>]quinoline-2,8(1 <i>H</i> ,9 <i>H</i>)-dione (46).....	195
10-Methoxy-4,6-dimethylpyrido[3,2- <i>g</i>]quinoline-2,8(1 <i>H</i> ,9 <i>H</i>)-dione (13)	196

8-Ethoxy-10-methoxy-4,6-dimethylpyrido[3,2- <i>g</i>]quinolin-2(1 <i>H</i>)-one (47).....	197
8-Ethoxy-10-hydroxy-4,6-dimethylpyrido[3,2- <i>g</i>]quinolin-2(1 <i>H</i>)-one (48).....	198
10-Ethoxy-6,8-dimethyl-2 <i>H</i> ,4 <i>H</i> -oxazolo[5,4,3- <i>ij</i>]pyrido[3,2- <i>g</i>]quinoline-4-one (DNM-O2).....	199
11-Ethoxy-7,9-dimethyl-2,3-dihydro-5 <i>H</i> -[1,4]oxazino[2,3,4- <i>ij</i>]pyrido[3,2- <i>g</i>]quinolin-5-one (6DNM-O2).....	200
12-Ethoxy-8,10-dimethyl-3,4-dihydro-2 <i>H</i> ,6 <i>H</i> -[1,4]oxazepino[2,3,4- <i>ij</i>]pyrido[3,2- <i>g</i>]quinolin-6-one (7DNM-O2).....	201
2,8-Diethoxy-10-methoxy-4,6-dimethylpyrido[3,2- <i>g</i>]quinoline (DNM-2O2).....	202
(<i>Z</i>)-3-(2,4-Dichloro-3-methoxy-5-((<i>Z</i>)-4-((4-methoxybenzyl)amino)-4-oxobut-2-en-2-yl)phenyl)- <i>N</i> -ethylbut-2-enamide (23).....	203
1-Ethyl-10-methoxy-9-(4-methoxybenzyl)-4,6-dimethylpyrido[3,2- <i>g</i>]quinoline-2,8(1 <i>H</i> ,9 <i>H</i>)-dione (24) ..	205
1-Ethyl-10-hydroxy-4,6-dimethylpyrido[3,2- <i>g</i>]quinoline-2,8(1 <i>H</i> ,9 <i>H</i>)-dione (25)	206
11-Ethyl-6,8-dimethyl-11-hydro-2 <i>H</i> ,4 <i>H</i> -oxazolo[5,4,3- <i>ij</i>]pyrido[3,2- <i>g</i>]quinoline-4,10-dione (DNM-2) ...	207
12-Ethyl-7,9-dimethyl-2,3-dihydro-5 <i>H</i> -[1,4]oxazino[2,3,4- <i>ij</i>]pyrido[3,2- <i>g</i>]quinoline-5,11(12 <i>H</i>)-dione (6DNM-2).....	208
13-Ethyl-8,10-dimethyl-3,4-dihydro-2 <i>H</i> ,6 <i>H</i> -[1,4]oxazepino[2,3,4- <i>ij</i>]pyrido[3,2- <i>g</i>]quinoline-6,12(13 <i>H</i>)-dione (7DNM-2).....	209
8,10-Dimethyl-3,4-dihydro-2 <i>H</i> ,6 <i>H</i> -[1,4]oxazepino[2,3,4- <i>ij</i>]pyrido[3,2- <i>g</i>]quinoline-6,12(13 <i>H</i>)-dione (7DNM-NH).....	211
1-Ethyl-10-(2-hydroxy-3-(piperidin-1-yl)propoxy)-4,6-dimethylpyrido[3,2- <i>g</i>]quinoline-2,8(1 <i>H</i> ,9 <i>H</i>)-dione (52) and 12-Ethyl-3-(hydroxymethyl)-7,9-dimethyl-2,3-dihydro-5 <i>H</i> -[1,4]oxazino[2,3,4- <i>ij</i>]pyrido[3,2- <i>g</i>]quinoline-5,11(12 <i>H</i>)-dione (6DNM-2-OH)	212
12-Ethyl-7,9-dimethyl-3-(piperidin-1-ylmethyl)-2,3-dihydro-5 <i>H</i> -[1,4]oxazino[2,3,4- <i>ij</i>]pyrido[3,2- <i>g</i>]quinoline-5,11(12 <i>H</i>)-dione (6DNM-2-L1A)	214
12-Ethyl-3-(hydroxymethyl)-7,9-dimethyl-2,3-dihydro-5 <i>H</i> -[1,4]oxazino[2,3,4- <i>ij</i>]pyrido[3,2- <i>g</i>]quinoline-5,11(12 <i>H</i>)-dione (6DNM-2-OH).....	216
3-(Chloromethyl)-12-ethyl-7,9-dimethyl-2,3-dihydro-5 <i>H</i> -[1,4]oxazino[2,3,4- <i>ij</i>]pyrido[3,2- <i>g</i>]quinoline-5,11(12 <i>H</i>)-dione (54)	217
(12-Ethyl-7,9-dimethyl-5,11-dioxo-2,3,11,12-tetrahydro-5 <i>H</i> -[1,4]oxazino[2,3,4- <i>ij</i>]pyrido[3,2- <i>g</i>]quinolin-3-yl)methyl morpholine-4-carboxylate (6DNM-2-L2B)	218
(12-Ethyl-7,9-dimethyl-5,11-dioxo-2,3,11,12-tetrahydro-5 <i>H</i> -[1,4]oxazino[2,3,4- <i>ij</i>]pyrido[3,2- <i>g</i>]quinolin-3-yl)methyl 4-methylpiperazine-1-carboxylate (6DNM-2-L2D)	219
(12-Ethyl-7,9-dimethyl-5,11-dioxo-2,3,11,12-tetrahydro-5 <i>H</i> -[1,4]oxazino[2,3,4- <i>ij</i>]pyrido[3,2- <i>g</i>]quinolin-3-yl)methyl 4-hydroxypiperidine-1-carboxylate (6DNM-2-L2E).....	221
12-Cyclopropyl-7,9-dimethyl-2,3-dihydro-5 <i>H</i> -[1,4]oxazino[2,3,4- <i>ij</i>]pyrido[3,2- <i>g</i>]quinoline-5,11(12 <i>H</i>)-dione (6DNM-Cyclo)	223
(Allyloxy)(<i>tert</i> -butyl)diphenylsilane (55).....	224
<i>tert</i> -Butyl(2,3-dibromopropoxy)diphenylsilane (56)	225
3-(Hydroxymethyl)-7,9-dimethyl-2,3-dihydro-5 <i>H</i> -[1,4]oxazino[2,3,4- <i>ij</i>]pyrido[3,2- <i>g</i>]quinoline-5,11(12 <i>H</i>)-dione (6DNM-NH-OH).....	226
2-Chloroethyl (4-bromo-3-chloro-2-fluorophenyl)carbamate (57)	227
2-((4-Bromo-3-chloro-2-fluorophenyl)amino)ethan-1-ol (58).....	228
7-Bromo-8-chloro-3,4-dihydro-2 <i>H</i> -benzo[<i>b</i>][1,4]oxazine (59)	229
1-(4-Hydroxy-3-methoxy-5-nitrophenyl)ethan-1-one (60).....	230
1-(3-Amino-4-hydroxy-5-methoxyphenyl)ethan-1-one (61).....	231
1-(7-Methoxybenzo[<i>d</i>]oxazol-5-yl)ethan-1-one (62).....	232
1-(7-Methoxy-2-methylbenzo[<i>d</i>]oxazol-5-yl)ethan-1-one (64)	233
1-(7-Methoxy-2-methyl-6-nitrobenzo[<i>d</i>]oxazol-5-yl)ethan-1-one (65) and 1-(7-methoxy-2-methyl-4-nitrobenzo[<i>d</i>]oxazol-5-yl)ethan-1-one (70)	234
1-(6-Amino-7-methoxy-2-methylbenzo[<i>d</i>]oxazol-5-yl)ethan-1-one (66)	235
<i>N</i> -(5-Acetyl-7-methoxy-2-methylbenzo[<i>d</i>]oxazol-6-yl)acetamide (67) and 1-(6-chloro-7-methoxy-2-methylbenzo[<i>d</i>]oxazol-5-yl)ethan-1-one (68).....	236
<i>N</i> -(2-Methoxyphenyl)-3-oxobutanamide (71)	237
8-Methoxy-4-methylquinolin-2(1 <i>H</i>)-one (72).....	238
8-Hydroxy-4-methylquinolin-2(1 <i>H</i>)-one (73).....	239
8-Methoxy-4-methyl-6-nitroquinolin-2(1 <i>H</i>)-one (74).....	240
1-Bromo-2-methoxy-3-nitrobenzene (75)	241
3-Bromo-2-methoxyaniline (77)	242

<i>N</i> -(3-Bromo-2-methoxyphenyl)-3-oxobutanamide (79)	243
7-Bromo-8-methoxy-4-methylquinolin-2(1 <i>H</i>)-one (81)	244
Methyl 2-methoxy-3-nitrobenzoate (76)	245
Methyl 3-amino-2-methoxybenzoate (78)	246
Methyl 2-methoxy-3-(3-oxobutanamido)benzoate (80)	247
1-Fluoro-2-methoxy-3-nitrobenzene (83)	248
<i>N</i> -(3-Fluoro-2-methoxyphenyl)-3-oxobutanamide (85)	249
7-Fluoro-8-methoxy-4-methylquinolin-2(1 <i>H</i>)-one (86)	250
7-Fluoro-8-methoxy-4-methyl-6-nitroquinolin-2(1 <i>H</i>)-one (87)	251
6,7-Diamino-8-methoxy-4-methylquinolin-2(1 <i>H</i>)-one (88)	252
4-Methoxy-8-methyl-3,5-dihydro-6 <i>H</i> -imidazo[4,5- <i>g</i>]quinolin-6-one (89)	253
2-Ethoxy-7-fluoro-8-methoxy-4-methyl-6-nitroquinoline (90) and 1-ethyl-7-fluoro-8-methoxy-4-methyl-6-nitroquinolin-2(1 <i>H</i>)-one (91)	254
7-Fluoro-8-hydroxy-4-methyl-6-nitroquinolin-2(1 <i>H</i>)-one (92)	256
10-Fluoro-7-methyl-9-nitro-2,3-dihydro-5 <i>H</i> -[1,4]oxazino[2,3,4- <i>ij</i>]quinolin-5-one (93)	257
10-Azido-7-methyl-9-nitro-2,3-dihydro-5 <i>H</i> -[1,4]oxazino[2,3,4- <i>ij</i>]quinolin-5-one (94)	258
9,10-Diamino-7-methyl-2,3-dihydro-5 <i>H</i> -[1,4]oxazino[2,3,4- <i>ij</i>]quinolin-5-one (95)	259
7-Methyl-2,3-dihydroimidazo[4,5- <i>g</i>][1,4]oxazino[2,3,4- <i>ij</i>]quinolin-5(11 <i>H</i>)-one (6Core2-NH)	260
11-Ethyl-7-methyl-2,3-dihydroimidazo[4,5- <i>g</i>][1,4]oxazino[2,3,4- <i>ij</i>]quinolin-5(11 <i>H</i>)-one (6Core2-NEtA) and 9-ethyl-7-methyl-2,3-dihydroimidazo[4,5- <i>g</i>][1,4]oxazino[2,3,4- <i>ij</i>]quinolin-5(9 <i>H</i>)-one (6Core2-NEtB)	261
5.3 Microbiology Protocols	263
5.3.1 Disc Preparations	263
5.3.2 Kirby-Bauer Disc Diffusion Assay ^{205,262}	263
5.3.3 Gene Deletion of TolC and AcrB from <i>E. coli</i>	264
5.3.4 Ethidium Bromide Cartwheel Assay	264
5.4 X-Ray Crystallography	265
5.4.1 The X-ray Crystal Structure of 44	265
5.4.2 The X-ray Crystal Structure of 49	265
5.4.3 References	268
5.4.4 Figures	268
6. References	269
7. Appendix	279
7.1 Failed Reaction Conditions	279
7.1.1 Table 1 - Scheme 5 Unsuccessful amide coupling of 2 to form 14	279
7.1.2 Table 2 - Scheme 5 Unsuccessful acetylation of 2 to form 15.	279
7.1.3 Table 3 - Scheme 10 Unsuccessful Suzuki-Miyaura cross-coupling of 22 and 19 to form 26.	279
7.1.4 Table 4 - Scheme 11 - Unsuccessful hydrolysis of ester 28 to acid 29.	280
7.1.5 Table 5 - Scheme 13 - Unsuccessful cyclisation of 30 to form 34.	280
7.1.6 Table 6 - Scheme 14 - Unsuccessful reduction of 30 to form 35.	280
7.1.7 Table 7 - Scheme 17 - Unsuccessful hydrolysis of ester 41 to acid 42.	281
7.2 Controls for the Kirby–Bauer disc diffusion assay	282
7.2.1 Kirby–Bauer disc diffusion with Amoxicillin (10 µg commercial disc)	282
7.2.2 Kirby–Bauer disc diffusion solvent controls (MeOH, EtOH and CHCl ₃)	284

1. Introduction

1.1 Why is Antibiotic Resistance a Problem?

The discovery of penicillin by Alexander Fleming was first reported in 1929 and revolutionised medicine.^{3,4} In his Noble Prize acceptance speech 16 years later he warned about the potential of antimicrobial resistance but this message was not heeded.⁵ Almost 80 years on from that first warning we find ourselves in grave danger of entering a 'post-antibiotic' era with recent evidence suggesting that we may already be there.⁶

Antimicrobial resistance (AMR) is the process where microorganisms (bacteria, archaea, fungi, algae, protozoa or viruses) undergo an adaptive change or changes in order to combat the effects of an antimicrobial agent. Disease causing microorganisms (microbes) are known as pathogens, however this is organism specific as a microbe can be capable of causing disease in one host (pathogenic) but can also be benign in another host (non-pathogenic). Antibiotic resistance is a subclass of AMR which addresses how bacteria adapt when exposed to an antibiotic agent.

Towards the latter half of the 20th century AMR was overlooked as an issue of any significance. The constant development of new antibiotics was faster than the rate bacteria could develop resistance against them. Unfortunately however, this is no longer the case.⁷ Another interesting thought is that those first antibiotic classes could be the most effective that may ever be discovered, and the chance of finding new "magic bullets" could be very low.⁸ This is due to the limited number of "ideal" druggable targets in bacterial cells that human cells don't possess and the ability of the bacteria to develop protection/resistance mechanisms for these finite targets.

The World Health Organisation (WHO) have called the rise of antibiotic resistance “one of the biggest threats to global health, food security, and development today”.⁹ It is a problem that can affect anyone, independent of health, in any country, at any time. It has been found in every country in the globe and it is undermining the progress made in a variety of areas including life expectancy, public health and increased food availability.⁶ The World Bank modelled the effects AMR would have on the global economy using a conservative approach that only considered the effects AMR would have on livestock productivity and labour supply. This simulation predicted a GDP shortfall of \$3.4 trillion dollars by 2030 and a loss of annual global GDP of 3.8 % by 2050.¹⁰ What this model predicted in real terms is that AMR, by 2030, would plunge an additional 24 million people into extreme poverty.¹⁰

In the US alone, the centre for disease control (CDC) estimated that at least 35,000 people die and 2.8 million people are infected as a direct result of resistant bacteria per year.⁶ However, according to a study by M. H. Kollef and co-workers, the true number is greater than 150,000 deaths;¹¹ almost seven times higher than the CDC estimate. In the CDC’s 2013 report, it was estimated that the direct cost to the US economy could be as great as \$20 billion, with that figure rising to \$35 billion if the cost to society *via* loss of productivity is taken into account.¹²

However, in the 2019 report, they acknowledge that the true value could be even greater.⁶

Another consequence that shouldn’t be underestimated is the effect that not having functioning antibiotics will have on other life-saving and life-improving modern medicine. Many cancer therapies, joint/organ replacements and treatments of chronic disease involve comprising the immune system and/or removing the body’s physical barriers to infection. This greatly increases the risk of bacterial infection.^{12,13} An example of this is a study by R. Smith and J. Coast. They disclosed that current rates of infection for hip operations were 0.5 - 2 %, whereas with no antibiotics, the infection rates were estimated to be between 40 – 50 % with

about 30 % of those infected leading to death.¹⁴ Antibiotic resistance will also extend the time spent in hospitals leading to increased healthcare costs and a higher chance of mortality. There is also evidence from previous outbreaks of resistant infection that the healthcare system will struggle to cope.¹⁵

As shown in Figure 1, global antimicrobial resistance (AMR) currently causes around 700,000 deaths per year at a low estimate.¹⁶ This figure is likely to be an underestimate as incidences are hard to attribute and sometimes not reported. This number however is projected to rise to around 10 million deaths in 2050.¹ That equates to one person every 3 seconds.

There are also concerns that once very treatable diseases like tuberculosis (TB) and typhoid could return with the rise of antibiotics resistance. Plagues used to cause mass extinction events every 100 years or so but with the discovery of antibiotics these events are a distant memory but for how much longer? The economic burden is also predicted to be colossal with the figures projected in the range of \$100 trillion when the morbidity and mortality is taken into account.¹⁷ If these projections are representative, AMR will become the greatest threat humanity has ever had to overcome.

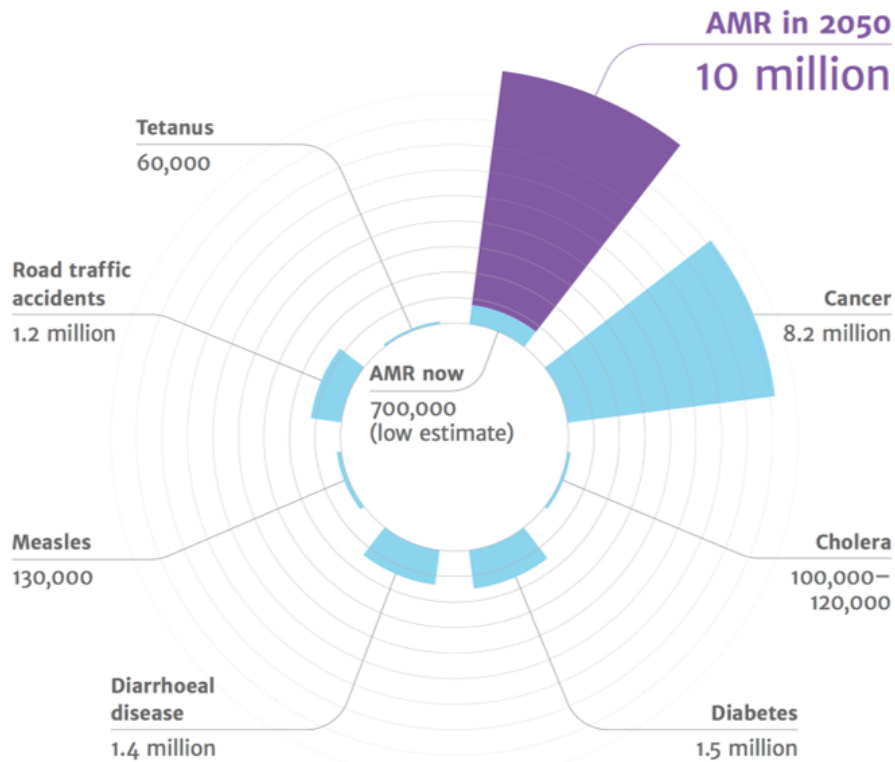


Figure 1 – Global annual causes of death in 2016. Figure taken from the J. O’NEILL report.¹ Data taken from the WHO facts sheets for causes of death. AMR has been attributed to 700,000 deaths in 2016 but that figure is projected to rise to 10 million by 2050.

1.2 Antibiotics and Agriculture

70 % of global antibiotic consumption is in agriculture and that is predicted to rise by 67 % by 2030.^{18,19} This is due to the high efficiencies demanded on agriculture by the consumer driving down the cost of the end product. The conditions used in most animal based food production methods wouldn’t be possible without antibiotics to maintain a healthy herd. They have also been used widely as growth promoters to increase meat production,²⁰ although this practice was banned in the European Union in 2006.²¹ Transmission of antibiotic resistance from animals to humans has been shown to occur and in some models it has been shown to have a larger effect on disseminating resistant bacteria than healthcare transmissions within humans.²²

1.3 Antibiotic Stewardship

Poor antibiotic stewardship, in terms of overuse and misuse, has been one of the main factors in the spread of AMR.²³ In the US from 2010 to 2011, 154 million prescriptions for antibiotics were written with 30 % of them being inappropriate.²⁴ One of the worst areas was acute respiratory conditions where 50 % of prescriptions were unsuitable.²⁴ A report in 2010 by the United Nations Office on Drugs Crimes (UNODC) stated that 50 - 60 % of antimicrobials tested in Africa and Asia had less active ingredient than advertised.²⁵ This is a huge issue as exposure of bacteria to sub-lethal amounts of antibiotics is an effective method for rapid generation of resistant mutants. It also elongates the time frame which someone is infected for, creating greater opportunity for spreading to others and can lead to complications and more severe infections. In 2013, 49 % of European people surveyed thought antibiotics were effective against viruses and 41 % thought that colds/flu could be treated by antibiotics.²⁶ It is worrying how high these numbers are and highlights the improvements in stewardship and education that need to be made. Also, as many of the antibiotics regularly used today were developed in the last century, they are no longer subjected to intellectual protection *via* the patent system. This has resulted in antibiotics being easy to access and cheap to acquire, adding to the overuse and misuse.²⁷

1.4 *De-novo* Antibiotic Development

Despite the dire predictions for the future consequences of antibiotic resistance, the pipeline of new antibiotics with novel modes of action is worryingly sparse.²⁸ The current problems with antibiotics are threefold. Firstly, bacteria are developing resistance to the current antibiotic strategies, addressed in Section 1.5. Secondly, due to lack of financial returns and a

broken funding structure, pharmaceutical research into the area has decreased significantly since the 'Golden Age' of Antibiotics,²⁹ addressed in Section 1.6. Thirdly, developing new antibiotics is one of the most challenging therapeutic areas, addressed in Section 1.7.

1.5 Bacteria Developing Resistance

1.5.1 Gram-Positive and Gram-Negative Bacteria

Bacteria are categorised into two groups depending on how they interact with Gram stain. This was first discovered by C. Gram in 1884 and is still used today.³⁰ Gram-positive bacteria are able to absorb the Gram stain and hence give the characteristic purple colour, whereas Gram-negative bacteria are unable to retain the Gram stain, giving them a pale pinkish colour. These differences in absorption can be explained by looking at the structural differences between the membranes in Gram-positive and Gram-negative bacteria as shown in Figure 2.

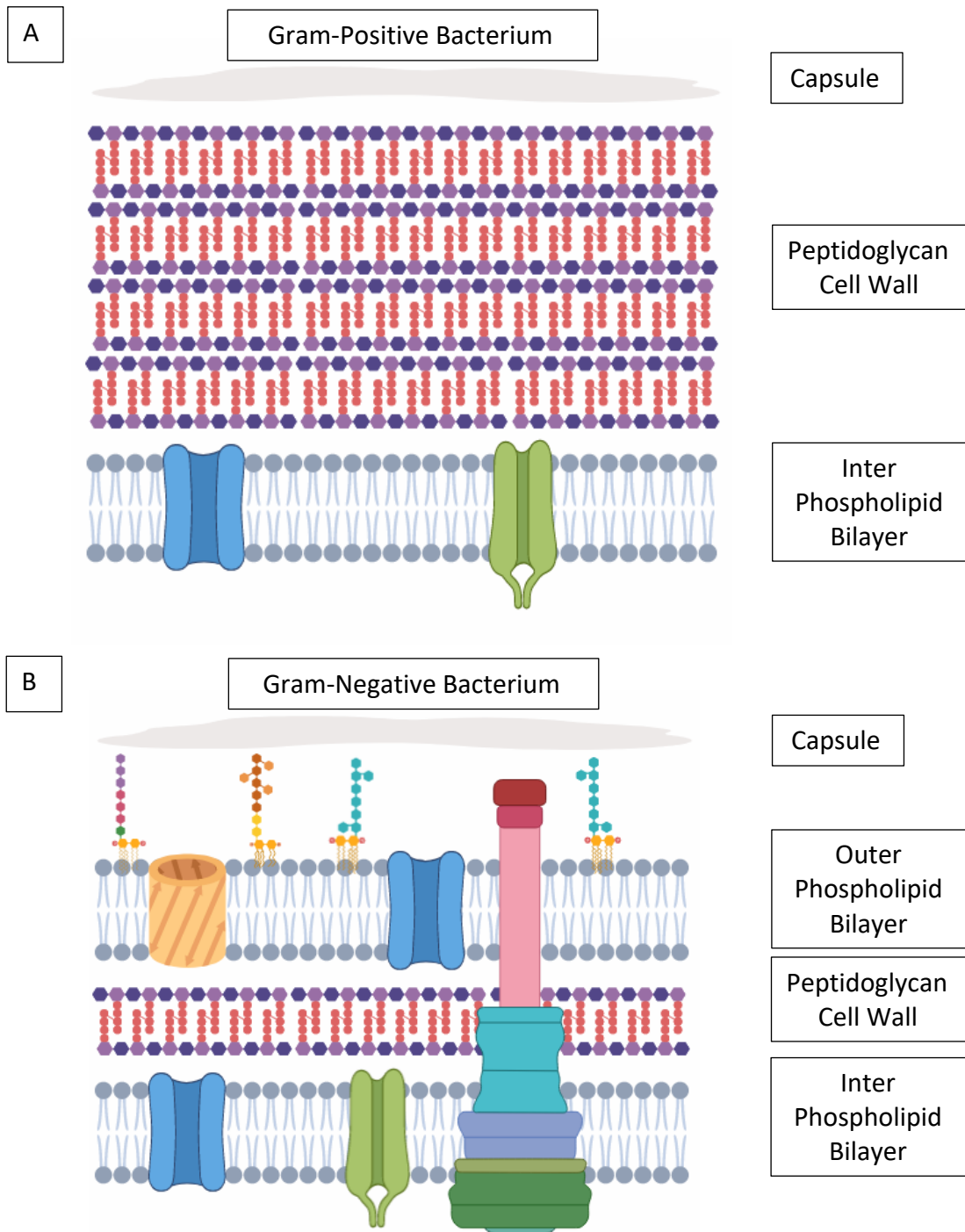


Figure 2 – Comparison of the Gram-positive versus the Gram-negative bacterial membranes. **A** - the Gram-positive membrane, includes an inter phospholipid bilayer with assorted membrane proteins, then a thick peptidoglycan cell wall and an outer capsule. **B** - the Gram-negative membrane, includes the same inter phospholipid bilayer with assorted membrane proteins, then a smaller peptidoglycan cell wall, an additional outer phospholipid bilayer, again with membrane proteins, including porins, and finally an outer capsule. It is much more difficult for antibiotics to penetrate into a Gram-negative cell as a result of the second phospholipid bilayer.

1.5.2 Developing Antibacterial Resistance

As soon as antibacterial compounds were discovered and used, it was apparent that bacteria were able to develop resistance against them.³¹ This is because resistance to antibiotics occurs naturally. Bacteria produce antibiotic compounds to impede the growth of other bacteria and outcompete them for resources in a process known as antibiosis,³² this is shown in Figure 3. In order to survive this antibiotic assault, resistance mechanisms needed to be developed, optimised and fine-tuned. The vast majority of antibiotics that have been sourced from nature have been co-evolved with corresponding resistance mechanisms.³³⁻³⁵ This is logical as it would be extremely beneficial for the bacteria that excretes the antibiotic to be immune to its effects. It has been reported in a study by G. D. Wright and co-workers, that bacteria isolated in a cave for over 4 million years, showed resistance to 14 structurally and mechanistically diverse antibiotics.³⁶ This provides strong evidence that antibiotic resistance is “natural, ancient, and hard wired in the shared genome of microbes”.³⁶ However, this is a process that has been accelerated by our overuse and misuse of antibiotics and negligence.^{19,37}

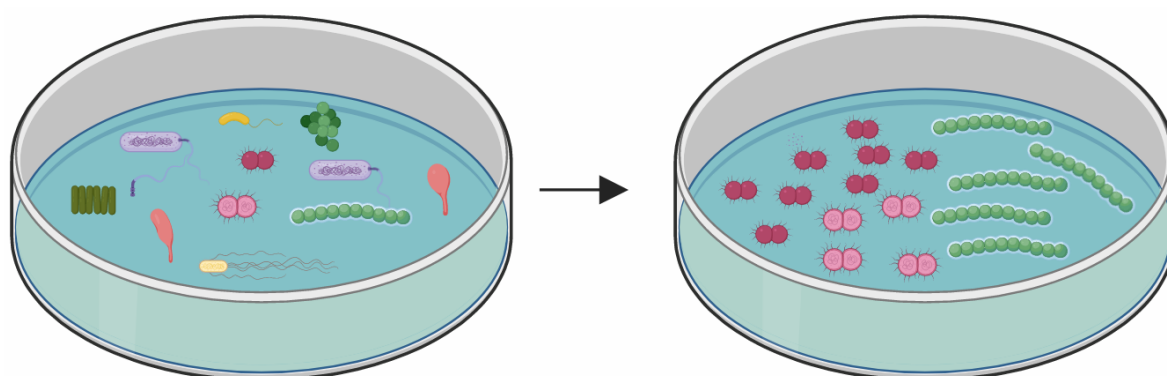


Figure 3 – Natural selection in bacteria. Bacteria are able to release antibiotic compounds that impede the growth or kill other species they are in competition with. This is a demonstration of Darwin’s concept of ‘survival of the fittest’ where the bacteria that are best able to attack and/or defend themselves survive.

1.5.3 Establishment and Transfer of Antibacterial Resistance

Bacteria are unique in the way they respond to a large variety of environmental pressures at the genetic level. It is a testament to their high genetic plasticity and their prolific reproduction rate. A colony of 10^9 bacterial cells per millilitre can be generated from a single bacterium after overnight growth in a nutrient rich environment.²³

To adapt to antibiotic attack, bacteria use two main strategies to acquire genetic resistance. The first is vertical evolution, shown in Figure 4. This involves the passage of beneficial mutations in the bacterial genome that infer a selection advantage to their progeny. High levels of resistance are typically achieved in a step-wise manner, with each mutation slightly increasing resistance. These slight increases in resistance are important as they can give the bacteria the time it needs for the development of more extreme resistance mechanisms that will confer a high-level of resistance.

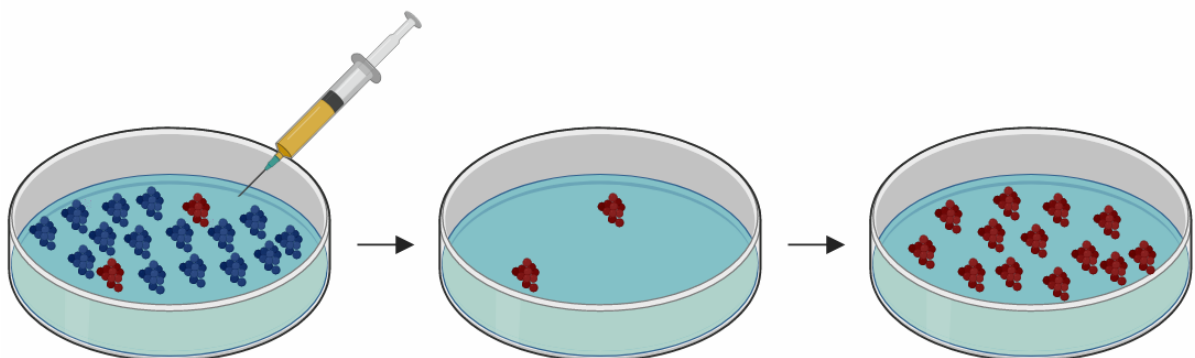


Figure 4 – Resistance of a population *via* vertical (endogenous) evolution. A mix population of susceptible (blue) and resistant (red) bacteria exist. After a drug is administered, the susceptible population is eliminated leaving behind the resistant bacteria. These resistant bacteria can then multiply to fill the newly created ecological void resulting in a resistant population to the antibiotic.

The second method is horizontal evolution *via* horizontal gene transfer (HGT), shown in Figure 5, which is the acquisition of mobile genetic elements (MGE) from a resistant species.

MGE are 'jumping genes' which include conjugative plasmids, integrons, transposons and insertion sequences.²³ These are responsible for the promiscuity of the dissemination of antibacterial resistance genes. Multiple resistance genes are often present in a single plasmid. This means that only one transfer event is needed for a susceptible strain to become multidrug resistant.³⁸ For example the NR1 (or R100) plasmid contains resistance genes for tetracycline, chloramphenicol, aminoglycosides, sulphonamides and mercury as well as transfer genes and coupling factors.³⁹ There are three main steps involved in this process; transduction, conjugation and transformation. Conjugation is the most common and important method of HGT. The mechanism for this transfer is *via* a '*pilus*', a hollow tubular structure that forms between two neighbouring bacteria to facilitate the transfer of the plasmid.⁴⁰ Transfer of the resistance plasmids, by conjugation, can occur with efficiencies approaching quantitative.³⁸

Transduction is the passage of genetic material from one bacterium to another *via* a vector which is typically a virus (bacterial viruses are known as phages). The phage extracts the bacterial resistance gene from the resistant bacteria and when the phage infects a new bacteria it also passes on the antibiotic resistance gene.⁴⁰

Transformation is the incorporation of free (or naked) DNA into the bacteria. These sections of free DNA typically exist when another bacterium has ruptured, releasing its cellular content. This mechanism gives the potential for opportunistic bacteria, which are recolonising an area post-antibiotic treatment, to pick up partial resistance to that antibiotic that may have existed pre-treatment.

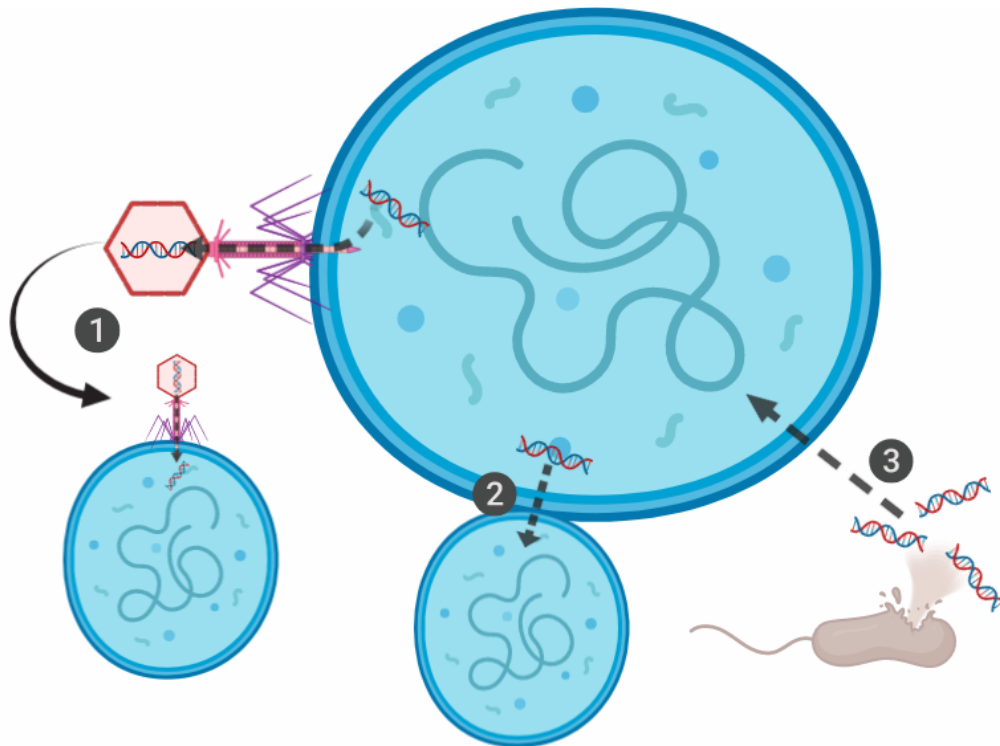


Figure 5 – Mechanisms for horizontal (exogenous) evolution. 1) Transduction, the process where a phage extracts genetic material from one bacterium and inserts it into another.
2) Conjugation, two bacterial cells are able to join and transfer genetic material.
3) Transformation, the process where bacteria are able to gather free genetic information.

1.5.4 Bacterial Resistance Mechanisms

Genetic resistance can be divided into five main bacterial resistance mechanisms: upregulation of efflux pumps, changes in membrane permeability, enzymes to deactivate antibiotics, point changes in the antibiotic targets and upregulation of alternative pathways/ use of additional proteins for key cellular function, shown in Figure 6.

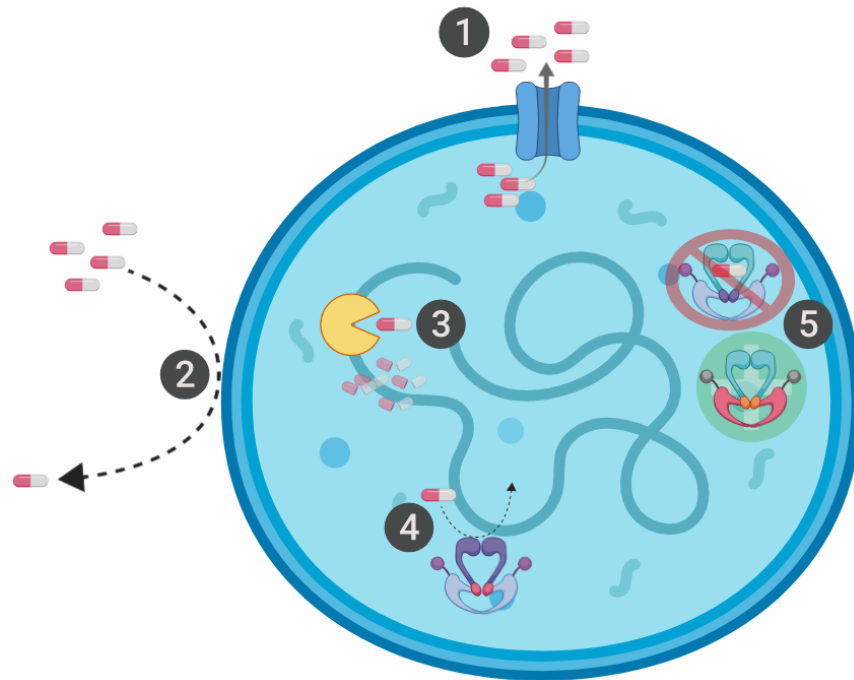


Figure 6 – Main resistance mechanisms in bacteria. 1) Upregulation of efflux pumps, 2) Changes in membrane permeability, 3) Enzymes to deactivate antibiotics, 4) Point changes in the antibiotic targets, 5) Upregulation of alternative pathways/ use additional proteins for key cellular function.

Upregulation of efflux pumps involves an increased expression of multi-drug efflux systems. These efflux systems effectively reduce the internal concentration of a vast array of structurally distinct antibiotics by actively transporting them out of the cell. As a result of their high substrate promiscuity, resistance can be achieved, in one step, to a variety of antibiotics. Changes in membrane permeability reduce the amount of antibiotic that can get into the cell, so there is no longer a sufficient internal concentration to have a therapeutic effect. This also includes down-regulation of channel proteins and ion channels if antibiotics are using these for assisted cell entry. In a last step to gain resistance to modern *Beta*-lactams, porins are significantly down regulated to stop the influx. However, this is also the mechanism needed for nutrients, so these strains are significantly adversely effected.³⁸ Other bacterial strains though have been able to make more subtle changes to the porin influx mechanism to exclude the bulkier *beta*-lactams without significant effect on nutrient influx.³⁸

Enzymes can be designed to target and deactivate antibiotics, again lowering the concentration of 'active' antibiotic inside the cell. This tends to be a resistance mechanism that has co-evolved with naturally occurring antibiotics as these enzymes are slow to develop. The most famous example of this mechanism is the *beta*-lactamase enzymes that target the penicillin class of antibiotics, an example of the key step in this degradation pathway is displayed in Figure 7.

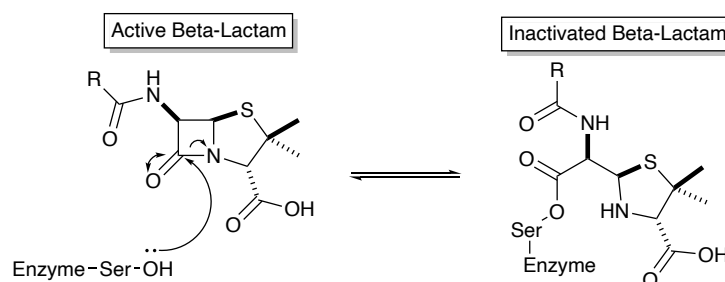


Figure 7 – Key step in the mechanism of inactivation of a *beta*-lactam antibiotic by a *beta*-lactamase enzyme. This step involves a nucleophilic attack from a serine in the enzyme on the lactam of the antibiotic. Zinc dependant *beta*-lactamases are also known and instead of forming a covalent intermediate with the enzyme, they function by activating a water molecule to perform the nucleophilic attack on the lactam in a mechanism similar to the example shown above.⁴¹

Single point changes of key amino acids in an antibiotic target can result in a dramatic decrease in affinity of the antibiotic for the target. This decrease in affinity means the required concentration of the antibiotic inside the cell to exert the therapeutic effect increases. An example of this is the single point mutations in DNA gyrase which allow for a bacterium to gain fluoroquinolone resistance – this will be described further in Section 1.8.4.

Upregulation of alternative pathways or use of orthogonal proteins to carry out the key cellular function is a way the bacteria can negate the effects of inhibition of a protein by finding other unaffected pathways. A good example of this is vancomycin, a naturally occurring antibiotic that binds to a *D*-ala-*D*-ala pentapeptide precursor needed for bacterial

cell wall synthesis. As this antibiotic doesn't directly bind a protein but a precursor that the protein requires, it was thought that it would be impossible to generate resistance as the bacteria cannot change the substrates it needs for cell wall production.³⁸ However, vancomycin resistance was indeed identified and was achieved by the substitution of a *D*-Ala with a *D*-Lac (or *D*-Ser). This resulted in a large reduction of the affinity of vancomycin towards the peptide and therefore cell wall production was less inhibited.⁴²

Resistance can be due to one or a multitude of these mechanism with them having an additive effect. A good example of this is how bacteria become resistant to fluoroquinolones. Bacteria are able to slowly acquire greater and greater resistance to this class of antibiotics by the incremental increase of resistance mechanisms. More information can be found in Section 1.8.4.

The activity of an antibiotic is measured using the minimum inhibitory concentration (MIC). This is the minimum concentration of antibiotic where no growth of bacteria is observed. It was once thought that resistance could only be generated at antibiotic concentrations below the MIC of the resistant mutant but above the MIC of the susceptible wild type. This results in the susceptible bacteria being killed and the resistant bacteria surviving to re-build the population. This was referred to as the "Mutant Selection Window Hypothesis".^{43,44} However, a study by D. I. Andersson and co-workers, showed how selection for resistant mutants and even *de novo* mutants can be generated using sub MIC concentration of antibiotics.⁴⁵ This was confirmed by work by J. H. Miller and co-workers.⁴⁶ These are similar conditions to what is experienced in the environment with the release of antibiotics or in certain compartments of the body after clinical administration and demonstrates another less well described mechanism for resistance generation. It also highlights another issue as, at low antibiotic concentrations, HGT is thought to dominate in terms of the passage of resistance.¹⁹ This

means that *in vitro* experiments with a single bacterial strain on agar are unlikely to be able to recreate the complexities occurring in nature.

1.5.5 Fitness Costs and Maintenance of a Resistance Phenotype

When a bacterium acquires resistance through a mutation, that mutation typically comes with a negative effect on cell homeostasis, also known as a fitness cost. This is the price a bacterium has to pay to survive under a different selection pressure. Bacteria usually carry resistance to multiple antibiotics (as well as heavy metals) in plasmids. Presence of these plasmids generally result in a significant fitness cost, inferring that for it to be maintained in the population a substantial selection pressure would be required. The underlying reason for this fitness cost is still poorly understood as it is a product of a wide variety of biochemical, environmental and genetic factors.^{47,48} It was hoped that removal of this selection pressure would result in the 'fitter' wild-type outcompeting the resistant variant. This would result in the re-sensitisation of the whole population to the current antibiotics as the resistant plasmid would have been lost.^{49,50} However, resistance seems to be rapid to acquire but slow to be lost.⁵¹ Bacteria are able to negate or greatly reduce the fitness cost without the loss of antibiotic resistance with different compensatory mutations.⁵⁰⁻⁵⁵ This means that bacteria are able to maintain the resistant plasmid, to be called upon when the selection pressure re-arises. Also, bacterial resistance genes can be co-located with other genes that offer growth advantages over the susceptible strain, making their maintenance beneficial.²³

Another explanation for the persistence of these resistance plasmids, even though they have a very low copy number, is the existence of 'killer' elements.^{38,56} The role of these 'killer' elements is to cause cell death if the plasmid is removed, therefore maintaining the plasmid in the population.⁵⁶

D. I. Andersson and co-workers showed that only low levels (>140 fold of MIC) of antibiotics (or heavy metals) were required to maintain the extended spectrum *beta*-lactamase (ESBL) plasmid.⁵⁷ This plasmid is of particular interest as it was implicated in outbreaks in clinical settings. They also showed that if the antibiotic resistance gene was moved from the plasmid to the chromosome, even less antibiotic was needed to maintain the resistance.⁵⁷ Most concerning, they disclosed that combinations of antibiotics and/or heavy metals could show synergistic effects and lower the amount needed to maintain resistance in a population.⁵⁷ This effect could explain why high levels of resistance are maintained in the environment where complex mixtures of antimicrobial substances exist.

Currently, susceptible bacterial strains are able to acquire resistance from “environmental reservoirs.”⁵⁸⁻⁶⁰ The transfer of resistance between the environment and the health care setting is concerning and an important route for the spread of resistance.⁶¹⁻⁶³ In 2012, a study by W. H. Gaze and co-workers has shown that there were 6.3 million exposure events to *Escherichia coli* (*E.coli*) resistant to third-generation cephalosporins through recreational water sport in coastal waters in England and Wales.⁶¹ A comprehensive two part review by K. Kümmerer summarises this area.^{64,65} A study by F. M. Aarestrup showed that a MSSA strain in humans (CC398) transferred to livestock and subsequently acquired resistance to tetracycline and methicillin. This strain has been implicated in an increase in MRSA infections in northern Europe.⁶⁶

1.6 Economics – Lack of Investment

Since 1990, 78 % of major drug companies have stopped or reduced their antibiotic portfolio.⁶⁷

This has largely been due to the inappropriate funding model and the very poor returns on investment when compared to other therapeutic areas.

The problem with the funding model is, unlike a new drug in a different disease indication that would become the 'gold standard' or 'blockbuster' and would immediately start repaying the significant investment costs, a new 'gold standard' or 'blockbuster' antibiotic would be kept in reserve to be used as a treatment of last resort. This means that only when there are no other viable alternatives would the new antibiotic be used and only in very severe cases. This means that companies would get poor returns on their substantial development costs and the antibiotic would likely lose its intellectual property protection by the time it was required for the mass market. Also, instead of the new drug being used to treat chronic conditions, where patient would need to take the drug for the rest of their life, the new antibiotic would likely only be prescribed for acute illnesses over short periods of time. This poor return on investment was shown in a review on antimicrobial resistance commission by the former UK Prime Minister David Cameron and the Wellcome Trust.⁶⁸ Even using the optimistic estimates, the new antibiotic takes around 23 years to become profitable and is almost out of patent protection when this happens,⁶⁸ shown in Figure 8. The result of this is that the company has a very short amount of time to get any returns on their investment, to fund future programs, and is unable to benefit from the revenues of the drug when it is at its most profitable. Antibiotic sales annually total \$ 40 billion, but only 12 % of that income is for patented compounds.¹ The on patent sales for antibiotics is around the same income as one of the top selling cancer drugs so it is clear which therapeutic area pharmaceutical companies

will preferentially invest in. This is a huge challenge in antibiotic development and will keep limiting the research in this area by large pharmaceutical companies until an alternative funding model can be implemented and this area can become commercially viable.^{29,68} The total investment in antibacterial research in the period of 2003 - 2013 was \$ 1.8 billion, less than 5 % of the total amount spent by pharma companies in research and development (\$ 38 billion).¹⁷

An interesting outcome of all of this is that 90 % of antibiotics currently in development (2019) are owned by companies outside the top 50 pharmaceutical companies by sales. This shows how this area has shifted away from the classic “big pharma” dominated environment and more pressure is on the small biotechnology firms to deliver, despite the fact that many have never brought a drug to market. Of course, this shift away from big pharma and towards smaller biotechnology companies and CROs is one which is happening across the pharmaceutical industry as a whole and not just in antibiotic research. There is a huge financial cost of developing a new chemical entity. For example, a phase III clinical trial of a novel antibiotic in a single disease indication costs around \$ 70 million.⁶⁷ Considering that if the antibiotic does make it to market, which is by no means guaranteed as the failure rate for infectious disease drugs is roughly 65 %, ⁶⁹ the potential returns are also limited as resistance can emerge at any point, it would become a treatment of last resort and mainly sold for short courses.

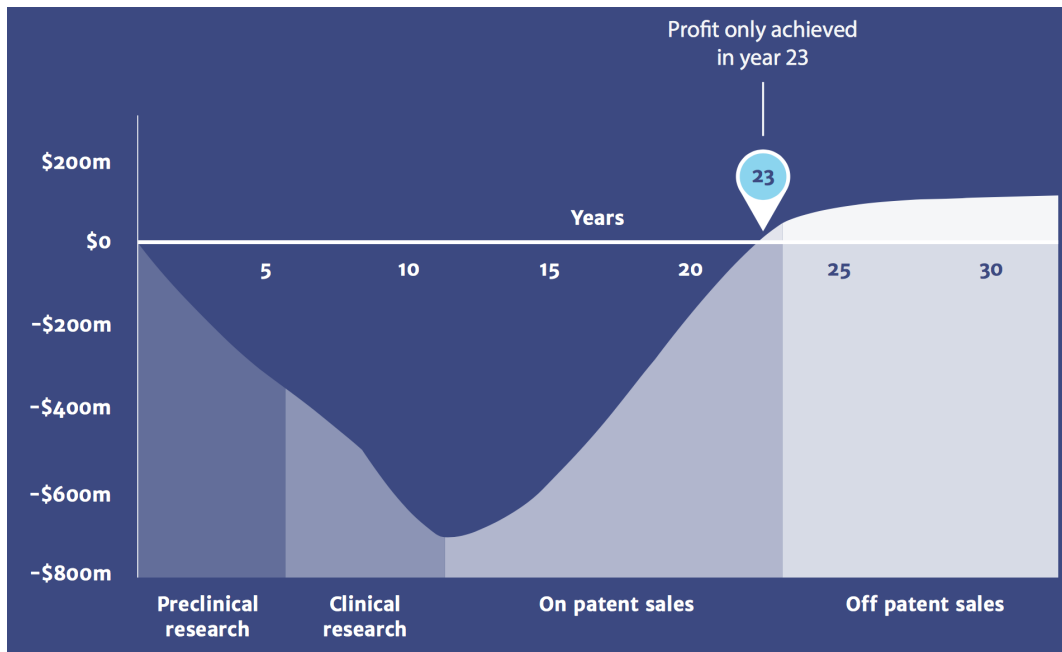


Figure 8 – Financial projections for antibiotic development.⁶⁸ Modelling done by the Review on Antimicrobial Resistance using data from the literature, IMS health UK and pharmaceutical companies. The model predicts an estimated \$ 700 million cost to bring a new antibiotic to market and a 23-year period before that cost is covered by the revenue.

1.7 Scientific Challenges of Developing Antibiotics

Development of new antibiotic compounds is scientifically challenging. In a review by L. Silver it was stated that even if money wasn't an obstacle and the issues with regulation were fixed, there would still be a stagnation with antibiotic drug discovery due to the significant scientific challenges of designing novel antibiotics.⁷⁰ An antibiotic compound is essentially a 'selective poison' that will kill bacteria but leave the host cells unaffected. In addition to properties required of a typical oral-administered drug, antibiotic compounds are also required to be:

1. Active against many variants of the target(s).
2. Ideally inhibit multiple targets.
3. Low frequency of resistance.
4. Aiming for total systemic exposure in order to treat any infection.
5. Treat a variety of infections.

6. Permeate bacterial cell walls/ membranes.
7. Evade efflux mechanisms.
8. High safety window that is compatible with a high dose regimen.

An antibiotic is required to be active against many variants of a protein as different bacterial species have variations in the same proteins. Antibiotics with a broad spectrum of activity must be able to achieve high affinity binding to all the variants of the target protein. Importantly though, they must be inactive against the human homologues, otherwise mechanism-based toxicity will cause complications. It is often understated how different bacterial species are from each other. Humans have more in common genetically with paramecia, a single celled organism, than *H. influenzae*, a Gram-negative bacteria, has to *S. pneumoniae*, a Gram-positive bacteria.^{71,72}

Ideally, antibiotics would have multiple biological targets. This would mean that changes to all targets would be required for high level resistance to be achieved. These agents are therefore less prone to resistance generation and as a result they have a higher likelihood to be a successful monotherapy.⁷³⁻⁷⁵ Enzymatic targets are probably a poor fit for antibiotic drug discovery due to their high propensity for rapid mutation and therefore resistance generation. This has been implicated in the lack of success for antibiotic discovery from genomic methods.⁷³

Low frequency of resistance in terms of both generation of resistant bacteria and low number of mutation events per generation are desired so the newly developed treatment will have a long clinical lifetime. A desired frequency of resistance is less than 1×10^{-10} as an infection can reach a maximum concentration as high as 1×10^9 cells per millilitre, which is the number of bacteria at the peak of an infection.^{76,77}

Ideally, antibiotics are also required to access a variety of compartments in the body. An infection can occur anywhere in the body, so the antibiotic will also need to get there at a therapeutically relevant concentration.⁷⁸

A variety of infections may need to be treated. These can vary greatly from urinary tract infections (UTI), to osteomyelitis (bone infections), to pneumonia (lung infections), and all require subtle differences to treat effectively.

It is key for an antibiotic to permeate a variety of bacterial cell walls/membranes containing diverse channel proteins/ porins. Specifically, cell membranes for Gram-positive bacteria and cell walls and cell membranes for Gram-negative bacteria, shown in Figure 2. This is especially difficult in Gram-negative bacteria as the outer membrane is largely impermeable but typically antibiotics can pass through it using porins or solute specific channels. This requires hydrophilic, charged compounds with a molecule weight (MW) less than 600 Da. The antibiotic then needs to pass through the cytoplasmic membrane which requires hydrophobic, uncharged compounds. Striking a balance between these two requirements is key for Gram-negative permeability and a very complex task to achieve with a single small molecule.

Evading resistance mechanism is key for the longevity of a new antibiotic. If resistance is easily generated or quick to acquire then even the most potent antibiotic will become useless in a relatively short period of time. These resistance mechanisms include enzymes specifically designed to inactivate compounds and removal of these compounds from the bacteria by highly promiscuous efflux pumps.⁷³ These efflux pumps can be located on the outer or cytoplasmic membranes and typically target hydrophobic compounds. Unfortunately, passive permeability is also linked to hydrophobicity, so the easier a compound can passively

permeate the cytoplasmic membrane, the more of a substrate for the efflux pumps it becomes.

The daily dose of an antibiotic tends to be a lot higher than most drugs, grams instead of milligrams. This has repercussions in terms of required safety and selectivity profile.

Generally speaking, antibiotic compounds exist outside C. A. Lipinski's 'rule of 5'.⁷⁹ A review of GSK's clinical efforts towards novel antibiotics, suggests that they require a distinct physicochemical profile as they tend to be larger and more hydrophilic than drugs for other therapeutic areas.⁷¹ Another study by H. E. Moser and co-workers found that, especially for targets in the cytoplasm of Gram-negative bacteria, where passive diffusion is the entry mechanism, the compounds require a MW less than 600 Da, high polar surface area (PSA) and to be charged at physiological pH.⁷⁰ This was further clarified in another study by L. L. Silver which looked at the 6 classes of antibiotics that have targets in the Gram-negative cytoplasm and found the MW was between 337 – 586 Da and a cLogP of -1.5 to 3.0.⁸⁰ If active transport was shown to be the entry mechanism the compounds tended to be even more polar.⁷⁰ Interesting Gram-positive agents tended to be less polar and have a higher MW.⁸⁰ Targets between gram negative and gram positive bacteria tend to be homologous, therefore this presumably means that permeability could be the reason for the lack of Gram-negative activity as passive permeability through the gram negative cell is limited. This is backed up by a study by Hergenrother and co-workers which showed that as long as a set of rigidity and shape criteria were met, adding a positively charged amine to a Gram-positive only antibiotic could increase the spectrum of activity to include Gram-negative bacteria.⁸¹ They postulate that this is due to a change in entry mechanism where the compound no longer relies on passive permeability but gains entry to the bacteria through porins.

To exemplify how difficult the development of an antibiotic is; 34 different companies, between 1996 and 2004, have conducted more than 125 high throughput screens (HTS) on 60 diverse targets, without a nominated development candidate.^{71,82} It's not surprising that finding structural moieties that have antibacterial activity is challenging when you consider that bacteria have been on the planet for over 3 billion years. In that time, they would have been exposed to most of the known chemical structural diversity and probably structural motifs that have yet to even be identified in the lab.²⁹

Another challenge is how to design the clinical trials for antibiotics that target resistant bacterial infections. Only a small subsection of patients contract these infections and meet the requirements to partake in the trials.⁸³

In summary, the consensus is starting to shift that we may have already entered the 'post-antibiotic' era and we must stop relying on one wonder drug to be the miracle cure.^{6,13} Instead the only way to efficiently combat this issue is a range of orthogonal treatments and for everyone to play their part, in both stopping infections in the first place and reducing the current overuse and misuse of antibiotics. An integrated, worldwide approach is possible, as shown by the global reaction to COVID-19, and action needs to be taken now to avoid a similar scenario but with multi-resistant bacteria unfolding.

1.8 Current Antibiotic Strategies – Fluoroquinolones

1.8.1 Development of Fluoroquinolones

Next, we will examine current strategies to combat AMR and focus on one of the most important and clinically relevant current classes of antibiotics - the fluoroquinolones. This class of antibiotics is used to treat a variety of Gram-positive and Gram-negative bacterial infections and are one of the most prescribed classes of antibiotics.⁸⁴ Some key examples of the fluoroquinolone class of antibiotics are displayed in Figure 9.

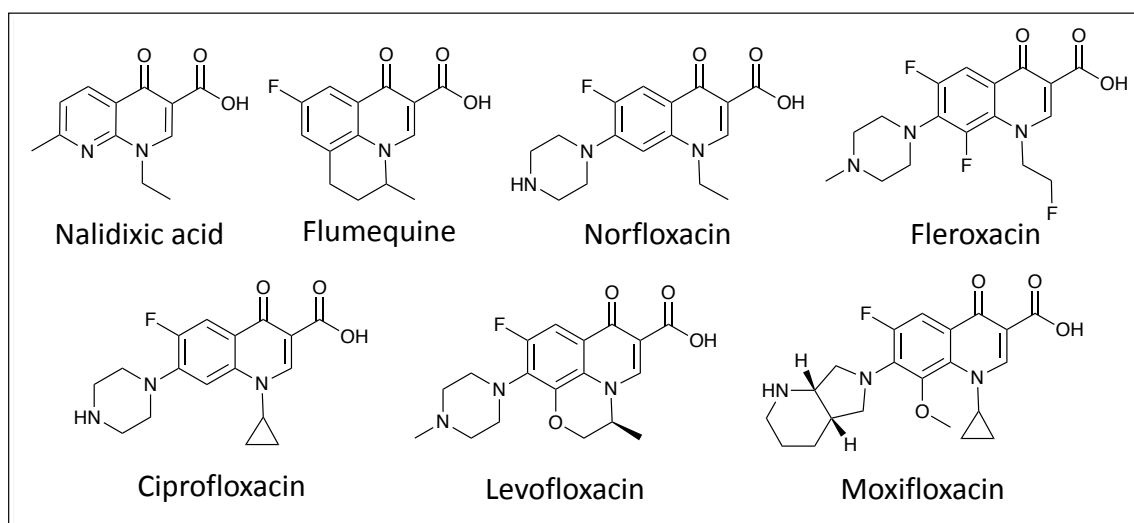


Figure 9 – Clinically relevant fluoroquinolones. This is not an exhaustive list but highlights the key improvements in the fluoroquinolone series.

Fluoroquinolones are a fully synthetic class of antibiotics that first entered the clinic in 1967 with the introduction of nalidixic acid.⁸⁵ Nalidixic acid was discovered fortuitously in 1962 as a by-product in the synthesis of Chloroquine and was quickly identified as an inhibitor of DNA synthesis,^{86,87} although the precise enzymatic target would not be identified until 1977.^{88,89} A significant improvement to Nalidixic acid came with the first-generation fluoroquinolone, Flumequine in 1976.⁹⁰ This compound had the quinolone core and a fluorine at the 6-position,

which gave the class its modern name 'fluoroquinolones'. The addition of this fluorine broadened the activity of the series and gave the first promise of increased Gram-positive activity. In general, the first generation fluoroquinolones had minimal systemic exposure and moderate Gram-negative activity, with little to no Gram-positive activity.⁹¹

The next step forwards, and the first of the second-generation fluoroquinolones, was Norfloxacin (sold under Noroxin) in 1978. The main advantage was improved Gram-negative activity and a longer half-life (3.5 h).⁹² Next was Fleroxacin (sold under Quinodis and Megalocin) in 1986. It had the first di-fluorinated core and a fluoroethyl group appended to the nitrogen of the quinolone. This was the first fluoroquinolone to allow for a once daily dosing scheme due to its longer half-life (~11 h), lower protein binding (23 %), good tissue penetration and excellent bioavailability (100 %).^{93,94} However clinical use of this compound was limited by side effects that included 'severe phototoxic reactions'.⁹⁵ The most clinically important second generation fluoroquinolone is Ciprofloxacin, discovered in 1981, and it is still in widespread clinical use today. Ciprofloxacin can be dosed orally or intravenously (IV), has a broad spectrum of activity and has successfully treated a large variety of infections.⁸⁵ The second generation fluoroquinolones have an expanded spectrum of activity which includes some atypical bacteria but limited activity towards Gram-positive bacteria.⁹¹ The third generation of fluoroquinolones expanded the spectrum of activity of the second generation fluoroquinolones by adding good Gram-positive activity.⁹¹ The most notable from this generation is Levofloxacin (sold under Levaquin), patented in 1985, as the *L*-isomer of Ofloxacin. It is shown to have higher aqueous solubility and potency than the racemate and was inside the top 200 drugs sold in America from 2007-2017.

The fourth generation of fluoroquinolones increased potency and spectrum of activity of the series including both atypical bacteria and anaerobes.⁹¹ An example of this subset is

Moxifloxacin (sold under Avelox) which was patented in 1988 and is currently on the WHO list of essential medicines.⁹⁶

1.8.2 Fluoroquinolones Currently in Development or Recently Released

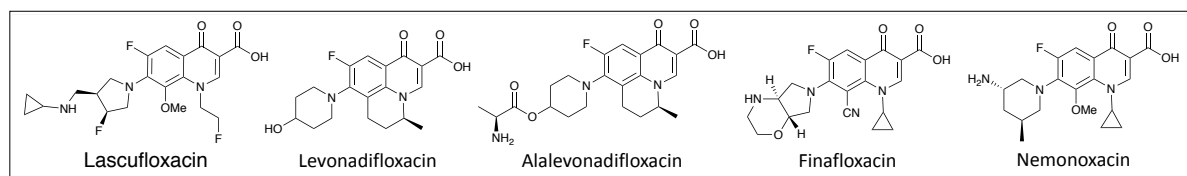


Figure 10 – Fluoroquinolones recently marketed or currently in final stages of clinical development.

Lascufloxacin (or KRP-AM1977), shown in Figure 10, was developed by Kyorin Pharmaceuticals for lower respiratory tract infections. It is potent against WT and resistant clinical isolates and has an excellent PK profile for once daily oral dosing.^{97,98} The new drug application was approved on 20/09/19 and it has been on sale from 08/01/2020.

Levonadifloxacin (or WCK 771), shown in Figure 10, is the active form of the orally bioavailable prodrug Alalevonadifloxacin (or WCK 2349) and is being developed by Wockhardt limited. Both versions have complete phase III trials in India and their new drug applications have been submitted (India DCGI) and are pending approval. The prodrug has a high safety window allowing for high doses which lead to plasma exposure 8 - 17 fold higher than other leading fluoroquinolones.⁹⁹ It shows good activity against WT and fluoroquinolone resistant clinical isolates.^{100,101}

Finafloxacin (or BAY-35-3377), shown in Figure 10, was initially discovered by Bayer AG and Novartis AG but is currently been developed by MerLion Pharmaceuticals GmbH. An otic formulation has been approved by the FDA (17/12/14) for treatment of acute otitis externa. A systemic formulation of Finafloxacin has not received approval in any country and phase II

clinical trials are ongoing. Unlike typical fluoroquinolones its optimal pH range for activity is 5.0 to 6.0. This means it is ideally designed to target infections in acidic body compartments, i.e. the stomach and urinary tract, and infections caused by *helicobacter pylori*.¹⁰²

Nemonoxacin (or TG-873870), shown in Figure 10, was initially developed by Procter & Gamble Pharmaceuticals and is now being advanced by TaiGen Biotechnology Company. It received approval by the Chinese FDA on 08/06/2016 and has moved into phase III trials in the US. It has been shown to be an effective treatment for community-acquired pneumonia (CAP).¹⁰³

1.8.3 Mode of Action of the Fluoroquinolones

1.8.3.1 Biological Target - Topoisomerases

Topoisomerase enzymes are involved with regulating the strain (or amount of supercoiling) on DNA during DNA replication.¹⁰⁴ They fulfil this function by causing transient breaks in DNA using a conserved catalytic tyrosine residue, forming a cleaved complex which is a covalent intermediate.¹⁰⁵ The topological change can then be completed and the DNA reconnected and released. Topoisomerases can be classified into type I - single strand breaks or type II - double strand breaks. These can be further divided into the A subfamily - linked to a 5' phosphate or B subfamily - linked to a 3' phosphate.

The fluoroquinolone series of antibiotics have been shown to target the homologues type IIA topoisomerase enzymes; DNA gyrase, by Tomizawa and co-workers in 1977,⁸⁹ and topoisomerase IV (topo IV), by H. Ikeda and co-workers in 1992.¹⁰⁶⁻¹⁰⁸ There is some overlap between the functions of the different topoisomerase enzymes, but they are optimised to their own specific topological function.

DNA gyrase was discovered in 1976 by H. A Nash and co-workers.¹⁰⁹ It has an A₂B₂ heterotetrameric structure made up of two units of 97 kDa gyrase A (GyrA) and two units of 90 kDa gyrase B (GyrB) and is encoded for by the *gyrA* and *gyrB* genes.^{110,111} It is the only known type II topoisomerase that can introduce negative supercoils into DNA. For enzymatic turnover and rapid kinetics this process requires a catalytic Mg(II) ion and hydrolysis of ATP.¹⁰⁵ It is essential for chromosome condensation leading to correct cell division.¹¹²

Topo IV, discovered in 1990 by H. Suzuki and co-workers,¹¹³ is mainly responsible for DNA decatenation,¹¹⁴ but has been shown to also introduce positive supercoils.¹¹⁵ It is homologous to DNA gyrase and has a similar C₂E₂ heterotetrameric structure made up of two units of 75 kDa ParC and two units of 70 kDa ParE (known as GrlA and GrlB in *Staphylococcus aureus*)¹¹⁶ and is encoded for by the *parC* and *parE* genes.^{110,111}

Gyrase and topo IV are ideal targets for antibacterial therapy as they are both essential for bacterial growth and are unique to bacteria.

Fluoroquinolones function by stabilising the covalent intermediate or cleaved complex of DNA gyrase (or topo IV) and DNA. Not only does this inhibit the enzyme from carrying out its critical cellular functions but it also results in fragmentation and release of cytotoxic DNA fragments which then cause death of the bacterial cells.^{54,117,118}

The binding mode of fluoroquinolone series in the cleaved complex is exemplified in Figure 11 with Moxifloxacin bound to DNA/ topo IV covalent intermediate of *A. baumannii*. The key interaction is the water-mediated magnesium ion bridge between the keto-acid on the fluoroquinolone and the serine and glutamic acid residues of the protein. The key residues can differ between bacterial species and the topoisomerase in question (gyrase or topo IV) but importantly they are four residues apart on the same face of the *alpha* helix and able to form the hydrogen bonding network to establish the interaction. The core of the

fluoroquinolone intercalates between the base pairs of the DNA forming a π - π stacking interaction. This binding mode is conserved between bacterial species and gyrase and topo IV hence fluoroquinolones typically have a broad spectrum of activity and are dual targeting. Due to the heterotetrameric structure of both DNA gyrase and topo IV, two fluoroquinolones bind per enzyme in a symmetrical pocket separate from the catalytic tyrosine.

The primary target of a fluoroquinolone can differ between bacterial species and the particular quinolone.^{119,120} A general rule is in Gram-negative bacteria DNA gyrase is the primary target and in Gram-positive bacteria topo IV is the primary target but this is not always the case.⁹¹

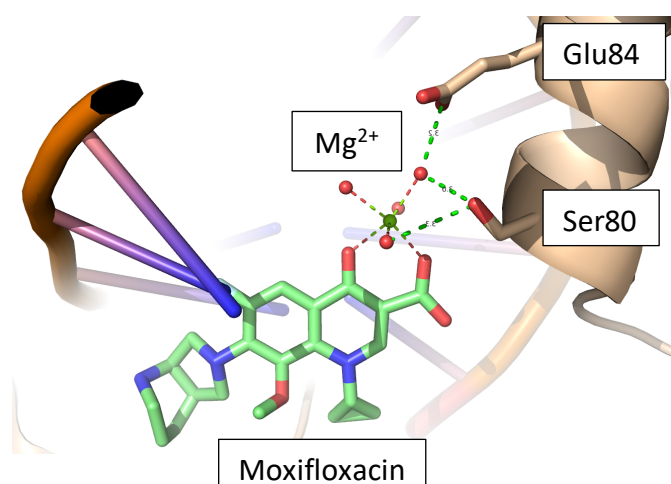


Figure 11 – X-ray crystal structure of Moxifloxacin in *Acinetobacter baumannii* topo IV (ParC-ParE fusion truncate). Created for pdb file 2XKK. Moxifloxacin (Fluoroquinolone antibiotic) in green, topo IV in light brown, DNA in orange and blue, magnesium ion in green and key waters in red. This displays the key water-mediated magnesium bridge with Ser80 and Glu84 (*A. baumannii* numbering).

1.8.4 Resistance Mechanism

There are two main resistance mechanisms that affect the fluoroquinolone series of antibiotics; single point mutations on the enzymatic target and decreased permeability/increased efflux. Enzymatic inactivation of fluoroquinolones was not thought to be possible

as they are a purely synthetic class of antibiotic and it was thought that this kind of resistance needed to co-evolve with the antibiotic over a substantial time period.¹¹⁰ However, in 2006 D. C. Hooper and co-workers showed that an enzyme capable of this inactivation did exist. It was a variant of the aminoglycoside *N*-acetyltransferase, which could acetylate the terminal piperazine nitrogen of Ciprofloxacin resulting in a four-fold increase of the minimum inhibitory concentration (MIC).^{121,122} This could be due to a decrease in binding affinity or simply an increase in clearance. Although this MIC increase only confers low level resistance, it was shown to be additive and an acquisition of a single plasmid could allow for clinically significant resistance to be obtained.¹²¹

The most common cause of resistance to fluoroquinolones occurs when there is a mutation in one of the key residues in the quinolone-resistance determining region (QRDR), this is shown in Figure 12.^{123,124} For gyrase, the most common site of mutation in clinical and laboratory setting in GyrA is Ser83 (*E. coli* numbering) with the second being Glu87, (*E. coli* numbering, this can be an Asp residue in some bacterial species).^{124–130} These mutations are hypothesised to disrupt the water-mediated bridge linking the fluoroquinolone to the protein *via* the non-catalytic Mg²⁺ ion,⁵⁴ as shown in Figure 12. The distribution in this water-mediated bridge results in a significant loss of activity for fluoroquinolones. For topo IV, the most common site of mutation in ParC are Ser80 (*E. coli* numbering, equivalent to position 83 in gyrase) and Glu84, (*E. coli* numbering, equivalent to position 87 in gyrase).^{127,131,132} This has the same effect as the gyrase mutants, disrupting the water-mediated magnesium bridge, with a similar result in terms of decreased activity. As fluoroquinolones are dual targeting and inhibit both gyrase and topo IV, mutations in both are required for high level resistance.¹⁰⁷ This is why the dual targeting motif is so desirable in antibiotic development. A balanced profile against two targets greatly decreases the chance of resistant mutant generation.¹³³

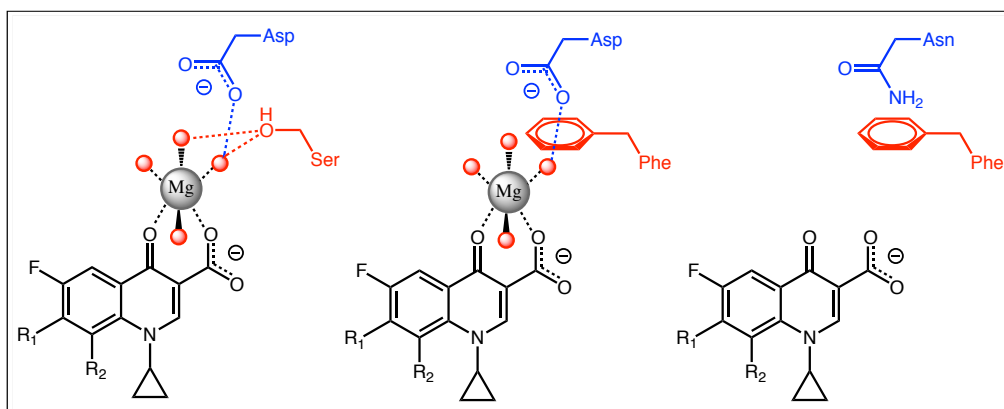


Figure 12 – Proposed role of single point mutation in distributing the water-mediated magnesium bridge. Left - WT structure with water-mediated magnesium bridge. Middle - single point mutation in gyrase (or topo IV) results in loss of key serine and partial distribution in the water network. Right – double mutation in gyrase (or topo IV) results in loss of key serine and acidic residue leading to complete distribution in the water network and loss of the Mg^{2+} ion.

Another frequent cause of fluoroquinolone resistance is diminished accumulation inside the bacterial cell either by decreased uptake or overexpression of efflux pumps. Fluoroquinolones can enter bacterial cells either through porins, protein channels to facilitate internalisation of nutrients, or passive diffusion through the phospholipid bilayer. The balance of these two methods of influx depend on the hydrophobicity of the fluoroquinolone in question.¹³⁴ Resistance due to a down regulation of porins is typically associated with Gram-negative bacteria and has a much greater effect on hydrophilic fluoroquinolones.^{135–137} Efflux pumps function by actively transporting compounds out of the bacterial cell, though a channel, at the expense of ATP. These systems are more effective at removing hydrophilic molecules from the cell.

Another less common mechanism of low-level quinolone resistance involves the protection of topoisomerases with Qnr (quinolone resistance) proteins.^{138–140} These proteins are thought to have originated as a protection mechanism for bacterial strains producing a natural occurring gyrase inhibitor microcin B17 to avoid self-inhibition.^{141–143} It has been shown that

Qnr can bind specifically gyrase haloenzyme without the need of DNA, ATP or the FQ,¹⁴⁴ but the exact mechanism of protection is still unknown. There are two plausible mechanisms which may be possible; Qnr binding could interfere with fluoroquinolone binding and therefore prevent the formation of the poisonous cleavage complex (DNA–gyrase–FQ) or Qnr binding could disfavour the cleavage complex, returning gyrase into a catalytically active form.^{144,145} The potential disadvantage in disruption of gyrase's key cellular activity is compensated for by the benefit of avoiding the release of cytotoxic DNA fragments that result from the fragmentation of the cleavage complex.

Another rare low-level resistance mechanism observed by D. C. Hooper and co-workers was the down regulation of topo IV in *s. aureus* on treatment with Premafloxacin.¹⁴⁶ This new strain was able to compensate with the lack of topo IV by upregulation of DNA gyrase and appear equally fit in growth competitions experiments presumably due to other compensatory mutations. This mechanism exemplifies the benefit of fluoroquinolones with a balanced inhibition profile against gyrase and topo IV, as this mechanism would not occur for these molecules.

Despite the dual targeting effect of the fluoroquinolones AMR is still on the rise with this class of antibiotics and despite being well studied, evading resistance mechanisms has proved challenging.¹¹⁹

1.8.5 General SAR of Fluoroquinolones

The general pharmacophore for the fluoroquinolone series of antibiotics is displayed in Figure 13. The optimal substituent off the quinolone nitrogen is cyclopropyl (Ciprofloxacin),¹⁴⁷ but ethyl (Norfloxacin), fluoroethyl (Feroxacin), aryl (Trovaflaxacin) or pyridyl (Delafloxacin) have all shown to be tolerated. At the 2-position hydrogen seems to be optimal and is consistent throughout the series. Positions 3 and 4 contain the magnesium chelating functionalities that are integral for activity so are conserved throughout the series. At the 5-position, small groups are tolerated but methyl (Grepafloxacin) or amino (Sparfloxacin) appear beneficial. However, this position is typically a hydrogen in the majority of the series. The fluorine at the 6-position is key as discussed earlier and gives a boost in gyrase activity of 2 to 17 fold and an increase in cell penetration by 1 to 70 fold.¹⁴⁸ This is thought to be due to how the fluorine effects the electronics of the quinolone core ring system and improves stacking interactions with the DNA base pairs.¹⁴⁹ As this substituent is so beneficial it has been maintained throughout the series. Position 7 has the greatest chemical diversity in the fluoroquinolone series. At this position both potency and pharmacokinetics (PK) can be fine-tuned. Either mono or bicyclic aliphatic amines give a good balance of potency and beneficial PK properties. The 8-position can be used to tune the *in vivo* and antibacterial activity. Fluoro (Sparfloxacin), chloro (Clinafloxacin), methyl (Ozenoxacin), methoxy (Moxifloxacin) and fused morpholine (Levofloxacin) are tolerated, as well as substitution of the carbon at position 8 for a nitrogen (Gemifloxacin). It has been shown by K. Drlica and co-workers that substitution of a hydrogen at this position to a halogen or methoxy group can enhance the antibacterial activity of the fluoroquinolone against both wild type (WT) and mutant strains.¹⁵⁰

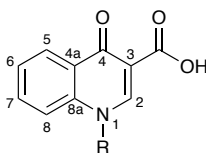


Figure 13 – Pharmacophore of the fluoroquinolone series.^{151–153} Pharmacophore for the fluoroquinolone series including the numbering of the positions around the quinolone core.

1.8.6 Fluoroquinolone Safety Profile

Generally, the fluoroquinolones are well tolerated but despite the benefits, they do possess some worrying side effects and have been given a black box warning by the FDA. These side effects are rare but serious and include tendonitis, arthralgia and mitochondria damage.^{154,155} The most common reactions are central nervous system (CNS) and gastrointestinal (GI) tract adverse events in 2 – 20 % of patients and slight QT interval prolongation is also observed.^{91,156–159}

1.8.7 Non-Fluoroquinolone Gyrase Inhibitors in the Clinical Development

Zoliflodacin (or ETX0914), shown in Figure 14, was previously discovered by AstraZeneca and is now being developed by Encases Therapeutics. It is currently in phase III clinical trials with an outcome estimated for August 2021. This molecule inhibits DNA gyrase and binds in the same pocket as the fluoroquinolones, however the key interactions are distinct with no magnesium binding.^{160–163} It is an orally active treatment and shows a very low frequency of resistance and no cross resistance with fluoroquinolones.¹⁶¹ Not only was it shown to be an effective monotherapy but it also shows promising results in combination with Ciprofloxacin, Ceftriaxone or Azithromycin.^{164,165}

Gepotidacin (or GSK2140944), shown in Figure 14, is being developed by GlaxoSmithKline and is currently in phase III clinical trials, with an estimated completion date of April 2021. This molecule is an orally active monotherapy and targets DNA gyrase but in a mechanistically

distinct way.¹⁶⁶ It binds in an orthogonal pocket between the two fluoroquinolone binding pockets and only one molecule binds per enzyme. As a result of this different mechanism of action, Gepotidacin doesn't show cross resistance with fluoroquinolones.¹⁶⁷ Interestingly, it causes double and single strand breaks in DNA whereas fluoroquinolones cause exclusively double strands breaks.

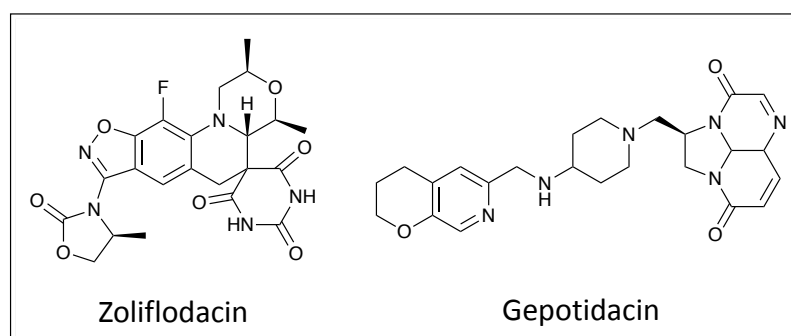


Figure 14 – Novel bacterial topoisomerase inhibitors (NBTIs) currently in the clinic. Non-fluoroquinolone DNA gyrase/ Topo IV inhibitors. Left – Zoliflodacin. Right – Gepotidacin.

1.9 Reverse Antibiotic Approach

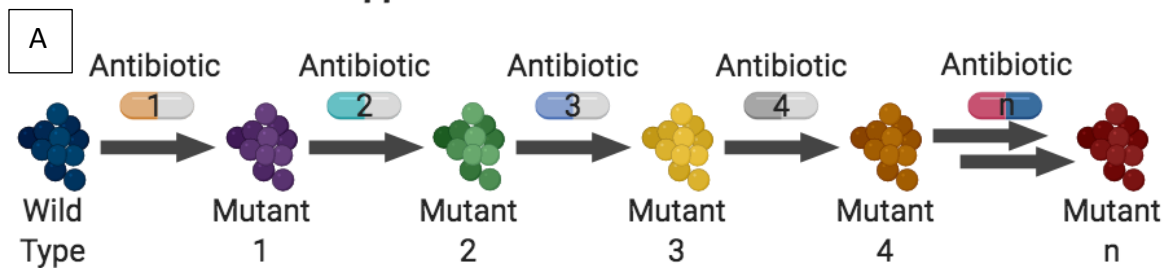
1.9.1 Introduction to the Reverse Antibiotic Approach

Fluoroquinolones have been one of the most clinically important classes of antibiotics, however with the increase in resistance, a method of re-instating their effectiveness would be highly desirable.

The concept of antibiosis has been previously discussed in Section 1.5.2 where competing bacteria emit inhibitory compounds in order to outcompete their rivals. One of these inhibitory compounds was shown to be the Nybomycin family of natural products. These fascinating compounds show intriguing activity and have been named 'Reverse Antibiotics'.^{2,168}

In a traditional approach, shown in Figure 15, an antibiotic is developed for a bacterial strain which over time then develops resistance. This results in a need for a new antibiotic to target the resistant mutant. This mutant can then develop further resistance to the new antibiotic and again a new drug will be needed. This cycle of new antibiotic - new resistance mechanism will continue indefinitely and will result in the constant need to develop new and novel treatments for bacterial resistance.

Traditional Antibiotic Approach



Reverse Antibiotic Approach

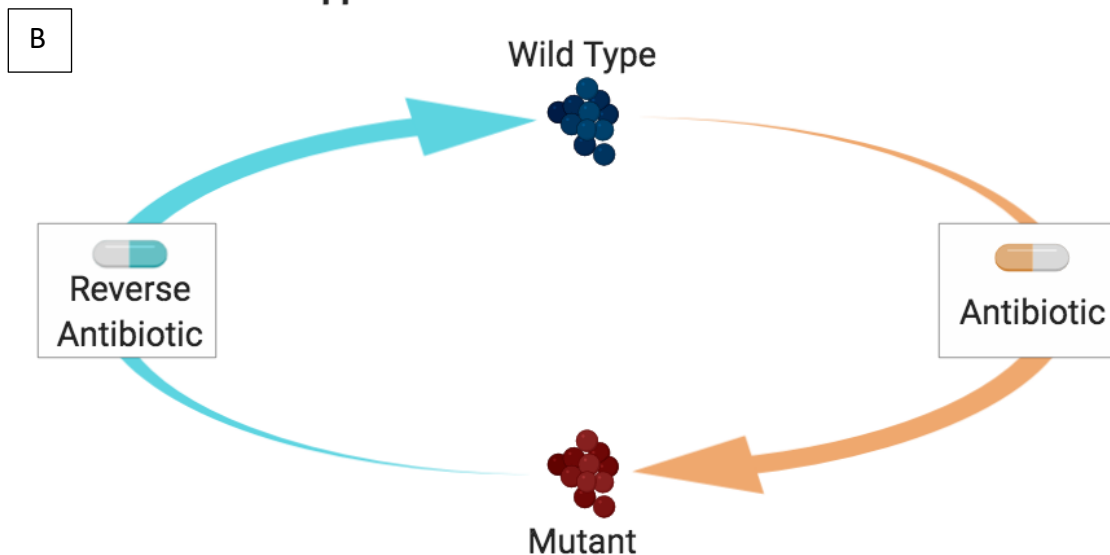


Figure 15 – Strategies of antibiotic development, A – traditional antibiotic approach, B – reverse antibiotic approach.^{2,169} Figure adapted from Bardell-Cox *et al.*¹⁶⁹

The concept behind the reverse antibiotic approach is being able to control the resistance pathway taken by the organism. As shown in Figure 15, treatment with the first antibiotic

leads to resistance so a new antibiotic is needed. However, unlike before, resistance to the second antibiotic can only be achieved by a back-mutation, thus re-sensitising the bacteria to the first antibiotic. The bacteria will be trapped in an 'evolutionary loop' where it will always be sensitive to either the antibiotic or the reverse antibiotic. This concept has been validated *in vitro* with Ciprofloxacin (fluoroquinolone antibiotic) and Nybomycin,^{2,170} shown in Figure 16. This could change the way FQR bacterial infections are treated and revive the fluoroquinolone class of antibiotics. However it is important to mention the caveats for this approach. This approach really only considers single point mutations as the process for resistance generation. It would be interesting if the bacteria could escape the 'evolutionary loop' by upregulating efflux or altering the permeability of the outer membrane.

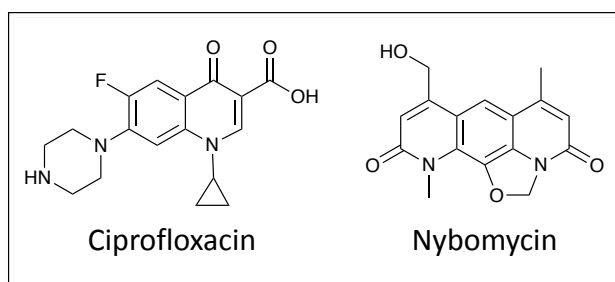


Figure 16 – A complementary pair of reverse antibiotics. Left – Ciprofloxacin. Right - Nybomycin.

1.9.2 Nybomycin Family of Natural Products

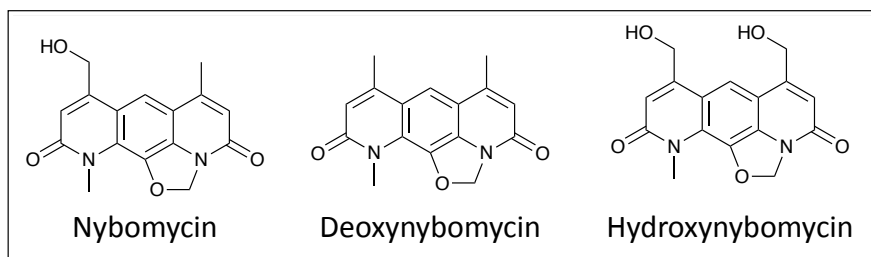


Figure 17 – Nybomycin family of nature products. Naturally occurring members of the Nybomycin family. Left – Nybomycin. Middle – Deoxynybomycin. Right – Hydroxynybomycin.

Nybomycin, shown in Figure 17, was first discovered and isolated from an unidentified *streptomycete* (A 717) from Missouri soil in 1955 by I. N. Asheshov and co-workers.¹⁷¹ It showed activity against some *E. coli* strains (B and FCb), *Klebsiella pneumoniae* (ATCC 9997), *B. subtilis* (ATCC 9633), *Mycobacterium smegmatis* (ATCC 10143), and *B. mycoides* (ATCC 9634) in a paper disc test by serial dilution.¹⁷¹ However no activity was observed against the standard laboratory test strain of *S. aureus* at the time (Heatley strain) or for *Pseudomonas aeruginosa* (ATCC 10145). They also showed Nybomycin was tolerated *in vivo*, using a mouse model with a 250 mg/Kg dose. Active material was found in faeces for 24 h and urine for 3 days after administration, showing good retention in the body and metabolic stability.¹⁷¹

The total synthesis of Nybomycin was first reported by K. L. Rinehart and co-workers in 1970.^{172,173} In the same year another member of the Nybomycin family, Deoxynybomycin, displayed in Figure 17, was isolated from *Streptomyces* (MB891-A1), in a soil sample from Okinawa, by H. Umezawa and co-workers.¹⁷⁴ This derivative has previously been described by K. L. Rinehart and co-workers *via* the dehydroxylation of Nybomycin under strongly acidic conditions.¹⁷⁵ It showed greater activity than Nybomycin on the strains tested which included; *S. aureus* (FDA 209 P, Terajima, Smith, 193, 52-34), *Mycobacterium smegmatis*

(ATCC 607), *Mycobacterium phlei* and *B. subtilis* (NRRL B-558).¹⁷⁴ It showed mild activity on the *E. coli* strain (NIHJ) but was less active than Nybomycin.¹⁷⁴

A third member of the Nybomycin family, Hydroxynybomycin, shown in Figure 17, was identified as a minor metabolite from *streptomyces* (sp. D-57) by K. L. Rinehart and co-workers in 1977.¹⁷⁶ Its activity was comparable with Deoxynybomycin in the strains tested and neither showed any activity against *S. aureus*.¹⁷⁶

There were no further reports of the Nybomycin family of natural products in the literature, no optimisation of the natural products was attempted, and no members of the family entered clinical use for more than 30 years. In 2012, Y. Akamatsu and co-workers reported results of their screen of compounds against a multi-resistant MRSA strain (Mu50).² The supernatant from *streptomyces hyalinum* (MB891-A1) showed an intriguing phenotype in that it displayed strong inhibition against the multi-resistant Methicillin-resistant *Staphylococcus aureus* (MRSA) strain (Mu50) but no activity against the globally susceptible *S. aureus* strain (FDA 209P). Further analysis of this supernatant showed it contained both Nybomycin and Deoxynybomycin. These were isolated and this mutant-selective phenotypic behaviour was confirmed on a panel of 77 *S. aureus* clinical isolates (including both Methicillin-sensitive *Staphylococcus aureus* (MSSA) and MRSA strains). After genetic analysis of the QRDR of GyrA and ParC the authors determined that the Nybomycin family targeted S84L GyrA mutant (*S. aureus* numbering) and were inactive against strains with WT GyrA. They hypothesised that gyrase was the primary enzymatic target as from the strain analysed the S84L mutant in GyrA was consistent for strong inhibition (MIC \leq 2 μ g/mL). However, for the greatest inhibition consistently (MIC \leq 0.06 μ g/mL) the quadruple mutant (S84L, E88G or E88K in GyrA and S80Y, E84G or E84K or E84V in ParC, *S. aureus* numbering) was required. To be able to confidently state the primary target, one would like to see the enzymatic inhibition

(supercoiling inhibition for gyrase, decatenation inhibition for topo IV) in both Gram-positive and Gram-negative strains. It could be that, like the fluoroquinolones, the Nybomycins target both GyrA and ParC. Generally, the more resistant to fluoroquinolones the bacterial strain becomes the more sensitive it becomes to the Nybomycins. The most important discovery was when Y. Akamatsu and co-workers attempted to generate mutants of the Mu50 strain to Deoxynybomycin.² Not only was the frequency of resistance very low (0.622×10^{-11} , average of two replicates at 2 mg/L) but all nine mutants independently underwent a back-mutation to a WT GyrA (L84S mutation) leading to a re-sensitisation to fluoroquinolones. The low frequency of resistance and the fact that only one mechanism of resistance was present in all isolates gives evidence that this reverse antibiotic approach may be clinically viable and escape from the cycle may be very difficult for the bacterium to achieve.

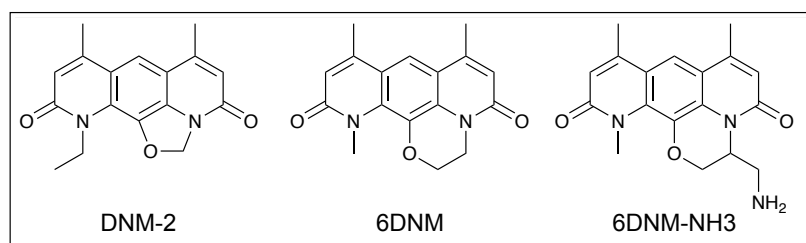


Figure 18 – Key synthetic analogues of Nybomycin. Designed by P. J Hergenrother and co-workers to probe the structure-activity relationship (SAR) and Gram-negative activity. The numbering regime used corresponds to the original names given to these compounds in the literature.^{81,170}

P. J. Hergenrother and co-workers in 2015 re-designed the synthetic route and produced a small array of analogues to probe the structure-activity relationship (SAR) around the core with longer and bulkier alkyl substituents.¹⁷⁰ The best compound they designed was **DNM-2**, shown in Figure 18. It showed comparable activity with Deoxynybomycin but had improved aqueous solubility. They reported the aqueous solubility of Deoxynybomycin was 9 μ M and

that the extended ethyl chain increased the aqueous solubility of **DNM-2** to 121 μM .¹⁷⁰ **DNM-2** also showed no inhibition of human topoisomerase II at 10 μM , with partial inhibition at 30 μM . The work showed inhibition of mutant GyrA (S83L and S83R, *E. coli* numbering) with Deoxynybomycin and **DNM-2** in a cleavage assay but didn't report IC_{50} values. They also commented that both single strand breaks and double strand breaks were observed in this assay and pointed out that this was a similar phenotype to another gyrase inhibitor, GSK 299423 (a compound created in the development of Gepotidacin),¹⁶⁶ whereas inhibition with fluoroquinolones like Ciprofloxacin forms exclusively double strand breaks.¹⁷⁷ This points to a slightly different mechanism of inhibition for the Nybomycin family compared to the fluoroquinolones. Either Nybomycins can inhibit gyrase at a different point in the catalytic cycle, the binding of one Nybomycin molecule does not catalyse the binding of a second as in the case of fluoroquinolones or Nybomycins can bind in an orthogonal pocket. The paper went on to confirm the low frequency of resistance to Deoxynybomycin in *S. aureus* (1.4×10^{-10} at 2 mg/L), (however found it to be 20-fold higher than Y. Akamatsu and co-workers)² and confirmed these resistant colonies had reverted to WT GyrA (L84S mutation, *S. aureus* numbering).¹⁷⁰ Interestingly, they also showed that co-treatment of Ciprofloxacin (4 $\mu\text{g}/\text{mL}$) and **DNM-2** (6 $\mu\text{g}/\text{mL}$) resulted in no mutant generation at a frequency of resistance $<1 \times 10^{-10}$.¹⁷⁰ **DNM-2** and Deoxynybomycin were also tested in a mouse model *in vivo* (50 mg/kg *via* oral gavage). **DNM-2** showed good peak serum exposure (42.6 μM , 12.8 $\mu\text{g}/\text{mL}$) and a half-life of 0.9 h.¹⁷⁰ It was commented that the aqueous solubility of these compounds can be used as a predictor for their oral bioavailability, although this is a very small subset of compounds. **DNM-2** showed a significant improvement in survival, compared with Ciprofloxacin and vehicle, in a mouse sepsis model with a fluoroquinolone resistance strain

(NRS3).¹⁷⁰ Although this *in vivo* works looks promising, further study is required before there is enough data for these compounds to be clinically viable.

In 2015, M. Kobayashi and co-workers showed Nybomycin inhibits *Mycobacterium* in both active and dormant states making this a good candidate for development for new treatments against Tuberculosis.¹⁷⁸

P. J. Hergenrother and co-workers in 2017 showed that certain parameters were required to increase accumulation of an antibiotic inside a Gram-negative bacteria; scaffold rigidity, shape, and a polarisable centre.⁸¹ These factors allowed for a new entry mechanism into the bacterial cell *via* the OmpF porin. Despite earlier reports of Gram-negative activity with Nybomycins,^{171,174} more recent work contradicts this.^{2,170} This study reports Gram-positive activity (MIC of 0.06 µg/mL for *S. aureus*) but no Gram-negative activity (MIC of > 32 µg/mL for *E. coli*) for a closely related analogue (**6DNM**, shown in Figure 18) with similar rigidity and shape to Deoxynybomycin. However, addition of a polarisable primary amine (**6DNM-NH3**, shown in Figure 18) gives a compound which maintains Gram-positive activity (MIC of 0.03 µg/mL for *S. aureus*) but now is active against the Gram-negative *E. coli* (MIC of 0.5 µg/mL). This was hypothesised to be due to increased accumulation inside the bacterial cell *via* this OmpF porin.⁸¹

1.9.3 Historical Context of Nybomycins

It is interesting to consider the timeline of events, shown in Figure 19, with regards to the Nybomycin series. The first quinolone, Nalidixic acid, was discovered in 1962 and used clinically from 1967.^{85,86} This led to quinolone resistance being observed in the clinic in the 1980's. However, Nybomycin which is reported to target the fluoroquinolone resistant mutated gyrase, was first discovered in nature in 1955.¹⁷¹ It doesn't seem logical that an antibiotic is present in nature before its biological target exists. But maybe we are thinking about this the wrong way around; what if bacteria mutated their gyrase to be resistant to Nybomycin and with the fluoroquinolone series, an inhibitor for this mutated gyrase was developed?

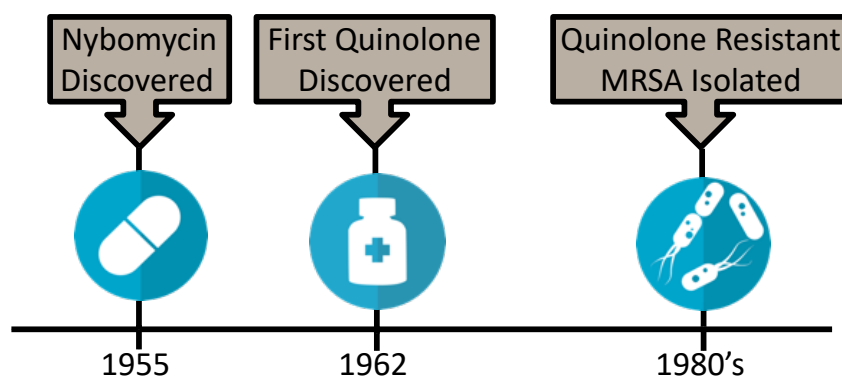


Figure 19 – Historical timeline of Nybomycin discovery and fluoroquinolone resistance.

1.9.4 Why Synthesise the Nybomycin Family of Natural Products?

The Nybomycin family of natural products have the potential to revolutionise antibiotic therapies. Only the two preliminary studies have been conducted and no further work has been attempted.^{2,170} There has not been a thorough exploration of the medicinal chemistry or microbiology around the scaffold and there remains substantial optimisation before the series is clinically relevant.

In order to facilitate this examination, a method with which to reliably obtain large quantities of the natural products and flexibility to explore novel analogues needs to be identified. Fermentation and isolation of the natural products was considered but the process is far from straight-forward and is inefficient (1,000 L reportedly gives between 200 – 350 mg of Nybomycin).^{179,180} It would also be complex to generate novel derivatives, even if you consider a semi-synthetic approach; the outputs would always be limited and lacking rational design or intellectual input. Therefore, it was concluded that a fully synthetic approach was the most appropriate for the aims of this project.

1.9.5 Why is the Nybomycin Series Currently Not a Drug?

The main limitations for the Nybomycin family of natural products are their very poor aqueous solubility. Even though Hergenrother and co-workers took initial steps to alleviate this liability, with **DNM-2** shown in Figure 18,¹⁷⁰ substantial optimisation is still required before this is an orally available drug. Another current limitation is that the mode of action for this series is still unclear, the primary target is still unknown and even the binding site is undetermined. A further potential cause for concern is the partial inhibition of human topoisomerase II at 30 μM .¹⁷⁰ This may not be problematic but typically a large safety window is required for an antibiotic as the dose is often significantly greater than in other disease indications.

2. Aims of the Project

With the above limitations in mind, the initial aim of this work was to reproduce the synthetic route to the best known Nybomycin analogue **DNM-2**¹⁷⁰ in order to validate the reported mutant-selective hypothesis. This work is outlined in Section 3.1.2 and describes the efforts to repeat the literature routes and where these routes encountered synthetic challenges, how these challenges were circumvented and routes were re-designed to successfully synthesise the best literature analogue **DNM-2**. With **DNM-2** in hand, profiling could then be carried out to test the effectiveness against FQS and FQR bacteria to confirm the literature reported mutant-selective phenotype. An aim here was to take a deeper look into the enzymatic targets of the series in order to identify the primary biological target; gyrase or topo IV, as well as investigating how efflux effects the ability of the series to inhibit *E. Coli*.

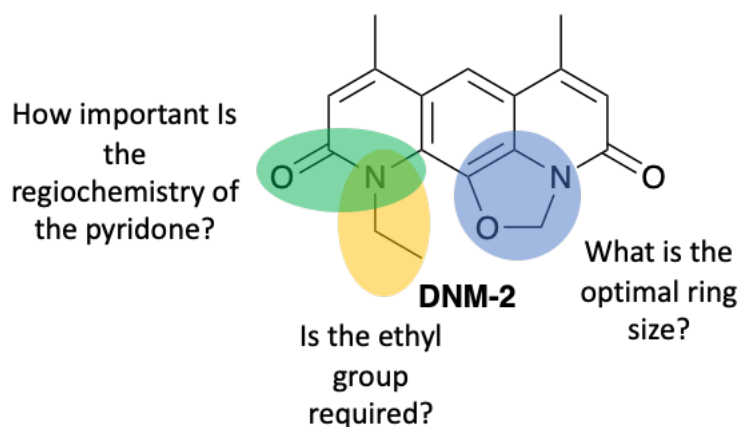


Figure 20 – Summary of the initial SAR explorations.

Once the reverse antibiotic premise had been confirmed, the aim of this project was to then design and synthesise novel Nybomycin derivatives to explore and expand the SAR of the series. Expansion of the 5-membered ring was planned to investigate the optimal ring size; the importance of the ethyl group was to be interrogated by planned synthesis of the des-ethyl

and the regio chemistry of the pyridone was to be evaluated. These initial SAR explorations are summarised in Figure 20.

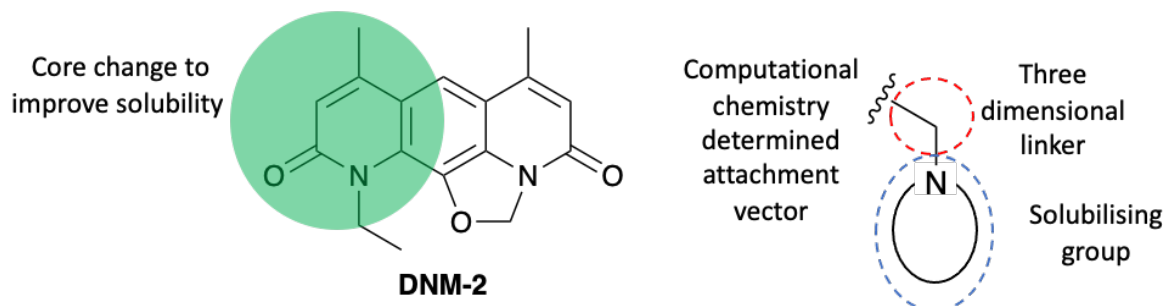


Figure 21 – Plans to increase aqueous solubility of the series.

The overall aim of this work was to explore whether the Nybomycin series of natural products could be turned into a drug. One of the reported liabilities of these compounds was extremely poor aqueous solubility and this would need to be addressed in order to progress this class further. With this in mind, an aim of this project was to design and synthesise novel analogues with much improved aqueous solubility which retained activity and the mutant-selective phenotype. It was thought that introducing polar amines and increasing the three-dimensionality of the series would have the desired effect on aqueous solubility. It was intended to use computational design in order to identify a vector in which to introduce these solubilising groups. This is outlined in Section 3.2.1 and exploration of the chemical synthesis is shown in Section 3.2.2. Diversification of the core was also planned as a more dramatic change to the original Nybomycin to investigate the importance of the electronics of the core system and potentially offer a more soluble starting point. The strategies to improve aqueous solubility are summarised in Figure 21.

3. Results and Discussion

3.1 Confirming the Mutant Selective Phenotype

3.1.2 Synthesis

3.1.2.1 Synthetic plan

As previously discussed in the introduction, **DNM-2**, shown in Figure 18, looked the most promising analogue from the Nybomycin family and so was selected as an initial target for synthesis and biological investigation. A review of the literature revealed three approaches to the synthesis of Deoxynybomycin (and therefore **DNM-2**), shown in Figure 21. They were all relatively low yielding with route 1 reported by Rinehart and Forbis in 1973 giving an overall yield of 0.84 %, ^{172,181} route 2 reported by Nussbaum and co-workers in 2009 giving an overall yield of 13 %¹⁸² and finally, route 3 reported by Hergenrother and co-workers in 2015 giving an overall yield of 11 %.^{170,183,184} Route 1 ignored the symmetrical nature of the molecule and constructed each side sequentially. This, and a few problematic steps, resulted in the lowest overall yield and highest number of linear steps. Routes 2 and 3 used the symmetrical nature of the molecule to reduce the number of linear steps and increase the overall yield. Therefore, these routes were used as starting points for the synthetic exploration of this work.

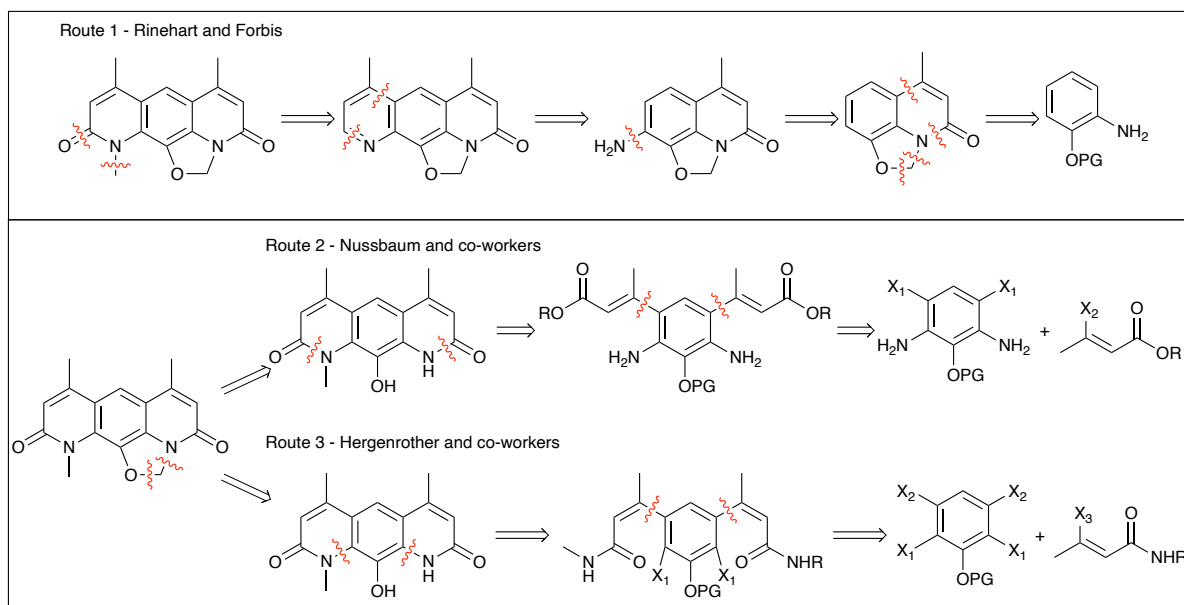
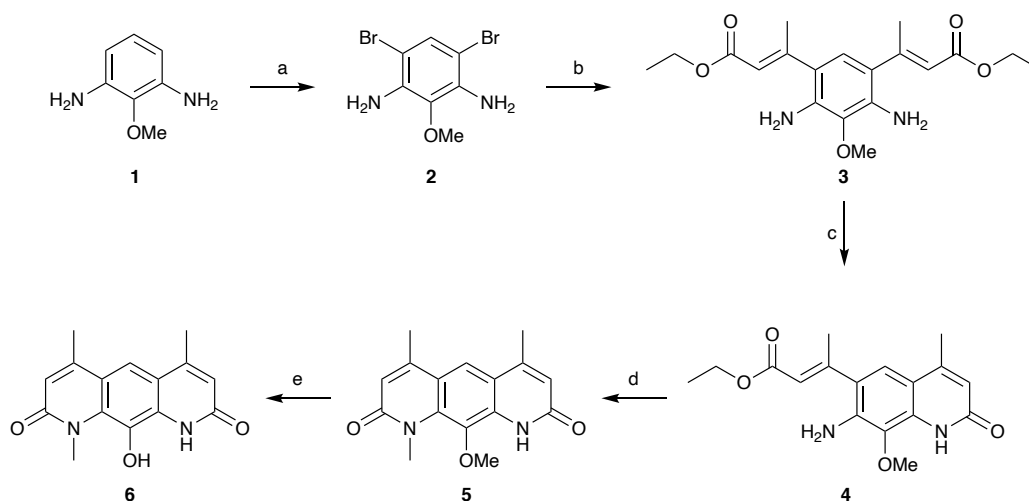


Figure 21 – Key retrosynthetic steps from the literature synthesis of Deoxynybomycin. Route 1 reported by Rinehart and Forbis in 1973.^{172,181} Route 2 reported by Nussbaum and co-workers in 2009.¹⁸² Route 3 reported by Hergenrother and co-workers in 2015.^{170,183,184} Figure adapted from Bardell-Cox *et al.*¹⁶⁹

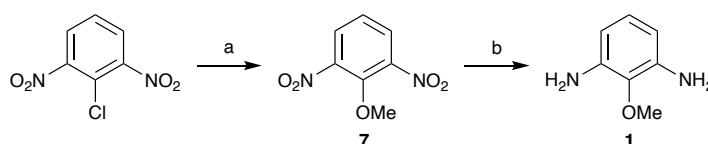
3.1.2.2 Route 2 – Nussbaum

The forward synthesis carried out by Nussbaum and co-workers is shown in Scheme 1. They took 2,6-diaminoanisole (**1**) and installed two bromine groups, in the *ortho/para* positions relative to the anilines, to give **2** in a good yield (69 %). These bromine atoms were then used for the installation of the alkene esters *via* a heck cross coupling to give **3** in a modest yield (27 %). Mono cyclisation was achieved in an excellent yield (95 %) under mildly acidic conditions using acetic acid to give **4**. Then methylation and the second cyclisation were achieved using methyl iodide and sodium hydride to give **5** in an acceptable yield (47 %). Then anisole **5** was de-methylated using hydrogen bromide to give **6** in a good yield (81 %). **6** could then be cyclised using dibromomethane to give Deoxynybomycin under the same conditions as Rinehart and co-workers.¹⁷²



Scheme 1 – Reported synthesis of 6 carried out by Nussbaum and co-workers. (a) NBS, NEt_3 , DCM, rt, 5 h, 69 %, (b) Ethyl crotonate, $\text{Pd}(\text{OAc})_2$, tri(*o*-tolyl) phosphine, NEt_3 , DMF, 110 °C, 12 h, 27 %, (c) Acetic acid, 45 °C, 4 h, 95 %, (d) MeI, NaH (60 % in mineral oil), DMF, rt, 2 h, 47 %, (e) i) HBr (aq., 48 %), 140 °C, 2 – 5 h, ii) NEt_3 , 81 %.

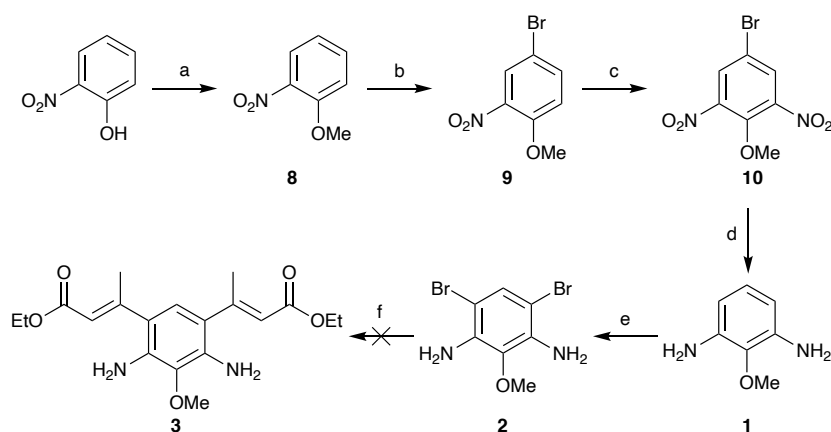
Nussbaum and co-workers used 2,6-diaminoanisole (**1**) as a starting material. It is commercially available but sales are regulated as it is an explosive precursor and its price was prohibitive. Hence a synthetic route was identified, shown in Scheme 2.



Scheme 2 – Synthesis of 2,6-diaminoanisole (1). (a) NaOMe, MeOH, rt, 18 h, 96 %, (b) Pd/C (10 %), H_2 , CH_2Cl_2 , MeOH, rt, 24 h, quantitative yield.

The planned route was envisaged to occur from 2-chloro-1,3-dinitrobenzene *via* a nucleophilic aromatic substitution ($\text{S}_{\text{N}}\text{Ar}$), followed by a reduction of the two nitro functional groups, shown in Scheme 2. The $\text{S}_{\text{N}}\text{Ar}$ with sodium methoxide proceeded well but the subsequent reduction caused problems. The first attempt at the di-nitro reduction used sodium dithionite, as this is a mild reagent with the simplest isolation protocols (precipitation with water). This is of particular importance due to the large scale this reaction would need

to be conducted on to facilitate the development of the series and the benefits of avoiding large quantities of iron or tin. Large quantities of iron can lead to difficulties in isolation and large quantities of tin are undesirable due to its toxicity. Sodium dithionite failed however and returned the unreacted di-nitro starting material **7**. After exploration, clean and quantitative conversion was achieved using hydrogenation conditions (10 % palladium on carbon and hydrogen) to yield the desired diaminoanisole **1**. However, although acceptable on the small scale, the cost of the starting material (2-chloro-1,3-dinitrobenzene) would again be prohibitive on the desired larger scales. This route was used to trial further downstream reaction conditions, but an alternative route to key intermediate **1** needed to be identified for the large-scale production of **DNM-2**. The next route shown in Scheme 3, utilises the very cheap 2-nitrophenol (~£ 0.2 per gram) as the starting material.



Scheme 3 – Alternative route to 2,6-diaminoanisole (1) and failed progression to intermediate 3. (a) NaH (60 %), MeI, DMF, 0 °C to rt, 3 days, 99 %, (b) Br₂, AcOH, 60 °C, 5 h, 96 %, (c) Triflic acid, HNO₃, CH₂Cl₂, 0 °C to rt, 5 h, quantitative yield, (d) Pd(OH)₂/C (10 %), MeOH, H₂, rt, 6 h, quantitative yield, (e) NBS, NEt₃, CH₂Cl₂, rt, 6 h, 91 %, (f) Ethyl crotonate, Pd(OAc)₂, P(*o*-tol)₃, NEt₃, DMF, 110 °C, 18 h or ethyl crotonate, Pd(dppf)Cl₂, NEt₃, acetonitrile, 85 °C, 18 h.

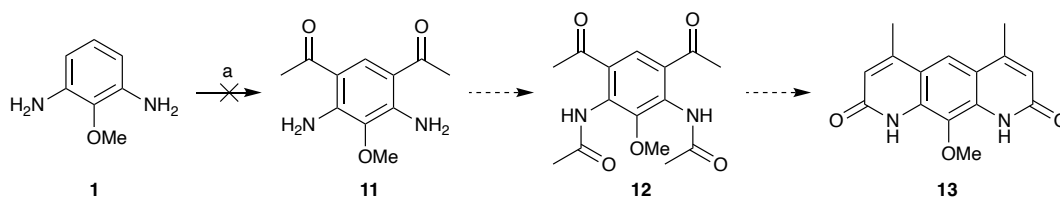
The first step was to methylate the phenol and was achieved using sodium hydride as a base and methyl iodide as the methylating agent. Attempts were trialed using a weaker base

(potassium carbonate), but resulted in worse conversion than the formal deprotonation conditions hence sodium hydride was used. The next step was a *para*-selective electrophilic bromination in order to block the *para*-position to avoid potential regiochemical issues with the subsequent nitration step. This approach was decided after a review of the literature seemed to suggest it was simpler and more efficient to perform a regioselective bromination rather than a regioselective nitration in this instance. Bromine was chosen as a suitable group for this purpose as it could be removed later in the synthesis under the same conditions as the nitro reduction, so this approach would only result in one additional step. Compound **9** was successfully formed by the desired regiospecific *para*-bromination using bromine in acetic acid with no detectable formation of the *ortho*-isomer. The next step was to install the second nitro functional group on the final electron rich position of the ring, giving compound **10**. The regiochemistry of the nitration could be fairly well predicted as the methoxy group is activating at the *ortho*-position and the nitro group is deactivating for the other two available positions (*meta* with regards to the methoxy). However, this step proved to be problematic with degradation being the main by-product under the standard nitration conditions (nitric acid/ sulfuric acid). This outcome could be explained as the system is both relatively electron poor and sterically hindered. Both these features are undesirable for electrophilic aromatic substitution and therefore result in degradation occurring faster than the desired reaction. After optimisation was attempted, conditions were found that resulted in clean and efficient conversion using nitronium trifluoromethanesulfonate (99 % yield).¹⁸⁵ The formation of diaminoanisole **1** required a global reduction, converting both nitro groups into amines and the removal of the bromine blocking group. This was envisaged in one step using the palladium-based hydrogenation conditions trialled previously, as many examples of these transformations are reported in the literature.^{186,187} However, this step proved very

problematic. Standard hydrogenations conditions using 10 % palladium on carbon and hydrogen caused reduction, but no de-halogenation. Attempts to increase the pressure or reaction time only caused degradation with no observable desired product. After trialling alternative conditions, Pearlman's catalyst (palladium hydroxide on carbon) proved to be a far superior catalyst for this reaction giving both clean reduction of the nitro groups and de-bromination in short reaction times (~2 h). It was unclear whether the equivalent of hydrogen bromide being produced in the reaction caused the degradation and this was quenched by the new catalyst, or whether a more active catalyst was required to successfully de-brominate.¹⁸⁸

Following Scheme 1, now with a large-scale route to 2,6-diaminoanisole (**1**), the next step was to di-brominate, shown in Scheme 3. This would give a synthetic handle for palladium-based cross-coupling which could in turn be cyclised to the desired Deoxynybomycin core **13**.

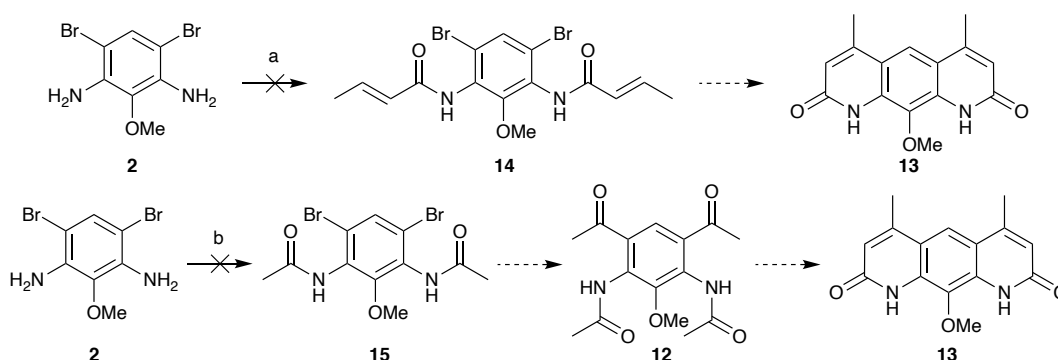
Although the bromination looked promising using the reported conditions and appeared to yield the desired product, there were major stability issues with both the starting material (2,6-diaminoanisole (**1**)) and the di-brominated product **2** that were not mentioned in the original paper.¹⁸² These stability issues likely caused the failure of the subsequent palladium-based functionalisation, shown in Scheme 3. Before abandoning this approach, a Friedel-Crafts type acylation was attempted using aluminium chloride and boron trichloride, with acetonitrile as the electrophile.¹⁸⁹ This was postulated to yield a di-imine intermediate which would then be hydrolysed upon work-up to afford the di-carbonyl **11**. From this di-carbonyl **11**, the anilines could be acetylated to give **12**, then treatment with a strong base would cause an aldol-type cyclisation to form the core of Deoxynybomycin **13**, shown in Scheme 4.



Scheme 4 – Proposed Friedel-Crafts type acylation of intermediate 8, then aldol type cyclisation.¹⁸⁹ (a) AlCl_3 , BCl_3 , acetonitrile, DCE, 80 °C, 18 h.

Unfortunately, the Friedel-Crafts type acylation failed, again thought to be due to the instability issues of the electron rich dianiline **1**.

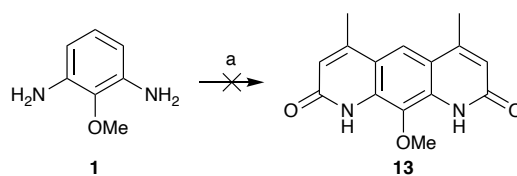
Another attempt to utilise route 2 was an amide formation on the di-bromo material **2** followed by a ring closure *via* an intramolecular Heck reaction or an aldol condensation. The amide formation on **2** was attempted with EDCI, crotonoyl chloride, crotonic anhydride, acetyl chloride and acetic anhydride, shown in Scheme 5, however none of these conditions yielded the desired amide product. These failures were again attributed to the instability of intermediate **2**.



Scheme 5 – Failed synthesis of intermediate 14 and 15 from intermediate 2 in order to trial the intramolecular Heck cross coupling and aldol-type cyclisation. For attempted reaction conditions see Appendix 7.1.1 Table 1 and 7.1.2 Table 2.

With the aim to attempt to utilise intermediate **1**, a direct formation of the Deoxynybomycin core **13** using conditions described by the Liu group; sodium persulfate, acetic anhydride, *para*-toluenesulfonic acid, ethyl crotonate and palladium(II) acetate,¹⁹⁰ shown in Scheme 6,

was attempted. This also failed, presumably due to the same stability issues observed previously.

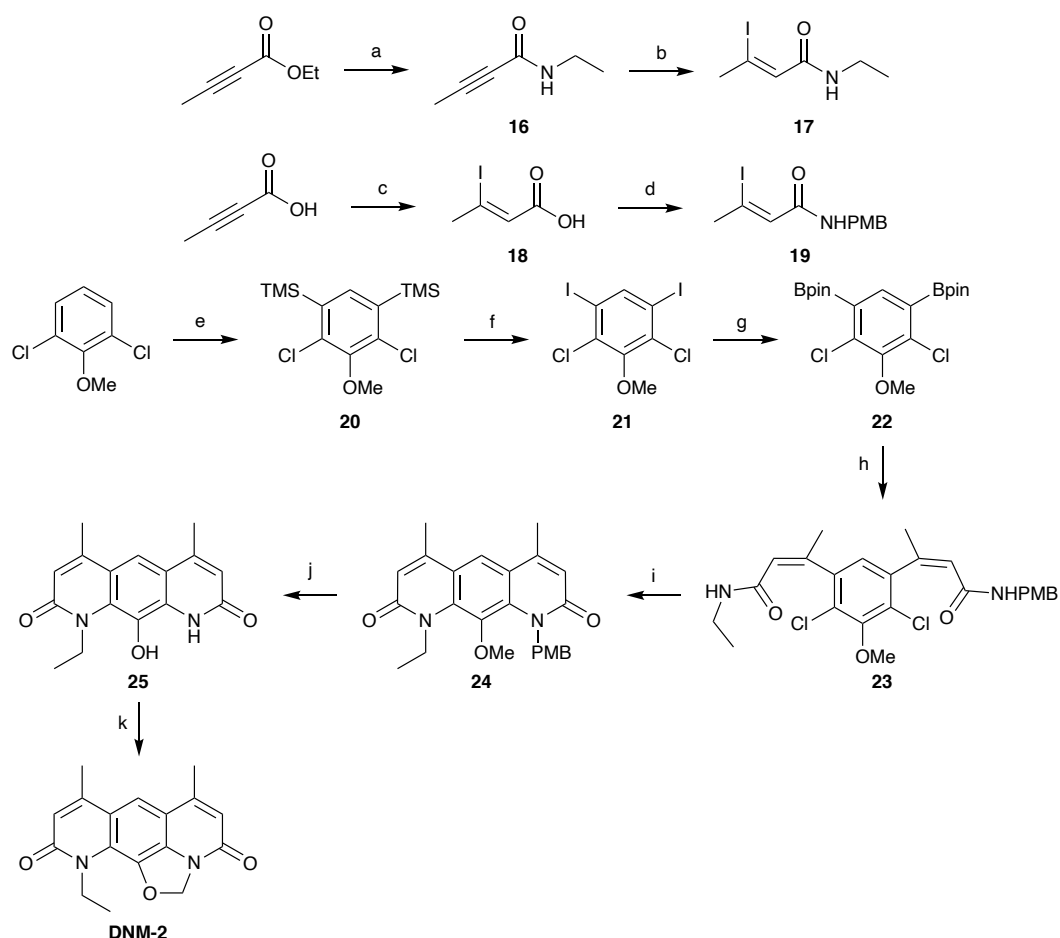


Scheme 6 – Proposed direct formation of the Deoxynybomycin core 13 from the di-aniline 1, using adapted methodology from the Liu group.¹⁹⁰ (a) Ac_2O , $\text{TsOH}\cdot\text{H}_2\text{O}$, ethyl crotonate, $\text{Na}_2\text{S}_2\text{O}_8$, $\text{Pd}(\text{OAc})_2$ toluene 100 °C, 4 h.

Methods were attempted to limit the duration of time spent handling the unstable intermediates (**1** and **2**) in hope that the rate of reaction would be faster than the rate of degradation. The 2,6-diaminoanisole (**1**) starting material was freshly made and apart from a filtration and concentration under reduced pressure, was telescoped directly into the subsequent reactions (bromination followed by cross coupling or amide formation). However, this still proved unsuccessful so route 2 was abandoned in preference of route 3, which avoided these unstable intermediates.

3.1.2.3 Route 3 – Hergenrother and Co-workers.

A summary of the retrosynthetic approach (Route 3) adopted by Hergenrother and co-workers is shown in Figure 21. This approach involved the palladium catalysed cross-coupling between two *Z*-iodo alkene amides (**17** and **19**) and a di-boronated core **22**. The product is then cyclised using Buchwald-Hartwig amination conditions, deprotected and finally the aliphatic ring is formed with dibromomethane to afford **DNM-2**. The full synthetic route carried out by Hergenrother and co-workers is shown in Scheme 7.



Scheme 7 – Literature route to DNM-2 reported by Hergenrother and co-workers.^{170,183,184}

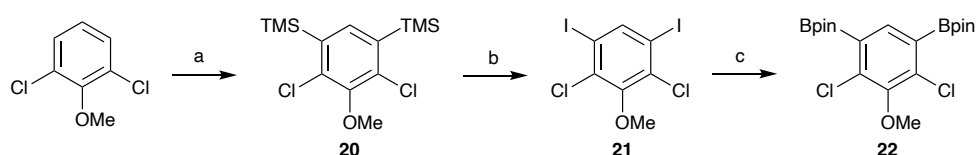
(a) EtNH₂, MeOH, 0 °C, 14 h, 83 % (b) NaI, HOAc, 110 °C, 8 h, 98 %, (c) NaI, HOAc, 110 °C, 3 h, 94 %, (d) i) (COCl)₂, CH₂Cl₂, 0 °C to rt, 5 h, ii) NH₂PMB, NEt₃, CH₂Cl₂, -78 °C to -40 °C, 2 h, 87 %, (e) LDA, TMSCl, THF, -65 °C, 14 h, 74 %, (f) ICl, CH₂Cl₂, 0 °C, quantitative, (g) PdCl₂(dppf), B₂pin₂, KOAc, DMSO, 85 °C, 19 h, 79 %, (h) **17**, **19**, PdCl₂(dppf), K₂CO₃, DME: H₂O (9:1), 80 °C, 3 h, yield not reported, (i) Pd/Xphos, Xphos, K₂CO₃, *i*-PrOH, 80 °C, 14 h, yield not reported, (j) HBr (aq., 48 %), 110 °C, 19 h, yield not reported, (k) CH₂Br₂, K₂CO₃, DMF, 85 °C, 4 h, 64 % (11 % yield over 4 steps from Bpin **22**).

The route began with the synthesis of the di-boronated intermediate **22**. As shown in Scheme 8, sequential deprotonation with lithium diisopropylamide then silylation with trimethylsilyl chloride were reproducible with comparable yields to the literature.^{183,184} This reaction formed **20** in a quantitative yield on the 100 mmol scale. Silylation was necessary instead of direct iodination because the aryl iodine has the potential to undergo a halogen dance under these reaction conditions which would lead to a mixture of the regioisomers.¹⁹¹

Direct borylation *via* a deprotonation and quench with an electrophilic boron source would also be problematic as the addition of the first boron would potentially change the regioselectivity of the second deprotonation. This would result in the 2,3-disubstituted product as opposed to the desired 2,4-product **22**.

The literature *ipso*-substitution of **20** proceeded very cleanly to give quantitative conversion to the di-iodinated material **21** when using iodine monochloride in dichloromethane.

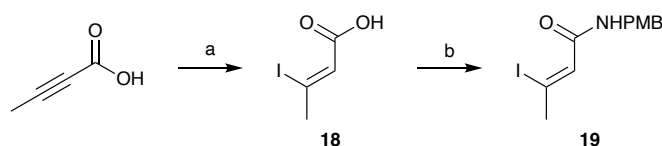
Borylation of **21** to form **22** proved challenging under the reported conditions¹⁸⁴ due to poor conversion and difficulties in isolation of the desired product. However, improvements in conversion and a quantitative isolated yield were achieved by swapping the solvent from dimethyl sulfoxide to 1,4-dioxane. Small amounts of bis(pinacolato)diboron starting material remained after both chromatography and recrystallization purification methods. However, small amounts of this reagent weren't thought to have a significantly negative effect on the subsequent Suzuki-Miyaura cross coupling as one-pot borylation Suzuki protocols are well established in the literature.^{192–195}



Scheme 8 – Synthesis of intermediate 22. a) LDA, TMSCl, THF, -78 °C, 18 h, quantitative yield, (b) ICl, CH₂Cl₂, rt, 2 h, 86 %, (c) PdCl₂(dppf), B₂pin₂, KOAc, 1,4-dioxane, 85 °C, 18 h, quantitative yield.

Next, attention was turned to synthesising the iodo amide coupling partner **19**, shown in Scheme 9. In accordance with Hergenrother and co-workers,^{183,184} this was achieved by iodination of but-2-ynoic acid with sodium iodide in acetic acid to give exclusively the *Z*-alkene

18. This was followed by an amide formation with *para*-methoxybenzylamine *via* the acyl chloride, as reported in the literature,^{183,184} to successfully afford **19**.



Scheme 9 – Literature synthesis of iodo amide coupling partner 19.¹⁸⁴ (a) NaI, HOAc, 115 °C, 5 h, 96 %, (b) i) (COCl)₂, CH₂Cl₂, 0 °C to rt, 3 h, ii) H₂NPMB, NEt₃, CH₂Cl₂, 0 °C to rt, 18 h, 74 %.

Unfortunately, the Suzuki-Miyaura cross coupling of the *Z*-iodo amide **19** with building block **22**, using the reported conditions^{183,184} that claimed a 42 % yield (over two steps from the di iodo intermediate **21**), were not reproducible, as shown in Scheme 10. A screen for alternative reaction conditions was then carried out altering the catalyst, ligand, base and solvent (for attempted reaction conditions see Appendix 7.1.3 Table 3). Regrettably, all these conditions failed to yield any of the desired coupled product **26**. A Heck cross-coupling reaction with the di-iodo core **21** and ethyl crotonate (Pd(Cl)₂dppf, NEt₃, acetonitrile, 85 °C, 18 h) also failed, although conditions for this type of cross-coupling were less extensively screened.

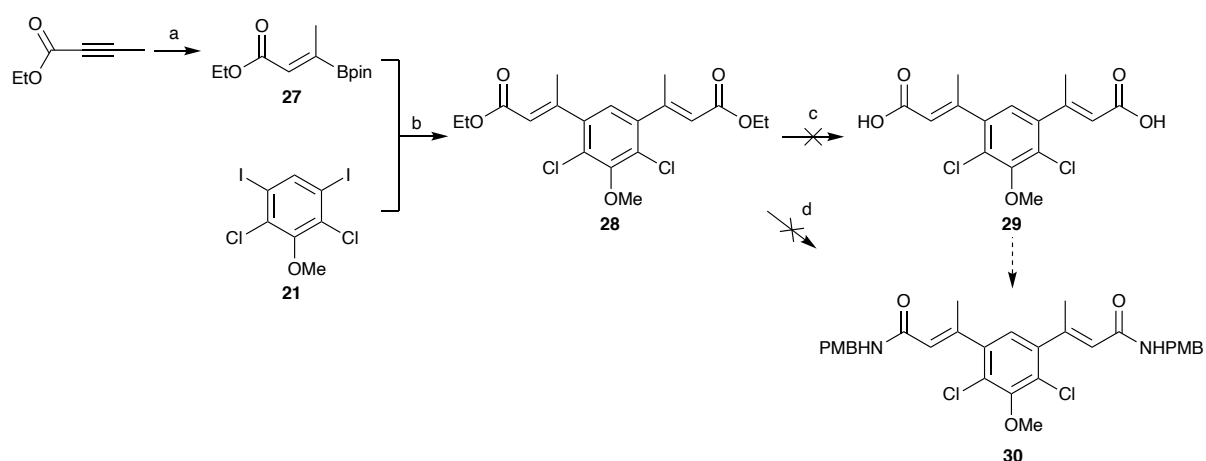


Scheme 10 – Failed reported literature coupling of 22 and 19 to form 26. For attempted reaction conditions see Appendix 7.1.3 Table 3.

As the aryl boronic ester **22** was relatively unreactive and the fact iodo alkene **19** could have base instability issues, it was proposed that a reversal of the coupling partners could be more successful.

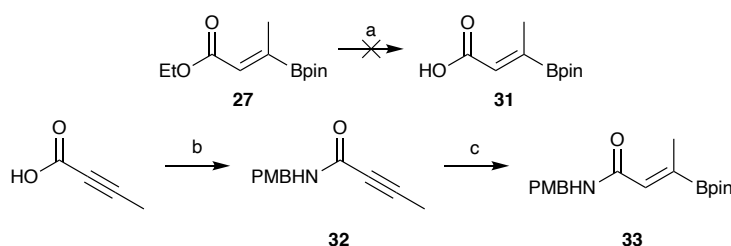
Firstly, synthesis of a borylated-alkene needed to be considered. As shown in Scheme 11, this was achieved using a method developed by Yun and co-workers which used copper(II) chloride, sodium *tert*-butoxide and bis(pinacolato)diboron.¹⁹⁶ Unfortunately this method would most likely afford the undesirable (*Z*) stereochemistry in the resulting alkene **27** as *syn*-additions would be the dominate pathway. This may cause issues when cyclisation is attempted further on in the synthesis but would be a useful 'proof-of-concept' starting material in the new cross-coupling reaction.

Gratifyingly, this reversal of the coupling partners had the desired effect. Successful coupling was achieved using the di-iodo core **21** and the borylated alkene coupling partner **27**, shown in Scheme 11. The coupling was achieved in excellent yields (90 %) to afford the di-coupled ester **28**. This result validated the reversal of the coupling partners and would facilitate the optimisation of future chemistry.



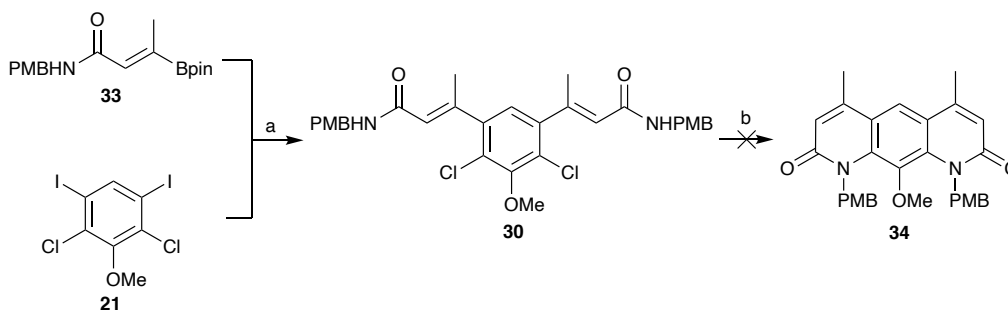
Scheme 11 – Successful cross-coupling of **27 and **21** to form **28** but failed synthesis of **29** and **30**.** (a) B₂pin₂, CuCl₂, NaO^tBu, xantphos, MeOH, THF, rt, 18 h, 77 %, (b) Pd(Cl)₂dppf, K₂CO₃, DME, H₂O, 90 °C, 3 h, 90 %, (c) For attempted reaction conditions see Appendix 7.1.4 Table 4, (d) H₂NPMB, AlMe₃, toluene 120 °C, 18 h.

The next step in this divergent route was the conversion of the ester **28** to the carboxylic acid **29** in order to form the desired amide **30** before the cyclisation could be attempted, shown in Scheme 11. However, base-mediated hydrolysis of di-ester **29** proved problematic and the desired product could not be identified, with degradation the main observed outcome. Acid-mediated hydrolysis was also attempted with similar disappointing outcomes. For details of the experimental conditions trialled please refer to Appendix 7.1.4 Table 4. Direct formation of the amide **30** from the ethyl ester **28** was attempted using a strong Lewis acid (trimethylaluminium) but also proved to be unsuccessful.



Scheme 12 – Failed hydrolysis of **27 to form **31** and successful synthesis of coupling partner **33**.** (a) LiOH (1 M), THF, rt, 18 h, (b) NH₂PMB, T3P (50 % in EtOAc), NEt₃, THF, 0 °C to rt, 18 h, 84 %, (c) B₂pin₂, CuCl₂, NaO^tBu, xantphos, MeOH, THF, rt, 18 h, 97 %.

The next strategy was to instal the amide before cross coupling to the di-iodo core **21** and so hydrolysis of the borylated alkene **27** was attempted. Unfortunately, and perhaps unsurprisingly, degradation occurred. This meant that the next step was to attempt the amide coupling before the borylation. Pleasingly, formation of **32** was achieved from but-2-ynoic acid using propylphosphonic anhydride as a coupling reagent in good yields (84 %), shown in Scheme 12. Alkyne amide **32** was then subjected to hydroboration using the aforementioned method to yield **33**.¹⁹⁷ This new coupling partner **33** was successfully reacted with the di-iodo core **21** under same conditions as before, to afford **30** in an excellent yield (80 %), shown in Scheme 13.



Scheme 13 – Synthesis of coupled amide product **30 and failed cyclisation to form intermediate **34**.** (a) Pd(Cl)₂dppf, K₂CO₃, DME, H₂O, 90 °C, 4 h, 80 %, (b) For attempted reaction conditions see Appendix 7.1.5 Table 5.

The next step was to cyclise intermediate **30** to form the Deoxynybomycin core **34**, under Buchwald-Hartwig amination conditions.^{170,184} However, using the reported conditions for this reaction, no cyclised product was observed and only starting material **30** remained. Alternative Buchwald conditions were screened; varying the catalyst, base and solvent and nucleophilic aromatic substitution (S_NAr) was also investigated (for attempted reaction conditions see Appendix 7.1.5 Table 5). None of these conditions were successful in forming the cyclised core **34** and starting material **30** was the major reaction component. A reason for the failure of both the coupling and S_NAr is most likely that the alkene amide **30** had the incorrect stereochemistry to cyclise. In deviating from the literature route and switching coupling partners to get chemistry to work, the *E* configuration of the alkene was synthesised rather than the *Z*. This was predicted as a likely problem as the *E* configuration of the alkene leads to the nitrogen of the amide being physically too far away from the aryl chloride to react, shown in Figure 22.

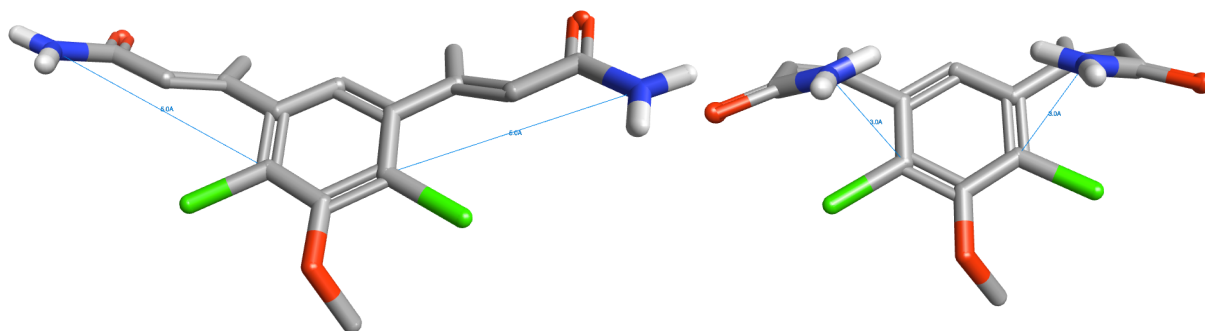


Figure 22: E/Z geometry of the double bond. 3D-conformations minimised using the conformational minimisation tool in Forge – a computational software package developed by Cresset.

It was hoped that a palladium or thermal *in situ* isomerisation of the alkene would occur under the reaction conditions and this would drive the progress of the reaction to desired product, as the small amount of alkene that isomerises would then cyclise. However, this evidentially was not the case.

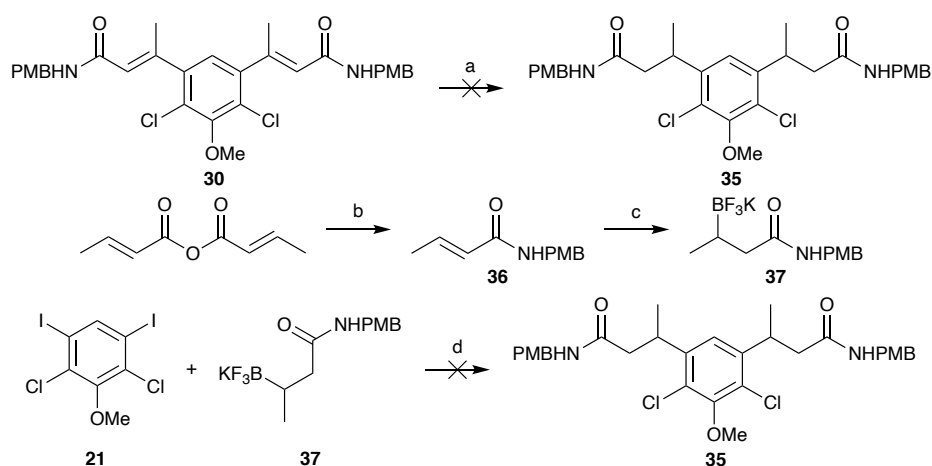
Three main strategies were hypothesised to resolve this problem:

1. Reduction from sp^2 to sp^3 carbon centre at the α and β carbons of the amide to give **35**. This would avoid the restricted rotation and give the molecule enough conformational freedom to cyclise, shown in Scheme 14.
2. Installation of the amine on the di-ester **28** then use amide formations for cyclisation, shown in Scheme 15.
3. Synthesis of the *E* boronic ester coupling partner, shown in Scheme 17. This has the pre-installed correct stereochemistry after coupling to cyclise as reported in the literature.^{183,184}

Strategy 1 - Reduction

Reduction conditions were trialled on the *E*-alkene amide **30** using hydrogen with palladium on carbon, sodium borohydride and polymethylhydrosiloxane with copper(I) chloride, for

conditions please refer to Appendix 7.1.6 Table 6. None of these conditions gave the reduced product **35** and gave either no reaction or degradation products. The next attempt was to synthesise the trifluoroborate salt **37**, shown in Scheme 14. This would allow for a sp^2 - sp^3 cross-coupling giving intermediate **35** which possesses the desired sp^3 hybridised centres. Isolation of the desired trifluoroborate salt **37** was very challenging with the best results for the isolation of the desired product obtained *via* Soxhlet extraction with methanol. Coupling this material to the di-iodinated core **21** failed and so this approach was abandoned.



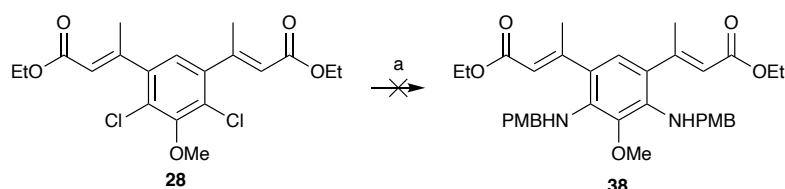
Scheme 14 – Failed reduction of **30 to form **35** but successful synthesis of coupling partner **37** from **36** and failed coupling with **21** to form **35**.**

(a) For attempted reaction conditions see Appendix 7.1.6 Table 6, (b) NH_2PMB , NEt_3 , DMF, rt, 3 h, 72 %, (c) i) B_2pin_2 , CuCl_2 , dppbz, NaO^tBu , MeOH, THF, rt, 18 h, ii) KHF_2 , MeOH, 0 °C to rt, 1 h, 92 %, (d) $\text{Pd}(\text{Cl})_2\text{dppf}$, K_2CO_3 , H_2O , DME, 90 °C, 20 h.

Strategy 2 - Cyclisation *via* Amide Formation

Goldberg coupling was attempted on ester building block **28**, using *para*-methoxybenzylamine, copper(I) iodide as the catalyst and an oxalamide ligand, shown in Scheme 15. This failed and produced no evidence of the desired product **38**. This could be due to the sterically demanding nature and/ or the relative lack of reactivity of the aryl

chloride. Further conditions could be trialled with smaller more nucleophilic ammonia surrogates, but this approach was deprioritised due to more attractive alternatives.



Scheme 15 – Attempted Goldberg coupling of di-ester **28 to form **38**.**¹⁹⁸ (a) H₂NPMB, CuI, *ortho*-oxalotoluidide, K₃PO₄, DMSO, 120 °C, 24 h.

Strategy 3- Synthesis of the *E* Boronic Ester Coupling Partner

Synthesis of the less thermodynamically favoured *E* isomer of the boronic ester coupling partner is challenging and there are very few reported methods in the literature with acceptable selectivities/ yields. Both regiochemical and stereochemical outcomes need to be considered. Classical hydroboration conditions tend towards the *anti*-Markovnikov product which would give the desired regiochemistry for the coupling partner. However, due to the *syn*-selectivity of the four-membered transition state, the stereochemistry would be incorrect to cyclise, as demonstrated above. Sawamura and co-workers have, however, reported a method of *anti*-hydroboration using a trialkyl phosphine catalyst that would result in both the desired regio- and stereochemistry in good selectivity.¹⁹⁹ Proposed mechanisms for both *syn*- and *anti*-hydroborations are outlined in Figure 23.

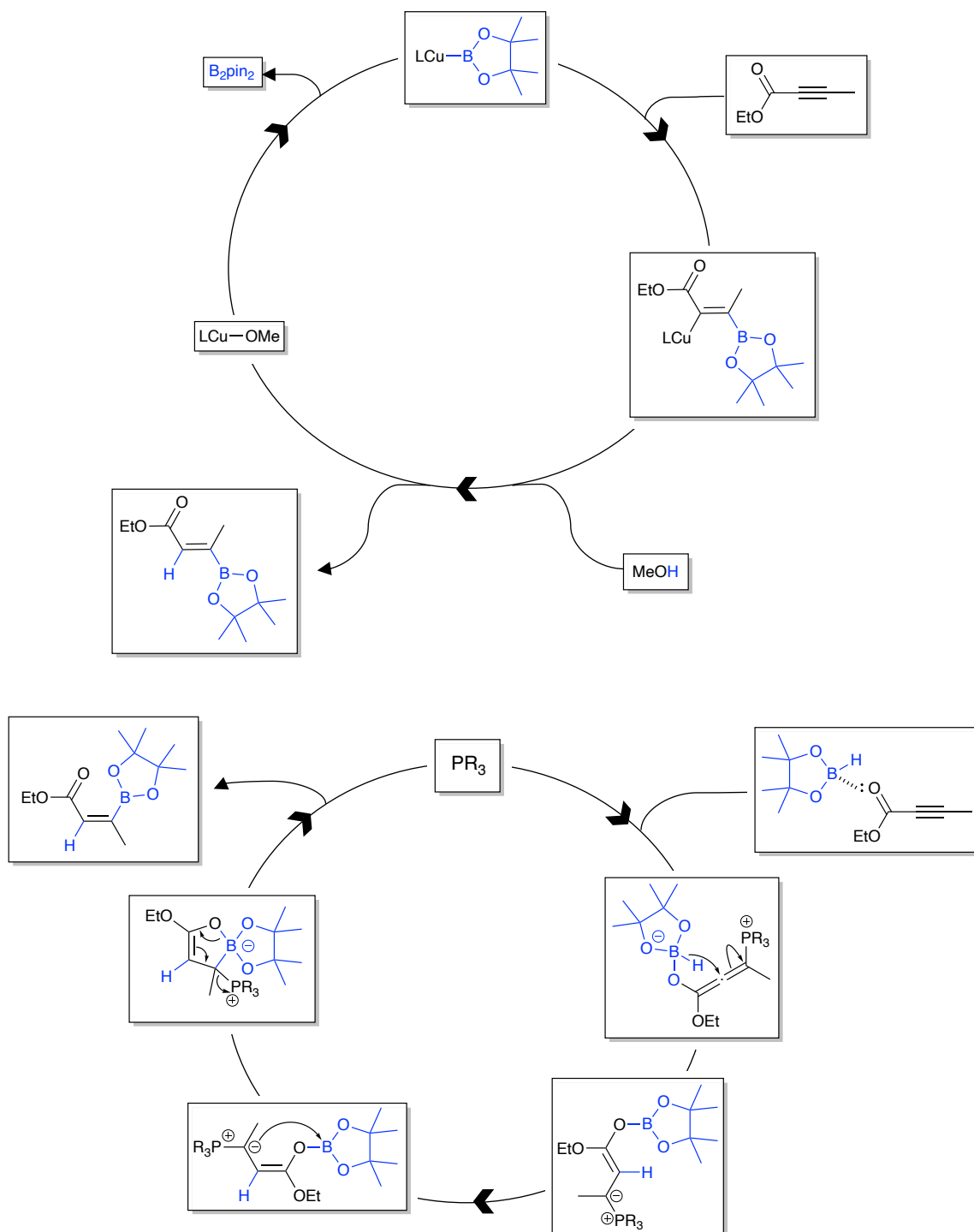
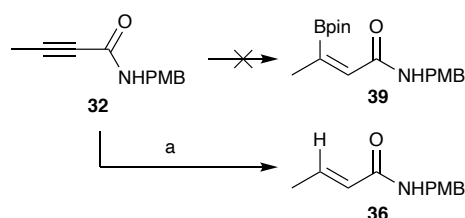


Figure 23 – Proposed mechanisms for *syn*- and *anti*-hydroboration. A – *Syn*-hydroboration mechanism proposed by Yun and co-workers,¹⁹⁶ B – *Anti*-hydroboration mechanism proposed by Sawamura and co-workers.¹⁹⁹

The approach was taken to synthesise the amide coupling partner prior to attachment to the core so the problematic hydrolysis step, shown in Scheme 11, could be avoided. Unfortunately, the reported *anti*-hydroboration chemistry wasn't compatible with the desired alkyne amide **39**. Instead of undergoing *anti*-hydroboration, either reduction or deborylation occurred to give *E*-*N*-(4-methoxybenzyl)but-2-enamide (**36**) as the major reaction product (47 % isolated yield), shown in Scheme 16. Attempts to use the methylated amide to remove the amidic NH that may have caused the side reaction, didn't yield any desired borylated material and resulted in a complex mixture of reaction products.

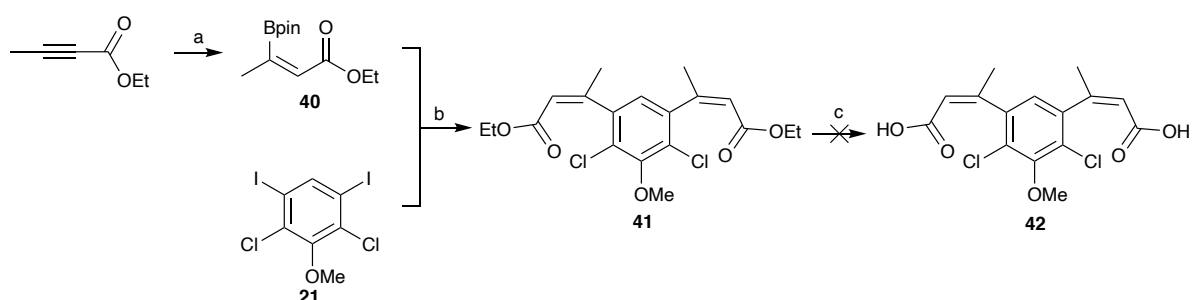


Scheme 16 – Undesired reduction of 32 to form 36 instead of hydroboration to form 39.

(a) PMe_3 (1M in toluene), HBpin, THF, 0 °C to rt, 18 h, 47 %.

Reluctantly, an ester coupling partner was returned to, shown in Scheme 17. *E*-selective *anti*-hydroboration of the ethyl but-2-ynoate was performed and gave reasonable yields (60 %) of **40** with regioselectivities of 9:1 *E*:*Z*. The assigned stereochemistry came from ^1H NMR data with a downfield shift of 0.43 ppm in the alkene proton and 0.22 ppm in the resonance of the CH of the alkene methyl group when compared to the previously synthesised *Z*-product **27**. Coupling of **40** to the di-iodo core **21** progressed with excellent yields (98 %) of intermediate **41**. Predictably, hydrolysis again proved to be problematic. Conditions were trialled using different hydroxide sources, temperatures, solvents and solvent ratios (for attempted reaction conditions see Appendix 7.1.7 Table 7). The best conditions yielded small amounts of crude di-acid product **42** but purification wasn't possible. Telescoping this mixture on to

the amide coupling using either propylphosphonic anhydride as a coupling agent or formation of the acyl chloride did not yield any of the desired bis-amide. Attempts were then made to directly convert the ester **41** to amide product **26** with the strong Lewis acid, trimethylaluminium. This also failed. The methyl ester was also synthesised using the same method shown above but suffered all the problems under the basic hydrolysis conditions that were observed with the ethyl ester.

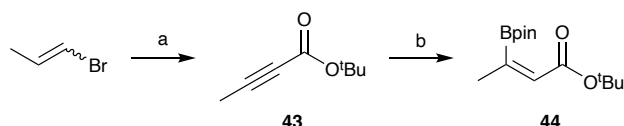


Scheme 17 – Formation of the coupling partner **40 successful coupling to form **41** but hydrolysis to form **42** failed.** (a) PMe_3 (1 M in toluene), HBpin, THF, 0 °C to rt, 3 days, 53 %, (b) $\text{Pd}(\text{Cl})_2\text{dppf}$, K_2CO_3 , DME, H_2O , 90 °C, 4 h, 98 %, (c) For attempted reaction conditions see Appendix 7.1.7 Table 7.

The next step was to find a starting material that would be compatible under the hydroboration conditions and could also be converted to the amide after it had been coupled to the core without the need for a base-mediated hydrolysis. The *tert*-butyl ester **44** was identified as a good substrate for this. It should be compatible under the hydroboration conditions but treatment with strong acids such as trifluoroacetic acid would liberate the free carboxylic acid *via* an acid-mediated *tert*-butyl cleavage. This could then be converted into the amide using standard amide coupling methodologies.

The starting *tert*-butyl alkyne **43** was synthesised *via* an elimination followed by deprotonation of 1-bromopropene with $n\text{BuLi}$, then trapping the lithiated alkyne anion

formed with di-*tert*-butyl dicarbonate. This method yielded **43** in excellent yields (98 %). Pleasingly, the hydroboration developed by Sawamura and co-workers¹⁹⁹ worked well on *tert*-butyl alkyne **43** to give the coupling partner **44** which was purified by distillation in an acceptable yield (52 %), shown in Scheme 18.



Scheme 18 – Synthesis of coupling partner 44. (a) $n\text{BuLi}$, Boc_2O , THF, $-78\text{ }^\circ\text{C}$ to rt, 18 h, 98 %, (b) PMe_3 (1 M in toluene), HBpin, THF, $0\text{ }^\circ\text{C}$ to rt, 18 h, 52 %.

Crystals of this material were grown from a mixture of pentane and diethyl ether so that X-ray crystal diffraction could be used for unequivocal structural assignment. As is evident from the X-ray structure, shown in Figure 24, the alkene is in the desired *E* configuration so after attachment to the core the geometry should be correct to undergo cyclisation.

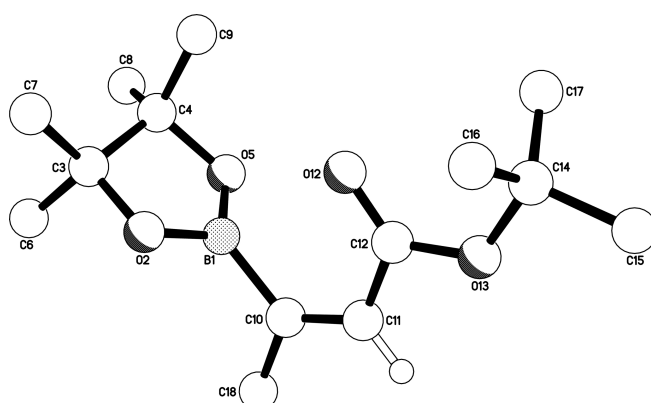
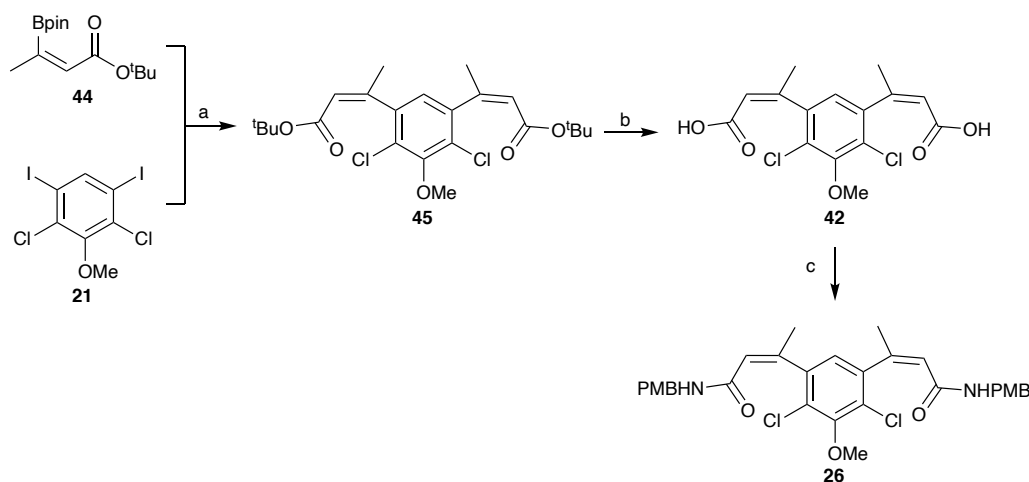


Figure 24 – X-ray crystal structure of 44, confirming the isomer as *E*. For 50% probability ellipsoids see Section 5.4.4 Figure S1.

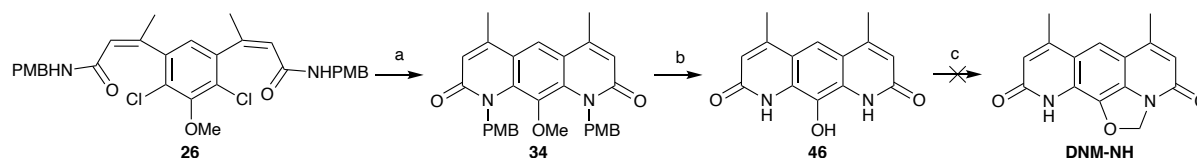
This material was coupled with the di-iodo core **21** using the previous method to afford **45** in a good yield (84 %). This method proved to be both robust and scalable to over 20 mmol. Treatment with trifluoroacetic acid at room temperature yielded the desired di-acid **42** in

excellent yields (94 %). This method avoided all the issues with the basic hydrolysis seen in the examples before. The di-acid **42** was then cleanly converted to the di-amide **26** in good yields (68 %) by first formation of the di-acyl chloride then treatment with *para*-methoxybenzylamine, shown in Scheme 19.



Scheme 19 – Successful formation of intermediate 26. (a) Pd(Cl)₂dppf, K₂CO₃, DME, H₂O, 85 °C, 18 h, 84 %, (b) TFA, CH₂Cl₂, rt, 2 h, 94 %, (c) i) (COCl)₂, CH₂Cl₂, 0 °C to rt, 4 h, ii) H₂NPMB, NEt₃, CH₂Cl₂, 0 °C to rt, 18 h, 68 %.

With key building block **26** in hand, the Deoxynybomycin core **34** could be synthesised, in an excellent yield (99 %), using a Buchwald-Hartwig amination, as used by Hergenrother and co-workers, shown in Scheme 20.^{183,184} A global deprotection with aqueous hydrobromic acid was used to remove both the *para*-methoxybenzyl protecting groups and demethylate the anisole in an excellent yield (96 %). The solubility of the resulting compound **46** was very poor and only small amounts were able to be solubilised using hot dimethyl sulfoxide. This lack of solubility is probably due to the planarity of the compound and its ability to π -stack with itself increasing the lattice enthalpy of the solid state. As an apparent result of this poor solubility, formation of the aliphatic ring for intermediate **DNM-NH** with this material failed.



Scheme 20 – Formation of the DeoxyNybomycin core 34 and failed synthesis of DNM-NH.

(a) Pd G2 xphos, xphos, K₂CO₃, *i*-PrOH, 90 °C, 18 h, 99 %, (b) HBr (aq., 48 %), 110 °C, 18 h, 96 %, (c) CH₂Br₂, K₂CO₃, DMSO, 85 °C, 18 h.

To avoid this insoluble intermediate **46**, only the *para*-methoxybenzyl protecting groups were removed. This was achieved using trifluoroacetic acid at room temperature, shown in Scheme 21. The resulting compound **13** was still poorly soluble in a range of organic solvents but did have slightly improved solubility when compared to the fully deprotected version **46**. Ethylation was achieved using iodoethane in dimethyl sulfoxide at 85 °C with potassium carbonate as the base. Analysis of the ¹³C NMR of the product and comparison with literature compounds, shown in Figure 25, with the same functionality gave evidence that the *O*-alkylated ethoxy pyridine product **47** had been formed as the major reaction product.¹⁷⁰ This was surprising as literature supported the *N*-alkylation of the pyridone as the major reaction product.^{200–202}

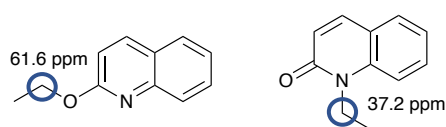
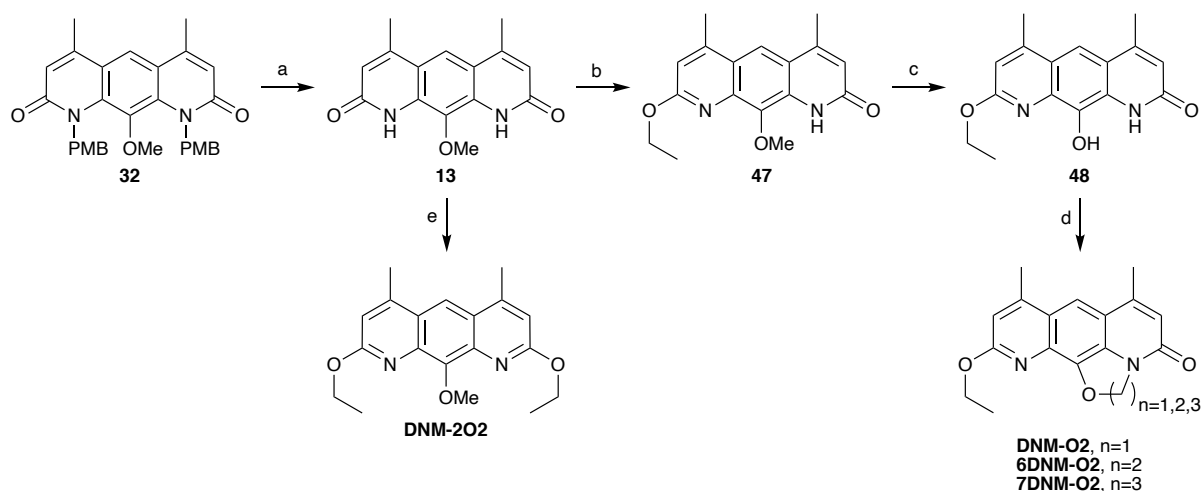


Figure 25 – Comparison of the chemical shift of the methylene carbon in ¹³C NMR. 2-Ethoxyquinoline from Ishizuka and co-workers²⁰³ and 1-ethylquinolin-2(1H)-one from Li and co-workers.²⁰⁴

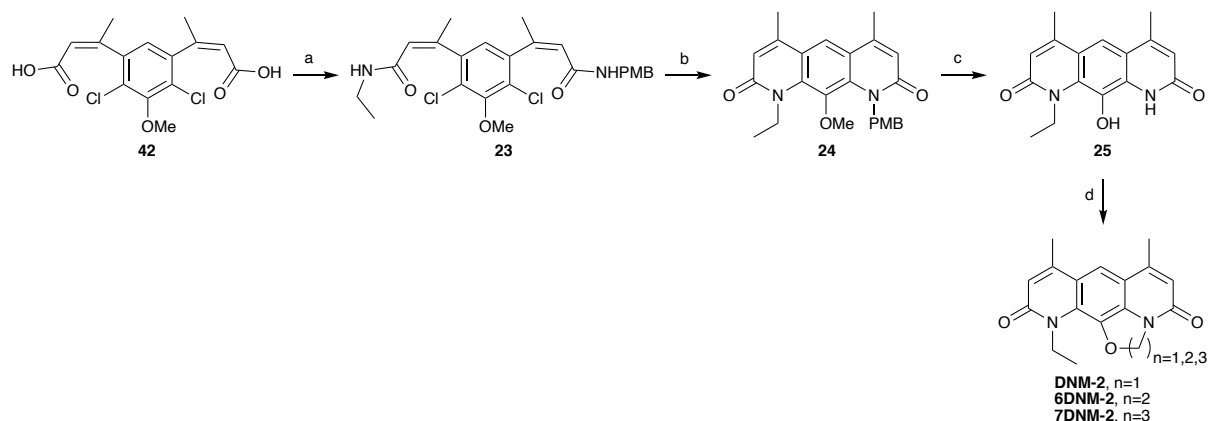
This presented an opportunity to explore a novel vector from the Nybomycin core in order to further probe the SAR of the series and possibly form new interactions with the protein. Selective demethylation of the anisole, in the presence of the ethoxy was achieved using boron tribromide to give intermediate **48**. This product was then successfully cyclised using

1,1-dibromomethane for **DNM-O2**, 1,2-dibromoethane for **6DNM-O2** and 1,3-dibromopropane for **7DNM-O2**. Intermediate **13** was also di-ethylated to yield **DNM-2O2** in order to probe the SAR further. This provided four novel analogues for microbiological evaluation.



Scheme 21 – Synthesis of the O-alkylated analogues – DNMO2, 6DNMO2, 7DNMO2 and DNMO2. (a) TFA, rt, 18 h, 98 %, (b) EtI, K₂CO₃, DMSO, 70 °C, 18 h, 59 %, (c) BBr₃ (1 M in CH₂Cl₂), CH₂Cl₂, 0 °C to rt, 18 h, 41 %, (d) CH₂Br₂, K₂CO₃, DMSO, 85 °C, 18 h, 14% for **DNM-O2**, BrCH₂CH₂Br, K₂CO₃, DMSO, 85 °C, 18 h, 13% for **6DNM-O2**, BrCH₂CH₂CH₂Br, K₂CO₃, DMF, 110 °C, 18 h, 18% for **7DNM-O2** (e) EtI, K₂CO₃, DMSO, 70 °C, 18 h, 40 %, 18% for **DNM-2O2**

After the successful synthesis of these novel analogues, attention was returned to how the O-alkylation could be avoided in preference for the N-alkylation. Due to the insolubility of intermediate **13**, options were limited in terms of how to affect the product distribution of this alkylation. Instead, a different approach was trialed using the unsymmetrical amide **23**. This was formed from the di-acid **42** and a 1: 1 mixture of ethylamine and *para*-methoxybenzylamine, shown in Scheme 22.



Scheme 22 – Synthesis of the *N*-alkylated analogues – DNM-2, 6DNM-2, 7DNM-2. (a) (i) $(\text{COCl})_2$, rt, 4 h, (ii) NH_2Et , NH_2PMB , NEt_3 , CH_2Cl_2 , rt, 18 h, 42 %, (b) Pd G2 Xphos, Xphos, K_2CO_3 , *i*-PrOH, 85 °C, 18 h, 85 %, (c) HBr, 110 °C, 18 h, 91 %, (d) CH_2Br_2 , K_2CO_3 , DMSO, 85 °C, 18 h, 33 % for **DNM-2**, $\text{BrCH}_2\text{CH}_2\text{Br}$, K_2CO_3 , DMSO, 110 °C, 18 h, 28 % for **6DNM-2**, $\text{BrCH}_2\text{CH}_2\text{CH}_2\text{Br}$, K_2CO_3 , DMF, 110 °C, 18 h, 44 % for **7DNM-2**.

This method yielded the statistical mixture of the amide products and these were separated by column chromatography with the desired amide **23** isolated in an acceptable yield (42 %). The undesired bis-PMB amide **26** could be recycled for the synthesis of the ethoxy-pyridines above. The other undesired bis-ethyl amide by-product **49** was recrystallised from dichloromethane and analysed by X-ray diffraction to prove that the *Z* double bond geometry had been maintained, shown in Figure 26.

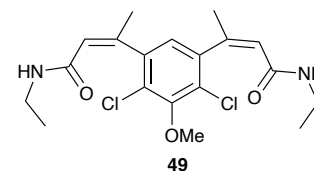
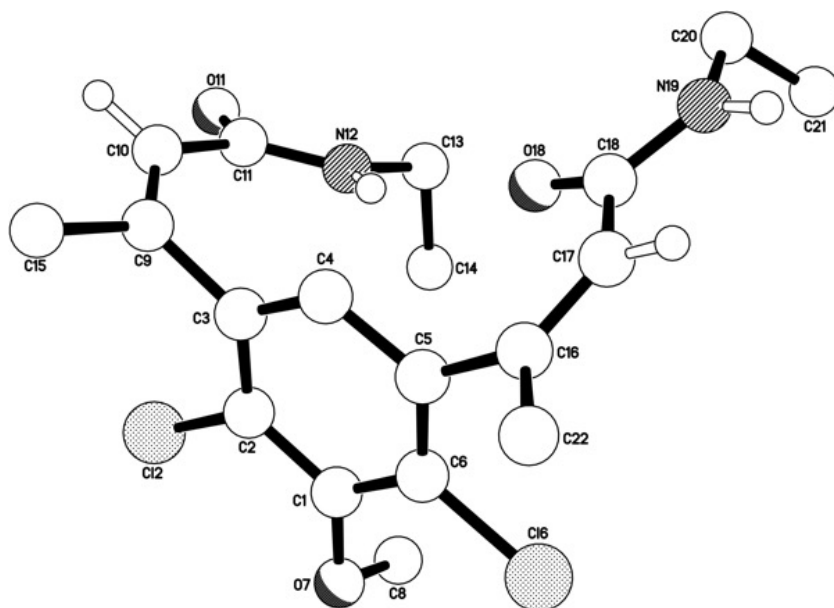
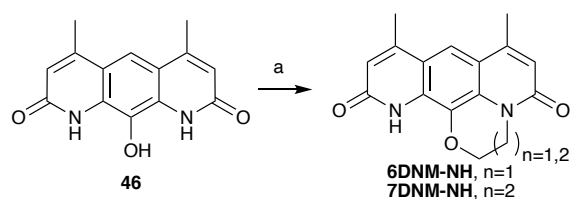


Figure 26 - X-ray crystal structure of 49, confirming the double bond geometry is maintained as *Z*. Confirmed the retention of double bond stereochemistry and showed that the compound now has the correct geometry to cyclise.

The unsymmetrical amide **23** was cyclised under the previously used Buchwald-Hartwig amination conditions to afford intermediate **24** in an excellent yield (85 %). Global deprotection using aqueous hydrobromic acid at reflux and isolation *via* precipitation with water afforded **25** in an excellent yield (91 %). Intermediate **25** was then cyclised using 1,1-dibromomethane to successfully form **DNM-2**. This key tool compound was isolated in 8 steps and could be synthesised robustly and on scale. As well as isolating **DNM-2**, two further analogues were synthesised by cyclising **25** with 1,2- dibromoethane for **6DNM-2** and 1,3-dibromopropane for **7DNM-2**.

In order to further explore the SAR, **6DNM-NH** and **7DNM-NH** were selected for synthesis, shown in Scheme 23. This was achieved using the cyclisation conditions previously used for the aliphatic ring formation, shown in Scheme 21 and 22. A potential explanation for the successful synthesis of the 6 and 7-membered rings where the 5-membered failed, could be the solubility of the intermediate formed after the first addition. Some evidence for this could

be the observation that the yield increases with increasing ring size (13 % for **6DNM-NH** vs 67 % for **7DNM-NH**). These compounds would provide a good opportunity for match pair analysis with **6DNM-2**, **7DNM-2**, **6DNM-O2** and **7DNM-O2** in order to thoroughly investigate the presence and position of the ethyl group on the pyridone ring. The 9 Nybomycin analogues successfully synthesised are shown in Figure 27.



Scheme 23 – Synthesis of the NH derivatives. (a) $\text{BrCH}_2\text{CH}_2\text{Br}$, K_2CO_3 , DMF, 110°C , 18 h, 13 % for **6DNM-NH**, $\text{BrCH}_2\text{CH}_2\text{CH}_2\text{Br}$, K_2CO_3 , DMF, 110°C , 18 h, 67 % for **7DNM-NH**.

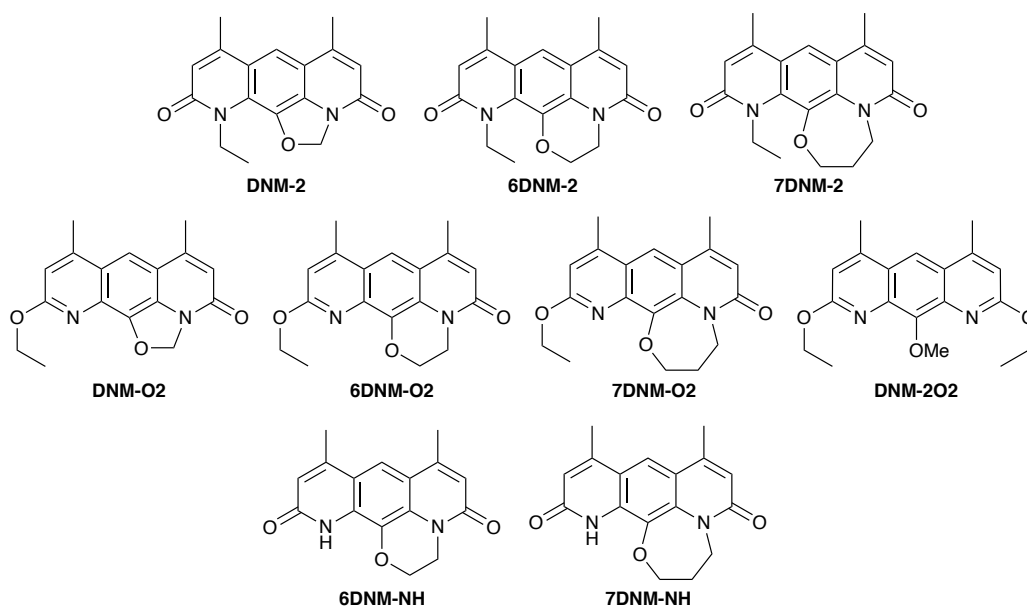


Figure 27 – Analogues successfully synthesised for microbiological evaluation.

3.1.3 Microbiology - Kirby-Bauer Disc Diffusion Assay

3.1.3.1 New DNM Analogues

With the key tool compound **DNM-2** and these novel analogues in hand (shown in Figure 27) the next step was to investigate their antibacterial activity and test the mutant selective hypothesis described in the literature.^{2,170} The Kirby-Bauer disc diffusion assay²⁰⁵ using the protocol described by Sridhar and co-workers²⁰⁶ was used. The zone of inhibition assay, shown in Figure 28, is a simple and rapid method for measuring antibiotic activity. An antibiotic of a known concentration is absorbed onto a disc, dried, and placed on an agar plate inoculated with a bacterial strain. The area around the disc where the bacteria can't grow due to antibiotic action is known as the zone of inhibition. The larger the zone of inhibition the more active the antibiotic is against that particular strain as antibiotic concentration decreases further from the disc.

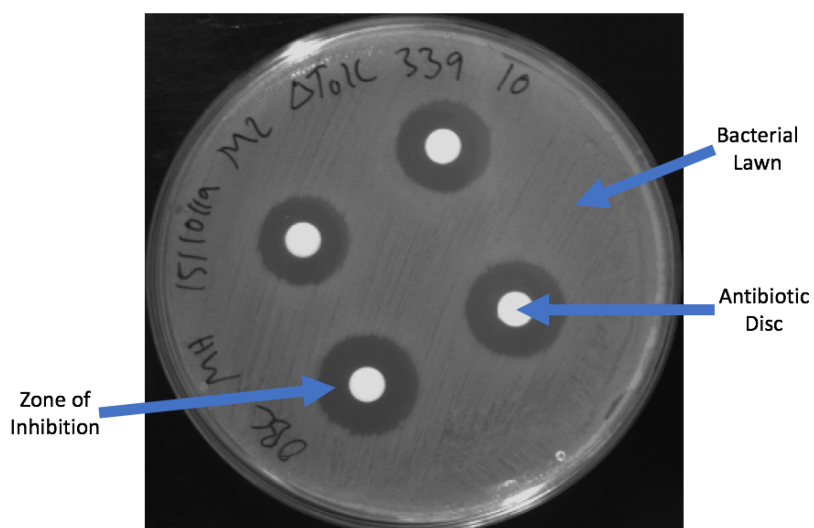


Figure 28 – Kirby-Bauer disc diffusion assay to measure the Zone of inhibition. The white circles are the discs containing the antibiotic, the light grey is the bacterial lawn and the dark circles around the antibiotic discs is the zone of inhibition. As antibiotic concentration decreases further from the disc, the larger the zone of inhibition the lower the concentration of antibiotic needed to stop the growth of bacteria and therefore the more active the antibiotic is.

In order to corroborate the reported mutant selective phenotype in the literature;^{2,170} in-house *S. aureus* strains SH1000 (fluoroquinolone sensitive (FQS) wild-type) and USA300 JE2 (FQR mutant) were chosen as model strains. The USA300 JE2 *S. aureus* strain was selected as the mutant strain as it possesses the GyrA S84L and ParC S80Y (*S. aureus* numbering) mutations that confer FQR and it also contains additional mutations that are responsible for resistance to other classes of antibiotics.²⁰⁷

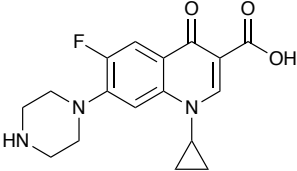
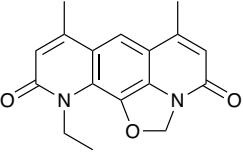
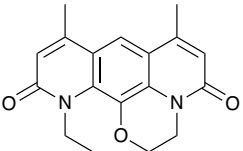
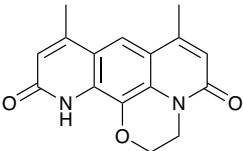
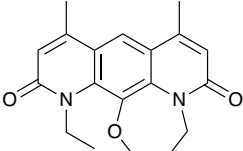
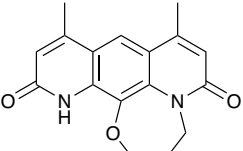
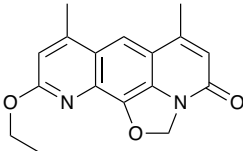
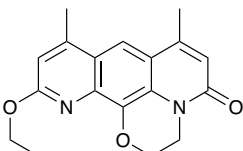
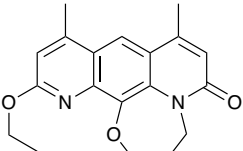
The results from this analysis are displayed in Table 1. As expected, Ciprofloxacin showed strong activity against the FQS strain (SH1000) and a marked decrease in activity against the FQR strain (USA300 JE2). Gratifyingly, **DNM-2** showed the reported mutant-selective phenotype in agreement with the literature.¹⁷⁰ This was a significant result for the project as there had been some speculation of the validity of this reported phenotype. Pleasingly, the novel ring expanded analogues (**6DNM-2** and **7DNM-2**) maintained the mutant-selective phenotype with **6DNM-2** (the 6-membered ring) cautiously showing the greatest activity against the FQR strain. This result would need to be confirmed by more precise susceptibility methods. The *N*-ethyl group appears important for activity as there is a marked decrease in activity when it's removed (**6DNM-2** vs **6DNM-NH** and **7DNM-2** vs **7DNM-NH**). This could indicate that the ethyl group is:

- Filling a hydrophobic pocket in the protein causing an increase in activity.
- Inducing a conformational change in the molecule that is important for activity
- Important for the solubility of the molecule.

However, this may also be explained by the fact that hydrogen bond donors (pyridonic NH) in this position are not tolerated.

The *O*-alkylated regioisomers (**DNM-O2** and **7DNM-O2**) showed no activity against either the FQS or FQR strains, apart from compound **6DNM-O2** that showed weak inhibition against the

FQR strain. Compound **DNM-02** was tested at elevated concentrations and still showed no inhibition of either the FQS or FQR strains at 32 mmol. This is a huge decrease in activity compared to the *N*-ethylated versions and shows the importance of the regiochemistry of the pyridone in this series. Molecular modelling/docking was used to explore the effect of regiochemistry of the pyridone but failed to rationalise the difference in activity. It is important to state that from this assay it is unclear whether the lack of activity in these analogues is due to a lack of target affinity or inability for the compound to access the target, whether that is due to a lack of permeability, solubility or a substrate for efflux. The symmetrical *O*-diethyl compound **DNM-202** showed no activity and appeared to degrade overtime. An intermediate in the synthesis, bis-PMB compound **34**, was tested and showed no inhibition on either strain, suggesting that the steric environment around the pyridone is important, in agreement with the literature of the more bulky alkyl substituents.¹⁷⁰

Compound	Structure	Zone of Inhibition (cm)			
		FQS		FQR	
		1 mmol	10 mmol	1 mmol	10 mmol
Ciprofloxacin		1.8	3.1	0	1.2
DNM-2		0	1.8	1.4	2.9
6DNM-2		0	2.2	1.8	3.2
6DNM-NH		0	1.1	0	2.0
7DNM-2		0	2.3	0	2.7
7DNM-NH		0	0	0	2.0
DNM-O2		0	0	0	0
6DNM-O2		0	0	0	1.0
7DNM-O2		0	0	0	0

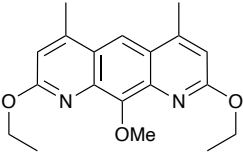
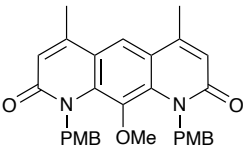
DNM-202		0	0	0	0
34		0	0	0	0

Table 1 - Zone of inhibitions (in cm) of known compounds Ciprofloxacin and DNМ-2 and novel analogues 6DNМ-2, 6DNМ-NH, 7DNМ-2, 7DNМ-NH, DNМ-O2, 6DNМ-O2, 7DNМ-O2, DNМ-202 and 34 SH1000 was used as the FQS strain and USA300 JE2 was used as the FQR strain. Compounds were tested at 1 and 10 mmol using the Kirby–Bauer disc diffusion assay with 7 replicates.

3.1.4 Gene Editing in *E. coli*

The next step was to look in more detail about how different mutation states in gyrase/ topo IV effected the antibacterial activity of the series. This was achieved by comparing the activity of the Nybomycin derivatives against the collection of in-house *E. coli* mutants shown in Table 2. These strains were *E. coli* with *S. typhi* gyrase and topoisomerase IV genes, with the desired mutations shown in Table 2, integrated into the genome, replacing the endogenous *E. coli* homologues. These strains are ideal to make comparisons to determine the effect that different mutation states in the topoisomerase enzymes have on antibiotic activity because they are exact genetic clones of each other only varying in the position of interest. This is important as it removes some of the variables common in whole cell assays using bacteria, such as influx, efflux and alterations to other enzymes. This means that any changes in antibiotic activity can be directly attributed to the change in the target gene and not an effect of differences elsewhere in the bacterium.

<i>E. coli</i> Strain	Mutation
M	BW25113 – Wild type original
M0	Wild type optimised
M1	GyrA S83F
M2	GyrA S83A
M3	GyrA S83F D87N
M4	GyrA D87N
M5	ParC S80I
M6	GyrA S83F D87N ParC S80I

Table 2 – Mutations in the in-house *E. coli* strains. These strains are genetically identical but have had their gyrase/ topo IV replaces with an *S. typhi* variant with the described mutation.

Ideally this work would have been done using a Gram-positive strain since it is a lot easier to get to the site of action compared to a Gram-negative strain like *E. coli*. However the protocols to undergo the desired genetic mutations were optimised for *E. coli* hence more easily accessible. Another advantage for using *E. coli* is it is considered less of a bio-safety risk. The Kirby–Bauer disc diffusion assay was used with 7 replicates and the change in zone of inhibition was compared. Firstly, Amoxicillin (an antibiotic with an orthogonal mechanism of action) was used as a positive control and showed no change in the zone of inhibition on all the in-house *E. coli* strains, shown in Appendix 7.2.1. This confirmed that there was no intrinsic difference in susceptibility of the strains across the collection. Next, several commercial fluoroquinolone antibiotics (Ciprofloxacin, Levofloxacin, Norfloxacin and Moxifloxacin) were tested against the wild-type (WT) strain (M0) and the most resistant mutant strain (M6). They showed the expected strong inhibition against the WT (M0) and weak or no inhibition against the triple mutant (M6). This was expected and confirmed that the changes in activity are due to the mutations in gyrase/ topo IV. This gave good evidence

for the use of these strains to confirm the mutant selective hypothesis of the Nybomycin family. Next, the tool compound **DNM-2** was tested against the panel of strains but no activity was observed on either the wild-type (M0) or the triple mutant (M6). This result contradicted the earlier reports of activity of the Nybomycin family against *E. coli*,^{171,174} but was in agreement with the most recent studies which suggested insufficient concentrations of the Nybomycins were reaching the target.^{2,170} The structure of the antibiotic could be altered to gain entry into Gram-negative bacteria using approaches akin to Hergenrother and co-workers, adding a small charged amine, as the structure already met the rigidity and shape criteria.⁸¹ However, for this study this approach wasn't appropriate as this structural change may result in a change in binding that may compromise the results. Another option could be to co-administer a membrane potentiator with the Nybomycin analogue. This has been shown to be an effective strategy in multiple studies with other antibiotics.²⁰⁸⁻²¹¹ However again this approach was not appropriate for this study as having a second compound may increase the difficulty in deconvoluting the data. Another approach that could be explored was permeabilising the bacterial strains. This has the benefits of not affecting the antibiotic or target and any difference to the wild type should be consistent for all the mutants and therefore won't affect the relative activities. A study by I. A. Osterman and co-workers showed that the MIC for Nybomycin against a wild-type *E. coli* strain (BW25513) was > 10 mg/L but for an efflux compromised *E. coli* strain (JW5503 Δ TolC) the MIC decreased to 0.4 mg/L.²¹² This indicated that the antibiotic was efficacious against *E. coli* but sufficient concentrations were not reaching the target due to the removal from the cell *via* efflux. By using an efflux compromised strain they showed that efflux was the cause for the lack of activity in *E. coli* not influx (permeability). A patent published by Hergenrother and co-workers also demonstrated a similar effect with **DNM-2**. They showed no inhibition (MIC > 24 mg/L)

against two wild-type *E. coli* strains (ATCC 25922, MG1655) but good inhibition (MIC = 2 mg/L) against a permeabilised *E. coli* strain (MG1655 Δ AcrB).¹⁶⁸ Again, this demonstrated that efflux was the issue and more specifically the AcrAB/TolC efflux system was the main contributor to decreased antibiotic activity for **DNM-2**. This system, shown in Figure 29, comprises of the outer membrane TolC protein, an inner membrane protein AcrB and an adaptor/fusion protein AcrA. The AcrAB/TolC efflux system has been implicated in increased antibiotic resistance in *E. coli* multiple times in the literature.^{213–223}

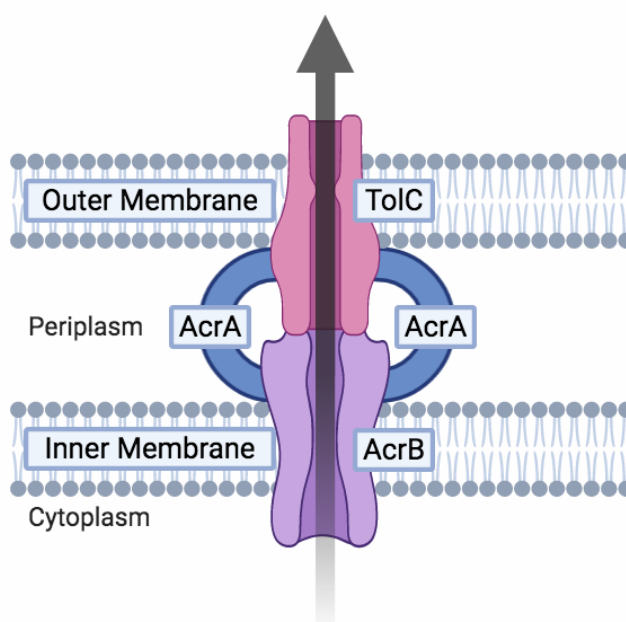


Figure 29 – The *E. coli* AcrAB/TolC efflux system.^{213,214} This system comprises of an outer membrane TolC protein, an inner membrane AcrB protein and a periplasmic adaptor/fusion AcrA protein.

The AcrAB/TolC efflux system, given the effect on antibacterial activity, is an attractive target to be ‘knocked-out’ to examine the activity of the Nybomycin derivatives in the in-house *E. coli* strains. A Red[®]/ET[®] recombination gene deletion kit was used to knock out AcrB and TolC separately as both have been shown to sensitise *E. coli*.^{168,212}

The Red[®]/ET[®] recombination gene deletion kit involves taking advantage of the recombination machinery in *E. coli* to replace the target gene with a cassette containing kanamycin resistance, shown in Figure 30.

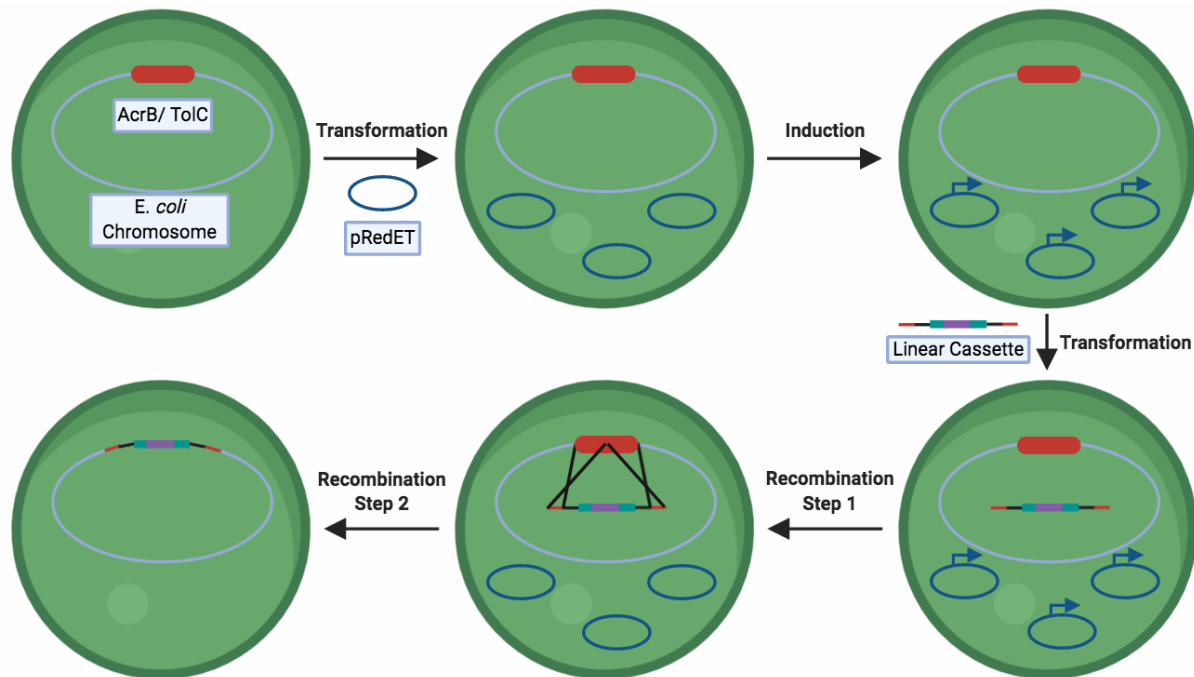


Figure 30 - Red[®]/ET[®] Recombination gene deletion kit in *E. coli*. This involves transformation of the pRedET plasmid into the bacterium. Induction of the plasmid followed by another transformation step to introduce the linear cassette with pre-installed homology arms to target the desire sequence. *In vivo* recombination can then occur which replaces the target gene with the linear cassette.

The strain can then be grown on agar containing kanamycin and only the bacterium that had undergone recombination will be able to grow. The removal of the original locus and incorporation of the new cassette in the correct location can be confirmed by using polymerase chain reaction (PCR) and gel electrophoresis. PCR is used to amplify the sequences of DNA and then gel electrophoresis is used to visualise the size of these amplified

sequences. To prove the insertion had occurred at the desired location internal and external primers to the incorporation cassette were used, shown in Figure 31.

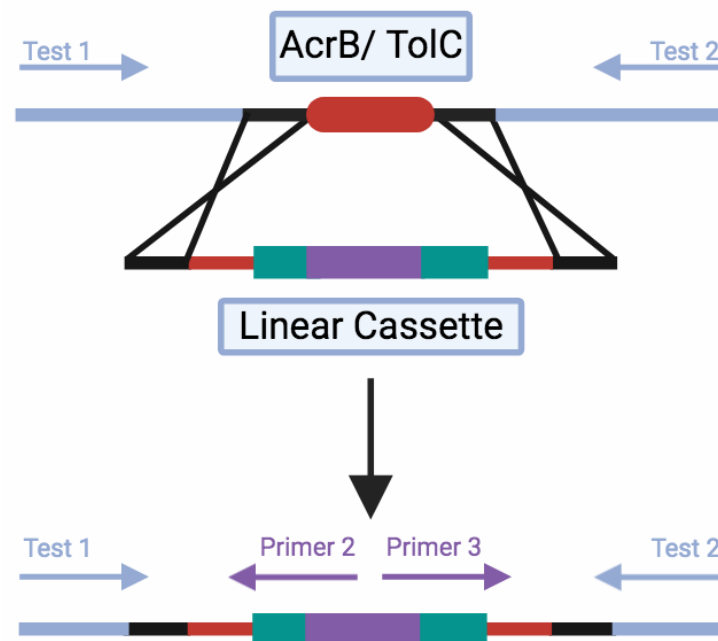


Figure 31 – Proof of integration to the host *E. coli* using PCR and gel electrophoresis. PCR is used to amplify the genetic sequence between the specific primers which is then analysed by gel electrophoresis. Before integration, there should be a band between the primers (Test 1 and Test 2). After integration, the band between primers (Test 1 and Test 2) should have changed size and new bands between the primers (Test 1 and Primer 2) and (Primer 3 and Test 2) should appear. This proves both that the target gene has been removed and that the integration has occurred at the correct position.

The correct incorporation was proved by PCR using the primers: Test 1, Test 2, Primer 2 and Primer 3, shown in Figure 31. Test 1 and Test 2 are primers just upstream and downstream of TolC or AcrB and Primer 2 and Primer 3 are internal primers in the cassette that is being inserted. Before incorporation only bands for Test 1 to Test 2 were visible. However, after incorporation had occurred the length of the Test 1 to Test 2 sequence had changed and new

bands for Test 1 to Primer 2 and Primer 3 to Test 2 were observed. These results from the gel electrophoresis are shown in Figure 32. These results confirmed the removal of TolC/AcrB from the *E. coli* DNA and the insertion of the new cassette.

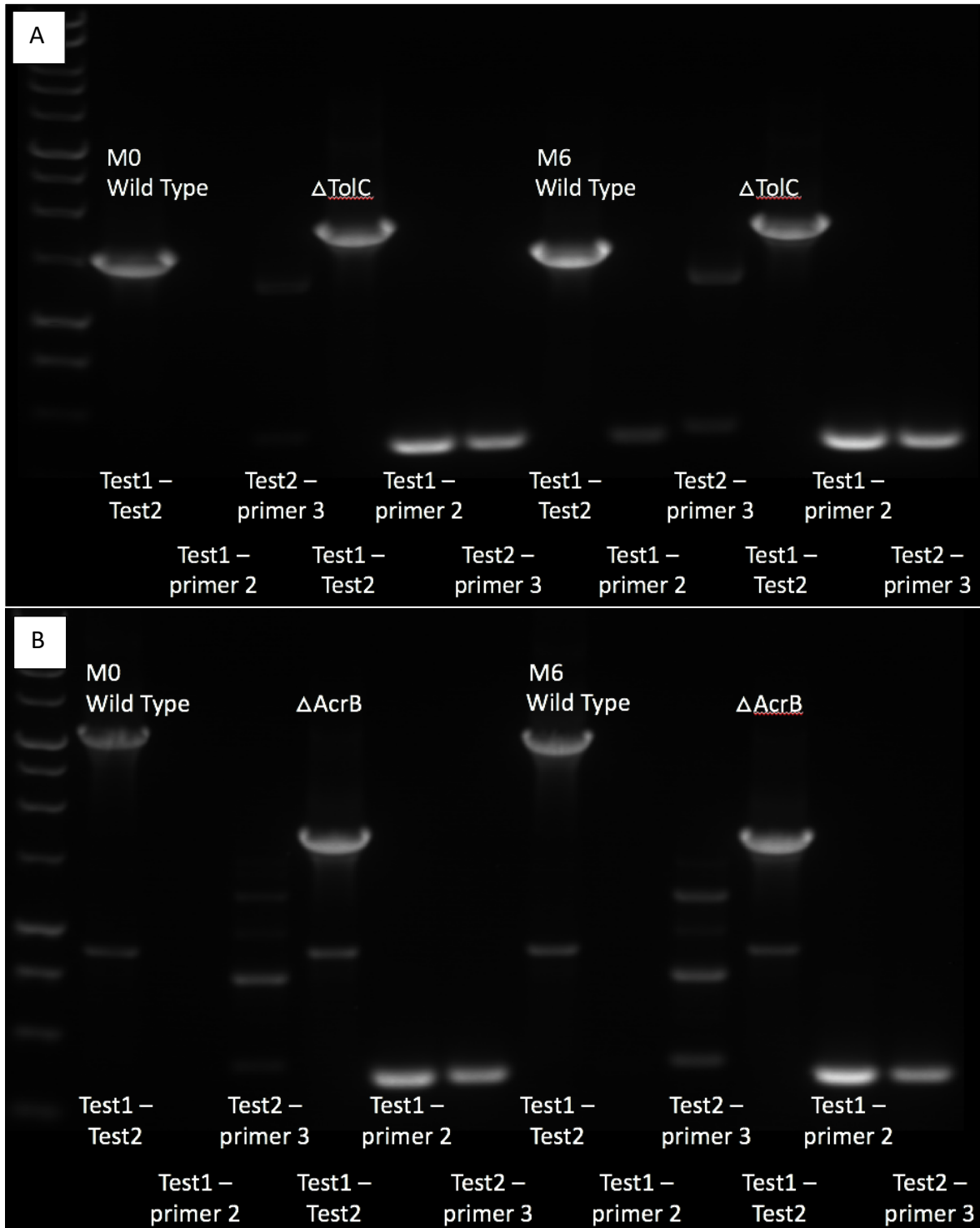


Figure 32 – Results from the gel electrophoresis confirming correct insertion of the new cassette at the position of TolC/ AcrB. A – Results for the removal of TolC in strains M0 and M6, B – Results for the removal of AcrB in strains M0 and M6. Both show the expected strong band between the primers (Test 1 and Test 2) before integration. After integration, this band (primers Test 1 and Test 2) changed size, indicating that there has been a change in the sequence between the two primers. Also new bands are observed between the primers (Test 1 and primer 2) and (primer 3 and Test 2) indicating that the linear cassette has been integrated at the desire position. 1 kilobase DNA ladder was used for A and B.

The effect that removing TolC/ AcrB had on bacterial efflux was examined by using the ethidium bromide-agar cartwheel assay that was optimised by L. Amaral and co-workers.^{224,225} This assay tests the levels of efflux in a bacterial strain and involves streaking a bacterial strain on an agar plate containing a known efflux substrate, ethidium bromide (EtB). After incubation overnight the plates can be visualised under UV light. The more EtB localised inside the bacterial cell, the brighter the cell appears under UV light as shown in Figure 33. As EtB is an efflux substrate, the higher the rate of efflux the lower the concentration of EtB inside the cell and therefore less UV absorbance is observed.

This assay was trialled using 6 strains (M0 WT, M0 Δ TolC, M0 Δ AcrB, M6 WT, M6 Δ TolC and M6 Δ AcrB) at four concentrations of EtB with two repeats. Only the M0 and M6 variants were chosen to be used as a proof of concept for this assay and the results from these strains should be indicative of the others. The results are displayed in Figure 33, and showed that the strains without TolC or AcrB appear much brighter and hence have lower rates of efflux than the WT strains. This gave phenotypic evidence for the removal of TolC or AcrB from these strains and demonstrated the effect this removal had on efflux.

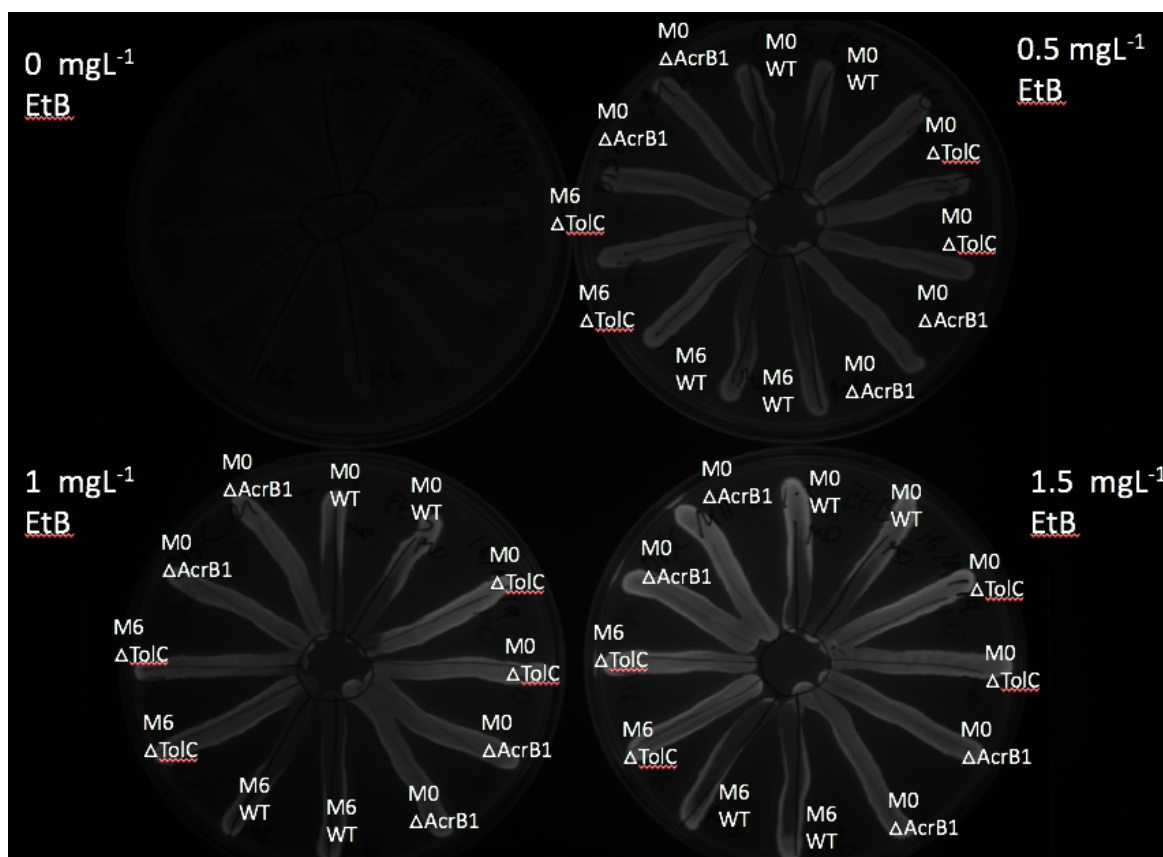
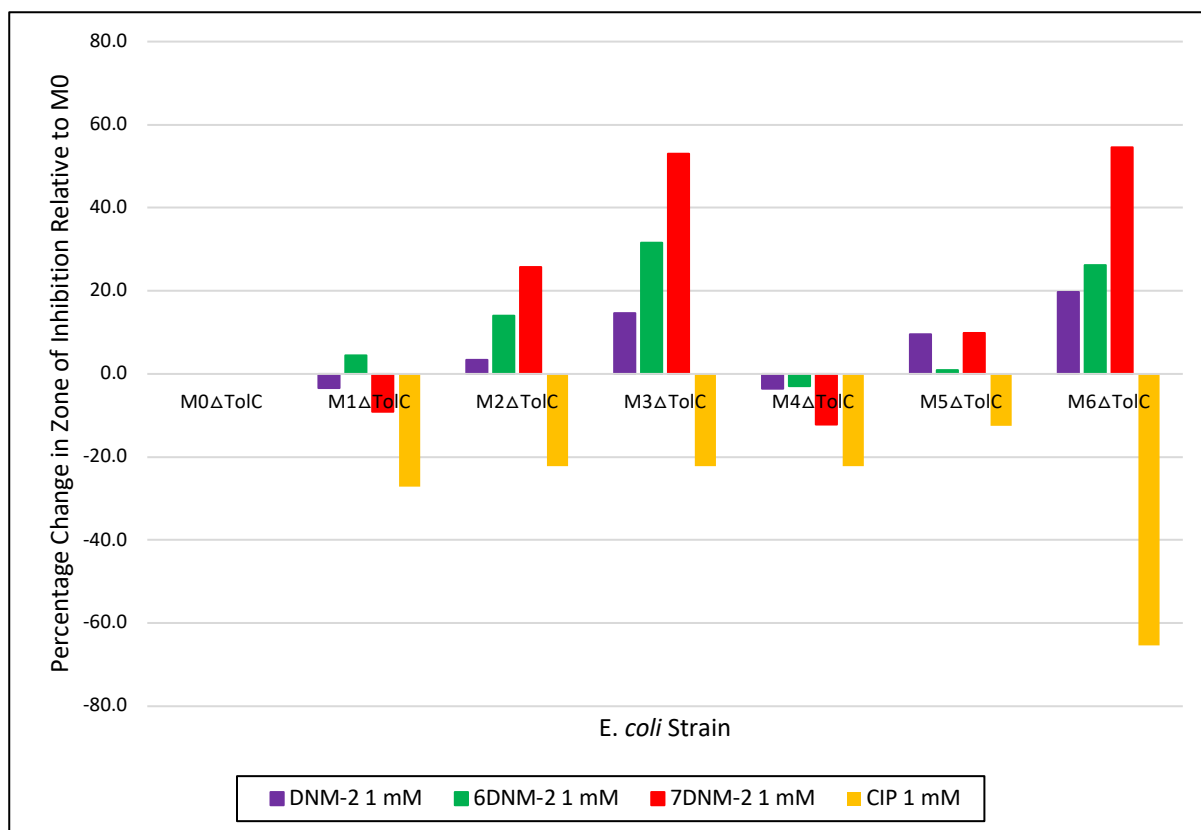


Figure 33 – Ethidium bromide-agar cartwheel assay to show effect on efflux by removing TolC or AcrB.^{224,225} In this assay the strains (M0 WT, M0 Δ TolC, M0 Δ AcrB, M6 WT, M6 Δ TolC and M6 Δ AcrB) are grown on agar containing increasing concentrations (0 , 0.5, 1, 1.5 mgL⁻¹) of ethidium bromide (EtB). After 18 h, the plates are visualised under UV light. The brighter the strain appears, the higher the internal concentration of EtB. As EtB is an efflux substrate the brighter the strain appears the less the strain is able to externalise EtB and therefore has lower rates of efflux.

With these reduced efflux mutants of the in-house *E. coli* collection in hand, the antibiotic activity of the tool compound **DNM-2** and the most interesting novel derivatives **6DNM-2** and **7DNM-2** could now be evaluated using the Kirby–Bauer disc diffusion assay. In order to compare the change in zone of inhibition with different mutations in GyrA/ ParC, the results were plotted on a graph as percent change in the zone of inhibition compared to the wild-type strain (M0), shown in Graph 1. As can be seen from Graph 1, for Ciprofloxacin, GyrA seems to have more of an effect on the zone of inhibition in the in-house *E. coli* strains (M1,

M2, M3, M4 vs M5) but the triple mutant (M6) causes a drastic decrease in activity. This is in agreement with the literature in terms of gyrase being the primary target for fluoroquinolones against a Gram-negative bacterium. Next the Nybomycin tool compound **DNM-2** and novel derivatives **6DNM-2** and **7DNM-2** were tested and evaluated. Single mutants in GyrA and ParC caused a minimal change in zone of inhibition with the GyrA S83A mutation (M2) resulting in the largest increase in zone of inhibition. The double mutant in GyrA S83F D87N (M3) caused a large increase in the zone of inhibition and was comparable with the triple mutant (M6). The similarity in the activity against M3 and M6 indicated that the mutation in topo IV (ParC S80I) resulted in a minimal change in activity. This gave tentative evidence that topo IV is the secondary target for the Nybomycin derivatives but enzymatic assays are needed to confirm this. Overall, the more resistant the strain became to Ciprofloxacin, the more sensitive they became to the Nybomycin derivatives. This is in agreement with the published data for this series.^{2,170}



Graph 1 – Comparison of the percentage change in zone of inhibition relative to the wild-type (M0). This difference is calculated and displayed as a percent change. This allows for rapid comparison between the antibiotic activity of the inhibitors against the panel of *E. coli* strains to identify which mutations are key for activity. Overall, the more resistant the stains become to Ciprofloxacin the more sensitive they are to the Nybomycin derivatives.

An interesting observation was made during the zone of inhibition assays. Some of the colonies were able to grow inside the zone of inhibition, shown in Figure 34A. PCR analysis of the TolC region (primers Test 1 to Test 2) showed that the colonies had reintroduced TolC and were therefore able to become resistant to **DNM-2**. This observation is uncommon for this kind of ‘knock out’ as the old gene (TolC/ AcrB) should have been completely removed. This is definitely the case for AcrB as no revertant colonies were observed in any of the plates and the band for Test1-Test2 in M0ΔAcrB and M6ΔAcrB is shorter than the band for Test1-Test2 in the WTs (M0 and M6), shown in Figure 34B. However, for ΔTolC, where in some instances

revertant colonies were observed, there appears to be a slight lengthening in the band for Test1-Test2 in M0 Δ TolC and M6 Δ TolC compared with the band for Test1-Test2 in the WTs (M0 and M6), shown in Figure 34A. Interestingly, comparing the length of the new band to the ladder doesn't appear to indicate the new band is long enough to be the old gene plus the cassette and so further work would need to be done to establish the exact mechanism the bacteria is using to revert. This revertant issue was not an issue for the zone of inhibition assay as the zone was still clearly visible. However, this would need to be further investigated for MIC determination as the end point of the assay is the miscibility of the solution and a small amount of these revertant colonies would cause a significant error.

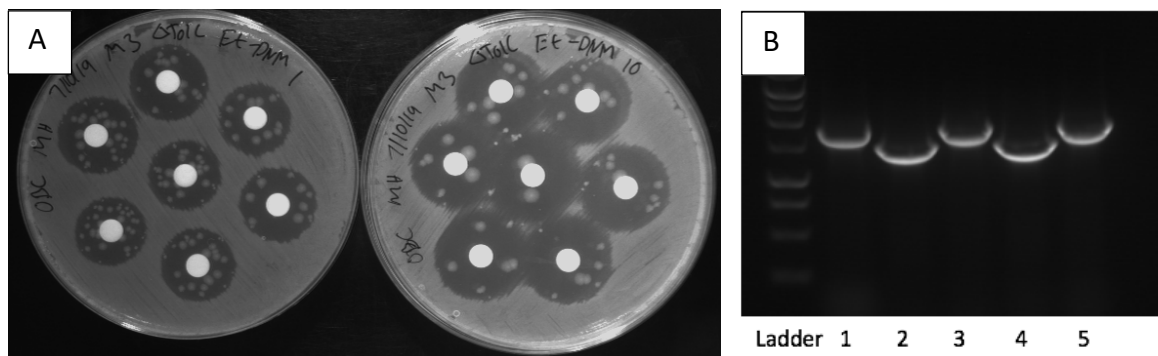


Figure 34 – Revertant colonies in zone of inhibition assay. A - two agar plates where revert colonies were observed. B – PCR analysis of the colonies: 1) Original M3 Δ TolC, 2) Single colony from 1 nM **DNM-2** M3 Δ TolC, 3) Bacterial lawn from 1 nM **DNM-2** M3 Δ TolC, 4) Single colony from 10 nM **DNM-2** M3 Δ TolC and 5) Bacterial lawn from 10 nM **DNM-2** M3 Δ TolC.

3.1.5 Enzymatic inhibition of the Key Derivates Conducted in Collaboration with

Inspiralis

In order to gain further insight into the SAR of the Nybomycin series and to help deconvolute and confirm the data obtained from the whole cell zone of inhibition assays, the inhibition of the isolated enzymes was determined. This work was conducted in collaboration with professor Tony Maxwell at the John Innes Centre and Inspiralis Ltd.

Firstly, the inhibition of *S. aureus* gyrase, both WT and S84L mutant was determined. In this assay the substrate, relaxed DNA (pBR322), is supercoiled by gyrase. The compounds inhibit this function of gyrase and the two topologies of DNA formed (relaxed and supercoiled) can be separated by gel electrophoresis to determine the compounds activity, shown in Figure 35.

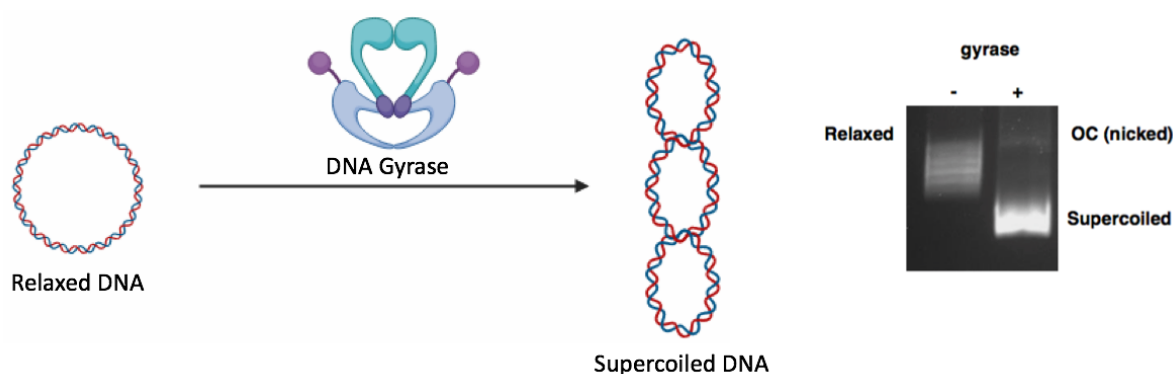
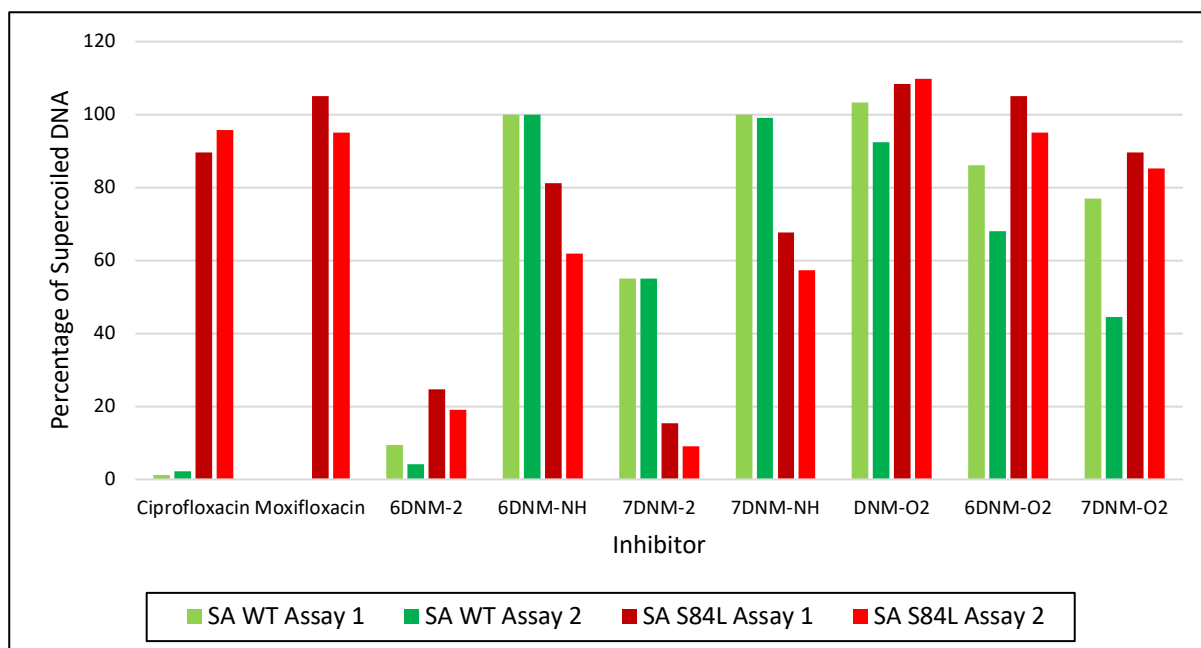


Figure 35 – Inhibition of the function of *S. aureus* DNA gyrase to supercoil relaxed DNA. In this assay DNA gyrase is incubated with relaxed DNA (pBR322). Then the reaction is stopped and analysed by gel electrophoresis.

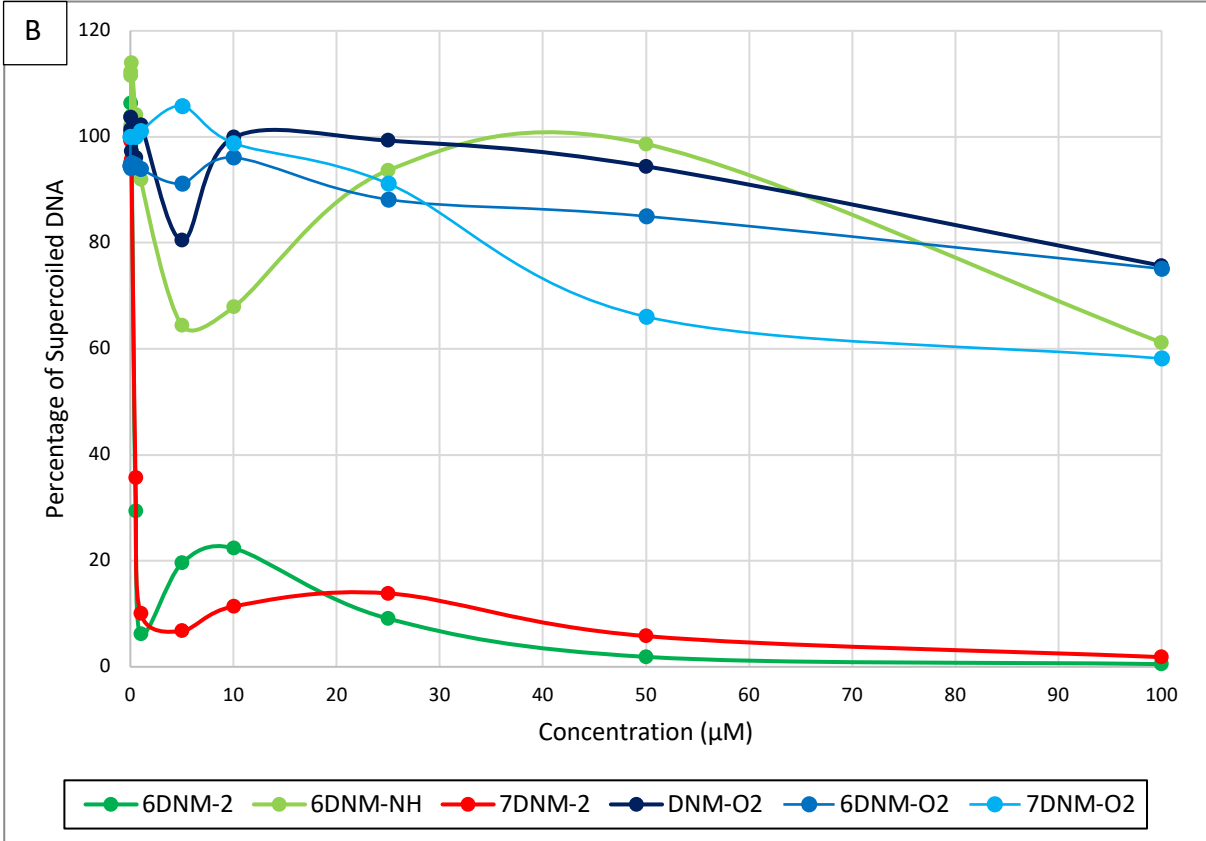
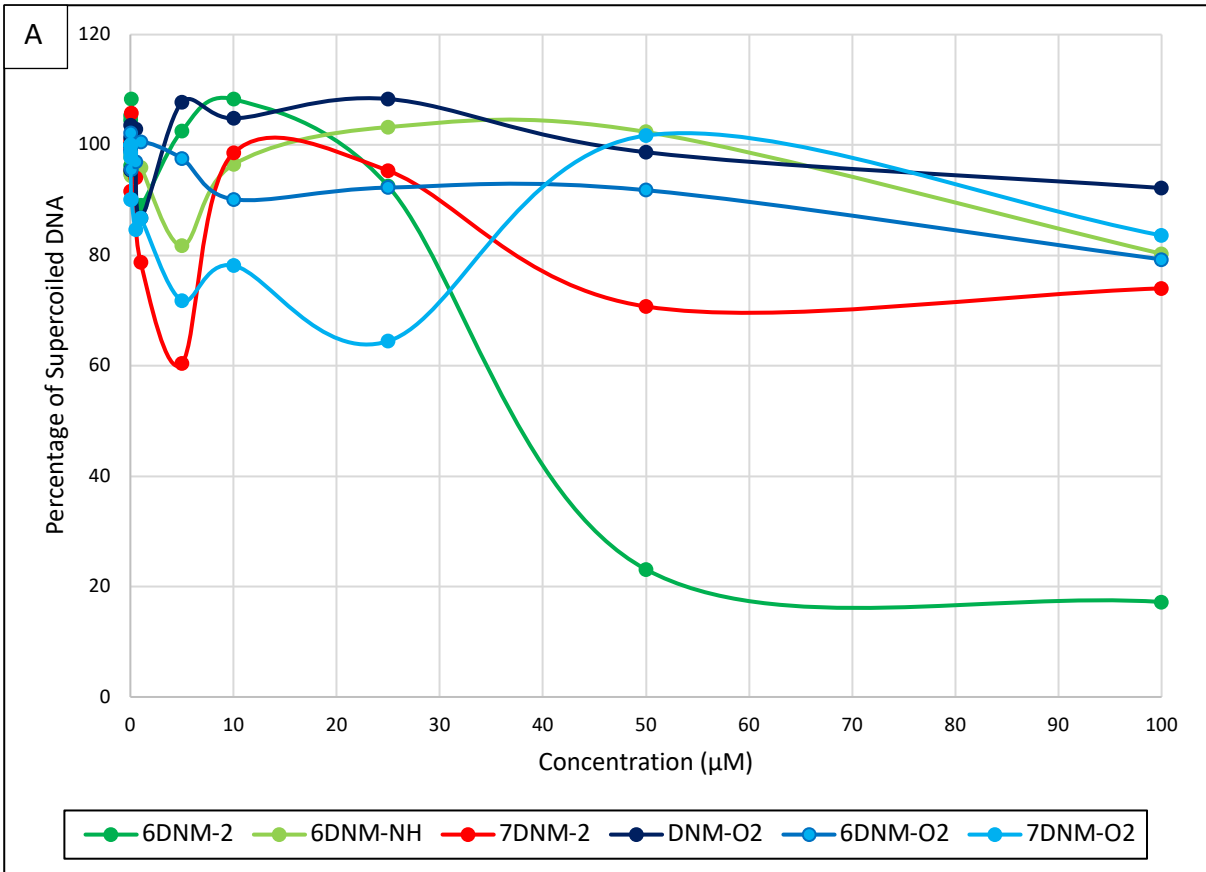
To get a rough idea of the activity of the Nybomycin analogues, a percentage inhibition at 50 μ M was measured in duplicate, this data is displayed in Graph 2. Ciprofloxacin and Moxifloxacin were used as controls and as expected showed strong inhibition against WT gyrase and weak inhibition against mutant (S84L) gyrase. This confirmed that the WT/ mutant gyrase chosen is a good model system to test the mutant selective phenotype. Compounds

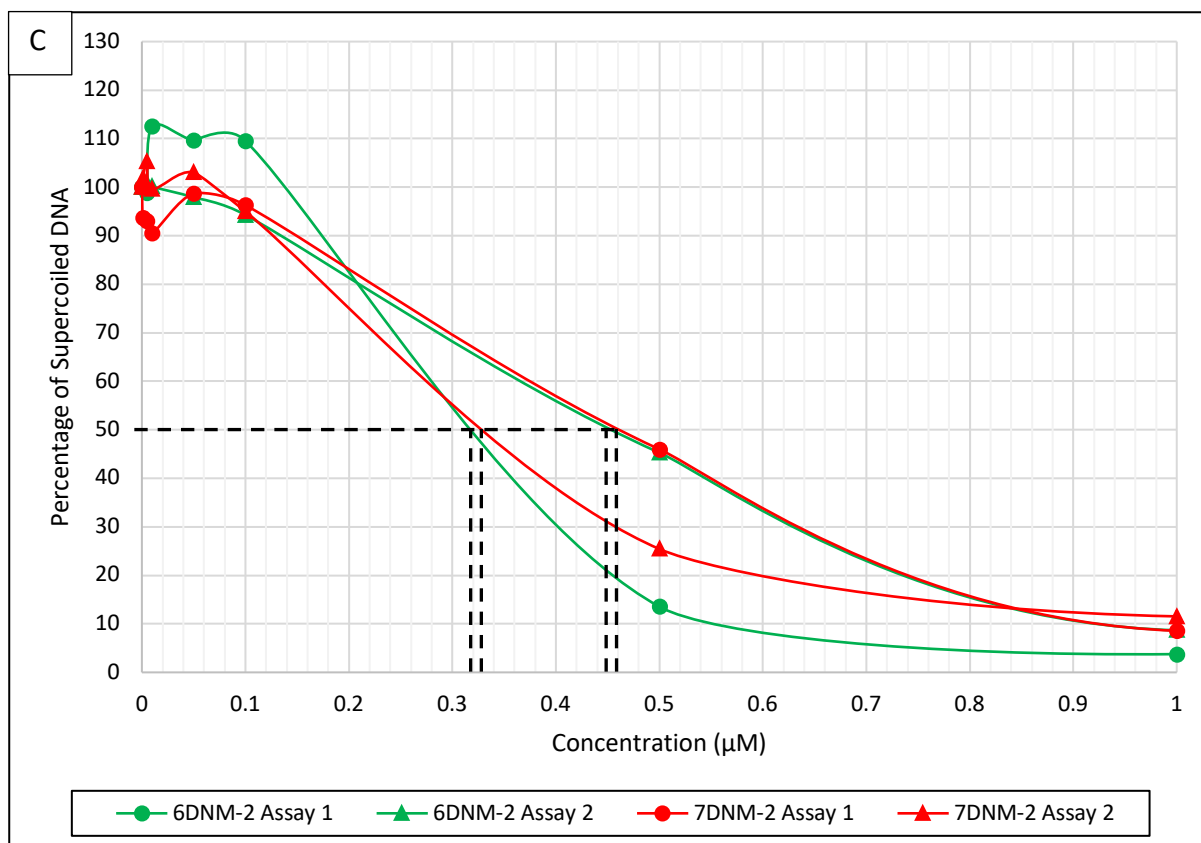
6DNM-NH, **7DNM-2** and **7DNM-NH**, under these assay conditions, showed more activity on the mutant gyrase than the WT. This confirmed the reported mutant selective phenotype from the literature. The most potent Nybomycin derivative under these assay conditions was **6DNM-2**; it showed strong inhibition on both the WT and mutant gyrase. At the concentration tested (50 μ M) there was no distinguishable difference between the activity on the WT and mutant gyrase. It seems that the concentration of **6DNM-2** was too high to observe a difference in activity, a lower concentration would hopefully show the difference in activity that was observed with the other analogues (**6DNM-NH**, **7DNM-2** and **7DNM-NH**). Expansion to a 7-membered ring **7DNM-2** caused a reduction in WT inhibition but mutant inhibition was maintained. Removal of the ethyl group (**6DNM-2** vs **6DNM-NH** and **7DNM-2** vs **7DNM-NH**) causes a significant reduction in activity in both WT and mutant inhibition. The *O*-alkylated regioisomers (**DNM-O2**, **6DNM-O2** and **7DNM-O2**) showed very weak inhibition on WT and mutant gyrase. This is in line with the whole cell data where these compounds showed no activity and confirmed that their lack of activity was target based and not a result of their inability to get to the target. Overall, the data from this assay is in agreement with the Kirby-Bauer disc diffusion assay, with the same trends observed.



Graph 2 – Percentage inhibition of WT and mutant (S84L) *S. aureus* DNA gyrase supercoiling spot test at 50 μ M of inhibitor. This assay was run in duplicate with WT *S. aureus* DNA gyrase in green and mutant (S84L) *S. aureus* DNA gyrase in red.

Since the Nybomycin analogues showed activity in the percentage inhibition assay, a more accurate IC_{50} value was next determined by testing the compounds at multiple concentrations against WT and S84L mutant *S. aureus* gyrase, displayed in Graph 3. None of the compounds appeared to inhibit WT gyrase (Graph 3A), with only **6DNM-2** achieving 50 % inhibition at $\sim 37 \mu$ M. This could be due to the lack of affinity against the WT enzyme or the poor solubility of the compounds under the aqueous assay conditions. Pleasingly, two compounds showed strong inhibition against the S84L mutant *S. aureus* gyrase (Graph 3B) with IC_{50} values of 0.39μ M for **6DNM-2** and 0.40μ M for **7DNM-2** (Graph 3C). To put these values into context, the IC_{50} values in the same assay for Ciprofloxacin was 210μ M and Moxifloxacin was 600μ M, making the Nybomycin analogues around 500 times more potent against the mutant. Solubility issues were again observed for all the compounds.





Graph 3 – Supercoiling inhibition of WT and mutant (S84L) *S. aureus* DNA gyrase. A – WT *S. aureus* DNA gyrase, B - mutant (S84L) *S. aureus* DNA gyrase, C – mutant (S84L) *S. aureus* DNA gyrase concentrations between 0 and 1 µM.

Next the ability of the compounds to inhibit WT gyrase DNA cleavage function was examined, shown in Figure 36. In this assay gyrase was allowed to form an equilibrium between supercoiled and re-ligated DNA. The inhibitor was then added and a new equilibrium was established. Protein denaturing agents such as sodium dodecyl sulphate (SDS) were then added to stop the interconversion and the equilibrium products were separated using gel electrophoresis. This assay can give insights into the mechanism of action by examining the distribution of products formed (nicked DNA (single strand breaks) vs linear DNA (double strand breaks)).

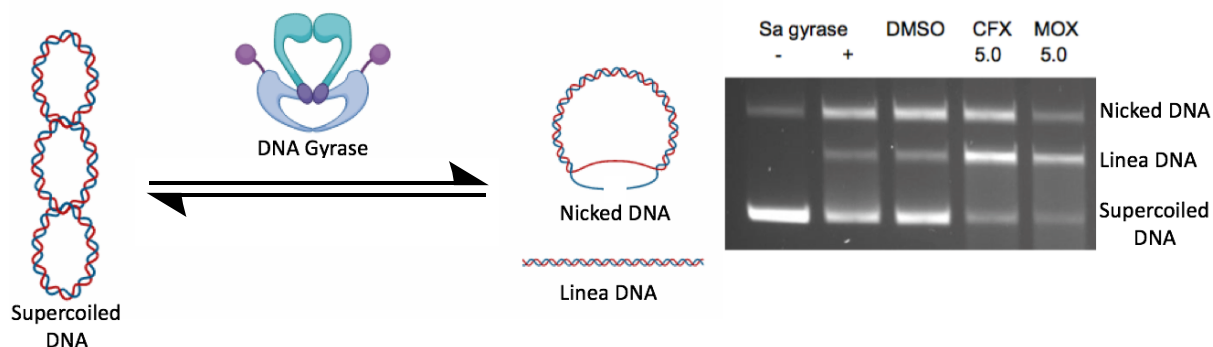
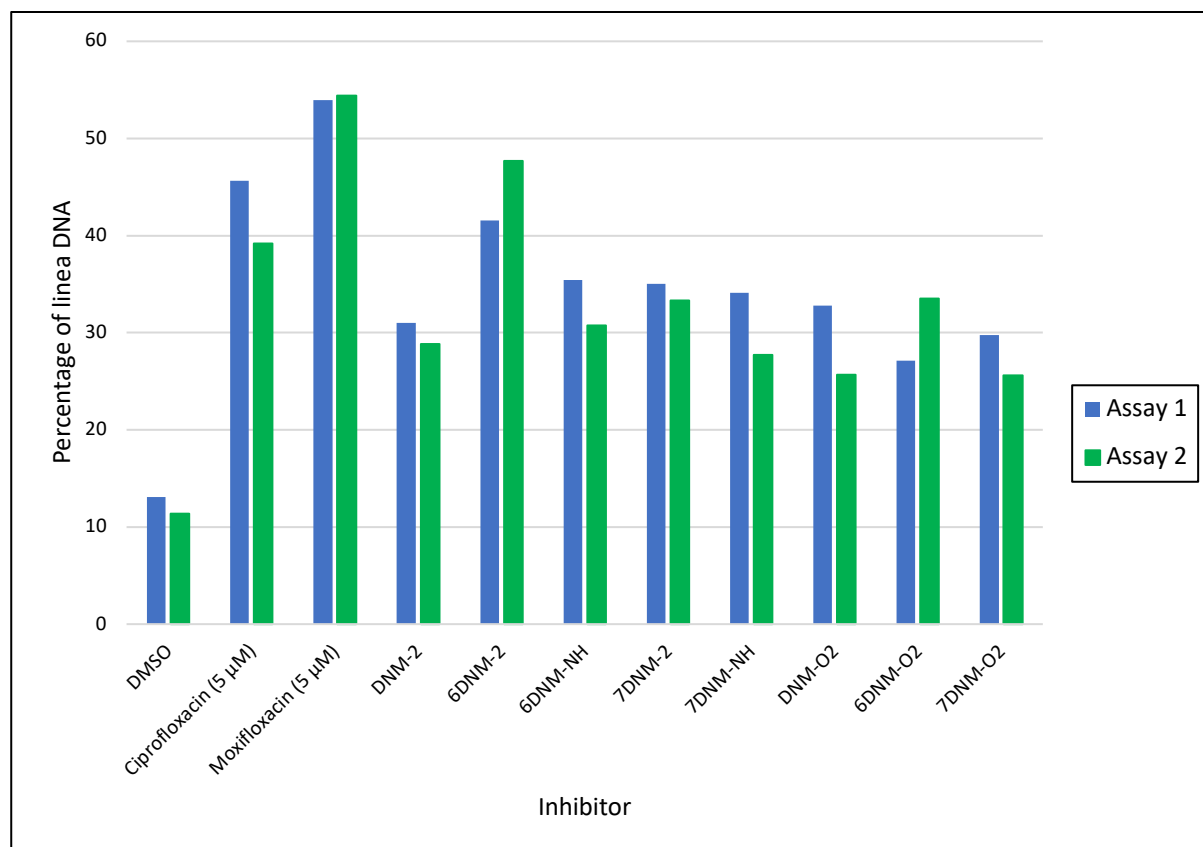


Figure 36 – Inhibition of the function of *S. aureus* DNA gyrase to cleave supercoiled DNA. In this assay DNA gyrase is incubated with supercoiled DNA (pBR322). SDS and proteinase K are added and after further incubation, the reaction was stopped and analysed by gel electrophoresis.

The results of this assay are displayed in Graph 4. The DNA cleavage levels for the majority of the compounds looked very similar and showed poor activity. This could be expected looking at the poor supercoiling inhibition data on the WT gyrase. This poor inhibition could be a result of the series' low aqueous solubility and/or a low affinity for WT gyrase. The one exception was **6DNM-2** as it gave slightly elevated cleavage levels, which was in agreement with the supercoiling results and indicated this was the most potent derivative. The dimethyl sulfoxide control showed around 10 % background DNA cleavage levels. The Nybomycin derivatives also cause single strand breaks which was difficult to quantify using this assay, so their activity was understated. This mode of action is more in line with Gepotidacin (a GSK topoisomerase inhibitor) than the fluoroquinolones. CC_{50} values were determined for the most potent analogue **6DNM-2** as well as Ciprofloxacin and Moxifloxacin. As expected, Moxifloxacin was the most potent with a CC_{50} value of 3.2 μ M followed by Ciprofloxacin at $CC_{50} = 6.2 \mu$ M. Pleasingly, **6DNM-2** was close in potency at $CC_{50} = 6.9 \mu$ M. An interesting follow up experiment would be to look at the cleavage levels with mutant (S84L) gyrase and compare how the results differ from the WT. One would expect to see a dramatic increase in activity as seen for the change from WT to mutant (S84L) gyrase in the supercoiling assay for **6DNM-2**.

It is surprising to see that **6DNM-2** appears to show stronger inhibition for WT gyrase in the cleavage assay than the supercoiling assay. This is a rare pattern of activity but has been reported before for the bactericidal peptide Microcin B17 so may be genuine for this series of compound.¹⁴³



Graph 4 – Percentage inhibition of WT *S. aureus* DNA gyrase cleavage spot test at 50 μM of inhibitor with 5 % DMSO. This assay was run in duplicate with the first run in blue and the second in green. Around 10 % background DNA was identified in the DMSO control. The fluoroquinolones (Ciprofloxacin and Moxifloxacin) were tested at 5 μM due to their activity.

Next the activity at topo IV of the Nybomycin analogues was considered. This was determined using an *S. aureus* topo IV decatenation assay. This assay measured the ability of the compounds to inhibit topo IV releasing the mini circles of DNA from the linked DNA, shown in Figure 37. These released mini circles were separated from the linked DNA using gel electrophoresis.

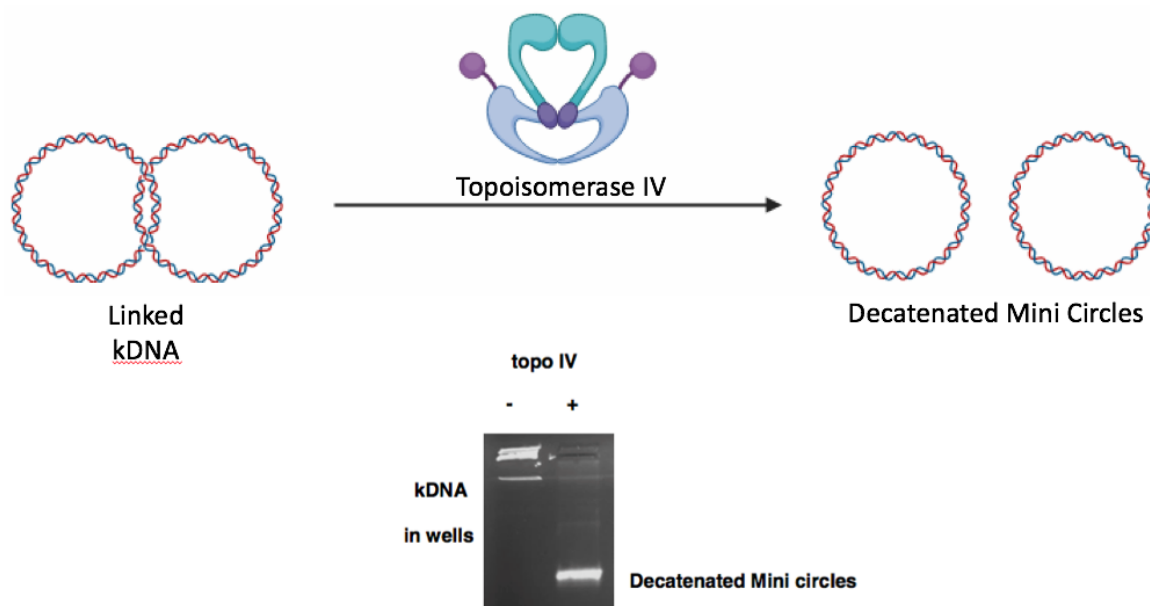
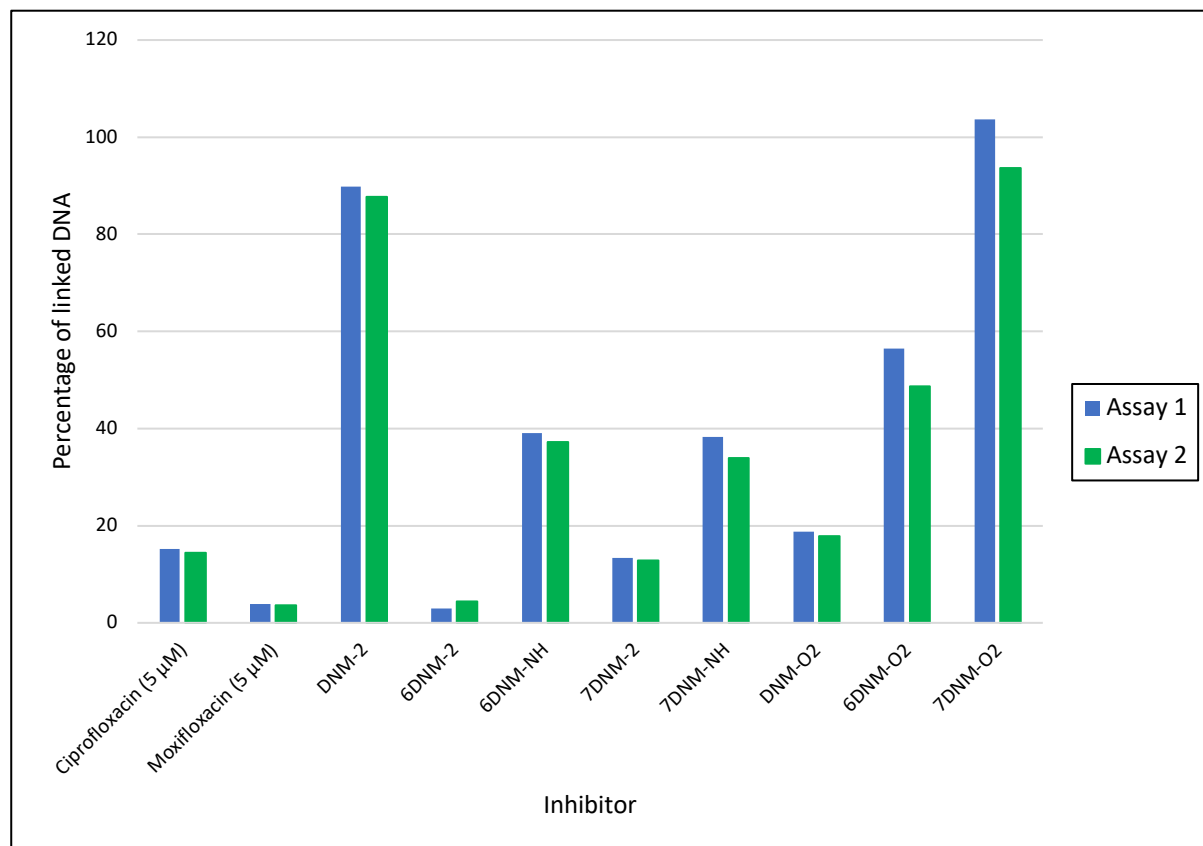


Figure 37 – Inhibition of the function of *S. aureus* topoisomerase IV to decatenate linked DNA. In this assay topo IV is incubated with kDNA. The reaction is stopped and analysed by gel electrophoresis.

The results for the decatenation assay are displayed in Graph 5. The majority of derivatives showed good inhibition of WT topo IV with **6DNM-2** again as the most potent. Surprisingly, **DNM-2** showed poor inhibition against topo IV, however this could be due to solubility or binding effects rather than affinity for the target as very similar analogues **6DNM-2** and **7DNM-2** showed strong inhibition. Similar trends in SAR to the DNA gyrase supercoiling assay were observed in terms of *N*-ethylation. Interestingly, the regioisomers **DNM-O2** and **6DNM-O2** showed good to moderate inhibition of topo IV. This was intriguing as they showed no activity on the whole cell zone of inhibition assay. All the compounds appeared to be more active on WT topo IV than WT gyrase under these assay conditions suggesting that topo IV may be the primary target. Literature shows that this is generally the case for the fluoroquinolones against a Gram-positive strain and it is interesting to see that the Nybomycins potentially follow this trend. Further experiments would be very interesting to

see their activity on mutant topo IV and how that compares with the wild type topo IV and mutant gyrase.



Graph 5 – Percentage inhibition of WT *S. aureus* topoisomerase IV decatenation spot test at 50 μ M of inhibitor. This assay was run in duplicate with the first run in blue and the second in green. The fluoroquinolones (Ciprofloxacin and Moxifloxacin) were again tested at 5 μ M due to their activity.

3.1.6 Section Conclusion

In summary, it has been shown that the Nybomycin series of natural products are more active against FQR than FQS bacteria, thus confirming the reported mutant selective hypothesis.^{2,170}

In terms of the SAR of the series, pleasingly there was agreement between the whole cell zone of inhibition assay and enzymatic assays. A summary of the SAR is displayed in Figure 38.

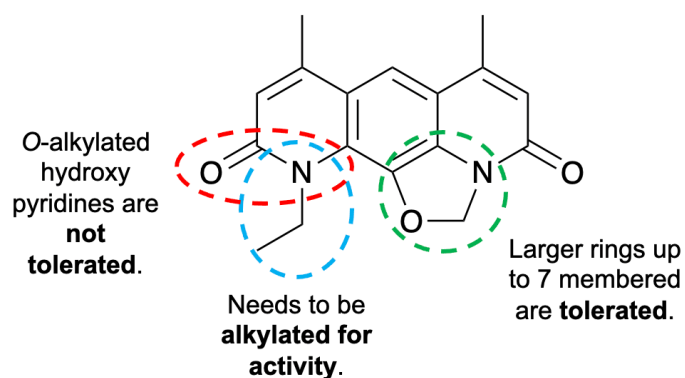


Figure 38 – Summary of Initial Nymbomycin SAR. Red – importance of regiochemistry of the pyridone, the ethoxy pyridines were not tolerated. Blue – *N*-ethylation increases activity compared with NH. Green – ring expansion from 5 membered rings to 6 or 7 membered rings is tolerated with 6 membered potentially the most active.

The main discovery was that the ethyl group on the pyridone is very important for activity. It has been shown that the regiochemistry (**6DNM-2** vs **6DNM-O2**) and its presence (**6DNM-2** vs **6DNM-NH**) dramatically changes the activity. Small alkyl substituents seem optimal at this positions when you consider the lack of activity of **34** alongside the previous work of Hergenrother and co-workers.¹⁷⁰ Ring expansion also provides an opportunity to increase the three-dimensionality and possibly the potency of **DNM-2**, with the 6-membered ring **6DNM-2** tentatively the most active. The 7-membered ring **7DNM-2** was the least active of the 3, but still tolerated.

Another important finding is the role that the AcrAB/TolC efflux channel plays in the lack of activity seen with this series in *E. coli*. Removal of AcrB or TolC results in good activity against *E. coli*, hence neither permeability nor target engagement are the reason for lack of activity in Gram-negative bacteria but instead efflux is the issue. After the removal of AcrB/TolC our in-house *E. coli* strains were used to probe the importance of various mutations in gyrase/topo IV. As the mutations caused greater resistance to Ciprofloxacin, they became more sensitive to the Nymbomycin derivatives – this finding is key for the compound's mutant

selective profile, which is important for the compound's ability to act as a reverse antibiotic. Additionally, these strains gave evidence for gyrase being the primary target in *E. coli*. This appears to be in-line with the general trends with fluoroquinolones where gyrase tends to be the primary target in Gram-negative bacteria.

The enzymatic data generated by Inspiralis confirmed the biological targets for this series as DNA gyrase and topo IV. **6DNM-2** and **7DNM-2** showed at least 500-fold greater inhibition than Ciprofloxacin and Moxifloxacin against mutant (S84L) DNA gyrase supercoiling. The Nybomycin derivatives caused both single and double strand breaks in the cleavage assay with WT gyrase. This phenotypic behaviour is more similar to Gepotidacin (a GSK inhibitor with a different mechanism of action) than the fluoroquinolones and potentially points to a different binding mode or inhibition at a different point of the gyrase catalytic cycle. The activity of the Nybomycin derivatives were also tested against *S. aureus* WT topo IV. They showed stronger inhibition against *S. aureus* WT topo IV than *S. aureus* WT gyrase, indicating that topo IV is the primary target in Gram-positive bacteria. However, it would worthwhile to investigate if this is still applicable with the mutant topoisomerases. There is a significant difference in activity between WT and mutant (S84L) gyrase supercoiling so it would be very interesting to see if the same effect happens with a similar mutation in topo IV. An important caveat for all the enzymatic data is the poor aqueous solubility of all the compounds. It is very hard to differentiate between these compounds showing a lack of activity versus just not being in solution under the assay conditions. For the series to be progressed further aqueous solubility will need to be drastically improved in order for the microbiology assays to be more reliable and robust.

3.2 Increasing Aqueous Solubility

3.2.1 Design of New Analogues

3.2.1.1 Designs of New Analogues Containing a Solubilising Handle

Section 3.1 of this work has successfully confirmed the mutant selective hypothesis for the Nybomycin series of compounds as reported in the literature.^{2,170} As well as this, an initial inspection of the SAR of this series has been undertaken. The major issue with the series so far, as highlighted particularly in the enzymatic assays, is aqueous solubility. The remainder of this work therefore details strategies to improve both the solubility and potency of this series with a view to progressing this exciting series of compounds towards a potential therapeutic.

The first strategy considered was to increase the three-dimensional character of the compounds, reducing intermolecular π -stacking and therefore lowering the overall lattice enthalpy of their solid form. Another strategy was the addition of a polarisable (basic) nitrogen which, once protonated at physiological pH, would be able to form ionic interactions with solvent and therefore aid aqueous solubility. These two strategies were explored with one set of compounds by adding an alkyl linker and a solubilising group to the **6DNM-2** scaffold.

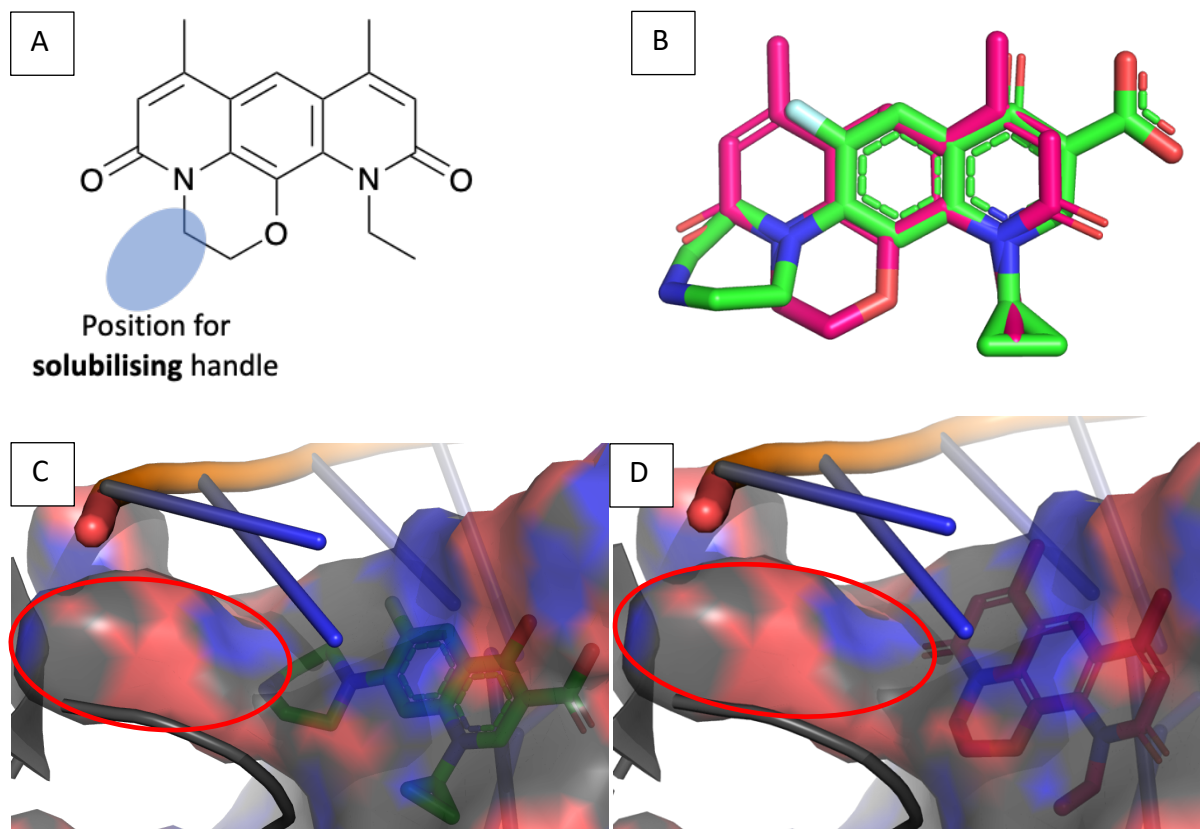


Figure 39 – Strategy to improve aqueous solubility and visualisation of free position to add solubilising handle. **A** – Position to add the solubilising handle to the **6DNM-2** scaffold, **B** – Overlay of Ciprofloxacin (green) and **6DNM-2** (pink) after molecular overlay in Forge, confirms good alignment of the cores were achieved, **C** – PyMol visualisation of the X-ray crystal structure of *S. aureus* DNA gyrase complexed with DNA (orange) and Ciprofloxacin (green) (pdb file 2XCT) with the surface displayed, red indicates negative potential and blue indicates positive potential. The free pocket highlighted with a red circle, **D** - PyMol visualisation of **6DNM-2** (pink) overlaid in to the aforementioned crystal structure with free pocket highlighted with a red circle. Molecular alignment was performed using the Forge™ software package developed by Cresset using the ‘Normal’ Alignment and ‘Very Accurate but Slow’ Conformation Hunt.

Firstly, the location of where to add the solubilising linker to the Nybomycin scaffold needed to be identified. The binding mode of the fluoroquinolone series is discussed in Section 1.8.3.1. As discussed previously, the phenotypic behaviour of the Nybomycins in the DNA cleavage assay is more similar to Gepotidacin (a GSK inhibitor with a different mechanism of action) than the fluoroquinolones and potentially points to a different binding mode or inhibition at a different point of the gyrase catalytic cycle. However, due to the

structural similarities of the Nybomycin series with the fluoroquinolones and the impact a single point mutation (S84L in *S. aureus*² and as discussed in Section 1.8.4, S83L and S83R in *E. coli*¹⁷⁰) has on the activity of the compounds, the binding mode for the Nybomycins is predicted to be in the same pocket as the fluoroquinolones. Based on this assumption, molecular overlay studies of the Nybomycin **6DNM-2** into the fluoroquinolone pocket were conducted using the software ForgeTM developed by Cresset and Molecular Operating Environment (MOE) from Chemical Computing Group ULC. The fluoroquinolone (Ciprofloxacin) was used as a reference molecule and the Nybomycin derivative was overlaid and the conformation was minimised. The structure was then inspected to check for any steric clashes with the protein and the lowest energy binding modes were analysed. The results from this study showed **6DNM-2** overlaid well into the fluoroquinolone binding site and indicated some space projecting from the aliphatic ring of **6DNM-2**, shown in Figure 39. This therefore seemed a good position to place the solubilising handle as there looked to be sufficient space and hydrophilic residues to target, demonstrated by the red (negative potential) and blue (positive potential) on the surface view. This was also confirmed by a study from Hergenrother and co-workers where a methylene amine (CH₂NH₂) was added, at the same position, and this compound retained activity.⁸¹ This design also had the advantage of extending the activity profile of this compound to a Gram-negative bacteria as discussed earlier.⁸¹

This pose, shown in Figure 39B, overlays the bicycle of the fluoroquinolone scaffold very nicely with the two rings of **6DNM-2**. The planned expansion off the 6-membered aliphatic ring in **6DNM-2** would correlate to the C-7 expansion off the fluoroquinolone scaffold (i.e., target the same pocket). This is a promising result as this position has been shown to be very fruitful

with numerous fluoroquinolone derivatives differentiating at this position making it into the clinic, for more details see Section 1.8.5.

Following this analysis, compounds were designed introducing three-dimensionality in the form of a linker and an amine solubilising handle coming off the 6-membered ring of **6DNM-2**.

A two by five library was designed to explore the new pocket using 2 different linker lengths to probe the pocket size; a methylene linker and a carbamate linker shown in Figure 40.

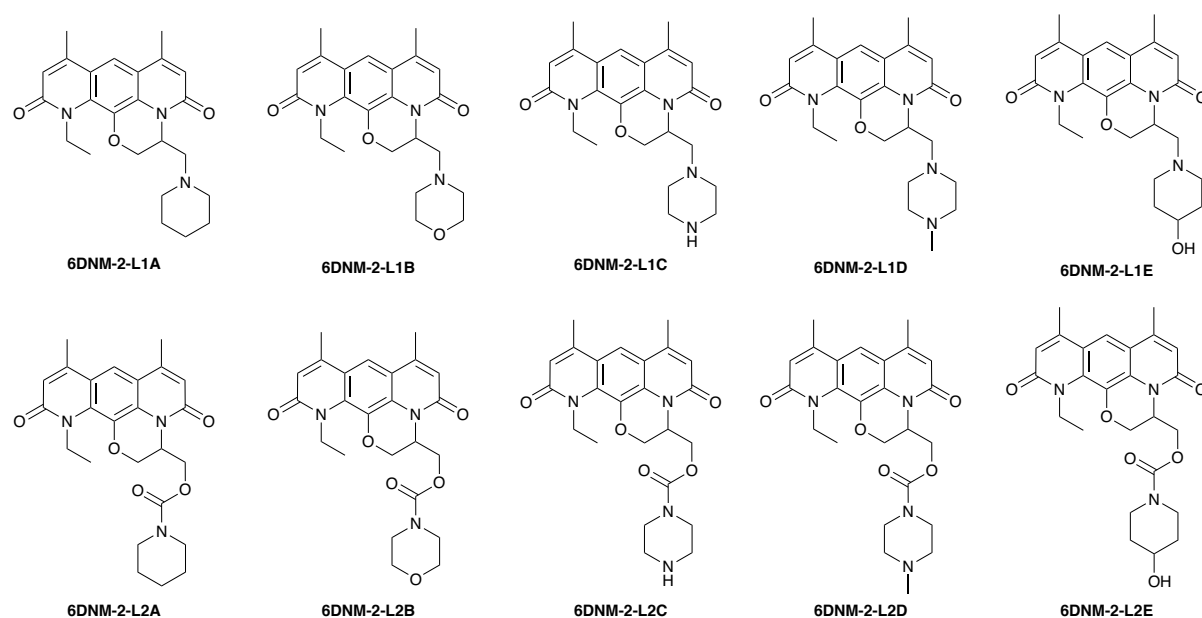


Figure 40 – Two by five library to explore the new pocket.

These linkers were chosen as they differ in length and both should be stable in a physiological context. Five different amines were included in the array containing different hydrogen bond donors/ acceptors to explore the electrostatics of the pocket and potentially pick up hydrogen bonds. These amines were chosen as they were close spatial analogues of each other but would allow for a comparison of the HBD/HBA effects. Molecular overlays of these compounds were then performed using the Forge™ software package developed by Cresset,

shown in Figure 41. Pleasingly, the lowest energy binding pose for these analogues overlaid the tricyclic core with **6DNM-2**, lending credibility to the identified binding pose and designs. Excitingly, the solubilising handle was placed into the empty pocket, shown in Figure 39. The best example of both the methylene (Figure 41A) and carbamate (Figure 41B) linkers are displayed. Looking at Figure 41, the binding pose suggests that potentially the methylene linked amine may not be optimally filling the pocket and in fact the longer carbamate linker in this position may be beneficial. Additionally, with the best-looking carbamate compound (41B), there was the potential to pick up a hydrogen bond with the NH₂ of the amide in Asn475 with the terminal OH on the piperidine of **6DNM-2-L2E**.

The binding poses suggested retainment of activity if not an improvement with these designed library compounds and the added three-dimensionality and solubilising handle was hoped to give the desired improvement in aqueous solubility compared to **6DNM-2**.

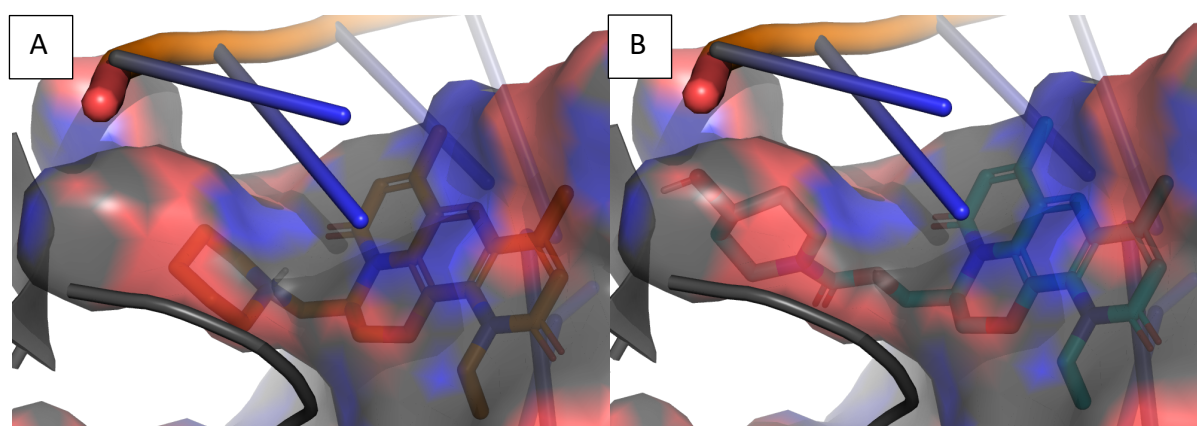


Figure 41 – Growth into the pocket. PyMol visualisation of the results of the molecular overlay study of the new Nybomycin derivatives into X-ray crystal structure of *S. aureus* DNA gyrase complexed with DNA (orange) (pdb file 2XCT) with the surface displayed, red indicates negative potential and blue indicates positive potential. The best derivative from each series is displayed. **A** – piperidine analogue **6DNM-2-L1A** (orange), starts to occupy the pocket, **B** – carbamate analogue **6DNM-2-L2E** (cyan), better occupation of the pocket, may be able to form a new hydrogen bond.

3.2.1.2 Designs of Cyclopropyl Analogues

The next change that could be beneficial for the Nybomycin series was to substitute the *N*-ethyl on the pyridone of **6DNM-2** for a cyclopropyl group. This substitution results in a dramatic increase in activity for the fluoroquinolone series, for example see this study by Easty and co-workers that showed that Ciprofloxacin (*N*-cyclopropyl) was more potent than Norfloxacin (*N*-ethyl) against all the strains they tested.²²⁶ This increase in potency is attributed to the cyclopropyl being better able to fill a small hydrophobic pocket in the receptor. It is hoped that a similar transformation with the Nybomycin series will lead to a similar increase in activity. Examining the lowest energy binding pose of **6DNM-2** overlaid on Ciprofloxacin gave evidence that this might be the case. The ethyl group from **6DNM-2** and the cyclopropyl group from Ciprofloxacin are positioned on top of each other, shown in Figure 42. This means that if this binding pose is valid for **6DNM-2** a similar boost in activity should be expected. This would also provide strong evidence that the Nybomycin derivatives and the fluoroquinolones share a common binding site/ position.

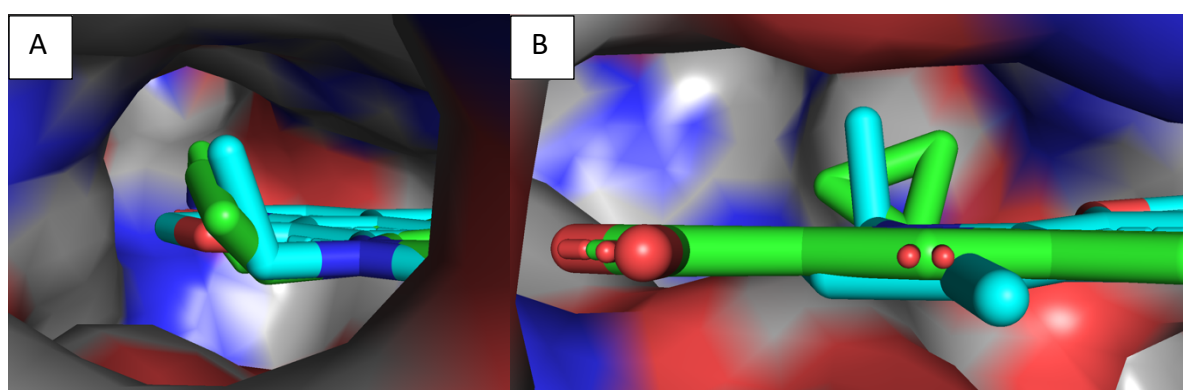


Figure 42 – Spatial position of Cyclopropyl (in Ciprofloxacin green) vs Ethyl (in 6DNM-2 cyan) binding pose. A – Side on view, B – view looking down the plane of the molecule (90-degree rotation from A). Created in PyMol using pdb file 2XCT.

The new cyclopropyl analogues **DNM-Cyclo**, **6DNM-Cyclo** and **7DNM-Cyclo** shown in Figure 43 were designed. These analogues will test the above ethyl to cyclopropyl hypothesis and also give another matched pair to analyse how the size of the aliphatic ring effects the activity of this series.

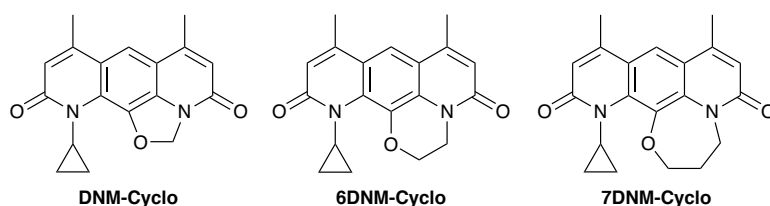


Figure 43 – New cyclopropyl analogues to synthesise.

Moving from an ethyl to a cyclopropyl may have an impact on the SAR observed with the different sized aliphatic rings since the torsion angle between the two substituents may be impacted as shown at a similar position in a closely related series of topoisomerase inhibitors, displayed in Figure 44, published by Huxley and co-workers.²²⁷

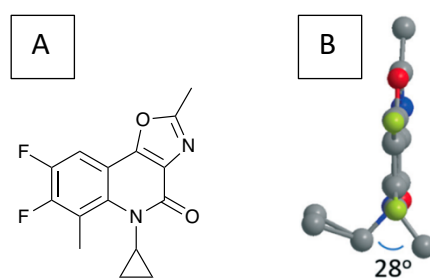


Figure 44 – Torsion angle between the cyclopropyl and methyl substituents of a closely related series of topoisomerase inhibitors developed by Huxley and co-workers.^{227,228} A – Chemical structure of the core of the series of topoisomerase inhibitors. B – X-ray crystal structure of A. Demonstrating the torsion angle between the cyclopropyl and methyl substituents is 28°. Figure taken from Huxley and co-workers.²²⁸

3.2.1.3 Designs of Novel Core Alteration

Finally, alterations to the Nybomycin core structure were considered. This presented the opportunity to modulate the electrostatic properties of the core in order to tune the π -stacking interaction with the base pairs of DNA. This strategy in turn has the potential to increase both the activity of the series and the aqueous solubility. Such diversification will also make the series more attractive from an intellectual property (IP) perspective. However, this approach was thought to be more speculative as, with more major changes to the core structure, there is no guaranty that activity will be maintained.

Molecular docking was performed using the software MOE on the S84F D88N *S. aureus* gyrase mutant, shown in Figure 45. This mutant was generated using the PyMol mutagenesis tool from the crystal structure 2XCT, mutating the residues Ser84 and Asp88 to Phe and Asn respectively and selecting the lowest energy position. This gyrase mutant was chosen as it resulted in high levels of resistance to fluoroquinolones in whole cell MIC assays in strains that also have similar mutations in ParC (S80Y, E84G).²

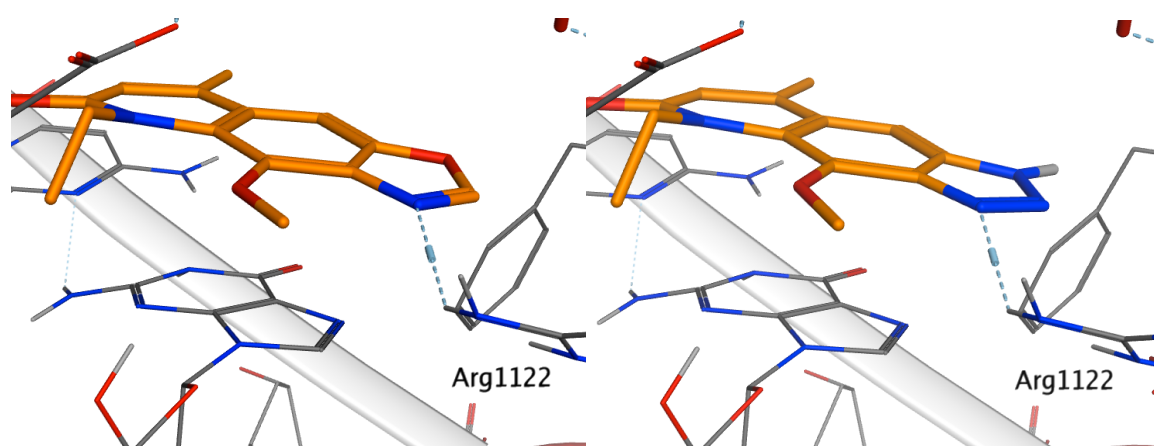


Figure 45 – Docking studies of the novel tricyclic cores (Left - Core1-NEt and Right - Core2-NEt) against the S84F D88N *S. aureus* gyrase mutant. The docking was performed using MOE and the mutant was created from pdb file 2XCT using the PyMOL mutagenesis tool.

The results from the docking showed that the substitution of one of the pyridone rings with an imidazole or oxazole had the potential to pick up a new interaction with the NH of Arg1122 (*S. aureus* numbering) with an HBA nitrogen of the new heterocycle, shown in Figure 46.

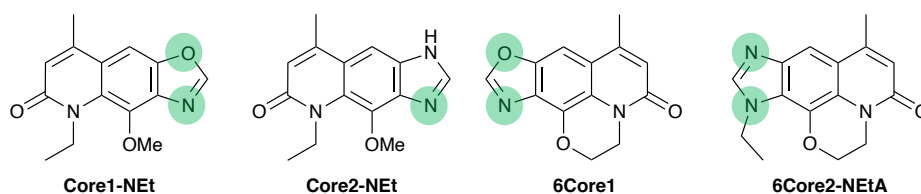


Figure 46 – Designs of the novel tricyclic cores. HBA atoms highlight with green circles. NH-imidazole **Core2-NEt** could exist as a mixture of tautomers so both the nitrogens of the imidazole have the potential to act as HBA.

3.2.2 Synthesis

3.2.2.1 Synthesis of Analogues Containing a Solubilising Handle

The first step was to design the synthetic methodologies that would allow for the preparation of the two by five library, shown in Figure 40. The retrosynthetic analysis of **6DNM-2-L1A** is shown in Figure 47. The target molecule **6DNM-2-L1A** could be disconnected to aldehyde **50**. Aldehyde **50** was chosen as a suitable disconnection as it would facilitate the use of library chemistry to diversify *via* reductive aminations. Aldehyde **50** could be disconnected to alcohol **6DNM-2-OH** which would also give a compound that is interesting to test in its own right. **6DNM-2-OH** can be disconnected back to intermediate **25** from the synthesis of **DNM-2** (Section 3.1.2.3 Scheme 22).

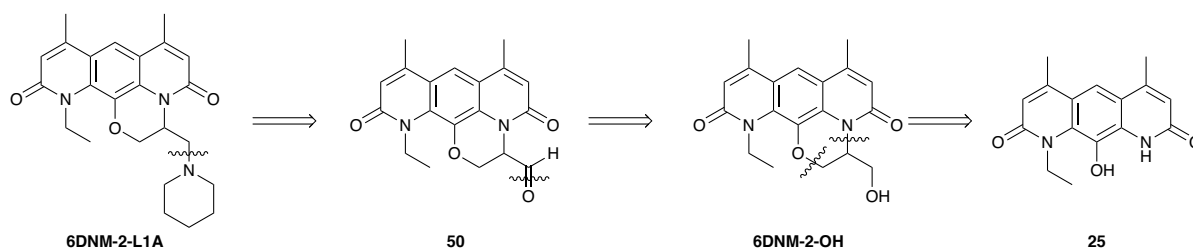
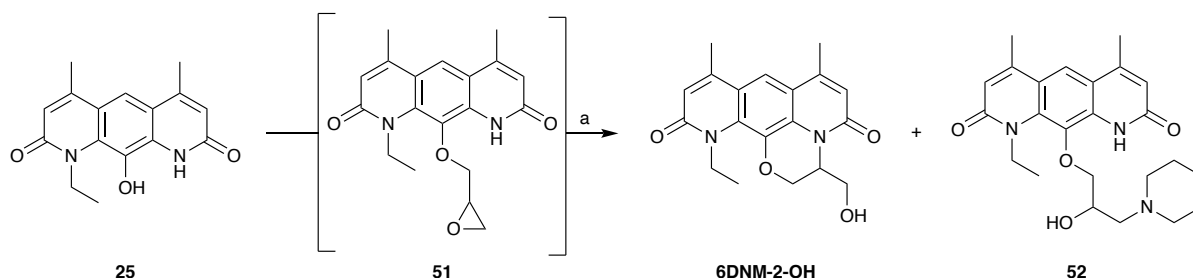


Figure 47 – Retrosynthetic analysis of methylene linked compound 6DNM-2-L1A.

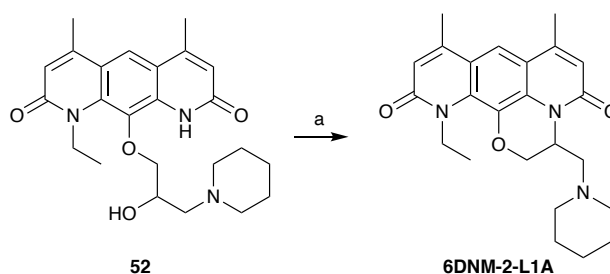
Firstly, the synthesis of **6DNM-2-OH** needed to be considered. After reviewing the literature, a one-pot method using epichlorohydrin by M. Cornebise and F. Reck was identified.²²⁹ Using the exact conditions (epichlorohydrin, catalytic piperidine, 1,4-dioxane/DMF, 85 °C) from the prior study, the reaction yielded some of the desired alcohol **6DNM-2-OH** (20 % isolated yield) but also a significant by-product (33% isolated yield). After NMR analysis the structure of the by-product was shown to be β -amino alcohol **51**, shown in Scheme 24.



Scheme 24 – Synthesis of the alcohol 6DNM-2-OH. (a) Epichlorohydrin, piperidine, DMF, 1,4-dioxane, 85 °C, 18 h, **6DNM-2-OH** - 20 %, **52** - 32 %.

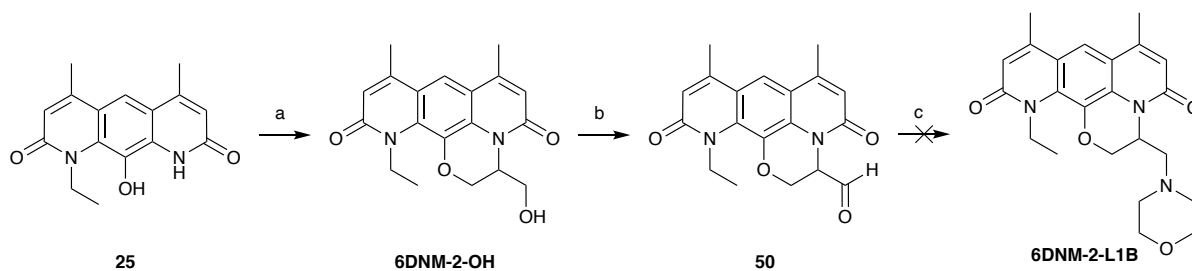
This was suspected to have come from interception of the epoxide intermediate **51** with piperidine instead of the desired intramolecular attack by the pyridonic nitrogen. However, this side reaction could prove to be very useful. If the epoxide intermediate could be intercepted by a range of amines it would remove the need for the reductive amination and after cyclisation, the array of methylene linked amine final products shown in Figure 40 could be generated. Therefore, ring closing methodologies of **52** were evaluated. Pleasingly mesylation

with methanesulfonyl chloride followed by a base catalysed intramolecular S_N2 reaction formed the final cyclised product **6DNM-2-L1A**, shown in Scheme 25.



Scheme 25 – Conversion of β -amino alcohol **52 to final product **6DNM-2-L1A**. (a) i) MsCl, NEt_3 , CH_2Cl_2 , $0\text{ }^\circ C$ to rt, 2 h, ii) K_2CO_3 , DMF, $40\text{ }^\circ C$, 18 h, 42 %.**

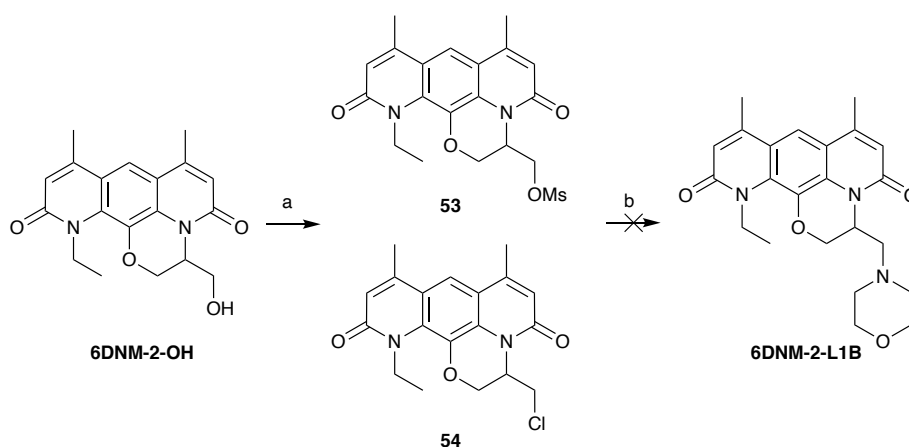
Next the formation of the β -amino alcohol using 1-boc-piperazine was investigated. However, this substrate failed to generate the β -amino alcohol. It was suspected that this amine intercepted the epichlorohydrin before it reacted with the core as the starting material **25** was isolated as the major reaction product. This result put into doubt how feasible this approach was for a variety of different amines. Attention was therefore returned to the initial route, *via* the alcohol **6DNM-2-OH** then aldehyde **50**, showed in Scheme 26. Pleasingly, changing the base to a non-nucleophilic inorganic base (potassium carbonate) prevented the formation of the β -amino alcohol **52** and led to clean conversion to alcohol **6DNM-2-OH**, in a much-improved yield (62 %). Formation of aldehyde **50** by oxidation using Dess–Martin periodinane worked well. However, the subsequent reductive amination (morpholine, catalytic AcOH, THF, rt then STAB) failed with no evidence for the formation of desired product. Further reductive amination conditions were not trialled due to restrictive amounts of aldehyde **50**.



Scheme 26 – Attempted formation of aldehyde 51 then failed reductive amination. a)

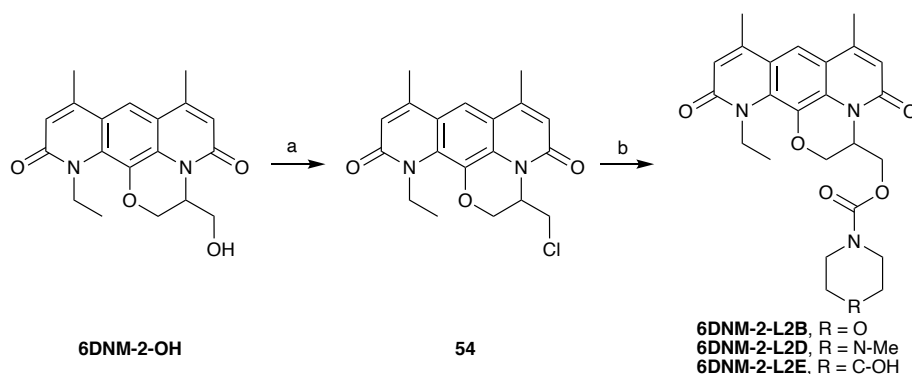
Epichlorohydrin, K_2CO_3 , DMF, 1,4-dioxane, 85 °C, 18 h, 62 %, b) DMP, CH_2Cl_2 , rt, 18 h, telescoped crude to next step, c) Morpholine, AcOH, mol. sieve, THF, rt to 70 °C, 18 h then STAB, 18 h, rt.

It was therefore apparent that other methodologies would need to be explored for the installation of the amines. The next approach was to use a mesylation reaction, shown in Scheme 27, with methanesulfonyl chloride. This approach converted alcohol **6DNM-2-OH** into a good leaving group and then used a nucleophilic substitution to install the amine. Mesylation however formed two products (mesylate **53** and chloride **54**) and this mixture was telescoped into the displacement reaction because of worries of the stability of mesylate **53**. The displacement reaction proved unsuccessful. Mesylate **53** appeared to degrade under the reaction conditions and chloride **54** was isolated in a 39 % yield (compared to starting material alcohol **6DNM-2-OH**).



Scheme 27 – Attempted displacement of mesylate 53. a) MsCl, NEt_3 , CH_2Cl_2 , 0 °C to rt, 20 h, telescoped into next step, **b)** Morpholine, Pyridine, MeCN, 70 °C, 18 h.

Attention was then turned to the displacement of the chloride intermediate **54**, shown in Scheme 28. Conditions were trialled using morpholine as the nucleophile with pyridine as a base in acetonitrile at 70 °C or neat in morpholine at 140 °C in a sealed system. Neither of these conditions yielded the desired product and resulted in either unreacted starting material or degradation. Conditions that used potassium fluoride to promote the nucleophilic substitution were trialled. The fluoride ion's capability to assist in these displacement reactions has been linked to its ability to form hydrogen bonds with the amine proton, hence increasing the amine's nucleophilicity.^{230–232} However, an interesting product was observed when potassium carbonate and potassium fluoride in acetonitrile and dimethylformamide were used. Instead of the desired displacement occurring, the isolated product formed was the carbamate, shown in Scheme 28. This was surprising and the exact mechanism for carbamate formation is unclear.



Scheme 28 – Synthesis of carbamate 6DNM-2-L2B, 6DNM-2-L2D and 6DNM-2-L2E. (a)

SOCl₂, CH₂Cl₂, rt, 18 h, 52 %, (c) Amine, K₂CO₃, KF, MeCN, DMF, 80 °C, 18 h, 30 % for **6DNM-2-L2B**, 28 % for **6DNM-2-L2D** and 43 % for **6DNM-2-L2E**.

Since the carbamate compounds were targets in their own right, this serendipitous reaction was successfully used to synthesise the morpholine **6DNM-2-L2B**, *N*-methyl pyrazine **6DNM-2-L2D** and 4-hydroxypiperidine **6DNM-2-L2E** derivatives. The piperidine **6DNM-2-L2A**

and pyrazine **6DNM-2-L2C** analogues were also attempted, however these reactions failed due to isolation difficulties. The successfully synthesised compounds are displayed in Figure 48. The other analogues were not re-synthesised due to time limitations on this project.

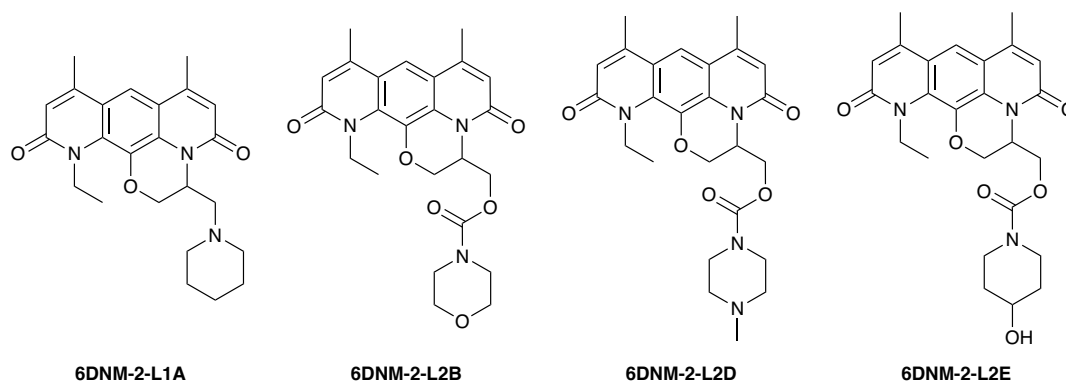
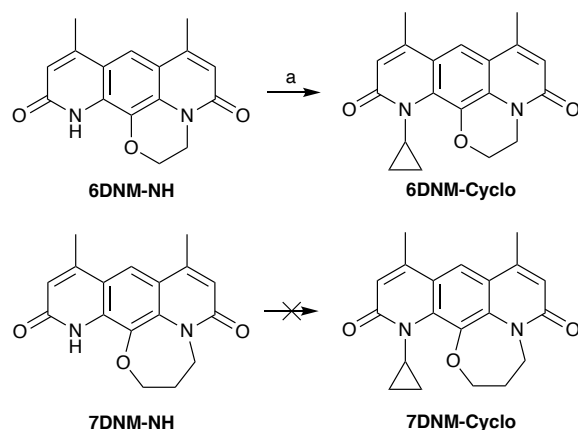


Figure 48 – Successfully synthesised Nybomycin analogues containing a linker and a solubility handle.

3.2.2.2 Synthesis of the Cyclopropyl Analogues

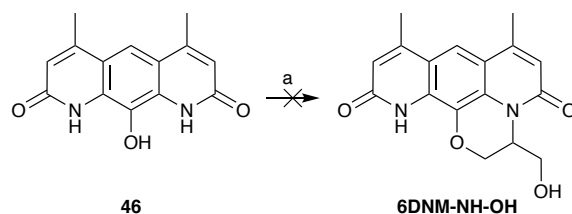
Next attention was turned to the synthesis of the cyclopropyl derivatives described in Section 3.2.1.2. They could be synthesised by changing the amines used in the unsymmetrical amide coupling (cyclopropylamine instead of ethylamine) but a potentially faster and more efficient approach could be repurposing intermediate **46**. The aliphatic ring was installed to give **6DNM-NH** and **7DNM-NH** as before and then a Chan-Lam cross coupling, described by Engle and co-workers,²³³ was attempted to introduce the cyclopropyl group, shown in Scheme 29.



Scheme 29 – Synthesis of cyclopropyl analogue 6DNM-Cyclo. (a) Potassium Cyclopropyltrifluoroborate, 1,10-phenanthroline, Cu(OAc)₂, K₂CO₃, Air, H₂O, toluene, 70 °C, 18 h, 7 %.

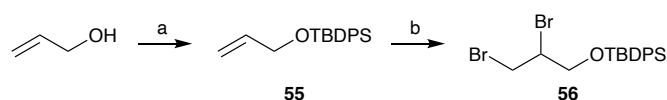
Unfortunately, formation of the 5-membered ring **DNM-NH** failed as before (Section 3.1.2.3 Scheme 20), likely due to its extremely poor solubility, meaning that the cyclopropylation could not be attempted. The Chan-Lam cross coupling was attempted and pleasingly was successful using **6DNM-NH** which yielded **6DNM-Cyclo**. This provided a match pair with **6DNM-2** so the exchange from ethyl to cyclopropyl could be evaluated. Unfortunately, the 7-membered ring **7DNM-NH** failed. This may be due to the increased steric hindrance, compared to **6DNM-NH**, around the site of reaction.

The chemistry to facilitate adding a solubilising handle to these new cyclopropyl analogues was also explored. Using a similar approach to the ethyl derivatives, epichlorohydrin was trialled for the ring closure on intermediate **46** (Scheme 30), but no reaction occurred and only starting material remained. This was attributed to the poor solubility of both the starting material and the reaction intermediates.



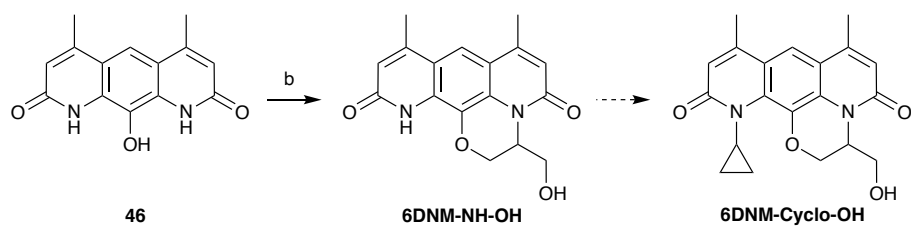
Scheme 30 – Failed reaction with intermediate 46 and epichlorohydrin to form 6DNM-NH-OH. a) Epichlorohydrin, K₂CO₃, DMF, 1,4-dioxane, 85 °C, 18 h.

To combat this solubility issue another approach was evaluated using TBDPS protected 2,3-dibromopropanol **56** as the electrophile. TBDPS was chosen as a protecting group as it is lipophilic and three-dimensional and it was hoped that this would improve the solubility of the reaction intermediates in the reaction solvent and lead to an easier to handle product. Compound **56** was successfully synthesised *via* protection of prop-2-en-1-ol with TBDPS-Cl then a bromination of the corresponding alkene **55**, shown in Scheme 31.



Scheme 31 – Synthesis of intermediate 57. a) TBDPS-Cl, Imidazole, DMF, rt, 18 h, 81 %, b) Br₂, CHCl₃, 0 °C to rt, 18 h, 87 %.

However, when this material was reacted with **46**, as before, no reaction occurred and only the starting material **46** remained. This indicated that steric hindrance of the electrophile is very important in this double substitution. The unprotected 2,3-dibromopropanol was also trialled as the electrophile and pleasingly this gave clean conversion to the desired product **6DNM-NH-OH**, shown in Scheme 32. In the future this material could then undergo cyclopropylation using similar conditions to above if the change from ethyl to cyclopropyl is beneficial in the 6-membered ring series. Due to time constraints, the generation of product **6DNM-Cyclo-OH** was not continued in the timescale of this project.



Scheme 32 – Route towards cyclopropyl analogues with solubility handles. (a)
 2,3-Dibromopropan-1-ol, K_2CO_3 , DMF, 110 °C, 18 h, 21 %.

3.2.2.3 Synthesis of Novel Core Alterations

Finally, work was begun on the Nybomycin core alterations shown in Section 3.2.1.3 Figure 45 and 46. The first approach was shown in Figure 49. The first disconnection was the new heterocycle as this would potentially allow for different heterocyclic cores to be synthesised from a common intermediate. Next the pyridone was disconnected, followed by the 6-membered ring.

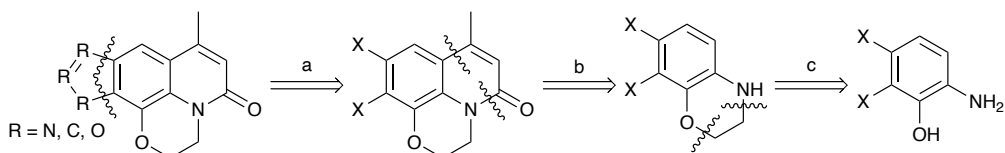
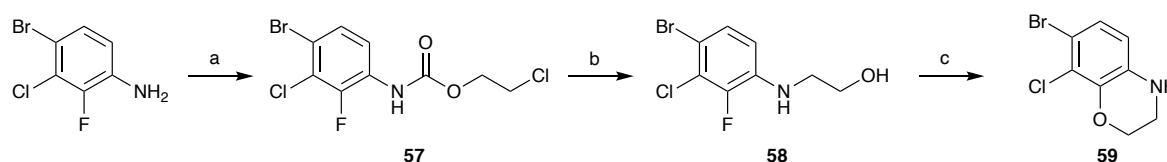


Figure 49 – Retrosynthetic plan for the novel core alterations. a) Heterocycle formation, b) Pyridone formation, c) 6-Membered ring formation.

The first step in this approach involved the synthesis of amino alcohol **58**, shown in Scheme 33. Particular care needs to be taken when forming this amino alcohol *via* nucleophilic substitution with the aniline as there is a potential for over-reaction. In order to avoid this potential issue of over addition products, the method shown in Scheme 33 was chosen. 4-Bromo-3-chloro-2-fluoroaniline was treated with 2-chloroethyl chloroformate to form the carbamate **57**. Then under basic conditions was cyclised to form the cyclic carbamate and then ring opened with hydroxide which led to a decarboxylation reaction to afford the amino alcohol **58**. Next the intramolecular S_NAr was attempted using sodium hydride but only

a disappointing isolated yield (19 %) of **59** was achieved. Optimisation was attempted by screening alternative bases (NEt₃, DIPEA, KOH, ^tBuOK), a range of temperatures (50 - 150 °C) in several solvents (THF, DMF, 1,4-dioxane), but none of these changes led to significant improvements. The challenge of this step seemed to be due to the very poor solubility of the product **59**, as exemplified by the need to run the ¹H NMR in *d*-TFA at elevated temperatures in order to observe any of the product resonances. As a result of the poor solubility of this intermediate and the difficulties that this would cause for large scale synthesis, this approach was abandoned.



Scheme 33 – Synthesis of 6-membered ring intermediate 59. (a) 2-Chloroethyl carbonochloridate, pyridine, CH₂Cl₂, 0 °C to rt, 5 h, quantitative yield, (B) KOH, EtOH, rt, 18 h, 88 %, (c) NaH (60 % mineral oil), THF, 50 °C, 18 h, 19 %.

The next approach involved pre-forming the heterocyclic ring prior to formation of the pyridone, shown in Figure 50. This had the benefit of being able to vary the pyridone substituent (ethyl, cyclopropyl or 6-membered ring) from a late-stage intermediate.

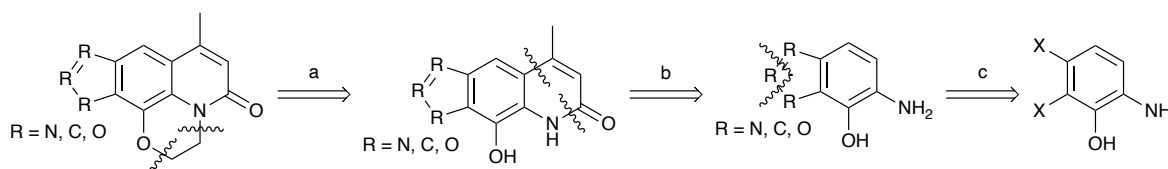
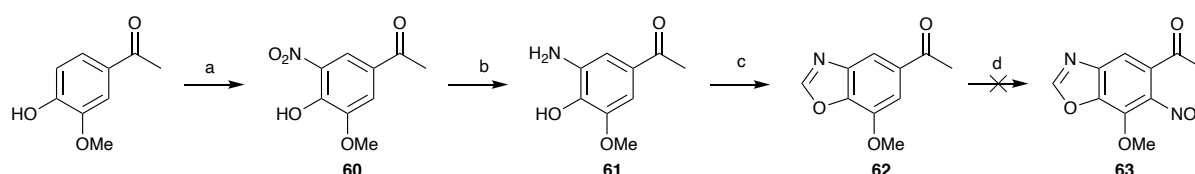


Figure 50 – Second retrosynthetic plan for the novel core alterations. a) 6-Membered ring formation, b) Pyridone formation, c) Heterocycle formation.

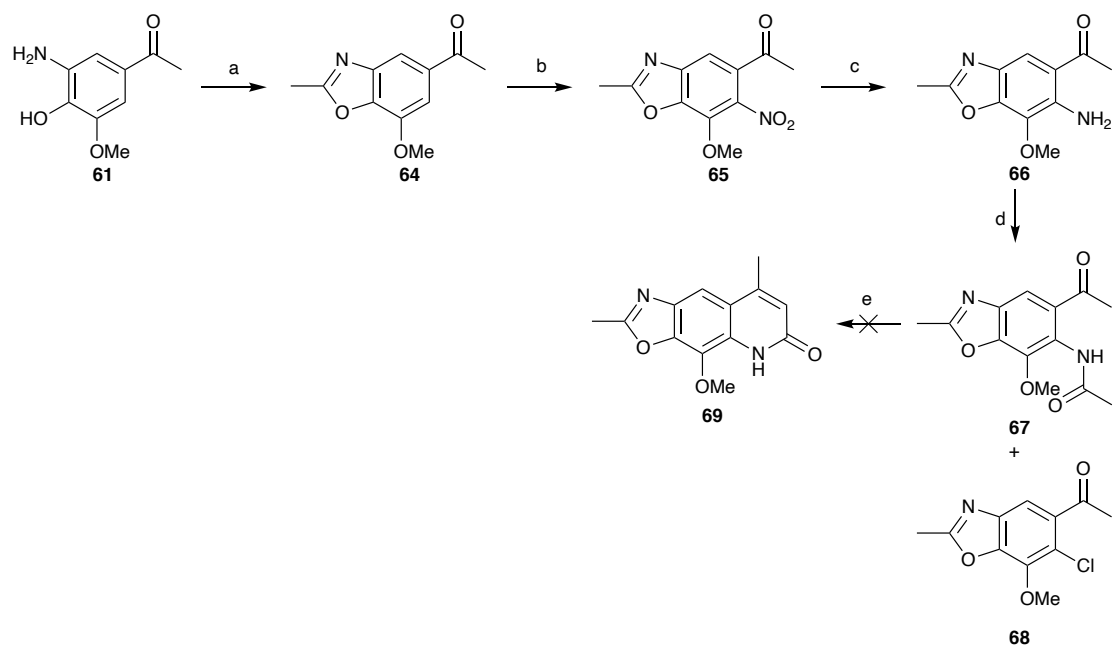
The first heterocycle to be selected for synthesis was the oxazole **Core1-NEt** (Figure 46) as it would test if it was possible to form the new interaction with Arg1122 (*S. aureus* numbering) as suggested by the docking, shown in Figure 46.

The first step in the formation of oxazole **62** was a nitration of 1-(4-hydroxy-3-methoxyphenyl)ethan-1-one, shown in Scheme 34. This was achieved in a good yield (67 %) to give intermediate **60** under the nitration conditions (nitric acid and acetic acid) reported by Learmonth and co-workers.²³⁴ Next the nitro functional group was reduced with hydrogen and palladium on carbon to form aniline **61** in a good yield (67 %) and then cyclised with triethyl orthoformate to afford oxazole **62** in an excellent yield (93 %). However, nitration of oxazole **62** proved to be problematic under standard conditions (nitric acid in acetic acid) or when using *ortho*-selective Menke conditions (copper(II) nitrate hexahydrate in acetic anhydride). The problem appeared to be the stability of the oxazole under the acidic reaction conditions.



Scheme 34 – Synthesis of oxazole **62 and failed nitration to **63**.** (a) HNO₃, AcOH, 0 °C to rt, 18 h, 67 %, (b) H₂, Pd/C (10 %), EtOH, rt, 18 h, 67 %, (c) Triethyl orthoformate, DMF, 105 °C, 18 h, 93 %, (d) HNO₃, HOAc, 0 °C to rt, 18 h, or Cu(II)(NO₂)₃·3H₂O, Ac₂O, 0 °C to rt, 18 h.

To combat this apparent acidic instability a methyl oxazole was instead selected for synthesis, shown in Scheme 35. Methyl oxazole **64** was formed from intermediate **61** using triethyl orthoacetate with an acid catalyst (trifluoroacetic acid) in excellent yields (98 %). Pleasingly, nitration on this material under Menke conditions afforded the *ortho*-isomer **65** in an acceptable yield (35 %).



Scheme 35 – Successful synthesis of methyl oxazole 67 and failed aldol ring closure to form 69. (a) Triethyl orthoacetate, TFA, rt, 18 h, 98 %, (b) $\text{Cu(II)(NO}_2)_3 \cdot 3\text{H}_2\text{O}$, Ac_2O , 0 °C to rt, 18 h, 35 %, (c) H_2 , Pd/C (10 %), EtOH, rt, 18 h, quantitative yield, (d) AcCl, NEt_3 , CH_2Cl_2 , rt, 18 h, **67** (54 %), **68** (23 %), (e) $^t\text{BuOK}$, $^t\text{BuOH}$, 50 °C, 18 h.

The regiochemical selectivity of this nitration was tolerable (1.6: 1, *ortho*: *para*, relative to the methoxy group). The regio isomers can be differentiated using Nuclear Overhauser effect (NOE) NMR, shown in Figure 51. When the aryl proton is excited, for the *ortho* isomer **65**, cross relaxation is seen in the ketone CH_3 (Figure 51A). For the *para* isomer **70**, when the same aryl proton is excited cross relaxation is observed in both the ketone CH_3 and methoxy CH_3 resonances (Figure 51B).

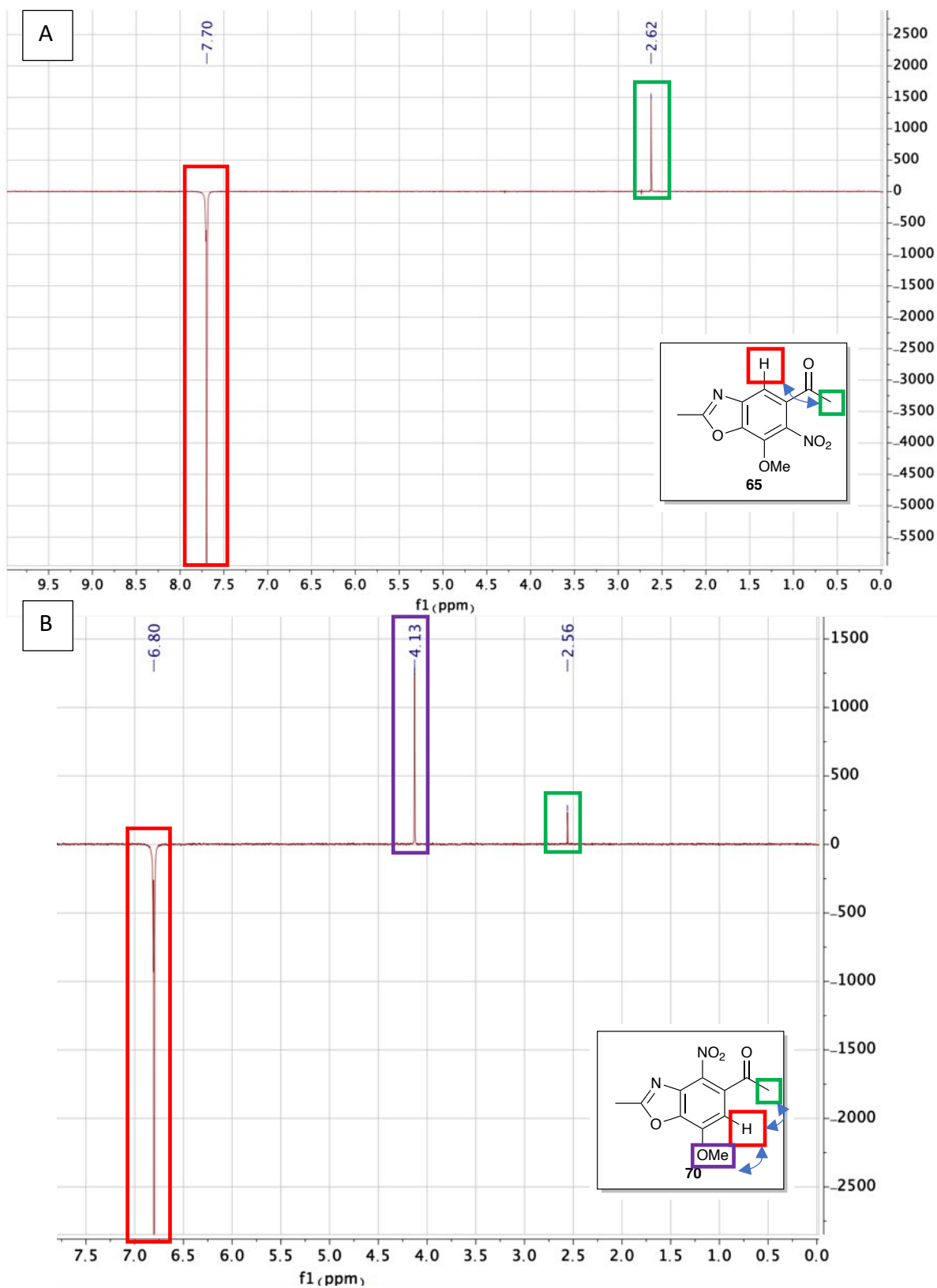


Figure 51 – Nuclear Overhauser effect (NOE) NMR spectra of both nitro isomers. A – NOE spectra of the *ortho* isomer **65. B - NOE spectra of the *para* isomer **70**.**

Compound **65** was then reduced using hydrogen and palladium on carbon to give the aniline **66** in a quantitative yield. Acetylation using acetyl chloride afforded two products, the desired acetylated intermediate **67** in an acceptable yield (54 %) and interestingly the chloride product **68** (isolated yield 23 %). The formation of the chloride **68** is probably due to steric crowding that results in the substitution by the chloride being energetically favourable despite the acetamide being a relatively poor leaving group. The next step was to form the novel oxazole core **69** via an aldol-type reaction using a strong base (potassium *tert*-butoxide). However, this reaction didn't result in cyclisation and instead degradation occurred. Following this result, this second approach was abandoned in preference for building the pyridone ring first, followed by formation of the heterocycle. The retrosynthetic analysis for this third approach is shown in Figure 52. This strategy has the added potential benefit of being able to form multiple novel cores from a common intermediate, varying both the heterocycle and substituents on the pyridone.

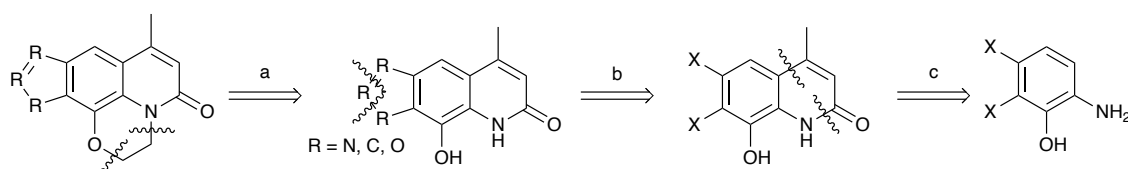
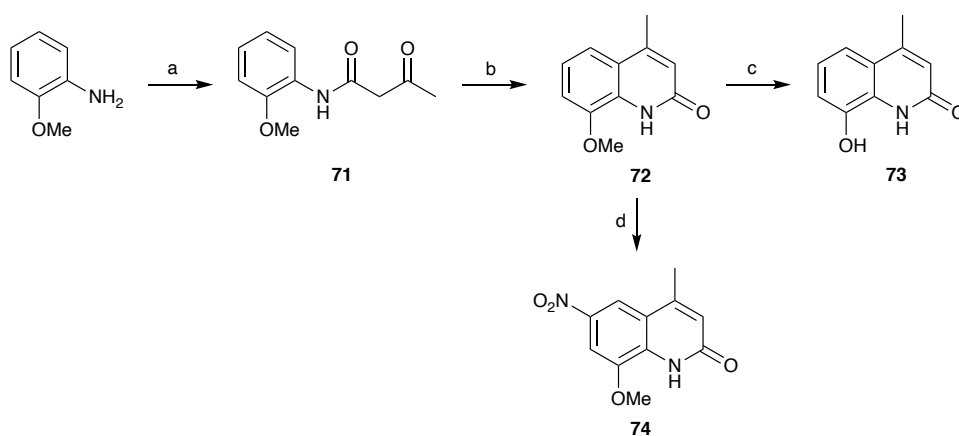


Figure 52 – Third retrosynthetic plan for the novel core alterations. a) 6-Membered ring formation, b) Heterocycle formation, c) Pyridone formation.

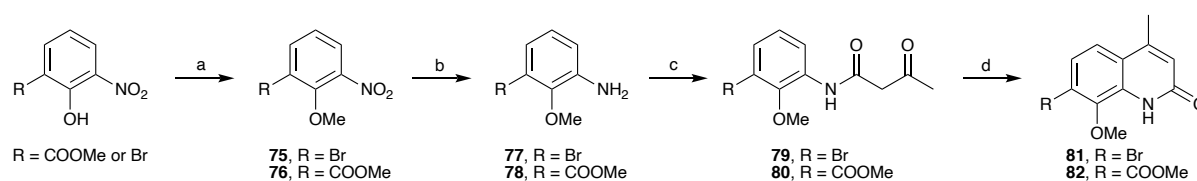
In order to facilitate the core diversification plans, a flexible intermediate would need to be synthesised that would allow for late stage derivatisation to a range of heterocycles. The first step was therefore to construct the fused 2-pyridone ring **72**. 2,2,6-Trimethyl-4*H*-1,3-dioxin-4-one was opened with *ortho*-anisidine to give the corresponding *ortho*-acetoacetanilide **71**, shown in Scheme 36. A cyclisation with triflic acid yielded the fused 2-pyridone ring **72** in a

good yield (80 %) with a simple purification (precipitation with water then filter). Deprotection of the methoxy to afford the free phenol **73** was achieved cleanly in excellent yields (99 %) using boron tribromide. This gave confidence that the cleavage of the methoxy group could be achieved in high yields and meant that the aliphatic ring, using the reaction conditions in Section 3.1.2.3 Scheme 21 Step d, could be installed at this stage if required. Next nitration of the fused 2-pyridone ring **72** was attempted and yielded the *meta*-isomer (with respect to the methoxide) as the major product **74** (2.3: 1, *meta*: *ortho/para*). The regioisomers can be differentiated by the magnitude of the coupling constant (*J* value) of the aryl protons. For the *meta* isomer **74** the *J* value is 2.1 Hz which is in the range for *meta* coupling in an aromatic system (*J* = 1 – 3 Hz). For the *ortho/para* isomer the *J* value is 8.6 Hz which is in the range for adjacent protons on an aryl system (6 – 10 Hz). This outcome suggests the *para*-directing amidic nitrogen dominates the *ortho/para*-directing nature of the methoxy group. This was an important finding as this regiochemical outcome wasn't anticipated and the major isomer (*meta* product **74**) provides a useful handle to start building a range of heterocycles.



Scheme 36 – Independent ring construction. (a) 2,2,6-Trimethyl-4*H*-1,3-dioxin-4-one, H₂O, 100 °C, 18 h, quantitative yield, (b) Triflic acid, CH₂Cl₂, 0 °C to rt, 4 h, 80 %, (c) BBr₃ (1 M), CH₂Cl₂, -78 °C to rt, 18 h, 99 %, (d) HNO₃, AcOH, 0 °C, 1.5 h, 66 % (NMR yield).

Building on the success of this approach to form the fused 2-pyridone ring **72**, both the *ortho*-bromo **81** and *ortho*-ester **82** derivatives of *ortho*-anisidine were selected for synthesis, shown in Scheme 37. These two compounds would allow assessment of the functional group tolerance (in terms of stability and electronics of the core) of this approach and afford intermediates with synthetic handles that would allow for further functionalisation once the cyclisation had occurred. The required anilines **77** and **78** could be synthesised from the corresponding commercially available nitro alcohols *via* a methylation to form **75** and **76**, then a nitro reduction. Both the anilines **77** and **78** successfully reacted with 2,2,6-trimethyl-4*H*-1,3-dioxin-4-one to form the corresponding *ortho*-acetoacetanisides **79** and **80**. However, only the *ortho*-bromo *ortho*-acetoacetaniside **79** underwent the cyclisation to form the fused *ortho*-bromo 2-pyridone ring **81**. This outcome demonstrates the importance of the electronics of the core for the cyclisation and the problems when using electron withdrawing substituents. In this instance, the aromatic ring in **80** was too electron-poor to undergo the desired cyclisation so instead amide hydrolysis was observed.

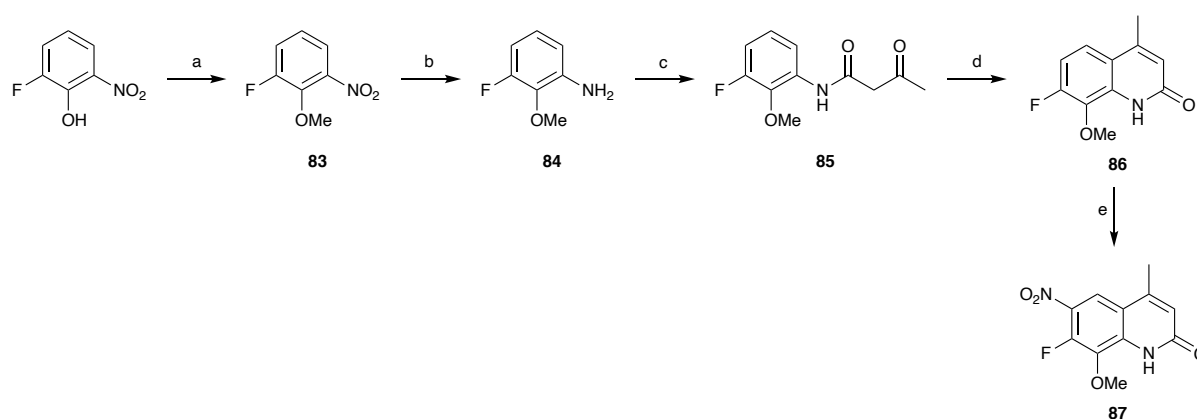


Scheme 37 – Acid cyclisation on more functionalised analogues. (a) MeI, K₂CO₃, DMF, 45 °C, 18 h, **75** - 87 %, **76** - 98 %, (b) H₂, Pd/C (10 %), THF, rt, 18 h, **77** - 85 %, **78** - 94 %, (c) 2,2,6-trimethyl-4*H*-1,3-dioxin-4-one, AcONa, THF, 85 °C, 22 h, **79** - 91 %, **80** - 96 %, (d) Triflic acid, CH₂Cl₂, 0 °C to rt, 24 h, **81** - 61 %, **82** reaction failed.

Building on the successful synthesis of the *ortho*-bromide derivative **81**, the *ortho*-fluoro analogue was selected for synthesis. The fluoride functional group is weakly electron withdrawing but to a much lesser extent than the methyl ester. It was therefore hoped that

this substrate would not be problematic for the cyclisation. As the fluoride is an ortho/ para directing group it may also increase the selectivity of the nitration.

Pleasingly, the synthesis using this substrate progressed well to the fused pyridone **86**, shown in Scheme 38. The product **86** was then nitrated (nitric acid and acetic acid in acetic anhydride) which formed a mixture of *meta* and *para*-isomers (2: 1 *meta*: *para*, with regards to the methoxy). The isomers were again differentiated by the magnitude of the coupling constant of the aryl proton and the fluoride. The *meta* isomer **87** had a J value of 7.3 Hz whereas the *para* isomer had a larger J value of 10.9 Hz indicating, that in this case, the proton was closer in proximity to the fluoride. While the fluoride substituent didn't appear to have a significant effect on the regiochemical outcome of the nitration, it did allow for isolation of the desired regioisomer **87** via trituration removing the need for a laborious separation using column chromatography.

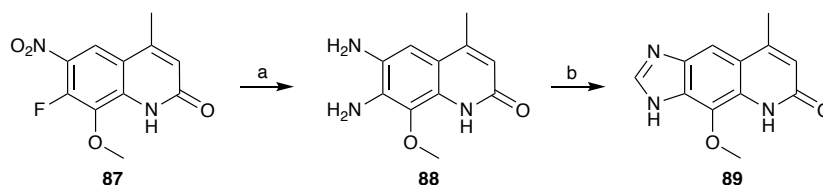


Scheme 38 – Synthesis of Nitro fluoro intermediate 87. (a) MeI, K₂CO₃, DMF, rt, 18 h, 76 %, (b) H₂, Pd/C (10 %), MeOH, rt, 18 h, 91 %, (c) 2,2,6-trimethyl-4H-1,3-dioxin-4-one, xylene, 120 °C, 18 h, 97 %, (d) Triflic acid, CH₂Cl₂, 0 °C to rt, 18 h, 81 %, (e) HNO₃, AcOH, Ac₂O, 0 °C to rt, 18 h, 44 %.

The next step attempted was to form imidazole **89** via an S_NAr reaction, shown in Scheme 39.

This was achieved using sodium azide as the nucleophile and then reduction with hydrogen

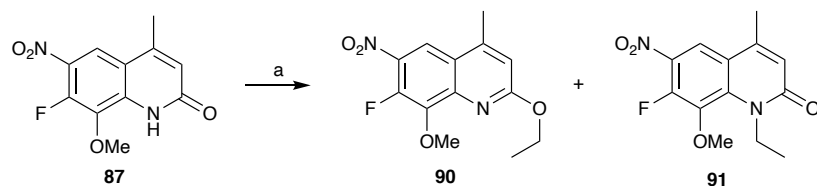
and palladium on carbon to yield the dianiline **88** (84 % yield over the two steps). This was then successfully cyclised to the novel imidazole core **89** using triethyl orthoformate and an acid catalyst in an excellent yield (96 %).



Scheme 39 – Formation of imidazole **89.** (a) i) NaN_3 , DMF, rt, 18 h, ii) H_2 , Pd/C (10 %), EtOH, rt, 18 h, 84 %, (b) Triethyl orthoformate, TFA, DMF, rt, 18 h, 96 %.

Ethylation of imidazole **89** was attempted and yielded a major and minor product. Unfortunately, the two products proved inseparable under normal phase conditions and so this approach was abandoned and the ethyl group would have to be pre-installed earlier in the synthesis.

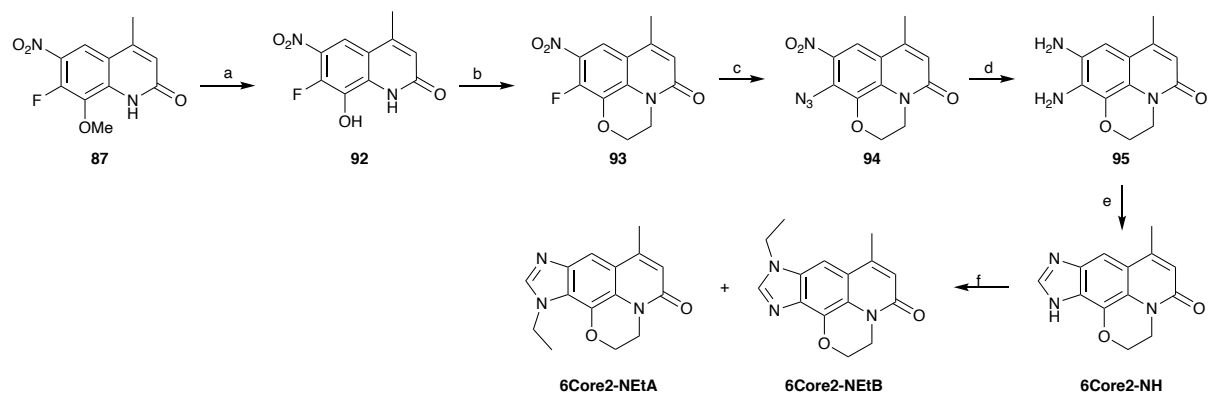
Now that synthesis of the imidazole core had been successful, attempts were made to form the match pairs of the best analogue from the initial work on **6DNM-2**. Ethylation was attempted on intermediate **87** but unfortunately it formed a mixture of regioisomers with the *O*-alkylated **90** (69 % isolated yield) as the major product and the desired *N*-alkylated **91** (11 % isolated yield) as the minor product, shown in Scheme 40.



Scheme 40 –Ethylation regiochemical issues. (a) NaH (60 % mineral oil), EtI, DMF, 50 °C, 2 h, **90** - 69 %, **91** - 11 %.

The regioisomers can be differentiated by the chemical shift of the carbon in the CH₂ of the ethyl group in a similar manner to previously seen in this work using the literature analysis shown in Figure 27. For the *O*-alkylated isomer the resonance of the CH₂ of the ethyl was at 62.6 ppm, whereas for the *N*-alkylated isomer the chemical shift of the same CH₂ was at 41.7 ppm. This result indicates that the ethylation needed to occur prior to the pyridone formation as this distribution of products is unacceptable given the previously established SAR.

Given the synthetic challenge of preparing the ethyl analogues, the synthesis of the cyclised analogues **6Core2-NEtA** and **6Core2-NEtB** were explored, shown in Scheme 41. Firstly, intermediate **87** was demethylated using boron tribromide to give intermediate **92** in a quantitative yield. The product was then cyclised using 1,2-dibromoethane to give intermediate **93** in a modest yield (30 %). The main by-product of this reaction (22 % isolated yield) was nucleophilic displacement of the fluoride with dimethylamine, presumably from partial decomposition of the solvent (DMF) at elevated temperature. Improvements to this step could therefore be made by swapping the solvent to 1,4-dioxane or DMSO. **93** was then converted to the imidazole core using the same method as before *via* the azide **94** (quantitative yield), dianiline **95** (quantitative yield) and cyclised to the imidazole **6Core2-NH** (60 %). The resultant product was then ethylated to give both regioisomers **6Core2-NEtA** (22 % yield) and **6Core2-NEtB** (14 % yield) for microbiological evaluation. The two ethylation regioisomers were assigned using two dimensional NOE NMR. For **6Core2-NEtB** a cross relaxation was observed for the CH₂ of the ethyl group and the aryl-H of the central aromatic core.



Scheme 41 – Synthesis of the novel imidazoles 6Core2-NEtA and 6Core2-NEtB. (a) HBr (aq.) 135 °C, 18 h, quantitative yield, (b) Dibromoethane, K₂CO₃, DMF, 110 °C, 18 h, 30 %, (c) NaN₃, DMF, rt, 18 h, quantitative yield, (d) H₂, Pd/C (10 %), CH₂Cl₂, EtOH, rt, 18 h, quantitative yield, (e) Triethyl orthoformate, TFA, DMF, rt, 18 h, 60 %, (f) NaH (60 % mineral oil), EtI, DMF, rt, 18 h, **6Core2-NEtA** - 22 %, **6Core2-NEtB** - 14 %.

The successful synthesis of these analogues, **6Core2-NEtA**, **6Core2-NEtB** and **6Core2-NH**, were not only important in terms of testing a novel Nybomycin core but these particular analogues also allowed for the importance of the ethyl group and its position to be explored.

3.2.3 Predictors for Aqueous Solubility.

Given the challenges experienced previously with the series, it was important to quantify how the structural changes made affected aqueous solubility. In the absence of an aqueous solubility assay, the melting point of the compounds were taken and the aqueous solubility of the compounds were predicted using the ADMETlab platform. Work by Yalkowsky and co-workers^{235,236} has shown that a compounds melting point has a very good correlation with the compounds aqueous solubility.²³⁷ The melting points and the predicted aqueous solubility score (logS), calculated using the ADMETlab platform, for selected Nybomycin analogues are shown in Table 3.

Number	Structure	Melting point (°C)	Predicted Aqueous Solubility (logS, log mol/L)	ClogP	ClogD
46		274.2	-3.472	1.692	-0.664
25		255.4	-3.798	2.185	0.215
6DNM-NH		289.7	-3.374	1.852	0.243
6DNM-Cyclo		277.7	-3.784	2.661	1.127
6DNM-2		239.5	-3.561	2.346	0.921
6DNM-2-OH		246	-3.605	1.879	0.59
6DNM-2-L1A		178.2	-4.172	3.373	1.553

Table 3 – Melting points of key Nybomycin derivatives. Predicted aqueous solubility score (logS) was calculated using the ADMETlab platform, a score of > -4 log mol/L is predicted to give a highly soluble compound.²³⁸ The values are coloured from green – most likely to give a highly aqueous soluble compound to red – less likely to give a aqueous soluble compound.

Firstly, the melting point of the undecorated core **46** was determined. Addition of the ethyl group **25** lowered its melting point by ~ 20 °C, this is in line with the idea from earlier that the ethyl group can add to the three-dimensionality of the molecule and help disrupt the π -stacking interactions lowering the overall lattice enthalpy of the solid form. However, addition of the 6-membered ring **6DNM-NH** increased the melting point by ~ 15 °C. This suggests that addition of the 6-membered ring doesn't disrupt the π -stacking. The combination of both these changes, **6DNM-2**, has an effect on the melting point, lowering it by 35 °C. This may suggest that the 6-membered ring may be helping to push the ethyl group out of the plane of the molecule, effecting the conformation of the molecule and disrupting the π -stacking, but this would need to be further investigated with an X-ray crystal structure of the compound. Interestingly though this affect is not seen with the cyclopropyl group **6DNM-Cyclo** as this has a very similar melting point to the undecorated core **46**. Small extensions (-CH₂OH, **6DNM-2-OH**) off the 6-membered ring have a negligible effect on the melting point. However, pleasingly a 100 °C decrease in melting point was achieved with the methylene piperidine **6DNM-2-L1A**. This compound should be significantly more soluble in water than the undecorated core **46** or even **DNM-2**, although further profiling with both kinetic and thermodynamic aqueous solubility methods would need to be undertaken to confirm this. Overall, this data indicates that the hypothesis of increasing the three-dimensionality and adding a polarisable centre to increase aqueous solubility is a valid one as highlighted by the most promising analogue **6DNM-2-L1A**.

Next the predicted properties could then be examined. The predicted aqueous solubility gave roughly the same rank order for the compounds as the melting point so more confidence can be given to the results. An interesting discrepancy was observed with the compound **6DNM-Cyclo**. Its predicted solubility score (-3.784 log mol/L) was one of the best whereas its melting

point (277.7 °C) would indicate it is one of the least soluble. A possible explanation for this could be that this compound formed a particularly stable polymorphic form which would require more energy to break up, hence the higher melting point. **6DNM-2-L1A** had the greatest solubility score (-4.172 log mol/L) and was predicted to have highly aqueous solubility. This was a great result and showed promising steps had been made to address the aqueous solubility to of the series.

However the predictions for ClogP and ClogD for this series of compounds are in do not add value to the discussion around thesis analogues. Take compound 44 for example with a ClogP of 1.7 and ClogD of -0.7 one would expect this compound to be extremely soluble in water. However practically this compound is extremely insoluble in water and it is isolated *via* precipitation with water. It would seem the calculations do not account for intermolecular π -stacking, making melting point a better surrogate for aqueous solubility than ClogP or ClogD as the solubility appears to be driven by lattice enthalpy. Also the dramatic differences in ClogP and ClogD would indicate that the model estimates a large proportion of the molecules are charged at pH 7.4. This seems very unlikely considering the pKa of the heteroatoms in question. Take 6DNM-2 for example with a reported ClogP of 2.3 and ClogD of 0.9 but where is the ionisable centre at pH 7.4?

3.2.4 Kirby–Bauer Disc Diffusion Assay for New Analogues

The next step was to evaluate the activity of the successfully synthesised compounds in the previously described Kirby–Bauer Disc Diffusion assay, shown in Table 4. **6DNM-2** and **7DNM-2** were used as controls as they were shown to be two of the most active analogues in the previous iteration (Table 1). The in-house *E. coli* bacterial strains with *S. Typhi* gyrase/topo IV were again chosen as the most appropriate to investigate the activity of these new derivatives. As in Part 1 of this work, both the wild type (M0) and triple mutant (M6) were used to investigate the mutant selective phenotype of these compounds. In Section 3.1 it was shown that all Nybomycin analogues appeared to be good efflux substrates *via* the AcrAB/TolC efflux channel. This meant that no activity was observed using the in-house *E. coli* strains and so the TolC knock-out strains were created, see Section 3.1.4. In this section the new compounds were tested against both the efflux competent M0 and M6 and also the reduced efflux M0 Δ TolC and M6 Δ TolC *E. coli* strains. This was to investigate whether any of the structural changes made had led to a change in efflux profile.

Firstly, the substitution of ethyl to cyclopropyl was evaluated. Unexpectedly, this change had a slight detrimental effect on activity. This was a disappointing result and also cast doubt on the binding pose of this compound compared with Ciprofloxacin. It seemed unlikely that if the binding mode did directly overlay the ethyl and cyclopropyl groups of these two molecules, that a similar effect on activity wouldn't be observed. However, the substitution of ethyl to cyclopropyl also had a detrimental effect on solubility shown in both the increased melting point, **6DNM-2** vs **6DNM-2-Cyclo** in Table 3, and also the difficulty in obtaining longer NMR analysis of **6DNM-2-Cyclo**. This poor solubility could potentially be a factor in explaining the lack of an increase in activity observed with the cyclopropyl compound since it may have

affected the actual concentration of compound being tested, although no visual precipitation was observed.

The undecorated cores **46** and **13** showed no activity against any of the strains tested. This was thought to be due to a lack of target affinity and demonstrated the importance of the aliphatic ring and ethyl substitution off the pyridone. Particularly poor solubility could also be a factor here. Interestingly, just the addition of the ethyl group **25** on the pyridone markedly increased the activity and solubility (in chloroform/ methanol) of the compound – again demonstrating the importance of the ethyl group.

Addition of the methylene OH **6DNM-2-OH** and the methylene piperidine **6DNM-2-L1A** were the two most promising results and these changes appeared to be at least as active if not more active than the previously most potent analogue **6DNM-2**. More quantitative antibiotic activity assays would need to be carried out in order to more accurately rank these compounds. This was a particularly promising result as these compounds also had improved solubility, at least when handling in chloroform/ methanol, compared to **6DNM-2**, and certainly **6DNM-2-L1A** had a significantly reduced melting point. It would be interesting to more thoroughly evaluate the solubility of these compounds *via* kinetic and thermodynamic solubility assays. Interestingly, addition of the methylene piperidine **6DNM-2-L1A** was the first compound in our collection to show activity on unaltered Gram-negative bacterial strains.

The carbamate derivatives **6DNM-L2B**, **6DNM-L2D**, **6DNM-L2E** showed reasonable inhibition with the hydroxy piperidine **6DNM-L2E** being the most potent. This was the analogue predicted by molecular overlay to be most active as it looked to be able to pick up a hydrogen bond. This compound showed comparable activity compared to the previously most potent analogue **6DNM-2** but did not show the activity boost predicted by the molecular overlay.

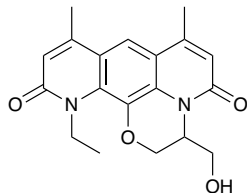
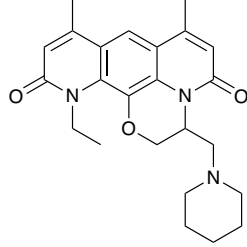
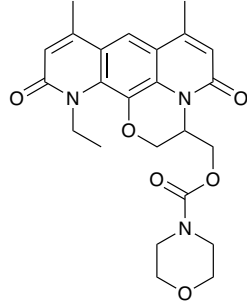
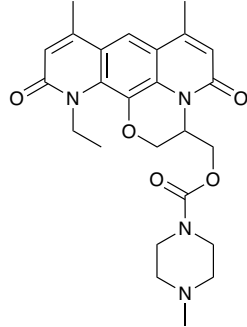
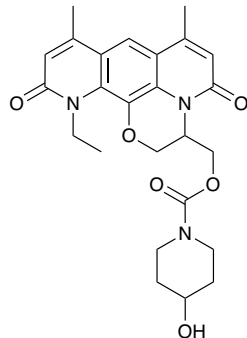
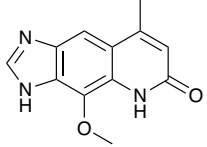
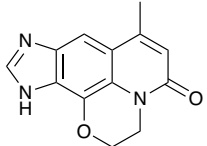
This lack of increase in activity would suggest that no additional hydrogen bonds were being picked up and would seem to disagree with the computational work– Figure 41B. Of course you also have additional entropic penalties with the carbamate derivatives that you do not have with **6DNM-2** which could go some way to explaining this lack of additional activity. However, the three carbamate linked analogues **6DNM-L2B**, **6DNM-L2D**, **6DNM-L2E** were also all less potent than the methylene linked **6DNM-2-L1A** suggesting that the methylene linker was favoured, again contradictory to the molecular overlays. One caveat of this is that the carbamate linked piperidine match pair of **6DNM-2-L1A** was unfortunately not successfully synthesised and so it would be interesting to have another attempt at synthesising this compound as future work to see whether it is this particular amine that is buying the activity or the linker, or both.

Finally, the novel imidazole core was evaluated. The undecorated core **89** showed no activity, however poor solubility meant that some precipitation was observed whilst running the assay. This means that the compound was likely to have been tested at a much lower concentration than desired and so may explain the lack of activity. Of course the lack of any decoration may also explain the lack of activity as seen previously with **46** and **13**. The cyclised analogue **6Core2-NH** showed mild inhibition on both the efflux compromised strains (M0 Δ TolC and M6 Δ TolC). This was a really promising result as such a drastic change in the core structure of the molecule had no guarantee of being able to maintain any activity against the target. Next the closest match pairs (**6Core2-NEtA** and **6Core2-NEtB**) to **6DNM-2** were analysed. The ethyl analogues showed improvements in activity compared to the NH imidazole **6Core2-NH** similar to the effect shown in the pyridone series. The regio chemistry on the ethylation of the imidazole appeared important for activity. It appeared to be in agreement to what would have been expected from superimposing these compounds with

6DNM-2 and suggests that this core may have a similar binding mode. The activity of **6Core2-NEtA** was a great result and for the first time showed it was still possible to maintain the mutant selective phenotype while being able to differentiate from the bis-pyridone core. An important observation across the data, was that for the majority of active compounds, a stronger inhibition was seen against the triple mutant strain (M6 Δ ToIC) than the WT (M0 Δ ToIC). This fits with the mutant selective phenotype of this series. **6DNM-2-L1A** was one of only three compounds to not show this phenotype at the higher concentration, however this could be due to the limit of the assay being reached in terms of limiting bacterial growth since the phenotype is observed at the lower concentration. The other two compounds **25** and **6Core2-NH** both suffered from poor solubility and precipitate being observed in the assay. The previously reported result about the importance of bacterial efflux by the TolC/AcrAB channel was also confirmed. In general, the new analogues showed no activity against the WT TolC strains and showed activity after TolC was removed. This meant that all the new compounds were still good substrates for efflux *via* the AcrAB/TolC efflux channel and were not able to compensate for this *via* uptake mechanisms. In agreement with the findings of Hergenrother and co-workers,⁸¹ the only exception to this was **6DNM-2-L1A**. This finding confirmed the importance of a polarisable nitrogen for activity against *E. coli* with competent efflux. It is important to state that the addition of the polarisable amine is thought to increase the uptake of the compound, *via* a porin-based mechanism, rather than have any effect on efflux directly. Interestingly **6DNM-L2D** showed no activity on the WT TolC strains. The pKa of methyl piperazine was approximated to be around 7.3, based on the experimentally determined pKa of a similar piperazine carbamate analogue studied by M. Harfenist.²³⁹ Although not fully ionised at physiological pH, it was hoped that partial ionisation may have assisted entry into *E. coli*. This appeared not to be the case, however lack of activity against

the unaltered *E. coli* could also be explained due to the shape parameters of the compound no longer being satisfied to increase the porin uptake compared to the methylene piperidine. Alternatively, the carbamate linked compound was not sufficiently potent to show activity against the unaltered *E. coli*.

Compound	Structure	Zone of Inhibition (cm)							
		WT TolC				Without TolC			
		M0		M6		M0		M6	
		1 mmol	10 mmol	1 mmol	10 mmol	1 mmol	10 mmol	1 mmol	10 mmol
6DNM-2		0	0	0	0	1.6	2	1.8	2.3
7DNM-2		0	0	0	0	1.1	1.5	1.7	2
6DNM-2-Cyclo		0	0	0	0	0	1.6	0.8	1.8
46*		0	0	0	0	0	0	0	0
13*		0	0	0	0	0	0	0	0
25*		0	0	0	0	1	1.8	1.2	1.8

6DNM-2-OH		0	0	0	0	1.6	2.2	2	2.6
6DNM-2-L1A		0	1	0	1	1.8	2.6	2	2.6
6DNM-L2B		0	0	0	0	0	1.2	0.8	2
6DNM-L2D		0	0	0	0	0	1.2	0	1.6
6DNM-L2E		0	0	0	0	0	1.6	1.2	2.2
89*		0	0	0	0	0	0	0	0
6Core2-NH*		0	0	0	0	0	0.8	0	0.8

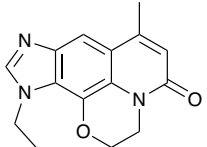
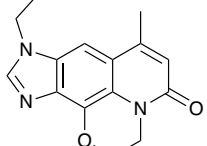
6Core2-NEtA		0	0	0	0	0	1	0	1.6
6Core2-NEtB		0	0	0	0	0	0	0	1

Table 4 – Antibiotic activity of new Nybomycin analogues. Compounds were tested at 1 mmol and 10 mmol using the Kirby–Bauer disc diffusion assay with 7 replicates. The *E. coli* strains used were M0, the optimised Wild type GyrA and ParC and M6, the triple mutant GyrA S83F D87N ParC S80I. * - denotes precipitate in the solution of the compound in CHCl₃/MeOH, these compounds were added to the discs as a suspension.

3.2.5 Section Conclusion

In summary, strategies were trialled to help improve the aqueous solubility of the Nybomycin family of natural products. The main attempt to do this involved increasing the three-dimensionality of the series and introducing a polarisable nitrogen. Molecular overlays were used in an attempt to rationalise where this solubilising handle could be placed on the Nybomycin core. A pocket was identified that looked to be the position exploited by the C-7 substituent of the fluoroquinolone series. According to the binding pose generated in this molecular overlay study this pocket was assessable from the aliphatic ring of **6DNM-2**. Two series were designed to explore this pocket, the methylene amines and the carbamates. These gave a varied linker length and different amines were used to explore the polarity and space in the pocket. After successful synthesis and analysis of the antibacterial activity of the compounds using the Kirby–Bauer disc diffusion assay, the methylene amine **6DNM-2-L1A** was found to be the most potent analogue to date and also possessed mild activity against efflux competent *E. coli*. The carbamate compounds (**6DNM-L2B**, **6DNM-L2D** and **6DNM-L2E**) although had moderate activity, were less potent than the methylene linked compound **6DNM-2-L1A**. The caveat here is that these compounds also had different solubilising amines attached and so a match pair is needed to confirm this SAR.

The effect on solubility of adding the methylene piperidine was also investigated. As there was no access to a kinetic or thermodynamic solubility assay, the melting points of the compounds were examined as a surrogate for their aqueous solubility. **6DNM-2-L1A** showed a significant drop in the melting point (~100 °C) when compared to the undecorated core **46**. This should correspond to a marked increase in aqueous solubility for **6DNM-2-L1A** as the lattice enthalpy of the solid form has greatly decreased. This gives good evidence that this strategy to improve aqueous solubility has been successful.

In conclusion, a novel compound **6DNM-2-L1A** has been designed and synthesised which is significantly more potent and more soluble than the literature Nybomycins. This can make an exciting tool compound for further mechanistic studies and potentially even crystallography to establish a binding site for this exciting class of antibiotics.

The substitution of ethyl to cyclopropyl was also explored for the Nybomycin series. This change gave a boost in activity for the fluoroquinolone series but unfortunately seemed negligible or slightly detrimental to the Nybomycin series, despite the promising molecular overlay result. This could suggest a subtle difference in the binding mode of the Nybomycin family compared to the fluoroquinolones.

More drastic changes to the core structure of the Nybomycin family were also examined. Synthesis of these new cores proved challenging but the imidazole match pairs to **6DNM-2 (6Core2-NEtA and 6Core2-NEtB)** were successfully synthesised. These compounds, although not as potent as **6DNM-2**, excitingly showed some moderate activity and displayed the same mutant selective phenotype as the initial Nybomycins. This was a very encouraging result and proved that the core could be altered without losing the important phenotypic activity of the Nybomycin series. The novelty of these initial compounds would make these an exciting new sub-series to explore in future work.

4. Concluding Thoughts and Future Work

4.1 Conclusion

In summary, a robust and scalable synthetic route to the Nybomycin series of natural products has been designed and successfully performed. This has led to the synthesis of the best literature compound **DNM-2** and 21 novel analogues. With the tool compound and these novel analogues in hand, the mutant selective phenotype required for a reverse antibiotic has been confirmed and the SAR around the series has been investigated.

The enzymatic activity of the compounds has been investigated in collaboration with Inspiralis Ltd. The most potent analogue tested **6DNM-2** was shown to have a 200-fold greater supercoiling inhibition for mutant (S84L) gyrase than Ciprofloxacin. The compounds were active on Gram-positive bacterial strains (*S. aureus*) but showed no activity on Gram-negative bacterial strains (*E. coli*). This lack of activity on *E. coli* was shown to be due to the compounds being good substrates for AcrAB/TolC mediated efflux. This issue was successfully circumvented by the removal of the TolC or AcrB genes from the *E. coli* strains.

The major issue with the series was aqueous solubility as demonstrated by the difficulty in handling the compounds and precipitation in the microbiology assays. Computational chemistry was used to design new compounds that aimed to alleviate this solubility issue resulting in **6DNM-2-L1A** with a greatly decreased melting point indicating a much improved aqueous solubility. This compound was also excitingly shown to be the most potent analogue made to date in the Kirby–Bauer disc diffusion assay on the *E. coli* strains (M0 Δ TolC and M6 Δ TolC).

Another important finding in this work was the first step to diversify the core of Nybomycin. It was shown the substitution of one of the pyridone rings for an ethyl imidazole was tolerate

albeit with a reduction in activity. This could prove to be an important step in improving the ‘drug likeness’ of the series and also offers more opportunities to modulate the PK properties further down the line.

The key compounds in this series are highlighted in Figure 53.

The limitation with this study was that the zone of inhibition was the only method used to determine antibiotic activity. It would be beneficial to confirm the trends disclosed herein with an alternative method like the MIC measurement. Also more antibiotic strains could be profiled to explore if the trends observed are unique to the strains studied or applicable in general. Eukaryotic toxicity data would be very interesting as this would be necessary for the advancement of this series of inhibitors into further clinical studies.

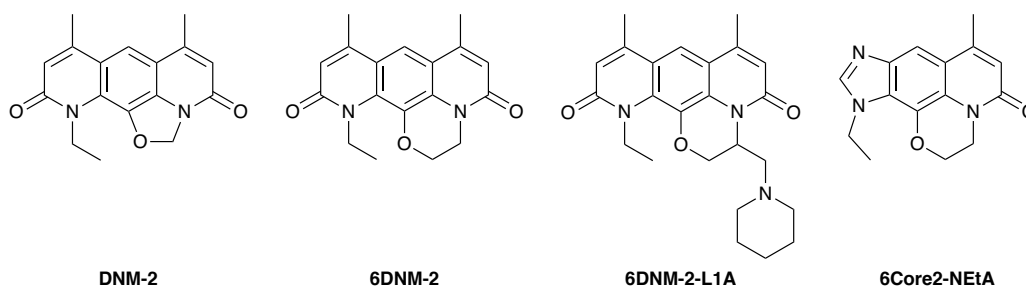


Figure 53 – Literature compound DNM-2 and key Nybomycin derivatives 6DNM-2, 6DNM-2-L1A and 6core2-NEtA.

4.2 Future work

Building on the success of **6DNM-2-L1A**, the next step would be to further investigate the SAR and synthesise the missing carbamate match pair to establish whether it is the piperidine binding potency or the methylene linker. Exploration around further heterocyclic core analogues could also be a very fruitful avenue for optimisation after the successful synthesis of the imidazole core analogues (**6Core2-NEtA** and **6Core2-NEtB**) which showed moderate potency at the higher concentration. Looking at different heterocyclic cores could be

beneficial as there may be more of an opportunity to balance potency with solubility. This would greatly aid the developability of the series. It would be informative to run all the Nybomycin derivatives through a quantitative solubility assay to confirm the melting point results.

In terms of designing novel Nybomycin analogues a crystal structure would help guide design efforts and streamline the process of developing the series. This crystal structure would confirm the binding mode of the Nybomycin series and also at which point of the catalytic cycle it binds. **6DNM-2-L1A** is a good candidate for co-crystallisation with its enhanced solubility and activity.

A thorough investigation of the PK of the series is needed and **6DNM-2-L1A** would be a great candidate here also. Metabolic hot spots in the Nybomycin core and also off target inhibition would need to be identified and these issues solved for this series to become a therapeutic option.

Another important next step for this series is to identify whether the primary biological target in a particular bacterial species is DNA gyrase or topo IV and see how this compares to the fluoroquinolone series. This can be achieved by examining the series activity on gyrase/topo IV at the enzymatic level in a particular species. This will help deconvolute whole cell data where the compound may be acting preferentially on one target over the other. Mutations in the preferred target could then be studied at both the whole cell and enzymatic level. This would allow for any single point mutations that would give the bacterial resistance to both the Nybomycin analogue and fluoroquinolones to be identified. This information is key in determining the clinical implications of the reverse antibiotic strategy.

Further studies on the reversibility of this process in different bacterial strains would also be of great interest and demonstrate how widely applicable this strategy is. It would be very

important to sequence the bacteria at each stage as there may be mutations elsewhere in the genome that would allow the bacterial to become resistant to both antibiotics. It would be intriguing to see how permeability or efflux mutants affect this process and how these potential issues could be overcome by compound design.

Another key area to examine is the effect the Nybomycin series has on the human topoisomerase homologs. Early derivatives published by Hergenrother and co-workers showed partial inhibition of human topoisomerase II at 30 μM .^{168,170} It would be desirable to test the new Nybomycin derivatives to see if this liability still remained as this could be a cause of mechanism-based toxicity and would be a red flag for the series.

5. Experimental

5.1 General Experimental

Unless otherwise stated, all reagents were obtained from commercial sources and were used as purchased. Moisture-sensitive reactions were undertaken in a nitrogen atmosphere using Schlenk techniques with oven-dried glassware. Anhydrous solvents were either purchased from commercial sources or dispensed using Pure Solv™ solvent drying towers (Innovative Technology Inc., China).

Reactions were analysed using thin layer chromatography (TLC) on pre-coated aluminium backed plates with Merck Kiesegel 60 F254 (230–400 mesh). Visualisation of the TLC plates were performed under UV light (254 nm, 365 nm) and where appropriate were stained with either KMnO₄ (aq. potassium permanganate), ninhydrin solution, bromocresol green, PMA (phosphomolybdic acid solution), vanillin solution, curcumin stain or 2,4-dinitrophenylhydrazine (DNP) solution.

Flash column chromatography was carried out on Fluorochem 60 silica gel (230–400 mesh, 40–63 μm) or Merck Kiesegel 60 silica gel (230–400 mesh, 0.040–0.063 mm) eluting with solvents as supplied under positive air pressure.

Microwave reactions were carried out using a Biotage™ Initiator (Biotage).

Hydrogenation reactions at higher than atmospheric pressures were carried out in a 3911 Parr shaker hydrogenator.

¹H, ¹¹B, ¹³C and ¹⁹F NMR spectra were obtained using a Bruker Advance 400 spectrometer at 400 MHz, 128 MHz, 101 MHz and 377 MHz respectively or ¹H and ¹³C on a Bruker Advance 500 spectrophotometer at 126 MHz and 500 MHz. Chemical shifts are downfield to tetramethylsilane (TMS) and referenced to the stated residual solvent peak - CDCl₃ (δH) =

7.26, (δ C) = 77.2; CD₃OD (δ H) = 3.31, (δ C) = 49.0; *d*6-DMSO (δ H) = 2.50, (δ C) = 39.5.²⁴⁰

Chemical shift (δ) are reported in parts per million (ppm) to the nearest 0.01 ppm for ¹H, ¹¹B and ¹⁹F and 0.1 ppm for ¹³C. Coupling constant (J) are measured in Hertz (Hz) and determined by analysis using the MestReNova[®] NMR software recorded to the nearest 0.1 Hz. ¹H-NMR spectra are reported as follows: chemical shift, signal splitting, coupling constant, integration). ¹³C-NMR spectra were recorded with broadband proton spin decoupling. The following abbreviations are used: singlet (s), d (doublet), t (triplet), q (quartet), m (multiplet), br. (broad).

Low and high resolution mass spectra (EI, ES, APCI) were recorded by the Imperial College London Department of Chemistry Mass Spectroscopy Service on a Micromass Platform II and Micromass AutoSpecQ spectrometers.

X-ray diffraction data was recorded by the Imperial College Department of Chemistry X-ray diffraction service by Dr A. J. P. White.

Melting points were determined using Stanford Research SRS Optimelt Automated Melting Point System (90–264 VAC (125 W)) with a 2 °C per min ramp from 50 °C to 350 °C and the values are uncorrected.

5.1.1 LCMS Conditions

INSTRUMENT-MASS SPEC

INSTRUMENT NAME: WATERS LCT PREMIER OPERATING IN ES+ OR ES- MODE

CONDITIONS FOR ES+

Capillary Voltage: 2.5kV

Sample Cone Voltage: 30 V

Desolvation Temperature: 350 degrees Celsius

Source Temperature: 120 degrees Celsius

Cone Gas Flow (Nitrogen): 10 l/hr

Desolvation Gas Flow (Nitrogen): 400 l/hr

MCP Voltage: 2.1kV

CONDITIONS FOR ES-

Capillary Voltage: 2.9kV

Sample Cone Voltage: 150 V

Desolvation Temperature: 350 degrees Celsius

Source Temperature: 120 degrees Celsius

Cone Gas Flow (Nitrogen): 10 l/hr

Desolvation Gas Flow (Nitrogen): 400 l/hr

MCP Voltage: 2.1kV

For Accurate mass: Samples referenced against Leucine Enkephalin or Sulfadimethoxine (depending on mass)

INSTRUMENT-WATERS ACQUITY UPLC SYSTEM

INSTRUMENT NAME: WATERS ACQUITY UPLC I-CLASS

Column: Waters BEH Acquity C18, 50mm x 2.1mm

Column Temperature: 40 degrees Celsius

Injection Volume: 10uL

Flow rate: 0.5ml/min

Time = 0 min 95% A 5%B (linear gradient)

Time = 3.2 min 5% A 95%B

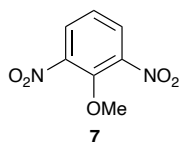
Time = 3.5 min 95% A 5%B

Total run time 4min Solvent A: 99.9% Water, 0.1% Formic Acid, Solvent B: 99.9% Acetonitrile, 0.1% Formic Acid

PDA: 210 to 300 nm

5.2 Synthetic Procedures

2-Methoxy-1,3-dinitrobenzene (7)



7 was obtained following experimental procedures previously described by Schrock and co-workers and their spectroscopic data correspond with those reported.²⁴¹

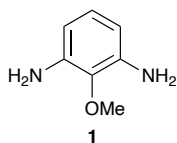
To a stirred solution of 2-chloro-1,3-dinitrobenzene (800 mg, 3.95 mmol) in dry MeOH (8 mL) under N₂ was added NaOMe (427 mg, 11.85 mmol). The reaction mixture was stirred for 18 h at rt, then NaOMe (427 mg, 11.85 mmol) was added. The reaction was stirred for a further 8 h and then NaOMe (300 mg, 5.56 mmol). The reaction was stirred for a further 18 h.

After completion of the reaction, monitored by TLC (1:1; CH₂Cl₂: pentane), water (50 mL) was added and the precipitate was isolated *via* filtration. This afforded the title compound 2-methoxy-1,3-dinitrobenzene (**7**) (749 mg, 96 %) as a yellow solid.

¹H NMR (400 MHz, CDCl₃) δ 8.05 (d, J = 8.2 Hz, 2H), 7.37 (t, J = 8.2 Hz, 1H), 4.08 (s, 3H). **TOF**

MS EI⁺ (m/z): [M⁺]⁺ calc'd for C₇H₆N₂O₅: 198.0277; found: 198.0255

2-Methoxybenzene-1,3-diamine (1) - Method 1



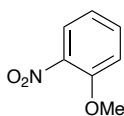
To a stirred solution of 2-methoxy-1,3-dinitrobenzene (**7**) (749 mg, 3.78 mmol) in CH₂Cl₂: MeOH (1:1; 14 mL) under N₂ was added Pd/C (10 %, 402 mg, 0.38 mmol). The atmosphere was changed to hydrogen and the reaction mixture was stirred for 24 h.

After consumption of the starting material, monitored by TLC (1:1; CH₂Cl₂: pentane), the reaction mixture was filtered through celite and eluted with CH₂Cl₂: MeOH (4:1; 100 mL). The filtrate was concentrated to afford the title compound **1** (552 mg, quantitative yield) as a yellow gum.

¹H NMR (400 MHz, CDCl₃) δ 6.72 (t, J = 7.9 Hz, 1H), 6.18 (d, J = 7.9 Hz, 2H), 3.77 (s, 3H). The sample was too unstable for analysis *via* mass spectrometry.

The spectroscopic data correspond with those previously reported.²⁴¹

1-Methoxy-2-nitrobenzene (8)



8

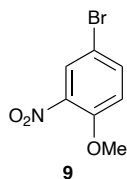
To a stirred solution of 2-nitrophenol (15.0 g, 107.8 mmol) in dry DMF (70 mL) under N₂ at 0 °C was added NaH (6.5 g, 161.7 mmol) portion-wise. The reaction mixture was stirred at 0 °C until the gas evolution ceased (~30 min). After this time, MeI (10.0 μL, 161.7 mmol) was added dropwise. The reaction mixture was then stirred at 0 °C for 2 h, then warmed to rt and stirred for 3 days.

After completion of the reaction, monitored by TLC (1:1; CH₂Cl₂: pentane), the reaction mixture was partitioned between EtOAc (100 mL) and water (100 mL). The layers were separated and the organic phase was washed with LiCl (5 % aq., 2 x 80 mL), brine (80 mL), dried over MgSO₄, filtered and concentrated. This afforded the title compound **8** (16.5 g, quantitative yield) as a yellow oil.

¹H NMR (400 MHz, CDCl₃) δ 7.84 (dd, J = 8.1, 1.7 Hz, 1H), 7.54 (ddd, J = 8.5, 7.4, 1.7 Hz, 1H), 7.09 (dd, J = 8.5, 1.1 Hz, 1H), 7.03 (ddd, J = 8.1, 7.4, 1.1 Hz, 1H), 3.96 (s, 3H). **¹³C NMR** (101 MHz, CDCl₃) δ 153.10, 134.33, 125.83, 120.41, 113.62, 56.61. Note: one of the aryl carbons (likely to be C-OMe) is not observed despite increase scans. **TOF MS ESI⁺** (m/z): [M+H]⁺ calc'd for C₇H₈NO₃: 154.0; found: 154.9.

The spectroscopic data correspond with those previously reported.²⁴²

4-Bromo-1-methoxy-2-nitrobenzene (9)



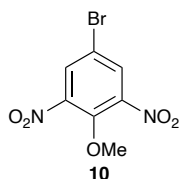
To a stirred solution of 1-methoxy-2-nitrobenzene (**8**) (16.5 g, 107.7 mmol) in acetic acid (155 mL) was added bromine (16.6 mL, 323.2 mmol). The reaction mixture was heated at 60 °C for 5 h.

After completion of the reaction, monitored by TLC (1:1; CH₂Cl₂: pentane), the reaction mixture was partitioned between EtOAc (150 mL) and NaHSO₃ (~15 % aq., 100 mL). The layers were separated and the organic phase was washed with NaHCO₃ (sat., 150 mL), water (100 mL), brine (100 mL), dried over MgSO₄, filtered and concentrated. This afforded the title compound **9** (24 g, 96 %) as an orange gum.

¹H NMR (400 MHz, CDCl₃) δ 7.98 (d, J = 2.5 Hz, 1H), 7.64 (dd, J = 9.0, 2.5 Hz, 1H), 6.99 (d, J = 8.9 Hz, 1H), 3.95 (s, 4H). **TOF MS ESI⁺** (m/z): [M+H]⁺ calc'd for C₇H₇BrNO₃: 231.9531; found: 231.9603.

The spectroscopic data correspond with those previously reported.²⁴³

5-Bromo-2-methoxy-1,3-dinitrobenzene (10)



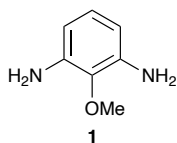
To a stirred solution of triflic acid (8.7 mL, 49.6 mmol) in CH₂Cl₂ (200 mL) under N₂, was added HNO₃ (2.1 mL) dropwise. The newly formed suspension was allowed to stir for 30 min at rt. After this time had passed, the mixture was cooled to 0 °C and 4-bromo-1-methoxy-2-nitrobenzene (**9**) (5.0 g, 21.5 mmol) in CH₂Cl₂ (150 mL) was added dropwise over 30 min. After the addition was complete, the reaction mixture was allowed to warm to rt and stirred for 5 h.

After completion of the reaction, monitored by TLC (20 % CH₂Cl₂ in pentane), the reaction mixture was partitioned between CH₂Cl₂ (150 mL) and water (200 mL). The layers were separated and the organic phase was washed with NaOH (1M, 100 mL), water (100 mL), brine (100 mL), dried over MgSO₄, filtered and concentrated. This afforded the title compound **10** (6.0 g, quantitative yield) as a brown solid.

¹H NMR (400 MHz, CDCl₃) δ 8.17 (s, 2H), 4.07 (s, 3H). **TOF MS EI⁺** (m/z): [M⁺]⁺ calc'd for C₇H₅BrN₂O₅: 275.9382; found: 275.9373.

The spectroscopic data correspond with those previously reported.²⁴⁴

2-Methoxybenzene-1,3-diamine (1) - Method 2



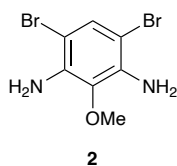
To a stirred solution of 5-bromo-2-methoxy-1,3-dinitrobenzene (**10**) (2.0 g, 7.2 mmol) in MeOH (40 mL) under N₂ was added Pd(OH)₂/C (1.0 g, 1.4 mmol). The atmosphere was changed to hydrogen and the reaction mixture was stirred for 6 h.

After completion of the reaction, monitored by TLC (1:1; CH₂Cl₂: EtOAc), the reaction mixture was filtered through celite and eluted with MeOH (150 mL). The filtrate was concentrated to afford the title compound **1** (1.5 g, quantitative yield) as a yellow gum.

¹H NMR (400 MHz, CDCl₃) δ 6.72 (t, J = 7.9 Hz, 1H), 6.18 (d, J = 7.9 Hz, 2H), 3.77 (s, 3H). Again, the sample was too unstable for analysis *via* mass spectrometry.

The spectroscopic data correspond with those previously reported.²⁴¹

4,6-Dibromo-2-methoxybenzene-1,3-diamine (2)



To a stirred solution of 2-methoxybenzene-1,3-diamine (**1**) (1.5 g, 10.9 mmol) in CH₂Cl₂ (33 mL) at 0 °C was added NEt₃ (9.0 mL, 65.0 mmol) and NBS (4.3 g, 23.9 mmol) portion-wise. The reaction mixture was stirred for 6 h at rt.

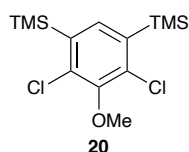
After completion of the reaction monitored by TLC (100 % CH₂Cl₂), the reaction mixture was concentrated. The resulting solid was purified by column chromatography using pentane: CH₂Cl₂ (1:1) and then 100 % CH₂Cl₂ to eluent the desired product. This yielded the title compound (2.9 g, 91 %) as a brown gum.

¹H NMR (400 MHz, CDCl₃) δ 7.28 (s, 1H), 4.13 (br. s, 4H), 3.78 (s, 3H). **TOF MS ESI⁺** (m/z):

[M+H]⁺ calc'd for C₇H₉Br₂N₂O: 294.9003; found: 294.9075.

Product appears to be unstable and degraded rapidly.

(4,6-Dichloro-5-methoxy-1,3-phenylene)bis(trimethylsilane) (20).



20 was obtained following experimental procedures previously described by Hergenrother and co-workers and their spectroscopic data correspond with those reported.^{183,184}

LDA Prep

To a stirred solution of diisopropylamine (17.8 mL) in dry tetrahydrofuran (THF) (132.2 mL) at -78 °C (dry ice, isopropanol (IPA) bath) was added *n*-butyl lithium (*n*-BuLi) (2.5 M, 100 mL) dropwise. The solution was stirred for 30 min at -78 °C then transferred to an ice bath for temporary storage.

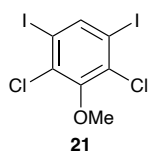
Reaction

To a stirred solution of 2,6-dichloroanisole (13.6 mL, 99.0 mmol) in dry THF (80 mL), under N₂, at -78 °C (dry ice, IPA bath) was added fresh LDA (1 M, 118.6 mL, 119.0 mmol) dropwise. The reaction mixture was stirred for 3 h taking care to keep the temperature between -78 °C to -65 °C. After this time had passed, TMSCl (15.0 mL, 119.0 mmol) was added dropwise and stirred for 1 h, keeping the temperature below -65 °C. The second portion of LDA (1 M, 128.5 mL, 129.0 mmol) was then added dropwise and stirred for 3.5 h. After the allotted time, TMSCl (17.5 mL, 129.0 mmol) was added and stirred for 18 h, while slowly allowing to -40 °C.

Water (50 mL) was added to quench the reaction. This turned the cloudy yellow solution to clear and colourless. HCl (1 M, 100 mL) was added and the product was extracted with EtOAc (2 x 150 mL). The organic phases were combined and washed with brine (100 mL), dried over MgSO₄, filtered and concentrated. This afforded the title compound **20** (33.4 g, quantitative yield) as an off-white solid.

¹H NMR (400 MHz, CDCl₃) δ 7.27 (s, 1H), 3.89 (s, 3H), 0.37 (s, 18H). ¹³C NMR (101 MHz, CDCl₃) δ 151.8, 138.6, 136.9, 136.6, 60.5, -0.6. **TOF MS EI⁺** (m/z): [M+]⁺ calc'd for C₁₃H₂₂OCl₂Si₂: 320.0586; found: 320.0590.

2,4-Dichloro-1,5-diiodo-3-methoxybenzene (21)



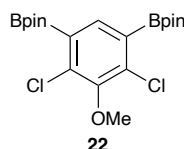
21 was obtained following experimental procedures previously described by Hergenrother and co-workers and their spectroscopic data correspond with those reported.^{183,184}

To a stirred solution of ICl (1 M in CH₂Cl₂, 100 mL, 97.0 mmol) at 0 °C was added 4,6-dichloro-5-methoxy-1,3-phenylene)bis(trimethylsilane) (**20**) (21.8 g, 67.8 mmol) in CH₂Cl₂ (80 mL) dropwise, taking care to control the exotherm. After the addition was complete, the reaction mixture was stirred at room temperature for 2 h.

After completion of the reaction, monitored by TLC (100 % pentane), NaHSO₃ (10 % in water, 60 mL) was added to quench the reaction. The desired product was extracted with EtOAc (2 x 80 mL) and the organics were combined, washed with brine, dried over MgSO₄, filtered and concentrated. The crude product was purified by recrystallization from hexane. This yielded the title compound **21** (25.0 g, 86 %) as yellow needles.

¹H NMR (400 MHz, CDCl₃) δ 8.17 (s, 1H), 3.90 (s, 3H). **¹³C NMR** (101 MHz, CDCl₃) δ 152.6, 144.3, 135.0, 97.6, 60.8. **TOF MS EI⁺** (m/z): [M]⁺ calc'd for C₇H₄OCl₂I₂: 427.7729; found: 427.7712.

2,2'-(4,6-Dichloro-5-methoxy-1,3-phenylene)bis(4,4,5,5-tetramethyl-1,3,2-dioxaborolane) (22)



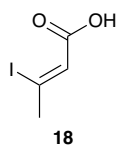
22 was obtained following experimental procedures previously described by Hergenrother and co-workers and their spectroscopic data correspond with those reported.^{183,184}

To a stirred solution of 2,4-dichloro-1,5-diiodo-3-methoxybenzene (**21**) (200 mg, 0.466 mmol), B₂pin₂ (261 mg, 1.026 mmol) and KOAc (275 mg, 2.798 mmol) in dry and degassed (sparged for 45 min) 1,4-dioxane (4 mL) under N₂, was added Pd(Cl)₂dppf (51 mg, 0.070 mmol). The reaction mixture was heated at 90 °C for 18 h.

After completion of the reaction, monitored by TLC (20 % ether in pentane), the reaction mixture was cooled to rt and partitioned between water (40 mL) and EtOAc (40 mL). The layers were separated and the organic phase was washed with brine (40 mL), dried over MgSO₄, filtered and concentrated under reduced pressure. The resulting solid was purified by column chromatography using pentane and then ether (20 %) in pentane to elute the desired product. This yielded the title compound (**22**) (230 mg, quantitative yield) as a white solid.

¹H NMR (400 MHz, CDCl₃) δ 7.70 (s, 1H), 3.88 (s, 3H), 1.40 (s, 24H). FTMS APCI⁺ (m/z): [M+H]⁺ calc'd for C₁₉H₂₉B₂Cl₂O₅: 429.1500; found: 429.1583.

(Z)-3-Iodobut-2-enoic acid (18)



18 was obtained following experimental procedures previously described by Hergenrother and co-workers and their spectroscopic data correspond with those reported.¹⁸⁴

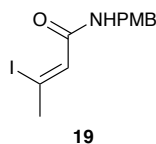
To a stirred solution of but-2-ynoic acid (5.0 g, 59.5 mmol) in acetic acid (22 mL) was added NaI (14.3 g, 95.2 mmol). The reaction mixture was stirred and heated at 115 °C for 5 h.

After completion of the reaction, monitored by TLC (20 % EtOAc in CH₂Cl₂), the reaction mixture was cooled to rt and partitioned between NaHSO₃ (10 %, 100 mL) and EtOAc (100 mL). The layers were separated and the organic phase was washed with brine (100 mL), dried over MgSO₄, filtered and concentrated under reduced pressure. This afforded the title compound (**18**) (12.1 g, 96 %) as a colourless oil.

¹H NMR (400 MHz, CDCl₃) δ 11.34 (br. s, 1H), 6.36 (q, J = 1.4 Hz, 1H), 2.77 (d, J = 1.4 Hz, 3H).

TOF MS ESI⁺ (m/z): [M+H]⁺ calc'd for C₄H₆IO₂: 212.9334; found: 212.9409.

(Z)-3-Iodo-N-(4-methoxybenzyl)but-2-enamide (19)



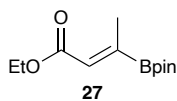
19 was obtained following experimental procedures previously described by Hergenrother and co-workers and their spectroscopic data correspond with those reported.¹⁸⁴

To a stirred solution of (*Z*)-3-iodobut-2-enoic acid (**18**) (2.5 g, 11.8 mmol) in dry CH₂Cl₂ (30 mL) under N₂ was cooled to 0 °C. Oxalyl chloride (3.0 mL, 35.4 mmol) was added dropwise. After the addition a colour change to light pink took place. The reaction mixture was allowed to warm to rt and stirred for 3 h. Small aliquot was taken and dried down under N₂. ¹H NMR analysis confirmed the formation of acyl chloride. The reaction mixture was concentrated and dried under vacuum. The gummy solid was re-dissolved in dry CH₂Cl₂ (25 mL) placed under N₂ and cooled to 0 °C. H₂NPMB (1.7 mL, 13.0 mmol) was added followed by NEt₃ (1.7 mL, 11.8 mmol) and the reaction mixture was stirred for 18 h.

After completion of the reaction, monitored by TLC (20 % EtOAc in CH₂Cl₂), the reaction mixture was partitioned between HCl (1 M, 50 mL) and CH₂Cl₂ (30 mL). The layers were separated and the organic phase was washed with brine, dried over MgSO₄, filtered and concentrated under reduced pressure. The resulting solid was triturated with hot hexane (20 mL) to afford the title compound (**19**) (1.7 g, 74 %) off white crystalline solid.

¹H NMR (400 MHz, CDCl₃) δ 7.30 – 7.21 (m, 2H), 6.91 – 6.83 (m, 2H), 6.24 (q, J = 1.5 Hz, 1H), 5.86 (br. s, 1H), 4.46 (d, J = 5.6 Hz, 2H), 3.80 (s, 3H), 2.65 (d, J = 1.5 Hz, 3H). TOF MS ESI⁺ (m/z): [M+H]⁺ calc'd for C₁₂H₁₅INO₂: 332.0069; found: 332.0138.

Ethyl (Z)-3-(4,4,5,5-tetramethyl-1,3,2-dioxaborolan-2-yl)but-2-enoate (27)



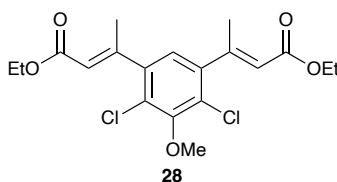
27 was obtained following experimental procedures previously described by Aggarwal and co-workers and their spectroscopic data correspond with those reported.¹⁹⁷

A mixture of CuCl₂ (20 mg, 0.15 mmol), NaO^tBu (29 mg, 0.30 mmol) and xantphos (87 mg, 0.15 mmol) was dissolved in dry THF (4.5 mL) and stirred for 30 min under N₂. B₂pin₂ (1.3 g, 5.0 mmol) in THF (3 mL) was added dropwise and the reaction mixture was stirred for 10 min. Ethyl but-2-ynoate (583 mL, 5.0 mmol), THF (2 mL) and MeOH (400 mL) were added sequentially and the reaction mixture was stirred for 18 h.

After completion of the reaction, monitored by TLC (100 % CH₂Cl₂), the reaction mixture was concentrated. The resulting solid was purified by column chromatography using CH₂Cl₂: pentane (1:1) to eluent the desired product. This yielded the title compound (**27**) (925 mg, 77 %) as a colourless oil.

¹H NMR (400 MHz, CDCl₃) δ 6.45 (q, J = 1.8 Hz, 1H), 4.17 (q, J = 7.1 Hz, 2H), 2.17 (d, J = 1.8 Hz, 3H), 1.30 – 1.25 (m, 15H). **TOF MS ESI⁺** (m/z): [M+H]⁺ calc'd for C₁₂H₂₂BO₄: 241.1533; found: 241.1606.

Diethyl 3,3'-(4,6-dichloro-5-methoxy-1,3-phenylene)(2*E*,2'*E*)-bis(but-2-enoate) (**28**)

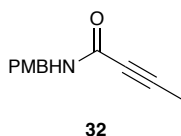


To a stirred solution 2,4-dichloro-1,5-diiodo-3-methoxybenzene (**21**) (50 mg, 0.1 mmol), ethyl (*Z*)-3-(4,4,5,5-tetramethyl-1,3,2-dioxaborolan-2-yl)but-2-enoate (**27**) (70 mg, 0.3 mmol) and K_2CO_3 (97 mg, 0.7 mmol) in DME (degassed with N_2 for 45 min prior to use, 0.9 mL) and H_2O (degassed with N_2 for 45 min prior to use, 0.1 mL) under N_2 was added $Pd(Cl)_2dppf$ (17 mg, 0.02 mmol). The reaction mixture was stirred and heated at 90 °C for 3 h.

After completion of the reaction, monitored by TLC (100 % CH_2Cl_2), the reaction was cooled to rt and partitioned between EtOAc (50 mL) and H_2O (50 mL). The layers were separated and the organic phase was washed with brine, dried over $MgSO_4$, filtered and concentrated under reduced pressure. The resulting solid was purified by column chromatography using pet. ether: CH_2Cl_2 (1:1) and then CH_2Cl_2 (100 %) to elute the desired product. This yielded the title compound (**28**) (42 mg, 90 %) as a colourless gum.

1H NMR (400 MHz, $CDCl_3$) δ 6.80 (s, 1H), 5.82 (q, $J = 1.4$ Hz, 2H), 4.22 (q, $J = 7.1$ Hz, 4H), 3.92 (s, 3H), 2.46 (d, $J = 1.5$ Hz, 6H), 1.31 (t, $J = 7.1$ Hz, 6H). **TOF MS ESI⁺** (m/z): $[M+H]^+$ calc'd for $C_{19}H_{23}Cl_2O_5$: 401.0844; found: 401.0912.

N-(4-Methoxybenzyl)but-2-ynamide (32)

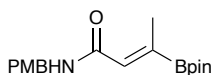


To a stirred solution of but-2-ynoic acid (3.0 g, 36.0 mmol), (4-methoxyphenyl)methanamine (5.1 mL, 39.0 mmol) and triethylamine (7.5 mL, 54.0 mmol) in dry THF (60 mL) under N₂ at 0 °C was added T3P (50 % in EtOAc, 31.8 mL, 54.0 mmol). The reaction mixture was allowed to warm to rt and stirred for 18 h.

After completion of the reaction, monitored by TLC (100 % CH₂Cl₂), the reaction mixture was partitioned between EtOAc (80 mL) and NaOH (2 M, 50 mL). The layers were separated and the aqueous phase was extracted with EtOAc (2 x 50 mL). The organic phases were combined, washed with brine, dried over MgSO₄, filtered and concentrated. The resulting solid was purified by recrystallization from diethyl ether to yield the title compound **32** (6.1 g, 84 %) as white crystalline solid.

¹H NMR (400 MHz, CDCl₃) δ 7.24 – 7.18 (m, 2H), 6.91 – 6.84 (m, 2H), 5.91 (br. s, 1H), 4.40 (d, J = 5.7 Hz, 2H), 3.80 (s, 3H), 1.93 (s, 3H). **TOF MS ESI**⁺ (m/z): [M+H]⁺ calc'd for C₁₂H₁₄NO₂: 204.1; found: 204.1.

(Z)-N-(4-Methoxybenzyl)-3-(4,4,5,5-tetramethyl-1,3,2-dioxaborolan-2-yl)but-2-enamide (33)



33

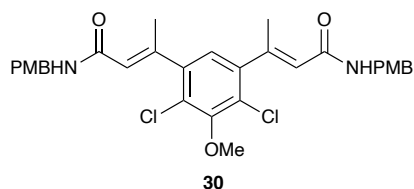
A mixture of CuCl₂ (99 mg, 0.74 mmol), NaO^tBu (142 mg, 1.48 mmol) and xantphos (429 mg, 0.74 mmol) was dissolved in dry THF (25 mL) and stirred for 30 min under N₂. B₂pin₂ (6.2 g, 24.6 mmol) in THF (20 mL) was added dropwise and the reaction mixture was stirred for 10 min. *N*-(4-Methoxybenzyl)but-2-ynamide (**32**) (5.0 g, 24.6 mmol), THF (5 mL) and MeOH (2 mL) were added sequentially and the reaction mixture was stirred for 18 h.

After completion of the reaction, monitored by TLC (100 % CH₂Cl₂), the reaction mixture was filtered through celite and concentrated under reduced pressure. The resulting solid was purified by recrystallization from diethyl ether. This yielded the title compound **33** in two batches (7.3 g) and (580 mg), overall a 97 % yield as yellow crystalline solid.

¹H NMR (400 MHz, CDCl₃) δ 7.23 – 7.19 (m, 2H), 6.88 – 6.83 (m, 2H), 6.39 (q, J = 1.8 Hz, 1H), 5.71 (br. s, 1H), 4.42 (d, J = 5.6 Hz, 2H), 3.80 (s, 3H), 2.16 (d, J = 1.8 Hz, 3H), 1.26 (s, 12).

TOF MS ESI⁺ (m/z): [M+H]⁺ calc'd for C₁₈H₂₇BNO₄: 332.2; found: 332.2.

(2E,2'E)-3,3'-(4,6-Dichloro-5-methoxy-1,3-phenylene)bis(N-(4-methoxybenzyl)but-2-enamide) (30)

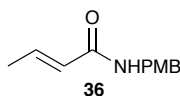


To a stirred solution of 2,4-dichloro-1,5-diiodo-3-methoxybenzene (**21**) (215 mg, 0.59 mmol), (Z)-N-(4-methoxybenzyl)-3-(4,4,5,5-tetramethyl-1,3,2-dioxaborolan-2-yl)but-2-enamide (414 mg, 1.253 mmol) (**33**) and K₂CO₃ (415 mg, 3.00 mmol) in DME (3.6 mL, degassed with N₂ for 45 min prior to use) and water (0.4 mL, degasses with N₂ for 45 min prior to use) under N₂ was added Pd(Cl)₂dppf (73 mg, 0.10 mmol). The reaction mixture was then heated at 90 °C for 4 h.

After reaction had gone to completion, monitored by TLC (100 % CH₂Cl₂), the reaction mixture was partitioned between EtOAc (50 mL) and water (50 mL). The aqueous layer was washed with EtOAc (2 x 50 mL) and the organic phases were combined, washed with brine, dried over MgSO₄, filtered and concentrated. The crude solid was then purified by trituration from CHCl₃. This yielded the title compound **30** (250 mg, 80 %).

¹H NMR (400 MHz, DMSO-*d*₆) δ 8.44 (t, J = 5.9 Hz, 2H), 7.23 – 7.17 (m, 4H), 7.04 (s, 1H), 6.92 – 6.85 (m, 4H), 5.87 (d, J = 1.6 Hz, 2H), 4.26 (d, J = 5.8 Hz, 4H), 3.84 (s, 3H), 3.73 (s, 6H), 2.39 (d, J = 1.4 Hz, 6H). **TOF MS ESI⁺** (m/z): [M+H]⁺ calc'd for C₃₁H₃₃Cl₂N₂O₅: 583.1688; found: 583.1909.

(E)-N-(4-Methoxybenzyl)but-2-enamide (36)



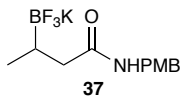
To a stirred solution of (4-methoxyphenyl)methanamine (476 mL, 3.65 mmol) in DMF (5 mL) was added NEt_3 (1.0 mL, 7.30 mmol) followed by crotonic anhydride (1.1 mL, 7.30 mmol). There was an exotherm after the addition of the anhydride. The reaction mixture was left to stir for 3 h.

After completion of the reaction, monitored by TLC (100 % CH_2Cl_2), water (50 mL) was added and the resulting solid was isolated *via* filtration. The solid was washed with water (50 mL) and dried under vacuum to yield the title compound **36** (542 mg, 72 %) as a yellow gum.

$^1\text{H NMR}$ (400 MHz, CDCl_3) δ 7.24 – 7.19 (m, 2H), 6.92 – 6.80 (m, 3H), 5.78 (dq, $J = 15.1, 1.7$ Hz, 1H), 5.61 (br. s, 1H), 4.43 (d, $J = 5.7$ Hz, 2H), 3.79 (s, 3H), 1.85 (dd, $J = 6.8, 1.7$ Hz, 3H). **TOF MS** ESI^+ (m/z): $[\text{M}+\text{H}]^+$ calc'd for $\text{C}_{12}\text{H}_{16}\text{NO}_2$: 206.1103; found: 206.1176.

The spectroscopic data correspond with those previously reported.²⁴⁵

Potassium *N*-(4-methoxybenzyl)-3-(trifluoro- λ^4 -boraneyl)butanamide (37)

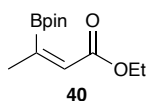


To a stirred solution of CuCl_2 (2 mg, 0.045 mmol) in dry THF (0.4 mL) under N_2 was added NaO^tBu (4 mg, 0.015 mmol) and dppbz (9 mg, 0.045 mmol). This was left to stir for 30 min at rt, then B_2pin_2 (125 mg, 0.537 mmol) in dry THF (0.3 mL) was added. This was left to stir for 30 min and then (*E*)-*N*-(4-methoxybenzyl)but-2-enamide (**36**) (100 mg, 0.488 mmol), dry THF (0.3 mL) and MeOH (40 mL) were added sequentially. The reaction mixture was left to stir for 18 h at rt. After completion of reaction, monitored by TLC (20 % EtOAc in CH_2Cl_2), the reaction mixture was filtered and concentrated under reduced pressure. The resulting solid was re-dissolved in MeOH (7 mL) and cooled to 0 °C. KHF_2 (323 mg, 4.146 mmol) in water (1.3 mL) was added slowly. After the addition was complete the reaction mixture was allowed to warm to rt and stirred for 1 h.

After completion of reaction, monitored by TLC (20 % EtOAc in CH_2Cl_2), the reaction mixture was concentrated and azeotroped with MeOH (3 x 30 mL). The resulting solid was purified by soxhlet extraction with MeOH (50 mL). The MeOH was concentrated to ~5 mL and Et_2O was added until a precipitation occurred. The solid was isolated via filtration to yield the title compound **37** (140 mg, 92 %) as a white solid.

$^1\text{H NMR}$ (400 MHz, $\text{DMSO}-d_6$) δ 7.85 (t, $J = 6.0$ Hz, 1H), 7.18 – 7.10 (m, 2H), 6.89 – 6.81 (m, 2H), 4.20 – 4.07 (m, 2H), 3.71 (s, 3H), 2.08 (dd, $J = 13.8, 3.5$ Hz, 1H), 1.64 (dd, $J = 13.8, 11.0$ Hz, 1H), 0.65 – 0.56 (m, 3H), 0.58 – 0.50 (m, 1H). **FTMS APCI** $^-$ (m/z): $[\text{M}-\text{F}]^-$ calc'd for $\text{C}_{12}\text{H}_{16}\text{BF}_2\text{NO}_2$: 254.1232; found: 254.1167.

Ethyl (Z)-3-(4,4,5,5-tetramethyl-1,3,2-dioxaborolan-2-yl)but-2-enoate (40)



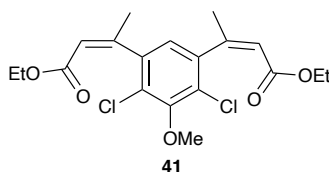
40 was obtained following experimental procedures previously described by Sawamural and co-workers and their spectroscopic data correspond with those reported.¹⁹⁹

To a stirred solution of ethyl but-2-ynoate (2.6 mL, 22.3 mmol) in dry THF (40 mL, degasses with N₂ for 45 min prior to use) under N₂ at 0 °C was added trimethylphosine (1 M in toluene, 2.2 mL, 2.2 mmol) and pinacolborane (4.9 mL, 33.5 mmol) dropwise. The reaction mixture was stirred for 5 min at 0 °C then allowed to warm to rt and stirred for 3 days.

After completion of the reaction monitored by TLC (10 % Et₂O in pentane), the reaction mixture was concentrated under reduced pressure and the resulting solid was purified by column chromatography. The title compound **40** was eluted with 10 % Et₂O in pentane in two batches, (batch 1 - 1.4 g, 96 % Z isomer, 25 % yield) and (batch 2 - 1.81 g, 83 % Z isomer, 28 % yield).

¹H NMR (400 MHz, CDCl₃) δ 6.04 – 6.01 (m, 1H), 4.18 (q, J = 7.1 Hz, 2H), 1.95 (d, J = 1.7 Hz, 3H), 1.35 (s, 12H), 1.26 (t, J = 7.1 Hz, 3H). ¹¹B NMR (128 MHz, CDCl₃) δ 31.06. **TOF MS ESI⁺** (m/z): [M+H]⁺ calc'd for C₁₂H₂₂BO₄: 241.1533; found: 241.1620.

Diethyl 3,3'-(4,6-dichloro-5-methoxy-1,3-phenylene)(2Z,2'Z)-bis(but-2-enoate) (41)

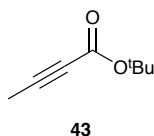


To a stirred solution of 2,4-dichloro-1,5-diiodo-3-methoxybenzene (**21**) (500 mg, 1.166 mmol), ethyl (*Z*)-3-(4,4,5,5-tetramethyl-1,3,2-dioxaborolan-2-yl)but-2-enoate (**40**) (616 mg, 2.564 mmol) and K_2CO_3 (967 mg, 6.994 mmol) in DME (4.5 mL, degasses with N_2 for 45 min prior to use) and water (0.5 mL, degasses with N_2 for 45 min prior to use) under N_2 was added $Pd(Cl)_2dppf$ (171 mg, 0.233 mmol). The reaction mixture was then heated at 90 °C for 4 h.

After reaction had gone to completion, monitored by TLC (100 % CH_2Cl_2), the reaction mixture was partitioned between EtOAc (50 mL) and water (50 mL). The aqueous layer was washed with EtOAc (2 x 50 mL) and the organic phases were combined, washed with brine, dried over $MgSO_4$, filtered and concentrated. The crude solid was then purified by column chromatography using 100 % CH_2Cl_2 then eluting the product with 10 % EtOAc in CH_2Cl_2 . This yielded the title compound **41** (459 mg, 98 %) as a pale tan solid.

1H NMR (400 MHz, $CDCl_3$) δ 6.58 (s, 1H), 5.99 (q, $J = 1.5$ Hz, 2H), 4.04 – 3.94 (m, 4H), 3.92 (s, 3H), 2.13 (d, $J = 1.5$ Hz, 6H), 1.13 – 1.04 (m, 6H). TOF MS ESI⁺ (m/z): $[M+Na]^+$ calc'd for $C_{19}H_{23}Cl_2O_5Na$: 423.04; found: 423.28.

tert-Butyl but-2-ynoate (43)



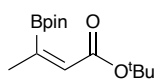
43 was obtained following experimental procedures previously described by Otaka and co-workers.²⁴⁶

To a stirred solution of 1-bromoprop-1-ene (9.7 mL, 113.6 mmol) in dry THF (120 mL) under N₂ at -78 °C was added ⁿBuLi (2.5 M in hexanes, 100 mL, 250.0 mmol) dropwise. The reaction mixture was stirred for 3 h at -78 °C. After this time had passed, Boc₂O (38.4 g, 176.0 mmol) in dry THF (42 mL) was added at -78 °C dropwise. After the addition was complete the reaction mixture was warmed slowly to room temperature overnight.

After this time had passed, the reaction mixture was quenched with water (300 mL) and extracted with CH₂Cl₂ (2 x 300 mL). The combined organic phases were washed with brine (100 mL), dried over MgSO₄, filtered and concentrated. The crude reaction product was purified using a silica plug flushing with 100 % pentane then eluting the title compound with 10 % Et₂O in pentane. This yielded the title compound **43** (15.6 g, 98 %) as a colourless oil.

¹H NMR (400 MHz, CDCl₃) δ 1.95 (s, 3H), 1.48 (s, 9H). ¹³C NMR (101 MHz, CDCl₃) δ 152.9, 83.1, 83.0, 73.9, 27.5, 3.9. TOF MS EI⁺ (m/z): [M]⁺ calc'd for C₈H₁₃O₂: 141; found: 141.

tert-Butyl (E)-3-(4,4,5,5-tetramethyl-1,3,2-dioxaborolan-2-yl)but-2-enoate (44)



44

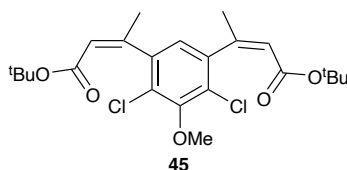
To a stirred solution of ethyl but-2-ynoate (**43**) (8 g, 57.1 mmol) in dry THF (80 mL, degasses with N₂ for 45 min) under N₂ at 0 °C was added trimethylphosine (1 M in toluene, 11.4 mL, 11.4 mmol) and pinacolborane (11.4 mL, 114.3 mmol) slowly. The reaction mixture was stirred for 5 min at 0 °C then allowed to warm to room temperature and stirred for 18 h.

After completion of the reaction monitored by TLC (10 % Et₂O in pentane) the reaction mixture was concentrated under reduced pressure and the resulting solid was purified using a silica plug flushing with 100 % pentane then eluting the title compound with 10 % Et₂O in pentane. This yielded the title compound **44** (7.9 g, 52 %) as a colourless oil.

¹H NMR (400 MHz, CDCl₃) δ 5.95 (q, J = 1.7 Hz, 1H), 1.91 (d, J = 1.7 Hz, 3H), 1.45 (s, 9H), 1.34 (s, 12H). ¹³C NMR (101 MHz, CHCl₃) δ 167.7, 152.2, 128.7, 83.6, 80.5, 28.2, 24.7, 20.4. ¹¹B NMR (128 MHz, CDCl₃) δ 31.1. TOF MS ESI⁺ (m/z): [M+H]⁺ calc'd for C₁₄H₂₆BO₄: 269.1924; found: 269.1932.

Di-*tert*-butyl 3,3'-(4,6-dichloro-5-methoxy-1,3-phenylene)(2*Z*,2'*Z*)-bis(but-2-enoate)

(45)

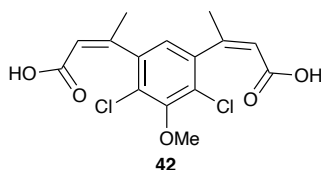


To a stirred solution of 2,4-dichloro-1,5-diiodo-3-methoxybenzene (**21**) (5.0 g, 11.7 mmol) in degasses (for 15 min with N₂) DME (100 mL) and water (10 mL) under N₂ was added *tert*-butyl (*E*)-3-(4,4,5,5-tetramethyl-1,3,2-dioxaborolan-2-yl)but-2-enoate (**44**) (7.0 g, 26.2 mmol), K₂CO₃ (9.7 g, 69.9 mmol) and Pd(Cl)₂dppf (1.7 g, 2.3 mmol). The reaction mixture was stirred for 18 h at 85 °C.

After completions of the reaction monitored by TLC (100 % CH₂Cl₂), the reaction was concentrated. The resulting solid was partitioned between CH₂Cl₂ (100 mL) and water (100 mL). The layers were separated, and the aqueous phase was extracted with CH₂Cl₂ (2 x 100 mL). The organic phases were then combined, washed with brine (150 mL), dried over MgSO₄, filtered and then concentrated under reduced pressure. The crude solid was purified by column chromatography starting with 100% CH₂Cl₂ and then using 10% EtOAc in CH₂Cl₂. The product containing fractions were combined and concentrated to yield the title compound **45** (4.5 g, 84 %) off-white crystalline solid.

¹H NMR (400 MHz, CDCl₃) δ 6.60 (s, 1H), 5.90 (q, *J* = 1.5 Hz, 2H), 3.92 (s, 3H), 2.08 (d, *J* = 1.5 Hz, 6H), 1.22 (s, 18H). ¹³C NMR (101 MHz, CDCl₃) δ 164.5, 152.4, 149.2, 140.8, 124.9, 122.8, 121.7, 80.2, 60.7, 27.9, 26.0. TOF MS ESI⁺ (*m/z*): [M+H]⁺ calc'd for C₂₃H₃₀O₅NaCl₂: 479.1368; found: 479.1374.

(2Z,2'Z)-3,3'-(4,6-Dichloro-5-methoxy-1,3-phenylene)bis(but-2-enoic acid) (42)

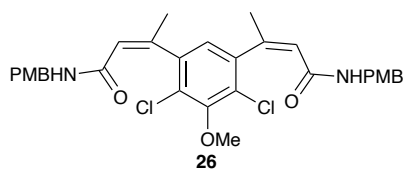


To a stirred solution of di-*tert*-butyl 3,3'-(4,6-dichloro-5-methoxy-1,3-phenylene)(I)-bis(but-2-enoate) (**45**) (52 mg, 0.114 mmol) in CH₂Cl₂ (1 mL) was added TFA (1 mL). The reaction mixture was stirred for 2 h at room temperature.

After completions of the reaction monitored by TLC (100 % CH₂Cl₂), the reaction was partitioned between CH₂Cl₂ (15 mL) and NaOH (1M, 15 mL). The layers were separated, and the aqueous phase was extracted with CH₂Cl₂ (2 x 20 mL). The aqueous phase was then acidified with HCL (1M, 30 mL) and extracted with CH₂Cl₂ (2 x 30 mL). These organic extracts were combined, washed with water (40 mL), brine (40 mL), dried over MgSO₄, filtered and concentrated under reduced pressure. This afforded the desired product **42** (37 mg, 94 %) as a white crystalline solid.

¹H NMR (400 MHz, CDCl₃) δ 6.52 (s, 1H), 5.97 (d, J = 1.6 Hz, 2H), 3.78 (s, 3H), 2.12 (d, J = 1.5 Hz, 6H). **¹³C NMR** (101 MHz, CDCl₃) δ 170.8, 153.7, 152.5, 139.9, 125.0, 120.3, 60.6, 26.4. **TOF MS** **ESI**⁺ (m/z): [M+CH₃CN+Na]⁺ calc'd for C₁₇H₁₇NO₅NaCl₂: 408.0381; found: 408.0383.

(2Z,2'Z)-3,3'-(4,6-Dichloro-5-methoxy-1,3-phenylene)bis(N-(4-methoxybenzyl)but-2-enamide) (26)



To a stirred solution of (2Z,2'Z)-3,3'-(4,6-dichloro-5-methoxy-1,3-phenylene)bis(but-2-enoic acid) (**42**) (1.8 g, 5.2 mmol) in dry CH₂Cl₂ (30 mL) under N₂ at 0 °C was added oxalyl chloride (2.6 mL, 31.2 mmol) dropwise. The reaction mixture was warmed to room temperature and stirred for 4 h.

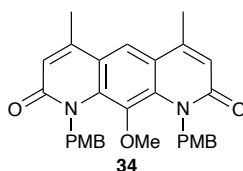
After this time had passed, the reaction mixture was concentrated under reduced pressure and the atmosphere was changed to N₂. The residue was re-dissolved in dry CH₂Cl₂ (30 mL) and cooled to 0 °C. H₂NPMB (1.7 mL, 13.0 mmol) the NEt₃ (1.8 mL, 13.0 mmol) were added. The reaction mixture was warmed to room temperature and stirred for 18 h.

After the allocated time had passed, the reaction mixture was partitioned between CH₂Cl₂ (50 mL) and HCl (1M, 80 mL). The layers were separated and the organic phase was washed with water (80 mL), brine (80 ml), dried over MgSO₄, filtered and concentrated under reduced pressure. The crude solid was purified by column chromatography using 100 % CH₂Cl₂ then 25 % EtOAc in CH₂Cl₂ as the eluent system. The product containing fractions were combined and concentrated to yielded the title compound **26** (2.1 g, 3.5 mmol, 68 %) as an off-white solid.

¹H NMR (400 MHz, DMSO-*d*₆) δ 7.03 (d, J = 8.4 Hz, 4H), 6.80 (d, J = 8.4 Hz, 5H), 6.07 (d, J = 1.7 Hz, 2H), 4.09 (d, J = 6.0 Hz, 4H), 3.75 (s, 3H), 3.70 (s, 6H), 2.01 – 1.93 (m, 6H). **¹³C NMR** (101 MHz, DMSO-*d*₆) δ 164.3, 158.6, 145.0, 140.8, 131.8, 129.3, 128.9, 124.3, 123.8, 123.5, 114.0, 61.0, 55.5, 41.7, 25.7. **TOF MS ESI⁺** (m/z): [M+Na]⁺ calc'd for C₃₁H₃₂N₂O₅NaCl₂: 605.1586; found: 605.1594.

The spectroscopic data correspond with those previously reported.²⁴⁷

10-Methoxy-1,9-bis(4-methoxybenzyl)-4,6-dimethylpyrido[3,2-*g*]quinoline-2,8(1*H*,9*H*)-dione (34)



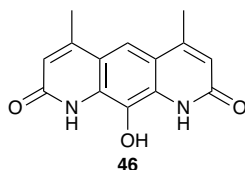
34 was obtained following experimental procedures previously described by Hergenrother and co-workers and their spectroscopic data correspond with those reported.²⁴⁷

To a stirred solution of (2*Z*,2'*Z*)-3,3'-(4,6-dichloro-5-methoxy-1,3-phenylene)bis(*N*-(4-methoxybenzyl)but-2-enamide) (**26**) (60 mg, 0.103 mmol) in dry *i*-PrOH (5 mL) under N₂ was added K₂CO₃ (86 mg, 0.619 mmol), Xphos (5 mg, 0.010 mmol) and Xphos G2 Pd (8 mg, 0.010 mmol). The reaction mixture was heated at 90 °C for 18 h.

After completion of the reaction, monitored by TLC (100 % CH₂Cl₂), the solvent was removed under reduced pressure. The resulting solid was portioned between CH₂Cl₂ (20 mL) and water (20 mL). The layers were separated and the organic phase was washed with brine (20 mL), dried over MgSO₄, filtered and concentrated under reduced pressure. The crude solid was purified by column chromatography using 100 % CH₂Cl₂ then 25 % EtOAc in CH₂Cl₂ as the eluent. The product containing fractions were combined and concentrated. The resulting solid was triturated with pentane (10 mL) to yield 10-methoxy-1,9-bis(4-methoxybenzyl)-4,6-dimethylpyrido[3,2-*g*]quinoline-2,8(1*H*,9*H*)-dione (**34**) (52 mg, 0.102 mmol, 99 %) as an off white solid.

¹H NMR (400 MHz, CHCl₃) δ 7.62 (s, 1H), 7.01 (d, J = 8.1 Hz, 4H), 6.74 (d, J = 8.3 Hz, 4H), 6.59 (d, J = 1.3 Hz, 2H), 5.79 – 5.18 (m, 4H), 3.73 (s, 6H), 2.90 (s, 3H), 2.48 (d, J = 1.2 Hz, 6H). **¹³C NMR** (101 MHz, CHCl₃) δ 164.1, 158.4, 146.2, 136.5, 130.2, 128.3, 120.8, 119.6, 116.8, 113.6, 61.7, 55.2, 29.7, 19.1. **TOF MS ESI⁺** (m/z): [M+H]⁺ calc'd for C₃₁H₃₁N₂O₅: 511.2233; found: 511.2213.

10-Hydroxy-4,6-dimethylpyrido[3,2-g]quinoline-2,8(1H,9H)-dione (46)



46 was obtained following experimental procedures previously described by Hergenrother and co-workers and their spectroscopic data correspond with those reported.²⁴⁷

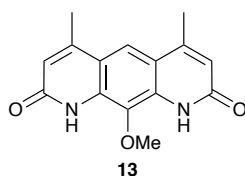
HBr (aq., 48 %, 12 mL) was added to 10-methoxy-1,9-bis(4-methoxybenzyl)-4,6-dimethylpyrido[3,2-*g*]quinoline-2,8(1*H*,9*H*)-dione (**34**) (500 mg, 0.98 mmol). The reaction mixture was stirred and heated at 110 °C for 18 h.

After the completion of the reaction, monitored by TLC (10 % MeOH in CH₂Cl₂), the reaction was cooled to rt and water (100 mL) was added. The formed precipitated was isolated *via* filtration and the resulting solid was washed with water (100 mL) and dried under vacuum. This yielded the title compound **46** (242 mg, 96 %) as a light brown solid.

¹H NMR (400 MHz, DMSO-*d*₆) δ 6.66 (s, 1H), 6.19 (d, *J* = 1.3 Hz, 2H), 2.41 (d, *J* = 1.2 Hz, 6H).

TOF MS ESI⁺ (m/z): [M+H]⁺ calc'd for C₁₄H₁₃N₂O₃: 257.0848; found: 257.0924. **m.p.** 274.2 °C (H₂O). LCMS (257.1 [M+H], 1.26 min, 100 %).

10-Methoxy-4,6-dimethylpyrido[3,2-*g*]quinoline-2,8(1*H*,9*H*)-dione (13)



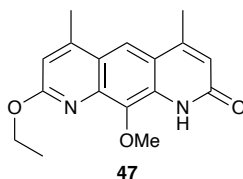
13 was obtained following experimental procedures previously described by Hergenrother and co-workers and their spectroscopic data correspond with those reported.²⁴⁷

10-Methoxy-1,9-bis(4-methoxybenzyl)-4,6-dimethylpyrido[3,2-*g*]quinoline-2,8(1*H*,9*H*)-dione (**34**) (236 mg, 0.463 mmol) was dissolved in TFA (2.3 mL) and stirred for 18 h.

After this time had passed water (30 mL) was added and the precipitated was collected *via* filtration and dried under vacuum. The solid was then triturated with Et₂O (10 mL) and the resulting solid was dried under vacuum. This yielded the title compound **13** (122 mg, 0.452 mmol, 98 %) as an off-white solid.

¹H NMR (400 MHz, DMSO-*d*₆) δ 11.20 (s, 2H), 7.74 (s, 1H), 6.36 (t, *J* = 1.6 Hz, 2H), 3.74 (s, 3H), 2.49 (s, 6H). ¹³C NMR (101 MHz, DMSO-*d*₆) δ 161.9, 148.2, 132.8, 130.8, 119.9, 116.8, 115.7, 61.4, 18.5. TOF MS ES⁺ (*m/z*): [M+H]⁺ calc'd for C₁₅H₁₅N₂O₃: 271.1083; found: 271.1082. LCMS (271.1 [M+H], 1.32 min, 100 %).

8-Ethoxy-10-methoxy-4,6-dimethylpyrido[3,2-*g*]quinolin-2(1*H*)-one (47)

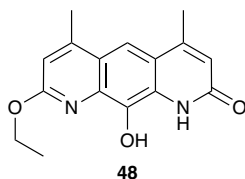


To a stirred solution of 10-methoxy-4,6-dimethylpyrido[3,2-*g*]quinoline-2,8(1*H*,9*H*)-dione (**13**) (200 mg, 0.735 mmol) in DMSO (10 mL) under N₂ was added K₂CO₃ (203 mg, 1.471 mmol) and EtI (59 mL, 0.735 mmol). The reaction mixture was heated at 70 °C for 18 h.

After this time had passed, water (80 mL) was added and the precipitate was collected *via* filtration and dried under vacuum. This afforded the title compound **47** (129 mg, 0.433 mmol, 59 %) as a white solid.

¹H NMR (400 MHz, CDCl₃) δ 9.14 (s, 1H), 7.87 (s, 1H), 6.72 (d, J = 1.1 Hz, 1H), 6.54 – 6.50 (m, 1H), 4.57 (q, J = 7.1 Hz, 2H), 4.28 (s, 3H), 2.66 (d, J = 1.1 Hz, 3H), 2.57 (d, J = 1.2 Hz, 3H), 1.47 (t, J = 7.1 Hz, 3H). **TOF MS ESI**⁺ (m/z): [M+H]⁺ calc'd for C₁₇H₁₉N₂O₃: 299.34; found: 299.14.

8-Ethoxy-10-hydroxy-4,6-dimethylpyrido[3,2-*g*]quinolin-2(1*H*)-one (48)



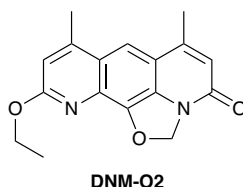
To a stirred solution of 8-ethoxy-10-methoxy-4,6-dimethylpyrido[3,2-*g*]quinolin-2(1*H*)-one (**47**) (298 mg, 0.993 mmol) in dry CH₂Cl₂ (10 ml) under N₂ at 0 °C was added BBr₃ (1 M in CH₂Cl₂, 5.9 mL, 0.880 mmol) dropwise. After the addition was complete the reaction mixture was allowed to warm to room temperature and stirred for 18 h.

After the completion of the reaction, monitored by TLC (100 % EtOAc), water (60 mL) was added to the reaction mixture and the resulting precipitate was isolated *via* filtration. The solid was dried under vacuum then washed through the filter with CH₂Cl₂: MeOH (100 mL, 4:1). The solvent was removed from the filtrate to afford the title compound **48** (115 mg, 0.405 mmol, 41 %) as an off-white solid.

¹H NMR (400 MHz, DMSO-*d*₆) δ 10.57 (s, 1H), 9.66 (s, 1H), 7.69 (s, 1H), 6.79 (d, J = 1.2 Hz, 1H), 6.42 (s, 1H), 4.62 (q, J = 7.0 Hz, 2H), 2.64 (d, J = 1.1 Hz, 3H), 2.53 (d, J = 1.2 Hz, 3H), 1.35 (t, J = 7.1 Hz, 3H). ¹³C NMR (101 MHz, DMSO-*d*₆) δ 161.8, 161.6, 153.7, 153.1, 148.6, 136.7, 135.0, 125.5, 121.5, 120.6, 112.5, 110.3, 62.0, 55.4, 19.2, 18.8, 15.0. TOF MS ESI⁺ (m/z): [M+H]⁺ calc'd for C₁₆H₁₆N₂O₃: 285.32; found: 285.13.

10-Ethoxy-6,8-dimethyl-2*H*,4*H*-oxazolo[5,4,3-*ij*]pyrido[3,2-*g*]quinoline-4-one

(DNM-O2)

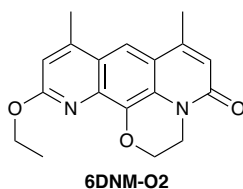


To a stirred solution of 8-ethoxy-10-hydroxy-4,6-dimethylpyrido[3,2-*g*]quinoline-2(1*H*)-one (**48**) (12 mg, 0.042 mmol) in DMSO (0.5 mL) under N₂ was added 1,1-dibromomethane (29 mL, 0.420 mmol) and K₂CO₃ (35 mg, 0.252 mmol). The reaction mixture was heated at 85 °C for 18 h.

After the completion of the reaction, monitored by TLC (10 % MeOH in CH₂Cl₂), the reaction mixture was partitioned between EtOAc (20 mL) and water (20 mL). The layers were separated and the organic phase was washed with brine (20 mL), dried over MgSO₄, filtered and concentrated. The crude solid was then purified using preparative TLC using 10 % MeOH in CH₂Cl₂ as the eluent. This yielded the title compound **DNM-O2** (1.8 mg, 0.006 mmol, 14 %) as a light yellow solid.

¹H NMR (400 MHz, CDCl₃) δ 7.58 (s, 1H), 6.69 (d, J = 1.2 Hz, 1H), 6.48 (s, 2H), 6.47 (q, J = 1.4 Hz, 1H), 4.54 (q, J = 7.1 Hz, 2H), 2.64 (dd, J = 2.8, 1.1 Hz, 3H), 2.54 (d, J = 1.3 Hz, 3H), 1.44 (t, J = 7.1 Hz, 3H). ¹³C NMR (101 MHz, CDCl₃) δ 162.7, 158.6, 147.8, 147.6, 142.5, 131.6, 130.0, 124.4, 122.2, 115.5, 113.5, 110.9, 86.9, 62.1, 19.9, 18.1, 14.6. TOF MS ESI⁺ (m/z): [M+H]⁺ calc'd for C₁₇H₁₇N₂O₃: 297.1239; found: 297.1235.

11-Ethoxy-7,9-dimethyl-2,3-dihydro-5H-[1,4]oxazino[2,3,4-*ij*]pyrido[3,2-*g*]quinolin-5-one (6DNM-O2)

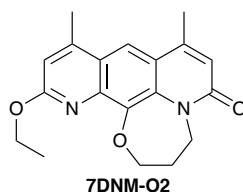


To a stirred solution of 8-ethoxy-10-hydroxy-4,6-dimethylpyrido[3,2-*g*]quinoline-2(1*H*)-one (**48**) (16 mg, 0.056 mmol) in DMSO (0.5 mL) under N₂ was added 1,2-dibromoethane (48 mL, 0.559 mmol) and K₂CO₃ (46 mg, 0.336 mmol). The reaction mixture was heated at 85 °C for 18 h.

After the completion of the reaction, monitored by TLC (10 % MeOH in CH₂Cl₂), the reaction mixture was partitioned between EtOAc (20 mL) and water (20 mL). The layers were separated and the organic phase was washed with brine (20 mL), dried over MgSO₄, filtered and concentrated. The crude solid was then purified using preparative TLC using 10 % MeOH in CH₂Cl₂ as the eluent. This yielded the title compound **6DNM-O2** (2.3 mg, 0.007 mmol, 13 %) as an off-white solid.

¹H NMR (400 MHz, CDCl₃) δ 7.79 (s, 1H), 6.79 (d, J = 1.2 Hz, 1H), 6.61 (d, J = 1.3 Hz, 1H), 4.67 – 4.58 (m, 4H), 4.38 (t, J = 4.7 Hz, 2H), 2.70 (d, J = 1.0 Hz, 3H), 2.60 (d, J = 1.2 Hz, 3H), 1.49 (t, J = 7.1 Hz, 3H). ¹³C NMR (126 MHz, CDCl₃) δ 163.0, 160.3, 147.2, 147.1, 136.9, 136.6, 125.0, 121.6, 120.6, 119.0, 113.6, 112.2, 64.4, 61.9, 39.7, 19.4, 19.1, 14.7. TOF MS ESI⁺ (m/z): [M+H]⁺ calc'd for C₁₈H₁₉N₂O₃ 311.1396; found: 311.1397.

12-Ethoxy-8,10-dimethyl-3,4-dihydro-2*H*,6*H*-[1,4]oxazepino[2,3,4-*ij*]pyrido[3,2-*g*]quinolin-6-one (7DNM-O2)

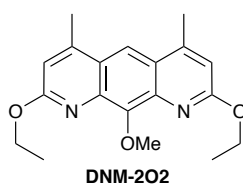


To a stirred solution of 8-ethoxy-10-hydroxy-4,6-dimethylpyrido[3,2-*g*]quinoline-2(1*H*)-one (**48**) (20 mg, 0.069 mmol) in DMF (1 mL) under N₂ was added 1,3-dibromopropane (7 mL, 0.069 mmol) and K₂CO₃ (58 mg, 0.420 mmol). The reaction mixture was heated at 85 °C for 18 h.

After the completion of the reaction, monitored by TLC (10 % MeOH in CH₂Cl₂), the reaction mixture was partitioned between EtOAc (20 mL) and water (20 mL). The layers were separated and the organic phase was washed with brine (20 mL), dried over MgSO₄, filtered and concentrated. The crude solid was then purified using preparative TLC using 5 % MeOH in CH₂Cl₂ as the eluent. This yielded the title compound **7DNM-O2** (4.0 mg, 0.012 mmol, 18 %) as an off-white solid.

¹H NMR (400 MHz, CDCl₃) δ 7.78 (s, 1H), 6.74 (q, J = 1.1 Hz, 1H), 6.55 (q, J = 1.2 Hz, 1H), 4.67 (t, J = 5.9 Hz, 2H), 4.59 (q, J = 7.1 Hz, 2H), 4.52 (t, J = 6.8 Hz, 2H), 2.65 (d, J = 1.1 Hz, 3H), 2.52 (d, J = 1.2 Hz, 3H), 2.43 – 2.35 (m, 2H), 1.45 (t, J = 7.1 Hz, 3H). ¹³C NMR (126 MHz, CDCl₃) δ 163.1, 162.8, 147.0, 146.5, 142.5, 140.7, 132.1, 122.0, 121.0, 120.5, 114.1, 113.5, 72.0, 61.9, 42.3, 27.9, 19.4, 19.0, 14.7. **TOF MS ESI**⁺ (m/z): [M+H]⁺ calc'd for C₁₉H₂₁N₂O₃ 325.1552; found: 325.1550. **LCMS** (325.2 [M+H], 2.10 min, 100 %).

2,8-Diethoxy-10-methoxy-4,6-dimethylpyrido[3,2-g]quinoline (DNM-2O2)

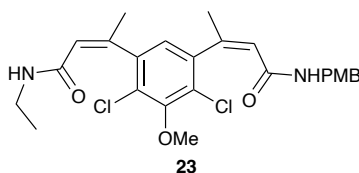


To a stirred solution of 10-methoxy-4,6-dimethylpyrido[3,2-g]quinoline-2,8(1*H*,9*H*)-dione (**13**) (100 mg, 0.368 mmol) in DMSO (5 mL) under N₂ was added K₂CO₃ (101 mg, 0.735 mmol) and EtI (38 mL, 0.478 mmol). The reaction mixture was heated at 70 °C for 18 h.

After completion of the reaction, monitored by TLC (5 % MeOH in CH₂Cl₂), water (80 mL) was added. The formed precipitate was collected *via* filtration and dried under vacuum. This solid was purified by preparative TLC (100 % EtOAc). This yielded the title compound **DNM-2O2** (6 mg, 5 %) as an off-white solid.

¹H NMR (400 MHz, CDCl₃) δ 8.08 (s, 1H), 6.74 (d, J = 1.3 Hz, 2H), 4.64 (q, J = 7.1 Hz, 4H), 4.29 (s, 3H), 2.70 (d, J = 1.1 Hz, 6H), 1.48 (t, J = 7.1 Hz, 6H). ¹³C NMR (101 MHz, CDCl₃) δ 161.53, 156.42, 146.92, 139.42, 123.40, 113.41, 113.29, 62.03, 61.60, 19.13, 14.59. **TOF MS ESI⁺** (m/z): [M+H]⁺ calc'd for C₁₉H₂₃N₂O₃: 327.1630; found: 327.1696.

(Z)-3-(2,4-Dichloro-3-methoxy-5-((Z)-4-((4-methoxybenzyl)amino)-4-oxobut-2-en-2-yl)phenyl)-N-ethylbut-2-enamide (23)

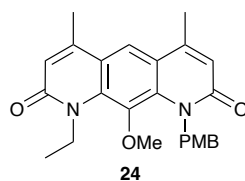


To a stirred solution of (2Z,2'Z)-3,3'-(4,6-Dichloro-5-methoxy-1,3-phenylene)bis(but-2-enoic acid) (**42**) (20 mg, 0.058 mmol) in dry CH₂Cl₂ (0.5 mL) under N₂ was added oxalyl chloride (41 mL, 0.349 mmol) dropwise. The reaction mixture was stirred at room temperature for 4 h. After this time had passed, the reaction mixture was concentrated under reduced pressure and the atmosphere was changed to N₂. The residue was re-dissolved in dry CH₂Cl₂ (1 mL) and cooled to 0 °C. NH₂Et (2M in THF, 29 mL, 0.058 mmol), NH₂PMB (8 mL, 0.058 mmol) and NEt₃ (41 mL, 0.291 mmol) were added sequentially. After the last addition the reaction mixture was allowed to warm to room temperature and stirred for 18 h.

After the reaction was complete, monitored by TLC (1:1 CH₂Cl₂: EtOAc), the reaction mixture was partitioned between CH₂Cl₂ (20 mL) and HCl (1 M, 20 mL). The layers were separated and the aqueous phase was extracted with CH₂Cl₂ (2 x 20 mL). The organic phases were then combined, washed with brine (50 mL), dried over MgSO₄, filtered and concentrated. The resulting solid was purified by column chromatography using 100 % CH₂Cl₂ then 1:1 CH₂Cl₂: EtOAc as the eluent. The yielded (Z)-3-(2,4-dichloro-3-methoxy-5-((Z)-4-((4-methoxybenzyl)amino)-4-oxobut-2-en-2-yl)phenyl)-N-ethylbut-2-enamide (**23**) (12 mg, 0.024 mmol, 42 %) as an off-white solid.

¹H NMR (400 MHz, DMSO-*d*6) δ 7.07 – 7.02 (m, 2H), 6.84 – 6.79 (m, 2H), 6.76 (br. s, 1H), 6.07 (q, *J* = 1.4 Hz, 1H), 5.98 (q, *J* = 1.5 Hz, 1H), 4.11 (d, *J* = 5.9 Hz, 2H), 3.77 (s, 3H), 3.70 (s, 3H), 2.96 (q, *J* = 7.0 Hz, 2H), 2.02 (d, *J* = 1.5 Hz, 3H), 1.97 (s, 3H), 0.89 (t, *J* = 7.2 Hz, 3H). **¹³C NMR** (101 MHz, DMSO-*d*6) δ 163.9, 163.7, 158.1, 153.3, 151.2, 144.6, 140.3, 131.4, 128.7, 128.5, 128.4, 123.9, 123.8, 123.3, 123.1, 113.6, 113.5, 60.2, 55.0, 41.3, 33.1, 25.2, 25.2, 14.6. **TOF MS ESI⁺** (*m/z*): [M+H]⁺ calc'd for C₂₅H₂₉N₂O₄Cl₂ 491.1504; found: 491.1987.

1-Ethyl-10-methoxy-9-(4-methoxybenzyl)-4,6-dimethylpyrido[3,2-g]quinoline-2,8(1*H*,9*H*)-dione (24)



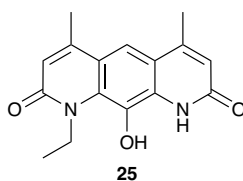
24 was obtained following experimental procedures previously described by Hergenrother and co-workers.²⁴⁷

To a stirred solution of (Z)-3-(2,4-dichloro-3-methoxy-5-((Z)-4-((4-methoxybenzyl)amino)-4-oxobut-2-en-2-yl)phenyl)-*N*-ethylbut-2-enamide (**23**) (11 mg, 0.022 mmol) in dry *i*-PrOH (1 mL) under N₂ was added K₂CO₃ (19 mg, 0.135 mmol), Xphos (1 mg, 0.002 mmol) and Xphos G2 Pd (2 mg, 0.002 mmol). The reaction mixture was heated at 90 °C for 18 h.

After completion of the reaction, monitored by TLC (100 % EtOAc), the solvent was removed under reduced pressure. The resulting solid was partitioned between CH₂Cl₂ (20 mL) and water (20 mL). The layers were separated and the organic phase was washed with brine (20 mL), dried over MgSO₄, filtered and concentrated under reduced pressure to afford the title compound **24** (8 mg, 0.019 mmol, 85 %) as a brown solid. This material was used in the next step without further purification.

¹H NMR (400 MHz, CDCl₃) δ 7.64 (s, 1H), 7.08 – 7.02 (m, 2H), 6.74 – 6.70 (m, 2H), 6.64 (d, J = 1.3 Hz, 1H), 6.51 (t, J = 1.3 Hz, 1H), 5.36 (d, J = 14.9 Hz, 2H), 4.18 (dq, J = 13.6, 6.8 Hz, 2H), 3.70 (s, 3H), 3.31 (s, 3H), 2.52 (d, J = 1.2 Hz, 3H), 2.45 (d, J = 1.2 Hz, 3H), 1.08 – 1.04 (m, 3H). **TOF MS ESI**⁺ (m/z): [M+H]⁺ calc'd for C₂₅H₂₇N₂O₄ 419.1971; found: 419.1987.

1-Ethyl-10-hydroxy-4,6-dimethylpyrido[3,2-g]quinoline-2,8(1H,9H)-dione (25)



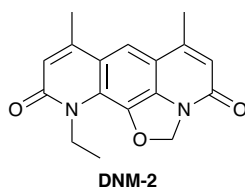
25 was obtained following experimental procedures previously described by Hergenrother and co-workers.²

To a round bottom flask containing 1-ethyl-10-methoxy-9-(4-methoxybenzyl)-4,6-dimethylpyrido[3,2-g]quinoline-2,8(1H,9H)-dione (**24**) (8 mg, 0.019 mmol) was added HBr (48 %, aq., 1 mL). The reaction mixture was stirred and heated at reflux (110 °C) for 18 h.

After completion of the reaction monitored by TLC (100 % EtOAc) water (20 mL) and the resulting precipitate was isolate *via* filtration. This afforded the title compound **25** (5 mg, 0.017 mmol, 91 %) as an off-white solid.

¹H NMR (400 MHz, DMSO-*d*₆) δ 7.65 (s, 1H), 6.93 (s, 1H), 6.44 (d, J = 1.3 Hz, 1H), 6.40 (d, J = 1.3 Hz, 1H), 4.59 (q, J = 6.8 Hz, 2H), 2.49 – 2.49 (m, 3H, under DMSO), 2.47 (d, J = 1.2 Hz, 3H), 1.16 (d, J = 6.8 Hz, 3H). **TOF MS ES⁻** (m/z): [M-H]⁻ calc'd for C₁₆H₁₅N₂O₃ 283.3; found: 283.1. **m.p.** 255.4 °C (H₂O). **LCMS** (285.1 [M+H], 1.46 min, 89 %).

11-Ethyl-6,8-dimethyl-11-hydro-2H,4H-oxazolo[5,4,3-ij]pyrido[3,2-g]quinoline-4,10-dione (DNM-2)



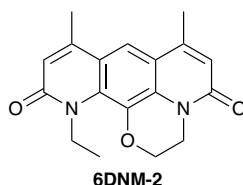
DNM-2 was obtained following experimental procedures previously described by Hergenrother and co-workers and their spectroscopic data correspond with those reported.¹⁶⁸

To a stirred solution of 1-ethyl-10-hydroxy-4,6-dimethylpyrido[3,2-g]quinoline-2,8(1*H*,9*H*)-dione (**25**) (5 mg, 0.017 mmol) in DMSO (0.5 mL) under N₂ was added K₂CO₃ (14 mg, 0.105 mmol) and dibromomethane (12 mL, 0.175 mmol). The reaction mixture was heated at 85 °C for 18 h.

After completion of the reaction monitored by TLC (10 % MeOH in CH₂Cl₂) the reaction mixture was partitioned between CH₂Cl₂ (20 mL) and water (20 mL). The layers were separated and the organic phase was washed with brine (20 mL), dried over MgSO₄, filtered and concentrated under reduced pressure. The resulting solid was purified by preparative TLC using 5 % MeOH in CH₂Cl₂ as the eluent (ran twice). This yielded the title compound **DNM-2** (1.7 mg, 33 %) as an off-white solid.

¹H NMR (400 MHz, CDCl₃) δ 7.48 (s, 1H), 6.52 (d, J = 1.3 Hz, 1H), 6.47 (q, J = 1.2 Hz, 1H), 6.41 (s, 2H), 4.54 (q, J = 7.0 Hz, 2H), 2.52 (d, J = 1.2 Hz, 3H), 2.50 (d, J = 1.2 Hz, 3H), 1.37 (t, J = 7.0 Hz, 3H). ¹³C NMR (101 MHz, CDCl₃) δ 161.7, 158.7, 147.6, 146.7, 135.1, 132.4, 125.1, 121.4, 121.1, 120.8, 113.6, 113.4, 86.1, 40.3, 20.3, 18.0, 15.0. **TOF MS ESI**⁺ (m/z): [M+H]⁺ calc'd for C₁₇H₁₇N₂O₃: 297.1239; found: 297.1234. **LCMS** (297.1 [M+H], 1.65 min, 87 %).

12-Ethyl-7,9-dimethyl-2,3-dihydro-5H-[1,4]oxazino[2,3,4-ij]pyrido[3,2-g]quinoline-5,11(12H)-dione (6DNM-2)

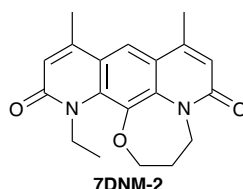


To a stirred solution of 1-ethyl-10-hydroxy-4,6-dimethylpyrido[3,2-g]quinoline-2,8(1H,9H)-dione (**25**) (20 mg, 0.069 mmol) in dry DMF (1 mL) under N₂ was added K₂CO₃ (58 mg, 0.420 mmol) and 1,2-dibromoethane (6 mL, 0.069 mmol). The reaction mixture was heated at 110 °C for 18 h.

After completion of the reaction monitored by TLC (10 % MeOH in CH₂Cl₂) the reaction mixture was partitioned between CH₂Cl₂ (20 mL) and water (20 mL). The layers were separated and the organic phase was washed with brine (20 mL), dried over MgSO₄, filtered and concentrated under reduced pressure. The resulting solid was purified by preparative TLC using 5 % MeOH in CH₂Cl₂ as the eluent (ran twice). This yielded the title compound the title compound **6DNM-2** (6.5 mg, 28 %) as an off-white solid.

¹H NMR (400 MHz, CDCl₃) δ 7.58 (s, 1H), 6.56 (d, J = 1.3 Hz, 2H), 4.60 (q, J = 6.9 Hz, 2H), 4.42 (t, J = 4.8 Hz, 2H), 4.32 (dd, J = 5.4, 4.1 Hz, 2H), 2.52 (d, J = 1.2 Hz, 3H), 2.48 (d, J = 1.2 Hz, 3H), 1.41 (t, J = 6.9 Hz, 3H). ¹³C NMR (101 MHz, CDCl₃) δ 163.2, 160.5, 146.6, 145.7, 130.8, 130.3, 127.9, 121.1, 119.8, 118.8, 116.7, 114.2, 63.7, 42.3, 40.0, 19.4, 19.0, 15.4. **TOF MS ESI⁺** (m/z): [M+H]⁺ calc'd for C₁₈H₁₉N₂O₃: 311.1396; found: 311.1387. **m.p.** 239.5 °C (MeOH: CH₂Cl₂). **LCMS** (311.1 [M+H], 1.75 min, 94 %).

13-Ethyl-8,10-dimethyl-3,4-dihydro-2*H*,6*H*-[1,4]oxazepino[2,3,4-*ij*]pyrido[3,2-*g*]quinoline-6,12(13*H*)-dione (7DNM-2)



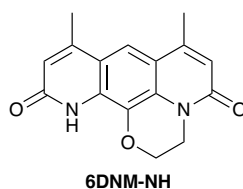
To a stirred solution of 1-ethyl-10-hydroxy-4,6-dimethylpyrido[3,2-*g*]quinoline-2,8(1*H*,9*H*)-dione (**25**) (20 mg, 0.069 mmol) in dry DMF (1 mL) under N₂ was added K₂CO₃ (58 mg, 0.420 mmol) and 1,3-dibromopropane (7 mL, 0.069 mmol). The reaction mixture was heated at 110 °C for 18 h.

After completion of the reaction monitored by TLC (10 % MeOH in CH₂Cl₂) the reaction mixture was partitioned between CH₂Cl₂ (20 mL) and water (20 mL). The layers were separated and the organic phase was washed with brine (20 mL), dried over MgSO₄, filtered and concentrated under reduced pressure. The resulting solid was purified by preparative TLC using 5 % MeOH in CH₂Cl₂ as the eluent (ran twice). This yielded the title compound the title compound **7DNM-2** (10 mg, 44 %) as an off-white solid.

¹H NMR (500 MHz, CDCl₃) δ 7.55 (s, 1H), 6.54 (d, J = 1.2 Hz, 1H), 6.53 (d, J = 1.2 Hz, 1H), 4.67 – 4.59 (m, 2H), 4.50 (q, J = 6.9 Hz, 2H), 4.35 (t, J = 6.7 Hz, 2H), 2.47 (d, J = 1.2 Hz, 3H), 2.46 (d, J = 1.2 Hz, 3H), 2.37 (p, J = 6.5 Hz, 2H), 1.44 (t, J = 6.8 Hz, 3H). **¹³C NMR** (126 MHz, CDCl₃) δ 163.7, 162.6, 146.4, 145.7, 137.7, 134.3, 134.3, 121.2, 120.6, 119.2, 118.5, 115.1, 72.3, 44.1, 42.0, 27.3, 19.4, 19.2, 15.0. **TOF MS ESI⁺** (m/z): [M+H]⁺ calc'd for C₁₉H₂₁N₂O₃: 325.1552; found: 325.1553.

7,9-Dimethyl-2,3-dihydro-5H-[1,4]oxazino[2,3,4-ij]pyrido[3,2-g]quinoline-5,11(12H)-dione

(6DNM-NH)

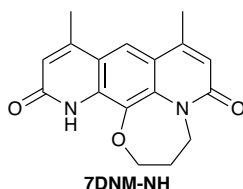


To a stirred solution of 10-hydroxy-4,6-dimethylpyrido[3,2-g]quinoline-2,8(1*H*,9*H*)-dione (**46**) (50 mg, 0.192 mmol) in DMF (2 mL) under N₂ was added K₂CO₃ (145 mg, 1.053 mmol) and dibromomethane (21 mL, 0.263 mmol). The reaction mixture was heated at 90 °C for 18 h. After completion of the reaction monitored by TLC (10 % MeOH in CH₂Cl₂), water (50 mL) was added to the reaction mixture and the resulting solid was isolated *via* filtration. This yielded the title compound **6DNM-NH** (30 mg, 13 %) as an off-white solid.

¹H NMR (500 MHz, CDCl₃) δ 8.95 (s, 1H), 7.56 (s, 1H), 6.54 (q, J = 1.3 Hz, 1H), 6.52 – 6.48 (m, 1H), 4.50 (dd, J = 5.3, 4.3 Hz, 2H), 4.33 (dd, J = 5.4, 4.2 Hz, 2H), 2.54 (d, J = 1.2 Hz, 3H), 2.53 (d, J = 1.2 Hz, 3H). ¹³C NMR (126 MHz, CDCl₃) δ 161.87, 160.28, 148.56, 147.17, 127.87, 126.47, 120.84, 119.95, 116.90, 116.33, 113.33, 64.48, 39.86, 19.31. Note: one of the aryl carbons (likely to be C-OCH₂-) is not observed despite increase scans. TOF MS ESI⁺ (m/z): [M+H]⁺ calc'd for C₁₆H₁₅N₂O₃: 283.1004; found: 283.1087. m.p. 289.7 °C (H₂O). LCMS (283.1 [M+H], 1.39 min, 100 %).

The spectroscopic data correspond with those previously reported.²⁴⁸

8,10-Dimethyl-3,4-dihydro-2H,6H-[1,4]oxazepino[2,3,4-ij]pyrido[3,2-g]quinoline-6,12(13H)-dione (7DNM-NH)

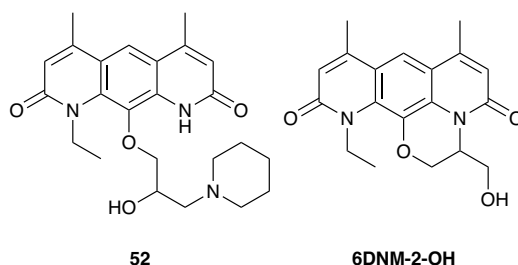


To a stirred solution of 10-hydroxy-4,6-dimethylpyrido[3,2-g]quinoline-2,8(1H,9H)-dione (**46**) (235 mg, 0.824 mmol) in DMF (5 mL) under N₂ was added K₂CO₃ (683 mg, 4.947 mmol) and 1,3-dibromopropane (71 mL, 0.824 mmol). The reaction mixture was heated at 110 °C for 18 h.

After completion of the reaction monitored by TLC (10 % MeOH in CH₂Cl₂), water (50 mL) was added to the reaction mixture and the resulting solid was isolated *via* filtration. This yielded the title compound **7DNM-2** (39 mg, 67 %) as an off-white solid.

¹H NMR (500 MHz, CDCl₃) δ 9.19 (s, 1H), 7.59 (s, 1H), 6.52 – 6.51 (m, 1H), 6.50 – 6.49 (m, 1H), 4.68 – 4.62 (m, 2H), 4.44 (t, J = 7.0 Hz, 2H), 2.52 (d, J = 1.2 Hz, 3H), 2.48 (d, J = 1.2 Hz, 3H), 2.42 – 2.36 (m, 2H). **¹³C NMR** (126 MHz, CDCl₃) δ 162.27, 162.01, 148.17, 146.53, 133.55, 133.21, 131.66, 120.79, 120.30, 118.35, 116.55, 115.28, 72.32, 41.38, 27.78, 19.26, 19.04. **TOF MS ESI⁺** (m/z): [M+H]⁺ calc'd for C₁₇H₁₇N₂O₃: 297.1161; found: 297.1236. **LCMS** (297.1 [M+H], 1.47 min, 100 %).

1-Ethyl-10-(2-hydroxy-3-(piperidin-1-yl)propoxy)-4,6-dimethylpyrido[3,2-g]quinoline-2,8(1*H*,9*H*)-dione (52) and 12-Ethyl-3-(hydroxymethyl)-7,9-dimethyl-2,3-dihydro-5*H*-[1,4]oxazino[2,3,4-*ij*]pyrido[3,2-*g*]quinoline-5,11(12*H*)-dione (6DNM-2-OH)



To a stirred solution of 1-ethyl-10-hydroxy-4,6-dimethylpyrido[3,2-*g*]quinoline-2,8(1*H*,9*H*)-dione (**25**) (50 mg, 0.176 mmol) in a mixture of dry dioxane (1 mL) and dry DMF (0.5 mL) under N₂ was added piperidine (1 drop) and epichlorohydrin (138 mL, 1.761 mmol). The reaction mixture was heated at 85 °C for 18 h.

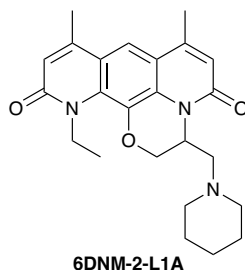
After completion of the reaction, monitored by TLC (10 % MeOH in CH₂Cl₂), the reaction mixture was concentrated under reduced pressure. The crude solid was then purified by column chromatography using 100 % EtOAc as the eluent.

This yielded:

The title compound **52** (25 mg, 32 %). ¹H NMR (400 MHz, CDCl₃, 328K) δ 11.06 (br. s, 1H), 7.71 (s, 1H), 6.53 – 6.50 (m, 2H), 4.80 (br. s, 1H), 4.53 (br. s, 1H), 4.18 – 4.09 (m, 1H), 3.97 (dd, *J* = 10.6, 2.5 Hz, 1H), 3.84 – 3.74 (m, 1H), 3.67 – 3.63 (m, 1H), 2.74 – 2.63 (m, 3H), 2.50 (d, *J* = 1.2 Hz, 3H), 2.48 (d, *J* = 1.2 Hz, 3H), 2.45 – 2.36 (m, 3H), 1.70 – 1.56 (m, 4H), 1.54 – 1.44 (m, 2H), 1.23 (t, *J* = 7.0 Hz, 3H). ¹³C NMR (101 MHz, CDCl₃) δ 163.2, 163.0, 147.5, 146.1, 134.3, 133.3, 131.3, 121.1, 120.3, 118.8, 117.4, 117.0, 77.0, 65.7, 59.2, 54.5, 39.4, 26.0, 24.2, 19.4, 18.9, 14.4. **TOF MS ESI⁺** (*m/z*): [M+H]⁺ calc'd for C₂₄H₃₂N₃O₄: 426.2315; found: 426.2390.

The title compound **6DNM-2-OH** (12 mg, 20 %) **¹H NMR** (400 MHz, CDCl₃) δ 7.61 (s, 1H), 6.58 (q, J = 1.2 Hz, 2H), 5.16 – 5.10 (m, 1H), 4.90 (dd, J = 11.4, 1.1 Hz, 1H), 4.68 – 4.59 (m, 2H), 4.04 – 3.99 (m, 1H), 3.99 – 3.93 (m, 1H), 3.92 – 3.84 (m, 1H), 3.03 (t, J = 6.0 Hz, 1H), 2.54 (d, J = 1.2 Hz, 3H), 2.49 (d, J = 1.2 Hz, 3H), 1.40 (t, J = 6.9 Hz, 3H). **¹³C NMR** (101 MHz, CDCl₃) δ 163.2, 161.2, 147.3, 145.6, 130.5, 130.3, 127.2, 121.2, 119.6, 118.9, 116.8, 114.5, 64.2, 61.4, 51.0, 42.2, 19.4, 19.1, 15.4. **TOF MS ESI⁺** (m/z): [M+H]⁺ calc'd for C₁₉H₂₁N₂O₄: 341.1423; found: 341.1509.

12-Ethyl-7,9-dimethyl-3-(piperidin-1-ylmethyl)-2,3-dihydro-5H-[1,4]oxazino[2,3,4-*ij*]pyrido[3,2-*g*]quinoline-5,11(12*H*)-dione (6DNM-2-L1A)



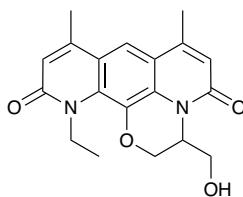
To a stirred solution of 1-ethyl-10-(2-hydroxy-3-(piperidin-1-yl)propoxy)-4,6-dimethylpyrido[3,2-*g*]quinoline-2,8(1*H*,9*H*)-dione (**52**) (25 mg, 0.058 mmol) in dry CH₂Cl₂ (1 mL) under N₂ at 0 °C was added MsCl (6 mL, 0.071 mmol) and NEt₃ (20 mL, 0.141 mmol). The reaction mixture was allowed to warm to rt and stirred for 2 h. Further MsCl (12 mL, 0.142 mmol) and NEt₃ (40 mL, 0.282 mmol) were added and the stirring was continued for 30 min.

After completion of the reaction, monitored by TLC (100 % EtOAc), the reaction mixture was concentrated under reduced pressure and dried under vacuum. The resulting solid was then placed under N₂ and re-dissolved in dry DMF (2 mL). K₂CO₃ (29 mg, 0.212 mmol) was then added and the reaction mixture was heated at 40 °C for 18 h.

After completion of the reaction, monitored by TLC (100 % EtOAc), the reaction mixture was partitioned between CH₂Cl₂ (30 mL) and water (30 mL). The organic phase was separated, washed with brine (40 mL), dried over MgSO₄, filtered and concentrated. The crude solid was purified by preparative TLC (ran in 1 % MeOH in CH₂Cl₂ then twice in 2.5 % MeOH in CH₂Cl₂). This yielded the title compound **6DNM-2-L1A** (12 mg, 42 %) as an off-white solid.

¹H NMR (400 MHz, DMSO-*d*₆) δ 7.66 (s, 1H), 6.54 – 6.51 (m, 1H), 6.50 – 6.48 (m, 1H), 5.00 – 4.88 (m, 1H), 4.80 (d, J = 11.0 Hz, 1H), 4.60 – 4.45 (m, 2H), 4.07 – 3.99 (m, 1H), 2.59 (s, 3H), 2.52 – 2.49 (m, 3H), 2.47 (d, J = 1.2 Hz, 3H), 2.41 – 2.32 (m, 2H), 2.31 – 2.22 (m, 1H), 1.61 – 1.45 (m, 4H), 1.43 – 1.34 (m, 2H), 1.27 (t, J = 6.8 Hz, 3H). **¹³C NMR** (101 MHz, CDCl₃) δ 163.2, 160.0, 146.4, 145.6, 130.6, 129.9, 127.4, 121.0, 120.0, 118.7, 116.8, 114.0, 64.5, 56.8, 55.4, 47.2, 41.9, 26.2, 24.3, 19.4, 19.0, 15.4. **TOF MS ESI⁺** (m/z): [M+H]⁺ calc'd for C₂₄H₃₀N₃O₃: 408.2209; found: 408.2291. **m.p.** 178.2 °C (MeOH: CH₂Cl₂). **LCMS** (408.2 [M+H], 1.33 min, 100 %).

12-Ethyl-3-(hydroxymethyl)-7,9-dimethyl-2,3-dihydro-5H-[1,4]oxazino[2,3,4-
ij]pyrido[3,2-g]quinoline-5,11(12H)-dione (6DNM-2-OH)



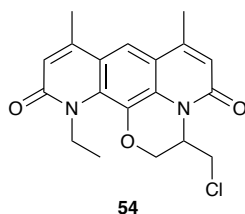
6DNM-2-OH

To a stirred solution of 1-ethyl-10-hydroxy-4,6-dimethylpyrido[3,2-*g*]quinoline-2,8(1*H*,9*H*)-dione (**25**) (162 mg, 0.570 mmol) in a mixture of dry dioxane (5 mL) and dry DMF (2.5 mL) under N₂ was added K₂CO₃ (157 mg, 1.141 mmol) and epichlorohydrin (89 mL, 1.141 mmol). The reaction mixture was heated at 85 °C for 18 h. After this time had passed epichlorohydrin (240 mL, 3.423 mmol) and dry DMF (2.5 mL) were added. The reaction mixture was heated for a further 24 h.

After completion of the reaction, monitored by TLC (5 % MeOH in CH₂Cl₂), the reaction mixture was partitioned between CH₂Cl₂ (40 mL) and water (40 mL). The layers were separated and the organic phase was washed with brine (40 mL), dried over MgSO₄, filtered and concentrated under reduced pressure. The crude solid was then purified by column chromatography using 100 % EtOAc as the eluent. This yielded the title compound **6DNM-2-OH** (120 mg, 62 %) as an off-white solid.

¹H NMR (400 MHz, CDCl₃) δ 7.61 (s, 1H), 6.58 (q, J = 1.2 Hz, 2H), 5.16 – 5.10 (m, 1H), 4.90 (dd, J = 11.4, 1.1 Hz, 1H), 4.68 – 4.59 (m, 2H), 4.04 – 3.99 (m, 1H), 3.99 – 3.93 (m, 1H), 3.92 – 3.84 (m, 1H), 3.03 (t, J = 6.0 Hz, 1H), 2.54 (d, J = 1.2 Hz, 3H), 2.49 (d, J = 1.2 Hz, 3H), 1.40 (t, J = 6.9 Hz, 3H). ¹³C NMR (101 MHz, DMSO-*d*₆) δ 162.1, 159.1, 147.2, 146.6, 130.0, 129.3, 127.4, 119.8, 119.2, 117.7, 116.1, 114.7, 63.2, 57.4, 49.9, 41.3, 18.8, 18.4, 15.3. **TOF MS ESI**⁺ (m/z): [M+H]⁺ calc'd for C₁₉H₂₁N₂O₄: 341.1423; found: 341.1509. **m.p.** 246.0 °C (EtOAc). **LCMS** (341.2 [M+H], 1.59 min, 100 %).

3-(Chloromethyl)-12-ethyl-7,9-dimethyl-2,3-dihydro-5H-[1,4]oxazino[2,3,4-
ij]pyrido[3,2-g]quinoline-5,11(12H)-dione (54)

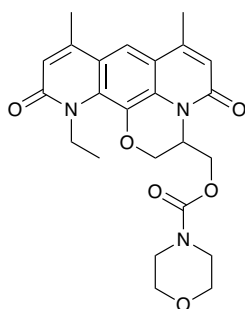


To a stirred solution of 12-ethyl-3-(hydroxymethyl)-7,9-dimethyl-2,3-dihydro-5H-[1,4]oxazino[2,3,4-ij]pyrido[3,2-g]quinoline-5,11(12H)-dione (**6DNM-2-OH**) (30 mg, 0.088 mmol) in CH₂Cl₂ (0.5 mL) was added SOCl₂ (10 mL, 0.132 mmol). The reaction mixture was stirred at room temperature for 18 h.

After completion of the reaction monitored by TLC (100 % CH₂Cl₂) the reaction mixture was partitioned between CH₂Cl₂ (10 mL) and water (10 mL). The layers were separated and the organic phase was washed with brine (10 mL), dried over MgSO₄, filtered and concentrated under reduced pressure. The crude solid was then purified by column chromatography using 10 % EtOAc in CH₂Cl₂ as the eluent. This yielded the title compound **54** (16 mg, 52 %) as an off-white solid.

¹H NMR (400 MHz, CDCl₃) δ 7.61 (s, 1H), 6.58 (d, *J* = 1.2 Hz, 1H), 6.55 (d, *J* = 1.3 Hz, 1H), 5.16 – 5.09 (m, 1H), 5.08 – 5.03 (m, 1H), 4.65 (q, *J* = 6.9 Hz, 2H), 4.03 – 3.96 (m, 1H), 3.85 – 3.78 (m, 1H), 3.63 (t, *J* = 10.6 Hz, 1H), 2.52 (d, *J* = 1.2 Hz, 3H), 2.48 (d, *J* = 1.1 Hz, 3H), 1.43 – 1.38 (m, 3H). **TOF MS ESI**⁺ (*m/z*): [M+H]⁺ calc'd for C₁₉H₂₀ClN₂O₃: 359.1084; found: 359.1152.

(12-Ethyl-7,9-dimethyl-5,11-dioxo-2,3,11,12-tetrahydro-5H-[1,4]oxazino[2,3,4-*ij*]pyrido[3,2-*g*]quinolin-3-yl)methyl morpholine-4-carboxylate (6DNM-2-L2B)

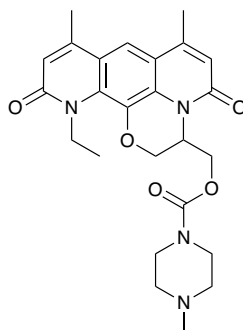


6DNM-2-L2B

To a stirred solution of 3-(chloromethyl)-12-ethyl-7,9-dimethyl-2,3-dihydro-5H-[1,4]oxazino[2,3,4-*ij*]pyrido[3,2-*g*]quinoline-5,11(12*H*)-dione (**54**) (16 mg, 0.045 mmol) in MeCN (0.5 mL) and DMF (0.5 mL) was added morpholine (10 μ L, 0.111 mmol), K_2CO_3 (15 mg, 0.111 mmol) and KF (18 mg, 0.111 mmol). The reaction mixture was heated at 80 $^{\circ}C$ for 18 h. After completion of the reaction monitored by TLC (100 % EtOAc) the reaction mixture was partitioned between CH_2Cl_2 (10 mL) and water (10 mL). The layers were separated and the organic phase was washed with brine (10 mL), dried over $MgSO_4$, filtered and concentrated under reduced pressure. The crude solid was then purified by preparative TLC (ran using 10 % MeOH in CH_2Cl_2). This yielded the title compound **6DNM-2-L2B** (6 mg, 30 %) as a white solid.

1H NMR (400 MHz, $CDCl_3$) δ 7.60 (d, $J = 2.5$ Hz, 1H), 6.59 – 6.53 (m, 2H), 5.33 – 5.06 (m, 1H), 4.94 – 4.73 (m, 1H), 4.69 – 4.54 (m, 2H), 4.47 – 4.36 (m, 1H), 4.11 – 3.98 (m, 1H), 3.98 – 3.82 (m, 1H), 3.73 – 3.52 (m, 2H), 3.46 (d, $J = 16.8$ Hz, 4H), 3.28 (s, 2H), 2.53 (s, 3H), 2.48 (s, 3H), 1.43 – 1.36 (m, 3H). ^{13}C NMR (126 MHz, $CDCl_3$) δ 163.2, 160.1, 154.6, 147.0, 145.9, 130.2, 127.4, 127.3, 121.0, 119.8, 118.8, 116.8, 114.5, 66.5, 66.3, 64.6, 62.6, 47.5, 44.2, 43.9, 42.4, 19.4, 19.1, 15.4. TOF MS ESI $^+$ (m/z): $[M+H]^+$ calc'd for $C_{24}H_{28}N_3O_6$: 454.1900; found: 454.1937. LCMS (454.2 $[M+H]$, 1.75 min, 100 %).

(12-Ethyl-7,9-dimethyl-5,11-dioxo-2,3,11,12-tetrahydro-5H-[1,4]oxazino[2,3,4-*ij*]pyrido[3,2-*g*]quinolin-3-yl)methyl 4-methylpiperazine-1-carboxylate (6DNM-2-L2D)



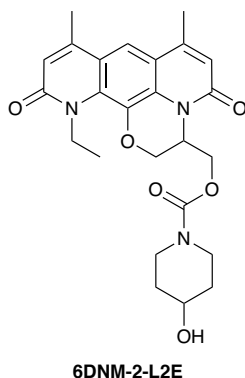
6DNM-2-L2D

To a stirred solution of 3-(chloromethyl)-12-ethyl-7,9-dimethyl-2,3-dihydro-5H-[1,4]oxazino[2,3,4-*ij*]pyrido[3,2-*g*]quinoline-5,11(12*H*)-dione (**54**) (25 mg, 0.070 mmol) in DMF (1 mL) was added 1-methylpiperazine (17 μ L, 0.154 mmol), K_2CO_3 (21 mg, 0.154 mmol) and KF (26 mg, 0.154 mmol). The reaction mixture was heated at 80 $^{\circ}C$ for 18 h.

After completion of the reaction monitored by TLC (10 % MeOH in CH_2Cl_2) the reaction mixture was partitioned between CH_2Cl_2 (10 mL) and HCl (1 M, 10 mL). The layers were separated and the aqueous phase was basified with K_2CO_3 (30 mL) and extracted with $CHCl_3$:IPA (3:1, 2 x 20 mL). The organic extracts were then combined washed with brine (10 mL), dried over $MgSO_4$, filtered and concentrated under reduced pressure. The crude solid was then purified by preparative TLC (ran three times using 5 % MeOH in CH_2Cl_2). This yielded the title compound **6DNM-2-L2D** (9 mg, 28 %) as an off-white solid.

¹H NMR (400 MHz, CDCl₃) δ 7.61 (s, 1H), 6.57 (d, J = 1.3 Hz, 1H), 6.53 (d, J = 1.3 Hz, 1H), 5.40 – 5.31 (m, 1H), 4.77 (dd, J = 11.5, 1.1 Hz, 1H), 4.67 – 4.56 (m, 2H), 4.53 – 4.44 (m, 1H), 4.42 – 4.32 (m, 1H), 4.07 (dd, J = 11.4, 2.6 Hz, 1H), 3.71 – 3.55 (m, 2H), 3.52 – 3.36 (m, 2H), 2.54 (d, J = 1.2 Hz, 3H), 2.49 (d, J = 1.2 Hz, 3H), 2.45 – 2.41 (m, 7H), 1.40 (t, J = 6.9 Hz, 3H). **¹³C NMR** (101 MHz, CDCl₃) δ 163.1, 160.1, 154.3, 147.7, 145.7, 136.6, 130.6, 129.9, 127.1, 126.3, 121.3, 116.8, 114.8, 64.9, 52.8, 52.4, 47.1, 43.7, 42.3, 41.0, 19.4, 19.2, 15.4. Note: one of the aryl carbons (likely to be C-OCH₂-) is not observed despite increase scans. **TOF MS ESI⁺** (m/z): [M+H]⁺ calc'd for C₂₅H₃₁N₄O₅: 467.2216; found: 467.2286. **LCMS** (467.2 [M+H], 1.31 min, 83 %).

(12-Ethyl-7,9-dimethyl-5,11-dioxo-2,3,11,12-tetrahydro-5H-[1,4]oxazino[2,3,4-*ij*]pyrido[3,2-*g*]quinolin-3-yl)methyl 4-hydroxypiperidine-1-carboxylate (6DNM-2-L2E)

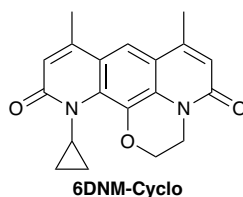


To a stirred solution of 3-(chloromethyl)-12-ethyl-7,9-dimethyl-2,3-dihydro-5H-[1,4]oxazino[2,3,4-*ij*]pyrido[3,2-*g*]quinoline-5,11(12*H*)-dione (**54**) (25 mg, 0.070 mmol) in DMF (1 mL) was added piperidin-4-ol (16 mg, 0.156 mmol), K₂CO₃ (21 mg, 0.156 mmol) and KF (26 mg, 0.156 mmol). The reaction mixture was heated at 80 °C for 18 h.

After completion of the reaction monitored by TLC (10 % MeOH in CH₂Cl₂) the reaction mixture was partitioned between CH₂Cl₂ (10 mL) and HCl (1 M, 10 mL). The layers were separated and the aqueous phase was basified with K₂CO₃ (30 mL) and extracted with CHCl₃:IPA (3:1, 2 x 20 mL). The organic extracts were then combined washed with brine (10 mL), dried over MgSO₄, filtered and concentrated under reduced pressure. The crude solid was then purified by preparative TLC (ran three times using 5 % MeOH in CH₂Cl₂). This yielded the title compound **6DNM-2-L2E** (14 mg, 43 %) as an off-white solid.

¹H NMR (500 MHz, CDCl₃) δ 7.61 (s, 1H), 6.62 (dd, J = 2.8, 1.4 Hz, 1H), 6.57 (d, J = 1.2 Hz, 1H), 5.33 – 5.25 (m, 1H), 4.79 (dd, J = 11.4, 1.0 Hz, 1H), 4.66 – 4.58 (m, 3H), 4.46 – 4.36 (m, 2H), 4.07 (dd, J = 11.4, 2.6 Hz, 1H), 3.86 – 3.79 (m, 2H), 3.70 – 3.58 (m, 1H), 3.16 – 2.90 (m, 2H), 2.54 – 2.53 (m, 4H), 2.50 (d, J = 1.1 Hz, 3H), 1.89 – 1.66 (m, 2H), 1.41 (t, J = 7.0 Hz, 3H). **¹³C NMR** (126 MHz, CDCl₃) δ 163.3, 160.1, 154.6, 147.1, 146.1, 130.3, 130.1, 127.3, 120.9, 119.8, 118.8, 116.9, 114.5, 67.1, 64.7, 62.5, 50.9, 47.5, 42.5, 41.3, 33.8, 19.4, 19.1, 15.4. **TOF MS ESI⁺** (m/z): [M+H]⁺ calc'd for C₂₅H₃₀N₃O₆: 468.2056; found: 468.2125. **LCMS** (468.2 [M+H], 1.61 min, 100 %).

12-Cyclopropyl-7,9-dimethyl-2,3-dihydro-5H-[1,4]oxazino[2,3,4-ij]pyrido[3,2-g]quinoline-5,11(12H)-dione (6DNM-Cyclo)

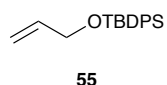


6DNM-Cyclo was obtained following experimental procedures previously described by Engle and co-workers.²³³

To a stirred solution 7,9-dimethyl-2,3-dihydro-5H-[1,4]oxazino[2,3,4-ij]pyrido[3,2-g]quinoline-5,11(12H)-dione (**6DNM-NH**) (30 mg, 0.106 mmol) in toluene (0.5 mL) and water (0.15 mL) was added potassium cyclopropyltrifluoroborate (47 mg, 0.319 mmol), 1,10-phenanthroline (5 mg, 0.027 mmol), Cu(OAc)₂ (5 mg, 0.027 mmol) and K₂CO₃ (29 mg, 0.212 mmol). Air was bubble through the reaction mixture and it was heated at 70 °C for 18 h. After completion of the reaction monitored by TLC (100 % EtOAc), the reaction mixture was partitioned between CH₂Cl₂ (10 mL) and water (10 mL). The layers were separated and the organic phase was washed with brine (10 mL), dried over MgSO₄, filtered and concentrated under reduced pressure. The crude solid was then purified by preparative TLC (ran twice using 5 % MeOH in CH₂Cl₂). This yielded the title compound **6DNM-Cyclo** (20 mg, 7 %) as a white solid.

¹H NMR (500 MHz, DMSO-*d*₆) δ 7.61 (s, 1H), 6.55 – 6.50 (m, 1H), 6.37 – 6.33 (m, 1H), 4.42 (t, J = 4.8 Hz, 2H), 4.13 (t, J = 4.9 Hz, 2H), 3.19 – 3.13 (m, 1H), 2.50 – 2.49 (m, 3H), 2.44 – 2.42 (m, 3H), 1.09 – 1.01 (m, 2H), 0.49 – 0.41 (m, 2H). ¹³C NMR (126 MHz, DMSO-*d*₆) δ 163.7, 159.4, 147.1, 146.2, 130.7, 130.5, 128.1, 120.3, 119.0, 118.0, 116.2, 114.1, 63.5, 48.6, 31.8, 18.5, 18.4, 10.5. **TOF MS ESI**⁺ (m/z): [M+H]⁺ calc'd for C₁₉H₁₉N₂O₃: 323.1317; found: 323.1384. **m.p.** 277.7 °C (MeOH: CH₂Cl₂). **LCMS** (323.1 [M+H], 1.65 min, 92 %).

(Allyloxy)(*tert*-butyl)diphenylsilane (55)



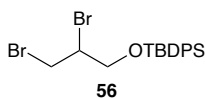
To a stirred solution of prop-2-en-1-ol (1.2 mL, 17.7 mmol) in dry DMF (40 mL) under N₂ was added imidazole (13.2 g, 194.0 mmol) and *tert*-butylchlorodiphenylsilane (5.1 mL, 19.4 mmol). The reaction mixture was stirred for 18 h at rt.

After completion of the reaction monitored by TLC (100 % CH₂Cl₂), the reaction mixture was partitioned between CH₂Cl₂ (100 mL) and HCl (1 M, 100 mL). The layers were separated and the organic phase was washed with water (80 mL), brine (80 mL), dried over MgSO₄, filtered and concentrated under reduced pressure. This afforded the title compound **55** (4.2 g, 81 %) as a colourless oil.

¹H NMR (400 MHz, CDCl₃) δ 7.76 – 7.65 (m, 4H), 7.48 – 7.34 (m, 6H), 6.00 – 5.86 (m, 1H), 5.44 – 5.33 (m, 1H), 5.17 – 5.08 (m, 1H), 4.27 – 4.18 (m, 2H), 1.07 (s, 9H). ¹³C NMR (101 MHz, CDCl₃) δ 137.1, 135.7, 133.8, 129.8, 127.8, 114.0, 64.8, 27.0, 19.4.

The spectroscopic data correspond with those previously reported.²⁴⁹

tert-Butyl(2,3-dibromopropoxy)diphenylsilane (56)



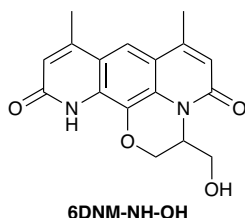
To a stirred solution of (allyloxy)(tert-butyl)diphenylsilane (**55**) (2.0 g, 6.8 mmol) in CHCl_3 (7 mL) under N_2 at 0°C was added bromine (380 μL , 7.4 mmol) in CHCl_3 (8 mL) dropwise. The reaction mixture was allowed to warm to rt and stirred for 18 h.

After completion of the reaction monitored by TLC (100 % pentane), the reaction mixture was partitioned between CH_2Cl_2 (70 mL) and sodium hydrosulfite (1 M, 80 mL). The layers were separated and the organic phase was washed with water (60 mL), brine (60 mL), dried over MgSO_4 , filtered and concentrated under reduced pressure. The crude solid was then purified by column chromatography using 100 % pentane then 10 % CH_2Cl_2 in pentane to elute the desired product. The pure product containing fractions were combined and concentrated to yield the title compound **56** (2.7 g, 87 %) as a colourless oil.

$^1\text{H NMR}$ (400 MHz, CDCl_3) δ 7.74 – 7.67 (m, 4H), 7.48 – 7.36 (m, 6H), 4.25 – 4.18 (m, 1H), 4.13 – 4.06 (m, 1H), 4.00 – 3.90 (m, 2H), 3.87 – 3.79 (m, 1H), 1.08 (s, 9H).

The spectroscopic data correspond with those previously reported.²⁵⁰

3-(Hydroxymethyl)-7,9-dimethyl-2,3-dihydro-5H-[1,4]oxazino[2,3,4-ij]pyrido[3,2-g]quinoline-5,11(12H)-dione (6DNM-NH-OH)

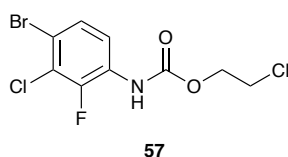


To a stirred solution of 10-hydroxy-4,6-dimethylpyrido[3,2-*g*]quinoline-2,8(1*H*,9*H*)-dione (**46**) (17 mg, 0.060 mmol) in dry DMF (1 mL) under N₂ was added K₂CO₃ (50 mg, 0.358 mmol) and 2,3-dibromopropan-1-ol (6 mL, 0.060 mmol). The reaction mixture was stirred and heated at 110 °C for 18 h.

After completion of the reaction, monitored by TLC (10 % MeOH in CH₂Cl₂), the reaction mixture was partitioned between CH₂Cl₂ (50 mL) and water (50 mL). The layers were separated and the organic phase was washed with brine (50 ml), dried over MgSO₄, filtered and concentrated. The resulting solid was purified by column chromatography using 5 % MeOH in CH₂Cl₂ as the eluent. This yielded the title compound **6DNM-NH-OH** (4 mg, 21 %) as a white solid.

¹H NMR (400 MHz, CDCl₃) δ 8.95 (br. s, 1H), 7.58 (s, 1H), 6.57 – 6.55 (m, 1H), 6.53 – 6.50 (m, 1H), 5.18 – 5.11 (m, 1H), 4.92 (dd, J = 11.4, 0.9 Hz, 1H), 4.14 (dd, J = 11.6, 2.7 Hz, 1H), 3.88 (d, J = 20.7 Hz, 2H), 2.54 (s, 6H). **TOF MS ESI⁺** (m/z): [M+H]⁺ calc'd for C₁₇H₁₇N₂O₄: 313.1110; found: 313.1185.

2-Chloroethyl (4-bromo-3-chloro-2-fluorophenyl)carbamate (57)

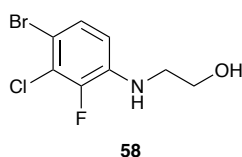


To a stirred solution of 4-bromo-3-chloro-2-fluoroaniline (5 g, 22.3 mmol) in dry CH₂Cl₂ (100 mL) under N₂ at 0 °C was added 2-chloroethyl carbonochloridate (2.4 mL, 22.3 mmol) slowly then pyridine (5.4 mL, 66.8 mmol) slowly. The reaction mixture was allowed to warm to rt and stirred for 5 h.

After completion of the reaction, monitored by TLC (1:1; pentane: CH₂Cl₂), the reaction mixture was partitioned between CH₂Cl₂ (50 mL) and HCl (1 M, 100 mL). The layers were separated and the organic phase was washed with water (100 mL), brine (100 mL), dried over MgSO₄, filtered and concentrated under reduced pressure. This afforded the title compound **57** (7.37 g, 100 %) as a light pink solid.

¹H NMR (400 MHz, CDCl₃) δ 8.00 – 7.90 (m, 1H), 7.41 (dd, J = 9.0, 2.1 Hz, 1H), 6.94 (br. s, 1H), 4.49 – 4.43 (m, 2H), 3.78 – 3.73 (m, 2H). ¹⁹F NMR (377 MHz, CDCl₃) δ -126.35.

2-((4-Bromo-3-chloro-2-fluorophenyl)amino)ethan-1-ol (58)

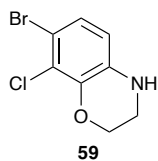


To a stirred solution of 2-chloroethyl (4-bromo-3-chloro-2-fluorophenyl)carbamate (**57**) (7.4 g, 25.2 mmol) in EtOH (250 mL) was added KOH (14.1 g, 251.6 mmol). The reaction mixture was stirred for 18 h at rt.

After completion of the reaction, monitored by TLC (100 % CH₂Cl₂), the reaction mixture was partitioned between CH₂Cl₂ (200 mL) and HCl (1 M, 200 mL). The layers were separated and the organic phase was washed with water (200 mL), brine (200 mL), dried over MgSO₄, filtered and concentrated under reduced pressure. This afforded the title compound **58** (5.89 g, 88 %) as a light pink oil.

¹H NMR (400 MHz, Chloroform-d) δ 7.22 (dd, J = 8.8, 2.0 Hz, 1H), 6.52 (t, J = 8.6 Hz, 1H), 4.34 (br. s, 1H), 3.90 – 3.82 (m, 2H), 3.36 – 3.27 (m, 2H), 1.75 (br. s, 1H). **¹³C NMR** (101 MHz, CDCl₃) δ 147.92 (d, J = 243.2 Hz), 137.01 (d, J = 12.1 Hz), 128.23 (d, J = 3.8 Hz), 121.88 (d, J = 17.3 Hz), 111.11 (d, J = 4.2 Hz), 108.84, 61.19, 45.66. **¹⁹F NMR** (377 MHz, CDCl₃) δ -130.87. **TOF MS ESI⁺** (m/z): [M+H]⁺ calc'd for C₈H₉BrClFNO: 267.9462; found: 267.9533.

7-Bromo-8-chloro-3,4-dihydro-2H-benzo[b][1,4]oxazine (59)

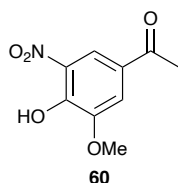


To a stirred solution of 2-((4-bromo-3-chloro-2-fluorophenyl)amino)ethan-1-ol (**58**) (100 mg, 0.375 mmol) in dry THF (3.6 mL) under N₂ was added NaH (60 %, 17 mg, 0.450 mmol). The reaction mixture was stirred and heated at 50 °C for 18 h.

After completion of the reaction, monitored by TLC (100 % CH₂Cl₂), the reaction mixture was partitioned between CH₂Cl₂ (50 mL) and HCl (1 M, 50 mL). The layers were separated and the organic phase was washed with brine (50 mL), dried over MgSO₄, filtered and concentrated. The resulting solid was purified by column chromatography using 100 % CH₂Cl₂ as the eluent. This yielded the title compound **59** (18 mg, 19 %).

¹H NMR (500 MHz, DMSO-*d*₆, at 393K) δ 7.21 (d, J = 8.8 Hz, 1H), 6.56 (d, J = 8.8 Hz, 1H), 4.31 – 4.26 (m, 2H), 3.39 – 3.35 (m, 2H). Mass spectrometry analysis using a range of techniques failed to give the correct mass. This was potentially due to the extremely poor solubility of the compound.

1-(4-Hydroxy-3-methoxy-5-nitrophenyl)ethan-1-one (60)



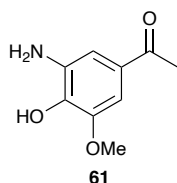
60 was obtained following experimental procedures previously described by Learmonth and co-workers and their spectroscopic data correspond with those reported.²³⁴

To a stirred solution of 1-(4-hydroxy-3-methoxyphenyl)ethan-1-one (1.0 g, 6.0 mmol) in acetic acid (14 mL) at 0 °C was added HNO₃ (422 mL, 6.62 mmol). Precipitate immediately started to form. The reaction mixture was then allowed to warm to room temperature and stirred for 18 h.

After completion of the reaction monitored by TLC (100 % CH₂Cl₂) water (10 mL) was added. The resulting precipitate was isolated *via* filtration, washed with Et₂O and dried under vacuum. This yielded the title compound **60** (831 mg, 67 %) as a yellow solid.

¹H NMR (400 MHz, CDCl₃) δ 11.15 (s, 1H), 8.31 (d, *J* = 2.0 Hz, 1H), 7.77 (d, *J* = 1.9 Hz, 1H), 4.01 (s, 3H), 2.63 (s, 3H). **TOF MS ESI⁻** (m/z): [M-H]⁻ calc'd for C₉H₈NO₅: 210.0481; found: 210.0410.

1-(3-Amino-4-hydroxy-5-methoxyphenyl)ethan-1-one (61)



61 was obtained following experimental procedures previously described by Wang and co-workers and their spectroscopic data correspond with those reported.²⁵¹

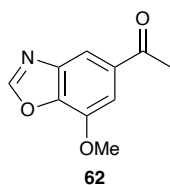
To a stirred solution of 1-(4-hydroxy-3-methoxy-5-nitrophenyl)ethan-1-one (**60**) (1.0 g, 4.7 mmol) in EtOH (40 mL) under N₂ was added Pd/C (10 %, 252 mg, 0.237 mmol). The atmosphere was changed to H₂ and the reaction mixture was stirred for 18 h.

After completion of the reaction, monitored by TLC (100 % CH₂Cl₂), the reaction mixture was filtered through celite with CH₂Cl₂/ MeOH (1:1, 60 mL) and the filtrate was concentrated under reduced pressure. This yielded the title compounds **61** (576 mg, 67 %) as a yellow solid.

¹H NMR (400 MHz, CDCl₃) δ 7.06 (d, *J* = 1.9 Hz, 1H), 7.03 (d, *J* = 1.9 Hz, 1H), 3.92 (s, 3H), 2.52

(s, 3H). FTMS APCI⁺ (m/z): [M+H]⁺ calc'd for C₉H₁₂NO₃: 182.0739; found: 182.0907.

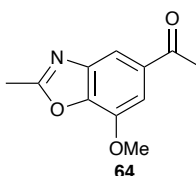
1-(7-Methoxybenzo[d]oxazol-5-yl)ethan-1-one (62)



To a stirred solution of 1-(3-amino-4-hydroxy-5-methoxyphenyl)ethan-1-one (**61**) (286 mg, 1.580 mmol) in triethyl orthoformate (20 mL) and DMF (5 mL) was heated at 105 °C for 18 h. After completion of the reaction, monitored by TLC (100 % CH₂Cl₂), the reaction mixture was concentrated under reduced pressure. This crude solid was taken onto the next step without further purification **62** (280 mg, 93 %) as a light brown solid.

¹H NMR (400 MHz, CDCl₃) δ 8.16 (s, 1H), 8.01 (d, *J* = 1.5 Hz, 1H), 7.61 (d, *J* = 1.4 Hz, 1H), 4.08 (s, 3H), 2.69 (s, 3H). FTMS APCI⁺ (*m/z*): [M+H]⁺ calc'd for C₁₀H₁₀NO₃: 192.0582; found: 192.0661.

1-(7-Methoxy-2-methylbenzo[d]oxazol-5-yl)ethan-1-one (64)

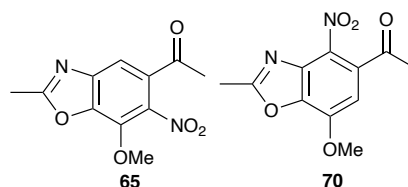


To a stirred solution of 1-(3-amino-4-hydroxy-5-methoxyphenyl)ethan-1-one (**61**) (576 mg, 3.18 mmol) in triethyl orthoacetate (10 mL) was added TFA (243 mL, 3.18 mmol). The reaction mixture was then stirred for 18 h at room temperature.

After completion of the reaction monitored by TLC (100 % CH₂Cl₂) the reaction mixture was diluted with sat. aq. K₂CO₃ (1 M, 50 mL) and stirred for 30 min. CH₂Cl₂ (50 mL) was then added and the layers were separated. The organic phase was washed with brine (50 mL), dried over MgSO₄, filtered and concentrated under reduced pressure. This yielded the title compound **64** (640 mg, 98 %) as a light brown solid.

¹H NMR (400 MHz, CDCl₃) δ 7.87 (d, *J* = 1.4 Hz, 1H), 7.54 (d, *J* = 1.4 Hz, 1H), 4.06 (s, 3H), 2.68 (s, 3H), 2.67 (s, 3H). **TOF MS ESI⁺** (*m/z*): [M+H]⁺ calc'd for C₁₁H₁₂NO₃: 206.0739; found: 206.0822.

1-(7-Methoxy-2-methyl-6-nitrobenzo[d]oxazol-5-yl)ethan-1-one (65) and 1-(7-methoxy-2-methyl-4-nitrobenzo[d]oxazol-5-yl)ethan-1-one (70)



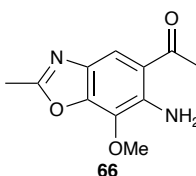
1-(7-Methoxy-2-methylbenzo[d]oxazol-5-yl)ethan-1-one (**64**) (100 mg, 0.488 mmol) was dissolved in acetic anhydride (5 mL) at 0 °C and Cu(II)(NO₂)₃·3H₂O (118 mg, 0.488 mmol) was added. The reaction was allowed to warm to rt and stirred for 18 h.

After completion of the reaction, monitored by TLC (100 % CH₂Cl₂) the reaction mixture was partitioned between CH₂Cl₂ (40 mL) and NH₄Cl (40 mL). The layers were separated and the organic phase was washed with brine (40 mL), dried over MgSO₄, filtered and concentrated. The crude solid was purified by preparative TLC (100 % CH₂Cl₂, ran four times). The yielded:

The title compound **65** (43 mg, 35 %). ¹H NMR (400 MHz, CDCl₃) δ 7.70 (s, 1H), 4.29 (s, 3H), 2.74 (s, 3H), 2.63 (s, 3H). TOF MS ESI⁺ (m/z): [M+H]⁺ calc'd for C₁₁H₁₁N₂O₅: 251.0590; found: 251.0663.

The title compound **70** (27 mg, 22 %). ¹H NMR (400 MHz, CDCl₃) δ 6.79 (s, 1H), 4.11 (s, 3H), 2.75 (s, 3H), 2.53 (s, 3H). TOF MS ESI⁺ (m/z): [M+H]⁺ calc'd for C₁₁H₁₁N₂O₅: 251.0590; found: 251.0665.

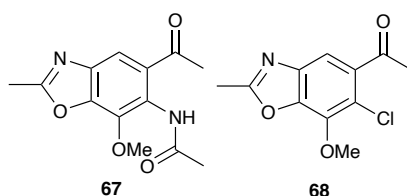
1-(6-Amino-7-methoxy-2-methylbenzo[d]oxazol-5-yl)ethan-1-one (66)



To a stirred solution of 1-(7-methoxy-2-methyl-6-nitrobenzo[d]oxazol-5-yl)ethan-1-one (**65**) (32 mg, 0.128 mmol) in EtOH (1 mL) under N₂ was added Pd/C (10 %, 14 mg, 0.013 mmol). The atmosphere was changed to H₂ and the reaction mixture was stirred for 18 h. After completion of the reaction, monitored by TLC (5 % MeOH in CH₂Cl₂), the reaction mixture was filtered through celite with CH₂Cl₂: MeOH (1:1, 60 mL) and the filtrate was concentrated under reduced pressure. This yielded the title compound **66** (32 mg, quantitative yield).

¹H NMR (400 MHz, CDCl₃) δ 7.09 (s, 1H), 3.97 (s, 3H), 2.64 (s, 3H), 2.59 (s, 3H). TOF MS ESI⁺ (m/z): [M+H]⁺ calc'd for C₁₁H₁₃N₂O₃: 221.0848; found: 221.0925.

N-(5-Acetyl-7-methoxy-2-methylbenzo[d]oxazol-6-yl)acetamide (67) and 1-(6-chloro-7-methoxy-2-methylbenzo[d]oxazol-5-yl)ethan-1-one (68)



To a stirred solution of 1-(6-amino-7-methoxy-2-methylbenzo[d]oxazol-5-yl)ethan-1-one (**66**) (32 mg, 0.128 mmol) in CH₂Cl₂ (1 mL) under N₂ was added acetyl chloride (26 μL, 0.384 mmol) and NEt₃ (53 μL, 0.384 mmol). The reaction mixture was stirred at rt for 18 h.

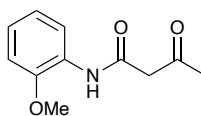
After completion of the reaction monitored by TLC (100 % EtOAc), the reaction mixture was partitioned between CH₂Cl₂ (40 mL) and HCl (1 M, 40 mL). The layers were separated and the organic phases was washed with brine (50 mL), dried over MgSO₄, filtered and concentrated.

This yielded:

The title compound **67** (18 mg, 54 %). ¹H NMR (400 MHz, CDCl₃) δ 7.20 (s, 1H), 4.07 (s, 3H), 2.70 (s, 3H), 2.66 (s, 3H), 2.28 (s, 3H). TOF MS ESI⁺ (m/z): [M+H]⁺ calc'd for C₁₃H₁₅N₂O₄: 263.0954; found: 263.1025.

The title compound **68** (7 mg, 23 %). ¹H NMR (400 MHz, CDCl₃) δ 7.20 (s, 1H), 4.07 (s, 3H), 2.66 (s, 3H), 2.28 (s, 3H). TOF MS ESI⁺ (m/z): [M+H]⁺ calc'd for C₁₃H₁₄N₂O₄: 239.0349; found: 239.2246.

N-(2-Methoxyphenyl)-3-oxobutanamide (71)



71

71 was obtained following experimental procedures previously described by Garden and co-workers.²⁵²

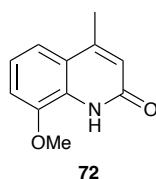
To a stirred solution of 2-methoxyaniline (4.6 mL, 40.7 mmol) in water (100 mL) at reflux was added 2,2,6-trimethyl-4*H*-1,3-dioxin-4-one (16.2 mL, 122.0 mmol). The reaction mixture was heated at reflux for 18 h.

After completion of the reaction monitored by TLC (100 % CH₂Cl₂), the reaction mixture was extracted with CH₂Cl₂ (2 x 60 mL) and the combined organic phases were washed with brine (50 mL), dried over MgSO₄, filtered and concentrated. This yielded the title compound **71** (9.8 g, quant).

¹H NMR (400 MHz, CDCl₃) δ 9.20 (br. s, 1H), 8.32 (dd, J = 7.9, 1.7 Hz, 1H), 7.06 (td, J = 7.8, 1.6 Hz, 1H), 6.95 (td, J = 7.8, 1.4 Hz, 1H), 6.89 (dd, J = 8.1, 1.4 Hz, 1H), 3.92 (s, 3H), 3.60 (s, 2H), 2.34 (s, 3H). **TOF MS ESI**⁺ (m/z): [M+H]⁺ calc'd for C₁₁H₁₄NO₃: 208.0895; found: 208.0973.

The spectroscopic data correspond with those previously reported.²⁵³

8-Methoxy-4-methylquinolin-2(1H)-one (72)



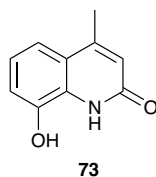
72 was obtained following experimental procedures previously described by Klumpp and co-workers and their spectroscopic data correspond with those reported.²⁵⁴

To a stirred solution of *N*-(2-methoxyphenyl)-3-oxobutanamide (**71**) (9.8 g, 47.5 mmol) in dry CH₂Cl₂ (110 mL) at 0 °C was added triflic acid (80 mL, 880 mmol) slowly. The reaction mixture was stirred for 4 h at rt.

After completion of the reaction monitored by TLC (1:1; CH₂Cl₂: EtOAc), the reaction mixture was cooled to 0 °C and water (200 mL) was slowly added. The reaction mixture was extracted with CH₂Cl₂ (2 x 100 mL) and the combined organic phases were washed with brine (100 mL), dried over MgSO₄, filtered and concentrated. This yielded the title compound **72** (7.3 g, 80 %).

¹H NMR (400 MHz, CDCl₃) δ 9.09 (br. s, 1H), 7.29 – 7.26 (m, 1H), 7.15 (t, J = 8.1 Hz, 1H), 6.99 (dd, J = 8.0, 1.1 Hz, 1H), 6.54 (d, J = 1.4 Hz, 1H), 3.97 (s, 3H), 2.47 (d, J = 1.2 Hz, 3H). **TOF MS** ESI⁺ (m/z): [M+H]⁺ calc'd for C₁₁H₁₂NO₂: 190.0790; found: 190.0860.

8-Hydroxy-4-methylquinolin-2(1H)-one (73)



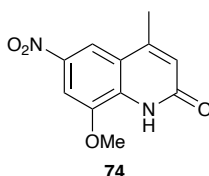
8-Methoxy-4-methylquinolin-2(1H)-one (**72**) (100 mg, 0.53 mmol) at -78 °C was dissolved in BBr₃ (1M in CH₂Cl₂, 3.2 mL, 3.19 mmol). This was left to stir for 2 h at -78 °C then warmed to rt and stirred for 18 h.

After complete conversion observed by TLC (1:1; EtOAc: CH₂Cl₂) the reaction mixture was quenched with NaHSO₃ (aq. Sat., 40 mL). The resulting solid was isolated *via* filtration. This wash dried under vacuum to yield the title compound **73** (93 mg, 99 %) as a tan solid.

¹H NMR (400 MHz, DMSO-*d*₆) δ 10.22 (br. s, 1H), 7.17 (dd, J = 8.0, 1.3 Hz, 1H), 7.02 (t, J = 7.8 Hz, 1H), 6.97 (dd, J = 7.8, 1.3 Hz, 1H), 6.39 (s, 1H), 2.39 (d, J = 1.1 Hz, 3H). Mass spectrometry analysis using a range of techniques failed to give the correct mass. This was potentially due to the poor solubility of the compound.

The spectroscopic data correspond with those previously reported.²⁵⁵

8-Methoxy-4-methyl-6-nitroquinolin-2(1H)-one (74)



To a stirred solution of 8-methoxy-4-methylquinolin-2(1H)-one (**72**) in Ac₂O (4 mL) at 0 °C was added a solution of AcOH (336 μL, 5.870 mmol) and HNO₃ (103 μL, 70 %, 1.566 mmol) dropwise. The reaction mixture was stirred for 1.5 h at 0 °C and was then quenched with water (40 mL).

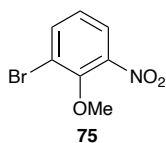
This afforded the crude solid (435 mg) as a mixture of the *meta* and *ortho/para* isomers. ¹H NMR analysis indicated a ratio of 2.3: 1 *meta*: *ortho/para*

74 - Meta isomer – ¹H NMR (400 MHz, CDCl₃) δ 8.29 (d, J = 2.1 Hz, 1H), 7.86 (d, J = 2.1 Hz, 1H), 6.70 – 6.65 (m, 1H), 4.12 (s, 3H), 2.57 (d, J = 1.2 Hz, 3H). – 66 % NMR conversion.

Ortho/para isomer – ¹H NMR (400 MHz, CDCl₃) δ 7.38 (d, J = 8.6 Hz, 1H), 6.97 (d, J = 8.6 Hz, 1H), 6.70 – 6.65 (m, 1H), 4.08 (s, 3H), 2.38 (d, J = 1.2 Hz, 3H). – 33 % NMR conversion.

Isolation wasn't attempted as separation could not be seen on TLC.

1-Bromo-2-methoxy-3-nitrobenzene (75)



75 was obtained following experimental procedures previously described by Moslin and co-workers.²⁵⁶

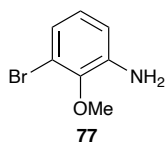
To a stirred solution of 2-bromo-6-nitrophenol (500 mg, 2.488 mmol) in DMF (5 mL) was added K_2CO_3 (1.12 g, 8.083 mmol) followed by MeI (496 mL, 7.960 mmol). The reaction mixture was heated at 45 °C for 18 h.

After completion of the reaction, monitored by TLC (100 % CH_2Cl_2), the reaction mixture was partitioned between CH_2Cl_2 (50 mL) and water (50 mL). The layers were separated and the organic phase was washed with brine (50 mL), dried over $MgSO_4$, filtered and concentrated. This afforded the title compound **75** (502 mg, 87 %).

1H NMR (400 MHz, $CDCl_3$) δ 7.80 (dd, $J = 8.0, 1.6$ Hz, 1H), 7.76 (dd, $J = 8.2, 1.6$ Hz, 1H), 7.12 (t, $J = 8.1$ Hz, 1H), 4.03 (s, 3H).

The spectroscopic data correspond with those previously reported.²⁵⁷

3-Bromo-2-methoxyaniline (77)

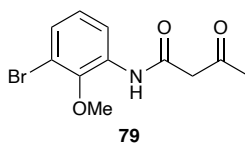


To a stirred solution of 1-bromo-2-methoxy-3-nitrobenzene (**75**) (504 mg, 2.51 mmol) in THF (12 mL) under N₂ was added Pd/C (10 %, 267 mg, 0.251 mmol). The atmosphere was changed to H₂ and the reaction mixture was stirred for 18 h.

After completion of the reaction, monitored by TLC (100 % CH₂Cl₂), the reaction mixture was filtered through celite with MeOH (30 mL) and the filtrate was concentrated under reduced pressure. This yielded the title compounds **77** (428 mg, 85 %).

¹H NMR (400 MHz, CDCl₃) δ 6.90 (dd, J = 8.0, 1.5 Hz, 1H), 6.78 (t, J = 8.0 Hz, 1H), 6.67 (dd, J = 7.9, 1.5 Hz, 1H), 3.91 (br. s, J = 4.5 Hz, 2H), 3.83 (s, 3H). ¹³C NMR (101 MHz, CDCl₃) δ 141.59, 125.87, 122.51, 117.26, 115.13, 59.67. Note: one of the aryl carbons (likely to be C-OMe) is not observed despite increase scans. TOF MS ESI⁺ (m/z): [M+H]⁺ calc'd for C₇H₉BrNO: 201.9789; found: 201.9860.

N-(3-Bromo-2-methoxyphenyl)-3-oxobutanamide (79)

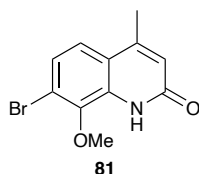


To a stirred solution of 3-bromo-2-methoxyaniline (**77**) (280 mg, 1.39 mmol) in THF (3 mL) was added AcONa (114 mg, 1.39 mmol) followed by 2,2,6-trimethyl-4*H*-1,3-dioxin-4-one (240 mL, 1.81 mmol). The reaction mixture was heated at 85 °C for 18 h then 2,2,6-trimethyl-4*H*-1,3-dioxin-4-one (240 mL, 1.81 mmol) was added. This was then heated for a further 4 h. After completion of the reaction, monitored by TLC (100 % CH₂Cl₂), the reaction mixture was partitioned between CH₂Cl₂ (50 mL) and HCl (1 M, 50 mL). The layers were separated and the organic phase was washed with water (50 mL), brine (50 mL), dried over MgSO₄, filtered and concentrated under reduced pressure. This afforded the title compound **79** (662 mg, 91 %).

¹H NMR (400 MHz, CDCl₃) δ 9.57 (br. s, 1H), 8.16 (dd, *J* = 8.2, 1.5 Hz, 1H), 7.12 (dd, *J* = 8.1, 1.5 Hz, 1H), 6.85 (t, *J* = 8.2 Hz, 1H), 3.78 (s, 3H), 3.56 (s, 2H), 2.20 (s, 3H).

The spectroscopic data correspond with those previously reported.²⁵⁸

7-Bromo-8-methoxy-4-methylquinolin-2(1H)-one (81)

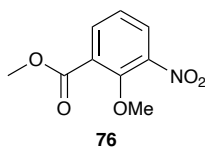


To a stirred solution of *N*-(3-bromo-2-methoxyphenyl)-3-oxobutanamide (**79**) (662 mg, 2.32 mmol) in dry CH₂Cl₂ (6 mL) was added triflic acid (2.5 mL, 27.9 mmol). The reaction mixture was stirred at rt for 18 h then triflic acid (1.5 mL) was added. The reaction mixture was stirred for a further 6 h.

After completion of the reaction, monitored by TLC (100 % CH₂Cl₂), the reaction mixture was partitioned between CH₂Cl₂ (50 mL) and water (50 mL). The layers were separated and the organic phase was washed with brine (50 mL), dried over MgSO₄, filtered and concentrated under reduced pressure. The resulting solid was purified by column chromatography using an eluent of 100 % CH₂Cl₂, CH₂Cl₂: EtOAc (1:1) then EtOAc (100 %) to eluent the product. This yielded the title compound **81** (380 mg, 61 %).

¹H NMR (400 MHz, CDCl₃) δ 7.32 (d, J = 8.7 Hz, 1H), 7.26 (d, J = 8.8 Hz, 1H), 6.54 (q, J = 1.2 Hz, 1H), 3.96 (s, 3H), 2.44 (d, J = 1.2 Hz, 3H). FTMS APCI⁺ (m/z): [M+H]⁺ calc'd for C₁₁H₁₁BrNO₂: 267.9895; found: 267.9968.

Methyl 2-methoxy-3-nitrobenzoate (76)



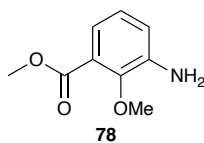
76 was obtained following experimental procedures previously described by Zeng and co-workers and their spectroscopic data correspond with those reported.²⁵⁹

To a stirred solution of methyl 2-hydroxy-3-nitrobenzoate (1.0 g, 5.00 mmol) in DMF (10 mL) was added K_2CO_3 (2.3 g, 3.25 mmol) followed by MeI (1.0 mL, 3.20 mmol). The reaction mixture was heated at 45 °C for 18 h.

After completion of the reaction. Monitored by TLC (100 % CH_2Cl_2), the reaction mixture was partitioned between CH_2Cl_2 (60 mL) and water (60 mL). The layers were separated and the organic phase was washed with brine (60 mL), dried over $MgSO_4$, filtered and concentrated. This afforded the title compound **76** (1.1 g, quantitative yield).

1H NMR (400 MHz, $CDCl_3$) δ 8.03 (dd, $J = 7.8, 1.8$ Hz, 1H), 7.91 (dd, $J = 8.1, 1.8$ Hz, 1H), 7.27 (t, $J = 8.0$ Hz, 1H), 4.01 (s, 3H), 3.96 (s, 3H). **TOF MS ESI⁺** (m/z): $[M+H]^+$ calc'd for $C_9H_{10}NO_5$: 212.0481; found: 212.0553.

Methyl 3-amino-2-methoxybenzoate (78)



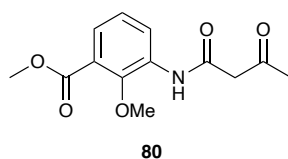
To a stirred solution of methyl 2-methoxy-3-nitrobenzoate (**76**) (1.1 g, 4.883 mmol) in EtOH (24 mL) under N₂ was added Pd/C (10 %, 266 mg, 0.488 mmol). The atmosphere was changed to H₂ and the reaction mixture was stirred for 18 h.

After completion of the reaction, monitored by TLC (100 % CH₂Cl₂), the reaction mixture was filtered through celite with MeOH (60 mL) and the filtrate was concentrated under reduced pressure. This yielded the title compounds **78** (830 mg, 94 %).

¹H NMR (400 MHz, CDCl₃) δ 7.19 (dd, J = 7.6, 1.9 Hz, 1H), 6.95 (t, J = 7.7 Hz, 1H), 6.90 (dd, J = 7.9, 1.9 Hz, 1H), 3.91 (s, 3H), 3.85 (s, 3H). **TOF MS ESI⁺** (m/z): [M+H]⁺ calc'd for C₉H₁₂NO₃: 182.0739; found: 182.0816.

The spectroscopic data correspond with those previously reported.²⁶⁰

Methyl 2-methoxy-3-(3-oxobutanamido)benzoate (80)

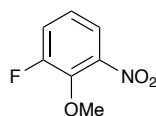


To a stirred solution of methyl 3-amino-2-methoxybenzoate (**78**) (830 mg, 4.586 mmol) in THF (8 mL) was added AcONa (376 mg, 4.586 mmol) followed by 2,2,6-trimethyl-4*H*-1,3-dioxin-4-one (791 mL, 5.961 mmol). The reaction mixture was heated at 85 °C for 18 h then 2,2,6-trimethyl-4*H*-1,3-dioxin-4-one (791 mL, 5.961 mmol) was added. This was then heated for a further 4 h.

After completion of the reaction, monitored by TLC (100 % CH₂Cl₂), the reaction mixture was partitioned between CH₂Cl₂ (80 mL) and HCl (1 M, 80 mL). The layers were separated and the organic phase was washed with water (80 mL), brine (80 mL), dried over MgSO₄, filtered and concentrated under reduced pressure. This afforded the title compound **80** (1.17 g, 96 %).

¹H NMR (400 MHz, CDCl₃) δ 9.74 (br. s, 1H), 8.53 (dd, J = 8.2, 1.7 Hz, 1H), 7.57 (dd, J = 7.9, 1.7 Hz, 1H), 7.14 (t, J = 8.0 Hz, 1H), 3.94 (s, 3H), 3.93 (s, 3H), 3.64 (s, 2H), 2.34 (s, 3H). **TOF MS ESI⁺** (m/z): [M+H]⁺ calc'd for C₁₃H₁₆NO₅: 266.0950; found: 266.1029.

1-Fluoro-2-methoxy-3-nitrobenzene (83)



83

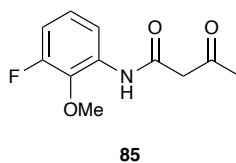
To a stirred solution of 1-fluoro-2-methoxy-3-nitrobenzene (1.0 g, 6.365 mmol) in DMF (5 mL) was added K_2CO_3 (1.32 g, 9.548 mmol) followed by MeI (594 μ L, 9.548 mmol). The reaction mixture was stirred at rt for 18 h.

After completion of the reaction, monitored by TLC (100 % CH_2Cl_2), the reaction mixture was partitioned between CH_2Cl_2 (50 mL) and HCl (1 M, 50 mL). The layers were separated and the organic phase was washed with brine (50 mL), dried over $MgSO_4$, filtered and concentrated. The crude solid was purified using flash column chromatography, eluted with CH_2Cl_2 (100 %). This yielded the title compound **83** (832 mg, 76 %).

1H NMR (400 MHz, $CDCl_3$) δ 7.56 (dt, $J = 8.3, 1.6$ Hz, 1H), 7.33 (ddd, $J = 10.8, 8.4, 1.6$ Hz, 1H), 7.13 (td, $J = 8.3, 4.9$ Hz, 1H), 4.05 (d, $J = 1.8$ Hz, 3H). **^{19}F NMR** (377 MHz, $CDCl_3$) δ -126.34. **TOF MS ESI⁺** (m/z): $[M+H]^+$ calc'd for $C_7H_7FNO_3$: 172.0332; found: 172.0404.

The spectroscopic data correspond with those previously reported.²⁶¹

N-(3-Fluoro-2-methoxyphenyl)-3-oxobutanamide (85)

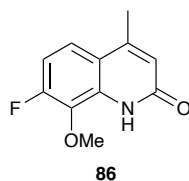


To a stirred solution of 3-fluoro-2-methoxyaniline (**84**) (1.7 mL, 14.2 mmol) in xylene (100 mL) was added 2,2,6-trimethyl-4*H*-1,3-dioxin-4-one (3.8 mL, 28.4 mmol). The reaction mixture was heated at 120 °C for 18 h.

After completion of the reaction, monitored by TLC (100 % CH₂Cl₂), the reaction mixture was partitioned between CH₂Cl₂ (250 mL) and water (250 mL). The layers were separated and the organic phase was washed with brine (250 mL), dried over MgSO₄, filtered and concentrated under reduced pressure. This afforded the title compound **85** (3.1 g, 97 %).

¹H NMR (400 MHz, CDCl₃) δ 9.60 (br. s, 1H), 8.11 (dt, J = 8.4, 1.4 Hz, 1H), 6.99 (td, J = 8.4, 5.7 Hz, 1H), 6.83 (ddd, J = 11.3, 8.5, 1.5 Hz, 1H), 4.03 (d, J = 1.8 Hz, 3H), 3.62 (s, 2H), 2.34 (s, 3H). ¹⁹F NMR (377 MHz, CDCl₃) δ -130.82. TOF MS ESI⁺ (m/z): [M+H]⁺ calc'd for C₁₁H₁₃FNO₃: 226.0801; found: 226.0877.

7-Fluoro-8-methoxy-4-methylquinolin-2(1H)-one (86)

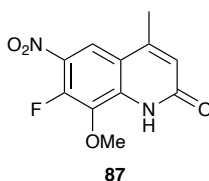


To a stirred solution of *N*-(3-fluoro-2-methoxyphenyl)-3-oxobutanamide (**85**) (116 mg, 0.516 mmol) in dry CH₂Cl₂ (5 mL) was added triflic acid (0.55 mL, 6.187 mmol). The reaction mixture was stirred at rt for 18 h.

After completion of the reaction, monitored by TLC (100 % CH₂Cl₂), the reaction mixture was partitioned between CH₂Cl₂ (50 mL) and water (50 mL). The layers were separated and the organic phase was washed with brine (50 mL), dried over MgSO₄, filtered and concentrated under reduced pressure. This yielded the title compound **86** (86 mg, 81 %).

¹H NMR (400 MHz, CDCl₃) δ 9.21 (br. s, 1H), 7.32 (dd, J = 9.1, 4.8 Hz, 1H), 6.97 (dd, J = 11.3, 9.1 Hz, 1H), 6.50 (s, 1H), 4.09 (d, J = 2.1 Hz, 3H), 2.45 (s, 3H). **¹⁹F NMR** (377 MHz, CDCl₃) δ -127.85. **TOF MS ESI⁺** (m/z): [M+H]⁺ calc'd for C₁₁H₁₁FNO₂: 208.0696; found: 208.0768.

7-Fluoro-8-methoxy-4-methyl-6-nitroquinolin-2(1H)-one (87)

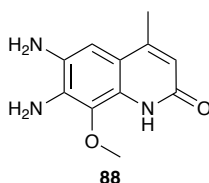


To a stirred solution of 7-fluoro-8-methoxy-4-methylquinolin-2(1H)-one (**86**) (1.74 g, 8.40 mmol) in Ac₂O (12 mL) at 0 °C was added AcOH (4 mL, 69.768 mmol) followed by HNO₃ (1.14 mL, 11.768 mmol) dropwise. The reaction mixture was allowed to warm to rt and stirred for 18 h.

After completion of the reaction, monitored by TLC (100 % CH₂Cl₂), water (200 mL) was added and the resulting solid was isolated *via* filtration. The solid was then triturated with CH₂Cl₂ leaving a pale tan solid. This solid was dried under vacuum to yield the title compound **87** (940 mg, 44 %).

¹H NMR (400 MHz, DMSO-*d*6) δ 11.81 (s, 1H), 8.21 (d, J = 7.3 Hz, 1H), 6.56 (s, 1H), 3.96 (d, J = 1.3 Hz, 3H), 2.46 (d, J = 1.2 Hz, 3H). ¹⁹F NMR (377 MHz, DMSO-*d*6) δ -135.45. TOF MS ESI⁺ (m/z): [M+H]⁺ calc'd for C₁₁H₁₀FN₂O₄: 253.0546; found: 253.0619.

6,7-Diamino-8-methoxy-4-methylquinolin-2(1H)-one (88)



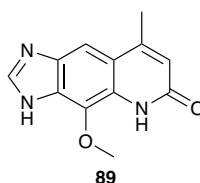
To a stirred solution of 7-fluoro-8-methoxy-4-methyl-6-nitroquinolin-2(1H)-one (**87**) (100 mg, 0.397 mmol) in dry DMF (1 mL) under N₂, was added NaN₃ (39 mg, 0.595 mmol). The reaction mixture was stirred for 18 h at rt.

After completion of the reaction, monitored by TLC (100 % EtOAc), the reaction mixture was partitioned between CH₂Cl₂ (50 mL) and water (50 mL). The layers were separated and the organic phase was washed with brine (50 mL), dried over MgSO₄, filtered and concentrated. The crude solid was used in the next reaction without purification.

To crude solid was dissolved in EtOH (1 mL) under N₂ and Pd/C (10 %, 42 mg, 0.040 mmol) was added. The atmosphere was changed to H₂ and the reaction mixture was stirred for 18 h. After completion of the reaction, monitored by TLC (5 % MeOH in CH₂Cl₂), the reaction mixture was filtered through celite with MeOH (60 mL) and the filtrate was concentrated under reduced pressure. This yielded the title compound **88** (73 mg, 84 %).

¹H NMR (400 MHz, CDCl₃) δ 6.74 (d, J = 2.9 Hz, 1H), 6.24 – 6.19 (m, 1H), 3.75 (d, J = 2.9 Hz, 3H), 2.32 (t, J = 1.9 Hz, 3H). **TOF MS ESI⁺** (m/z): [M+H]⁺ calc'd for C₁₁H₁₄N₃O₂ 220.1008; found: 220.1085.

4-Methoxy-8-methyl-3,5-dihydro-6H-imidazo[4,5-g]quinolin-6-one (89)

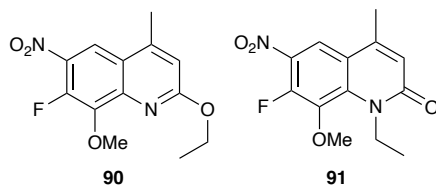


To a stirred solution of 6,7-diamino-8-methoxy-4-methylquinolin-2(1H)-one (**88**) (73 mg, 0.403 mmol) in DMF (1 mL) was added triethyl orthoformate (1 mL, 4.032 mmol) and TFA (26 μ L, 0.403 mmol). The reaction mixture was stirred for 18 h at rt.

After completion of the reaction, monitored by TLC (5 % MeOH in CH_2Cl_2), the reaction mixture was partitioned between CH_2Cl_2 (30 mL) and aqu. K_2CO_3 (sat., 30 mL). The layers were separated and the aqueous phase was concentrated under reduced pressure. The resulting solid was dissolved with CH_2Cl_2 : MeOH (4:1, 50 mL), filtered and concentrated. This yielded the title compounds **89** (89 mg, 96 %) as a white solid.

$^1\text{H NMR}$ (500 MHz, $\text{DMSO-}d_6$) δ 10.30 (br. s, 1H), 8.58 (s, 1H), 8.24 (d, $J = 1.2$ Hz, 1H), 7.58 (s, 1H), 6.32 (d, $J = 1.3$ Hz, 1H), 4.24 (s, 3H), 2.47 (d, $J = 1.1$ Hz, 3H). $^{13}\text{C NMR}$ (126 MHz, $\text{DMSO-}d_6$) δ 166.3, 161.6, 158.4 (major tautomer), 158.1 (minor tautomer), 148.6, 146.0, 134.1, 124.9, 119.6 (major tautomer), 119.0 (minor tautomer), 117.1 (major tautomer), 116.6 (minor tautomer), 103.1, 61.0, 19.6. **FTMS APCI⁺** (m/z): $[\text{M}+\text{H}]^+$ calc'd for $\text{C}_{12}\text{H}_{12}\text{N}_3\text{O}_2$: 230.0851; found: 230.0913. **LCMS** (230.1 $[\text{M}+\text{H}]$, 0.79 min, 100 %).

2-Ethoxy-7-fluoro-8-methoxy-4-methyl-6-nitroquinoline (90) and 1-ethyl-7-fluoro-8-methoxy-4-methyl-6-nitroquinolin-2(1H)-one (91)



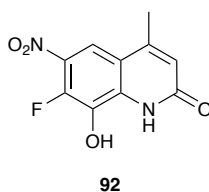
To a stirred solution of 7-fluoro-8-methoxy-4-methyl-6-nitroquinolin-2(1H)-one (**87**) (100 mg, 0.397 mmol) in dry DMF (1 mL) under N₂ was added NaH (60 %, 18 mg, 0.476 mmol) followed by EtI (38 μL, 0.476 mmol) dropwise. The reaction mixture was heated at 50 °C and stirred for 2 h.

After completion of the reaction, monitored by TLC (100 % CH₂Cl₂), water (50 mL) was added and the resulting solid was isolated *via* filtration. The crude solid was then purified by column chromatography using 100 % CH₂Cl₂ to yield the title compound **90** (77 mg, 69 %) and 1:1 CH₂Cl₂: EtOAc to yield the title compound **91** (12 mg, 11 %).

2-Ethoxy-7-fluoro-8-methoxy-4-methyl-6-nitroquinoline (**90**). ¹H NMR (400 MHz, CDCl₃) δ 8.38 (d, J = 7.4 Hz, 1H), 6.85 – 6.82 (m, 1H), 4.59 (q, J = 7.1 Hz, 2H), 4.22 (d, J = 0.5 Hz, 3H), 2.65 (d, J = 1.1 Hz, 3H), 1.47 (t, J = 7.1 Hz, 3H). ¹³C NMR (101 MHz, CDCl₃) δ 164.1, 147.7 (d, J = 139.5 Hz), 145.4, 138.8 (d, J = 3.7 Hz), 131.7 (d, J = 4.8 Hz), 121.0, 120.1, 114.9, 114.8, 62.6, 62.5 (d, J = 2.5 Hz), 18.9, 14.4. ¹⁹F NMR (377 MHz, CDCl₃) δ -137.66. TOF MS ESI⁺ (m/z): [M+H]⁺ calc'd for C₁₃H₁₄FN₂O₄: 281.0859; found: 281.0939.

1-Ethyl-7-fluoro-8-methoxy-4-methyl-6-nitroquinolin-2(1*H*)-one (**91**). **¹H NMR** (400 MHz, CDCl₃) δ 8.19 (d, *J* = 7.9 Hz, 1H), 6.63 (d, *J* = 1.3 Hz, 1H), 4.51 (q, *J* = 6.9 Hz, 2H), 4.05 (d, *J* = 1.7 Hz, 3H), 2.47 (d, *J* = 1.2 Hz, 3H), 1.36 (t, *J* = 7.0 Hz, 3H). **¹³C NMR** (101 MHz, CDCl₃) δ 162.5, 151.1 (d, *J* = 264.2 Hz), 145.7, 138.7 (d, *J* = 3.6 Hz), 137.5 (d, *J* = 13.9 Hz), 131.9 (d, *J* = 7.1 Hz), 122.6, 118.4 (d, *J* = 2.5 Hz), 117.6, 63.1 (d, *J* = 7.8 Hz), 41.7, 19.4, 14.8. **¹⁹F NMR** (377 MHz, CDCl₃) δ -129.77. **TOF MS ESI⁺** (*m/z*): [M+H]⁺ calc'd for C₁₃H₁₄FN₂O₄: 281.0859; found: 281.0942.

7-Fluoro-8-hydroxy-4-methyl-6-nitroquinolin-2(1H)-one (92)



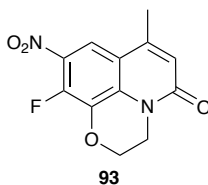
7-Fluoro-8-methoxy-4-methyl-6-nitroquinolin-2(1H)-one (**87**) (100 mg, 0.397 mmol) was dissolved in HBr (48 %, aq., 3 mL) and heated at 135 °C for 18 h.

After completion of the reaction, monitored by TLC (100 % EtOAc), water (50 mL) was added and the resulting solid was isolated *via* filtration. This afforded the title compound **92** (105 mg, quantitative yield) as an off-white solid.

¹H NMR (400 MHz, DMSO-*d*₆) δ 7.96 (d, *J* = 7.1 Hz, 1H), 6.52 (s, 1H), 2.45 (d, *J* = 1.2 Hz, 3H).

TOF MS ESI⁺ (*m/z*): [M+H]⁺ calc'd for C₁₀H₈FN₂O₄: 239.0390; found: 239.0462.

10-Fluoro-7-methyl-9-nitro-2,3-dihydro-5H-[1,4]oxazino[2,3,4-ij]quinolin-5-one (93)



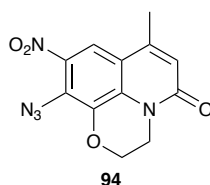
To a stirred solution of 7-fluoro-8-hydroxy-4-methyl-6-nitroquinolin-2(1H)-one (**92**) (270 mg, 0.944 mmol) in dry DMF (20 mL) under N₂ was added K₂CO₃ (781 mg, 5.659 mmol) and 1,2-dibromoethane (122 μL, 1.416 mmol). The reaction mixture was heated at 110 °C for 18 h. After completion of the reaction monitored by TLC (1:1 EtOAc: CH₂Cl₂) the reaction mixture was partitioned between CH₂Cl₂ (60 mL) and HCl (1 M, 60 mL). The layers were separated and the organic phase was washed with brine (60 mL), dried over MgSO₄, filtered and concentrated under reduced pressure. The resulting solid was purified by column chromatography using 100 % CH₂Cl₂ then EtOAc: CH₂Cl₂ (1:1) as the eluent.

This yielded:

The title compound **93** (76 mg, 30 %) as an off-white solid. ¹H NMR (400 MHz, CDCl₃) δ 8.08 (d, J = 7.0 Hz, 1H), 6.67 – 6.61 (m, 1H), 4.51 – 4.47 (m, 2H), 4.31 – 4.27 (m, 2H), 2.51 (d, J = 1.3 Hz, 3H). ¹⁹F NMR (377 MHz, CDCl₃) δ -136.83. TOF MS EI⁺ (m/z): [M⁺]⁺ calc'd for C₁₂H₉FN₂O₄: 264.0546; found: 264.0541.

By-product - 10-(Dimethylamino)-7-methyl-9-nitro-2,3-dihydro-5H-[1,4]oxazino[2,3,4-ij]quinolin-5-one (64 mg, 22 %). ¹H NMR (400 MHz, CDCl₃) δ 7.68 (s, 1H), 6.52 (d, J = 1.3 Hz, 1H), 4.43 (dd, J = 5.4, 4.2 Hz, 2H), 4.29 – 4.24 (m, 2H), 2.89 (s, 6H), 2.43 (d, J = 1.2 Hz, 3H). TOF MS ESI⁺ (m/z): [M+H]⁺ calc'd for C₁₄H₁₆N₃O₄: 290.1063; found: 290.1143.

10-Azido-7-methyl-9-nitro-2,3-dihydro-5H-[1,4]oxazino[2,3,4-*ij*]quinolin-5-one (94)



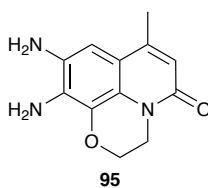
To a stirred solution of 10-fluoro-7-methyl-9-nitro-2,3-dihydro-5H-[1,4]oxazino[2,3,4-*ij*]quinolin-5-one (**93**) (76 mg, 0.288 mmol) in DMF (1 ml) was added sodium azide (28 mg, 0.432 mmol). The reaction mixture was stirred for 18 h at rt.

After completion of the reaction, monitored by TLC (1: 1 CH₂Cl₂: EtOAc), the reaction mixture was partitioned between EtOAc (40 mL) and water (40 mL). The layers were separated and the organic phase was washed with brine (40 mL), dried over MgSO₄, filtered and concentrated under reduced pressure.

This crude solid was used in the next step without further purification (91 mg).

TOF MS ESI⁺ (m/z): [M+H]⁺ calc'd for C₁₂H₁₀N₅O₄: 288.0655; found: 288.0724.

9,10-Diamino-7-methyl-2,3-dihydro-5H-[1,4]oxazino[2,3,4-ij]quinolin-5-one (95)



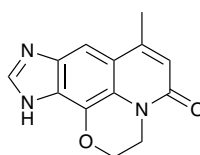
To a stirred solution of crude 10-azido-7-methyl-9-nitro-2,3-dihydro-5H-[1,4]oxazino[2,3,4-ij]quinolin-5-one (**94**) (91 mg, 0.317 mmol) in EtOH (1 mL) and CH₂Cl₂ (1 mL) under N₂ was added Pd/C (10 %, 34 mg, 0.032 mmol). The atmosphere was changed to H₂ and the reaction mixture was stirred for 18 h.

After completion of the reaction, monitored by TLC (1: 1 CH₂Cl₂: EtOAc), the reaction mixture was filtered through celite with MeOH (50 mL) and the filtrate was concentrated under reduced pressure. This yielded the title compound **95** (77 mg, quantitative yield).

¹H NMR (400 MHz, CDCl₃) δ 6.67 (s, 1H), 6.37 (s, 1H), 4.42 – 4.34 (m, 2H), 4.28 – 4.22 (m, 2H), 2.37 (d, J = 1.1 Hz, 3H). **TOF MS ESI⁺** (m/z): [M+H]⁺ calc'd for C₁₂H₁₄N₃O₂: 232.1008; found: 232.1085.

7-Methyl-2,3-dihydroimidazo[4,5-g][1,4]oxazino[2,3,4-ij]quinolin-5(11H)-one

(6Core2-NH)

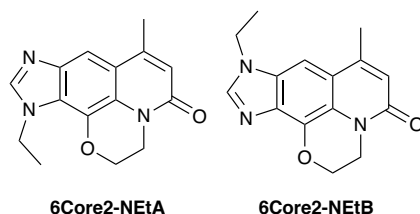


6Core2-NH

To a stirred solution of 9,10-diamino-7-methyl-2,3-dihydro-5H-[1,4]oxazino[2,3,4-ij]quinolin-5-one (**95**) (77 mg, 0.333 mmol) in DMF (2 mL) was added triethyl orthoformate (555 μ L, 3.333 mmol) and TFA (26 μ L, 0.333 mmol). The reaction mixture was stirred for 18 h at rt. After completion of the reaction, monitored by TLC (5 % MeOH in CH_2Cl_2), the reaction mixture was partitioned between CH_2Cl_2 (40 mL) and aq. K_2CO_3 (Sat., 40 mL). The layers were separated and the organic phase was washed with brine (40 mL), dried over MgSO_4 , filtered and concentrated under reduced pressure. This yielded the title compound **6Core2-NH** (48 mg, 60 %) as a white solid.

$^1\text{H NMR}$ (500 MHz, $\text{DMSO-}d_6$) δ 8.39 (s, 1H), 7.60 (s, 1H), 6.46 (d, $J = 1.2$ Hz, 1H), 4.49 (t, $J = 4.7$ Hz, 2H), 4.20 (t, $J = 4.7$ Hz, 2H), 2.49 (d, $J = 1.2$ Hz, 3H). **$^{13}\text{C NMR}$** (126 MHz, $\text{DMSO-}d_6$) δ 158.8, 147.2, 144.1, 135.1, 130.7, 128.1, 120.9, 118.5, 117.7, 103.4, 63.8, 39.4, 19.1. **TOF MS** **ESI**⁺ (m/z): $[\text{M}+\text{H}]^+$ calc'd for $\text{C}_{13}\text{H}_{12}\text{N}_3\text{O}_2$: 242.0851; found: 242.0933. **LCMS** (242.1 $[\text{M}+\text{H}]$, 0.80 min, 100 %).

11-Ethyl-7-methyl-2,3-dihydroimidazo[4,5-*g*][1,4]oxazino[2,3,4-*ij*]quinolin-5(11*H*)-one
(6Core2-NEtA) and 9-ethyl-7-methyl-2,3-dihydroimidazo[4,5-*g*][1,4]oxazino[2,3,4-*ij*]quinolin-5(9*H*)-one
(6Core2-NEtB)



To a stirred solution of 7-methyl-2,3-dihydroimidazo[4,5-*g*][1,4]oxazino[2,3,4-*ij*]quinolin-5(11*H*)-one (**6Core2-NH**) (37 mg, 0.154 mmol) in dry DMF (1 mL) under N₂ was added NaH (60 %, 7 mg, 0.169 mmol) followed by EtI (14 μL, 0.169 mmol) dropwise. The reaction mixture was stirred at rt for 18 h.

After completion of the reaction, monitored by TLC (10 % MeOH in CH₂Cl₂), water (20 mL) and CH₂Cl₂ (20 mL) was added and the layers were separated. The organic layer was washed with brine (20 mL), dried over MgSO₄, filtered and concentrated. The crude solid was then purified by preparative TLC (ran twice using 5 % MeOH in CH₂Cl₂).

This yielded:

The title compound **6Core2-NEtA** (9 mg, 22 %) as a white solid. ¹H NMR (500 MHz, DMSO-*d*₆) δ 8.43 (s, 1H), 7.68 (s, 1H), 6.46 (d, *J* = 1.2 Hz, 1H), 4.51 (t, *J* = 4.8 Hz, 2H), 4.45 (q, *J* = 7.2 Hz, 2H), 4.20 (t, *J* = 4.8 Hz, 2H), 2.49 (d, *J* = 1.2 Hz, 3H), 1.44 (t, *J* = 7.2 Hz, 3H). ¹³C NMR (126 MHz, DMSO-*d*₆) δ 158.9, 147.2, 145.9, 139.3, 129.0, 123.3, 121.7, 118.5, 117.8, 107.2, 64.1, 41.7, 40.0, 19.1, 17.0. **TOF MS ESI**⁺ (*m/z*): [M+H]⁺ calc'd for C₁₅H₁₆N₃O₂: 270.1164; found: 270.1239. **LCMS** (270.1 [M+H], 0.95 min, 100 %).

The title compound **6Core2-NEtB** (6 mg, 14 %) as a white solid. **¹H NMR** (500 MHz, DMSO-*d*₆) δ 8.49 (s, 1H), 7.62 (s, 1H), 6.50 (d, *J* = 1.2 Hz, 1H), 4.47 (t, *J* = 4.8 Hz, 2H), 4.36 (q, *J* = 7.3 Hz, 2H), 4.21 – 4.18 (m, 2H), 2.53 (d, *J* = 1.2 Hz, 3H), 1.45 (t, *J* = 7.3 Hz, 3H). **¹³C NMR** (126 MHz, DMSO-*d*₆) δ 159.1, 147.5, 145.9, 133.6, 133.1, 131.2, 121.2, 119.5, 118.6, 98.9, 64.2, 40.1, 39.8, 19.7, 15.6. **TOF MS ESI⁺** (*m/z*): [M+H]⁺ calc'd for C₁₅H₁₆N₃O₂: 270.1164; found: 270.1240. **LCMS** (270.1 [M+H], 0.95 min, 100 %).

5.3 Microbiology Protocols

Experimental procedures for the Kirby-Bauer disc diffusion assay were previously described by Sridhar and co-workers.²⁰⁶

5.3.1 Disc Preparations

Antibiotics were dissolved in a mixture of CHCl_3 and MeOH to make up 1 mmol and 10 mmol solutions. 20 μL of each solution was loaded onto a 6 mm whatmann paper disc (sterilised by autoclave) in a glass petri dish (sterilised by autoclave). 7 discs were used per antibiotic per concentration. The glass petri dishes containing the antibiotic discs were transferred to the oven (37 °C) for 30 min to dry.

5.3.2 Kirby-Bauer Disc Diffusion Assay^{205,262}

Purity of bacterial cultures were confirmed by streaking on Mueller-Hinton agar plates to single colonies and grown in the oven (37 °C) for 18 h. A single colony was taken and dissolved in sterilised Mueller-Hinton broth (10 mL) and grown in the incubator (37 °C) with aeration for 4 h to create the inoculum culture. The inoculum culture was then diluted with PBS to a turbidity of 0.5 McFarland standard solution. A Mueller-Hinton agar plate was then inoculated with the inoculum culture using a sterilised swap, swapping in three directions for even coverage on the plate. 7 antibiotic discs were transferred to the plate and the plate was incubated in the oven (37 °C) for 18 h. After this time the zone of inhibition was measured for each disc.

5.3.3 Gene Deletion of TolC and AcrB from *E. coli*.

Gene deletion was carried out using the **Gene bridges - Red[®]/ET[®] Recombination gene deletion kit in *E. coli*** - Product ID K006.

5.3.4 Ethidium Bromide Cartwheel Assay

Experimental procedures for the ethidium bromide cartwheel assay were previously described by Amaral and co-workers.²²⁵

Purity of bacterial cultures were confirmed by streaking on Mueller-Hinton agar plates to single colonies and grown in the oven (37 °C) for 18 h. A single colony was taken and dissolved in sterilised Mueller-Hinton broth (10 mL) and grown in the incubator (37 °C) with aeration for 4 h to create the inoculum culture. The inoculum culture was then diluted with PBS to a turbidity of 0.5 McFarland standard solution. A Mueller-Hinton agar plate containing ethidium bromide (0, 0.5, 1, 1.5 mgL⁻¹) were then inoculated with the inoculum culture using a sterilised swap, swapping once from the centre of the plate to the outside, taking care for the strains not to touch. The plates were then incubated in the oven (37 °C) for 18 h.

5.4 X-Ray Crystallography

5.4.1 The X-ray Crystal Structure of **44**

Crystal data for 44: C₁₄H₂₅BO₄, *M* = 268.15, orthorhombic, *P*2₁2₁2₁ (no. 19), *a* = 8.9148(5), *b* = 9.6905(8), *c* = 18.8528(13) Å, *V* = 1628.7(2) Å³, *Z* = 4, *D*_c = 1.094 g cm⁻³, μ(Mo-Kα) = 0.077 mm⁻¹, *T* = 173 K, colourless block, Agilent Xcalibur 3 E diffractometer; 2856 independent measured reflections (*R*_{int} = 0.0331), *F*² refinement,^[X1,X2] *R*₁(obs) = 0.0496, *wR*₂(all) = 0.1161, 2298 independent observed absorption-corrected reflections [*|F*_o| > 4σ(*|F*_o)], completeness to θ_{full}(25.2°) = 98.3%, 202 parameters. The absolute structure of **44** could not be determined from the diffraction data [Flack parameter *x* = -0.2(10)]. CCDC 1908213.

The (CMe₂)₂ portion of the (CMe₂)₂O₂B ring in the structure of **44** was found to be disordered. Two orientations were identified of *ca.* 74 and 26% occupancy, their geometries were optimised, the thermal parameters of adjacent atoms were restrained to be similar, and only the non-hydrogen atoms of the major occupancy orientation were refined anisotropically (those of the minor occupancy orientation were refined isotropically).

5.4.2 The X-ray Crystal Structure of **49**

Identification code	49	
Formula	C ₁₉ H ₂₄ Cl ₂ N ₂ O ₃	
Formula weight	399.30	
Temperature	173(2) K	
Diffractometer, wavelength	Agilent Xcalibur 3 E, 0.71073 Å	
Crystal system, space group	Triclinic, P-1	
Unit cell dimensions	<i>a</i> = 9.4885(5) Å	∠ = 105.996(6)°
	<i>b</i> = 9.9080(7) Å	∠ = 102.645(5)°
	<i>c</i> = 12.2752(8) Å	∠ = 107.611(5)°
Volume, <i>Z</i>	998.14(12) Å ³ , 2	
Density (calculated)	1.329 Mg/m ³	
Absorption coefficient	0.346 mm ⁻¹	

F(000)	420
Crystal colour / morphology	Colourless blocks
Crystal size	0.461 x 0.237 x 0.101 mm ³
θ range for data collection	2.386 to 28.069°
Index ranges	-8<=h<=12, -13<=k<=12, -16<=l<=15
Reflns collected / unique	5831 / 3936 [R(int) = 0.0286]
Reflns observed [F>4 σ (F)]	2925
Absorption correction	Analytical
Max. and min. transmission	0.969 and 0.913
Refinement method	Full-matrix least-squares on F ²
Data / restraints / parameters	3936 / 2 / 248
Goodness-of-fit on F ²	1.042
Final R indices [F>4 σ (F)]	R1 = 0.0494, wR2 = 0.1052
R indices (all data)	R1 = 0.0729, wR2 = 0.1231
Largest diff. peak, hole	0.246, -0.236 eÅ ⁻³
Mean and maximum shift/error	0.000 and 0.002

Table 2. Bond lengths [Å] and angles [°] for **49**.

C(1)-O(7)	1.366(3)
C(1)-C(2)	1.397(3)
C(1)-C(6)	1.400(4)
C(2)-C(3)	1.391(3)
C(2)-Cl(2)	1.737(2)
C(3)-C(4)	1.391(3)
C(3)-C(9)	1.494(3)
C(4)-C(5)	1.393(3)
C(5)-C(6)	1.385(4)
C(5)-C(16)	1.493(3)
C(6)-Cl(6)	1.741(2)
O(7)-C(8)	1.430(3)
C(9)-C(10)	1.327(3)
C(9)-C(15)	1.500(3)
C(10)-C(11)	1.482(3)
C(11)-O(11)	1.238(3)
C(11)-N(12)	1.341(3)
N(12)-C(13)	1.459(3)
C(13)-C(14)	1.501(4)
C(16)-C(17)	1.329(3)

C(16)-C(22)	1.505(3)
C(17)-C(18)	1.494(3)
C(18)-O(18)	1.231(3)
C(18)-N(19)	1.338(3)
N(19)-C(20)	1.454(3)
C(20)-C(21)	1.505(4)
O(7)-C(1)-C(2)	121.1(2)
O(7)-C(1)-C(6)	121.3(2)
C(2)-C(1)-C(6)	117.6(2)
C(3)-C(2)-C(1)	121.8(2)
C(3)-C(2)-Cl(2)	119.73(18)
C(1)-C(2)-Cl(2)	118.43(19)
C(4)-C(3)-C(2)	118.1(2)
C(4)-C(3)-C(9)	119.6(2)
C(2)-C(3)-C(9)	122.3(2)
C(3)-C(4)-C(5)	122.3(2)
C(6)-C(5)-C(4)	117.6(2)
C(6)-C(5)-C(16)	123.0(2)
C(4)-C(5)-C(16)	119.3(2)
C(5)-C(6)-C(1)	122.4(2)
C(5)-C(6)-Cl(6)	120.21(19)
C(1)-C(6)-Cl(6)	117.3(2)
C(1)-O(7)-C(8)	113.13(18)
C(10)-C(9)-C(3)	123.2(2)
C(10)-C(9)-C(15)	122.0(2)
C(3)-C(9)-C(15)	114.7(2)
C(9)-C(10)-C(11)	129.3(2)
O(11)-C(11)-N(12)	121.5(2)
O(11)-C(11)-C(10)	118.8(2)
N(12)-C(11)-C(10)	119.7(2)
C(11)-N(12)-C(13)	122.5(2)
N(12)-C(13)-C(14)	111.64(19)
C(17)-C(16)-C(5)	122.4(2)
C(17)-C(16)-C(22)	121.4(2)
C(5)-C(16)-C(22)	116.1(2)
C(16)-C(17)-C(18)	127.2(2)
O(18)-C(18)-N(19)	122.6(2)
O(18)-C(18)-C(17)	123.8(2)
N(19)-C(18)-C(17)	113.6(2)
C(18)-N(19)-C(20)	123.3(2)
N(19)-C(20)-C(21)	112.4(2)

5.4.3 References

- [X1] SHELXTL v5.1, Bruker AXS, Madison, WI, 1998.
[X2] SHELX-2013, G.M. Sheldrick, *Acta Cryst.*, 2015, **C71**, 3-8.

5.4.4 Figures

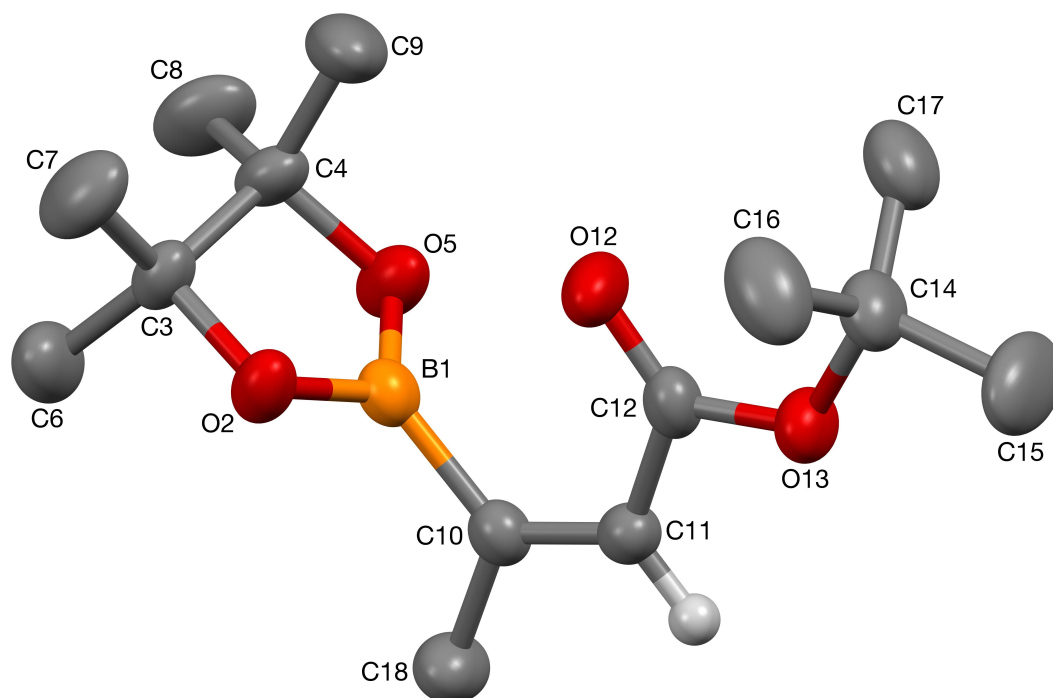


Fig. S1 - The crystal structure of **44** (50% probability ellipsoids).

6. References

- 1 J. O’Neill, (2016) *Tackling Drug-Resistant Infections Globally: Final Report and Recommendations*, Review on Antimicrobial Resistance. Report number: 1.
- 2 K. Hiramatsu, M. Igarashi, Y. Morimoto, T. Baba, M. Umekita and Y. Akamatsu, *Int. J. Antimicrob. Agents*, 2012, **39**, 478–485.
- 3 A. Fleming, *Br J Exp Pathol*, 1929, **10**, 226–236.
- 4 A. Fleming, *Br. Med. Bull.*, 1944, **2**, 4–5.
- 5 A. Fleming, in *Nobel Lecture*, 1945, pp. 83–93.
- 6 R. R. Redfield, *Antibiotic resistance threats in the United States*, 2019.
- 7 A. D. So, Q. Ruiz-Esparza, N. Gupta and O. Cars, *BMJ*, 2012, **344**, 1–4.
- 8 M. Cormican and A. Vellinga, *BMJ*, 2012, **344**, 3369.
- 9 WHO, Antibiotic resistance, <https://www.who.int/news-room/fact-sheets/detail/antibiotic-resistance>, (accessed 26 March 2020).
- 10 O. Jonas, A. Irwin, F. Berthe, F. Le Gall, P. V. Marquez, I. Nikolic, C. Plante, M. Schneidman, D. Shriber, A. Thiebaud, C. McCahan, B. McNulty, R. Seifman, A. Seiter, V. Solovyov, E. Sterlin, J. Voegelé and P. Zwaans, *Drug-Resistant Infections: A Threat to Our Economic Future.*, 2017.
- 11 J. P. Burnham, M. A. Olsen and M. H. Kollef, *Infect. Control Hosp. Epidemiol.*, 2019, **40**, 112–113.
- 12 T. Frieden, (2013) *Antibiotic resistance threats in the United States*, Centers for Disease Control and Prevention. Report number: 1.
- 13 R. Laxminarayan, A. Duse, C. Wattal, A. K. M. Zaidi, H. F. L. Wertheim, N. Sumpradit, E. Vlieghe, G. L. Hara, I. M. Gould, H. Goossens, C. Greko, A. D. So, M. Bigdeli, G. Tomson, W. Woodhouse, E. Ombaka, A. Q. Peralta, F. N. Qamar, F. Mir, S. Kariuki, Z. A. Bhutta, A. Coates, R. Bergstrom, G. D. Wright, E. D. Brown and O. Cars, *Lancet Infect. Dis.*, 2013, **13**, 1057–1098.
- 14 R. Smith and J. Coast, *BMJ*, 2013, **346**, 1–5.
- 15 R. Plowman, N. Graves, M. A. S. Griffin, J. A. Roberts, A. V. Swan, B. Cookson and L. Taylor, *J. Hosp. Infect.*, 2001, **47**, 198–209.
- 16 A. Mohammed, T. A. Ghebreyesus, J. Husu-Kallio, M. Khor and M. M. de Marinis, (2019) *No Time To Wait: Securing the Future from Drug-Resistant Infections*, IACG. Report number: 1.
- 17 M. J. Renwick, V. Simpkin, E. Mossialos and E. Schippers, *Heal. policy Ser.*
- 18 T. P. Van Boeckel, C. Brower, M. Gilbert, B. T. Grenfell, S. A. Levin, T. P. Robinson, A. Teillant and R. Laxminarayan, *Proc. Natl. Acad. Sci. U. S. A.*, 2015, **112**, 5649–5654.
- 19 W. Gaze and M. Depledge, (2017) *Frontiers 2017 - Emerging Issues Of Environmental Concern*, UN Environment. Report number: 1.
- 20 E. Angelakis, V. Merhej and D. Raoult, *Lancet Infect. Dis.*, 2013, **13**, 889–899.
- 21 C. Cogliani, H. Goossens and C. Greko, *Microbe*, 2011, **6**, 274–279.
- 22 D. L. Smith, J. Dushoff and J. G. Morris, *PLoS Med.*, 2005, **2**, 0731–0735.
- 23 G. P. Salmond and M. Welch, *Lancet*, 2008, **372**, S97–S103.
- 24 K. E. Fleming-Dutra, A. L. Hersh, D. J. Shapiro, M. Bartoces, E. A. Enns, T. M. File, J. A. Finkelstein, J. S. Gerber, D. Y. Hyun, J. A. Linder, R. Lynfield, D. J. Margolis, L. S. May, D. Merenstein, J. P. Metlay, J. G. Newland, J. F. Piccirillo, R. M. Roberts, G. V. Sanchez, K. J. Suda, A. Thomas, T. M. Woo, R. M. Zetts and L. A. Hicks, *JAMA - J. Am. Med.*

- Assoc.*, 2016, **315**, 1864–1873.
- 25 A. M. Costa, (2013) *The Globalization of Crime*, UNODC. Report number: 1.
- 26 European Commission, (2013) *Antimicrobial Resistance*, European Commission. Report number: 1.
- 27 P. Fernandes and E. Martens, *Biochem. Pharmacol.*, 2017, **133**, 152–163.
- 28 H. W. Boucher, G. H. Talbot, J. S. Bradley, J. E. Edwards, D. Gilbert, L. B. Rice, M. Scheld, B. Spellberg and J. Bartlett, *Clin. Infect. Dis.*, 2009, **48**, 1–12.
- 29 P. Fernandes, *Nat. Biotechnol.*, 2006, **24**, 1497–1503.
- 30 H. C. Gram, *Fortschr Med*, 1884, **2**, 185–189.
- 31 P. Courvalin, *J. Intern. Med.*, 2008, **264**, 4–16.
- 32 J. Brunelt, *J. Hist. Med. Allied Sci.*, 1951, **VI**, 287–301.
- 33 J. O’Brien and G. D. Wright, *Curr. Opin. Biotechnol.*, 2011, **22**, 552–558.
- 34 G. H. Cassell and J. Mekalanos, *J. Am. Med. Assoc.*, 2001, **285**, 601–605.
- 35 L. Katz and R. H. Baltz, *J. Ind. Microbiol. Biotechnol.*, 2016, **43**, 155–176.
- 36 K. Bhullar, N. Waglechner, A. Pawlowski, K. Koteva, E. D. Banks, M. D. Johnston, H. A. Barton and G. D. Wright, *PLoS One*, 2012, **7**, 1–11.
- 37 W. H. Gaze, L. Zhang, N. A. Abdousslam, P. M. Hawkey, L. Calvo-Bado, J. Royle, H. Brown, S. Davis, P. Kay, A. B. A. Boxall and E. M. H. Wellington, *Int. Soc. Microb. Ecol.*, 2011, **5**, 1253–1261.
- 38 H. Nikaido, *Annu Rev Biochem.*, 2009, **78**, 119–146.
- 39 C. A. Liebert, R. M. Hall and A. O. Summers, *Microbiol. Mol. Biol. Rev.*, 1999, **63**, 507–522.
- 40 A. J. Alanis, *Arch. Med. Res.*, 2005, **36**, 697–705.
- 41 R. Fernandes, P. Amador and C. Prudêncio, *Rev. Med. Microbiol.*, 2013, **24**, 7–17.
- 42 R. C. Arduino and B. E. Murray, *Curr. Opin. Infect. Dis.*, 1993, **6**, 715–724.
- 43 K. Drlica, *J. Antimicrob. Chemother.*, 2003, **52**, 11–17.
- 44 K. Drlica and X. Zhao, *Clin. Infect. Dis.*, 2007, **44**, 681–688.
- 45 E. Gullberg, S. Cao, O. G. Berg, C. Ilbäck, L. Sandegren, D. Hughes and D. I. Andersson, *PLoS Pathog.*, 2011, **7**, 1–9.
- 46 A. Liu, A. Fong, E. Becket, J. Yuan, C. Tamae, L. Medrano, M. Maiz, C. Wahba, C. Lee, K. Lee, K. P. Tran, H. Yang, R. M. Hoffman, A. Salih and J. H. Miller, *Antimicrob. Agents Chemother.*, 2011, **55**, 1204–1210.
- 47 T. Vogwill and R. C. Maclean, *Evol. Appl.*, 2015, **8**, 284–295.
- 48 P. Dorado-Morales, M. Pilar Garcillán-Barcia, I. Lasa and C. Solano, *MBio*, 2021, **12**, 1–18.
- 49 S. Hernando-Amado, F. Sanz-García, P. Blanco and J. L. Martínez, *Essays Biochem.*, 2017, **61**, 37–48.
- 50 D. I. Andersson and D. Hughes, *Nat. Rev. Microbiol.*, 2010, **8**, 260–271.
- 51 S. B. Levy and M. Bonnie, *Nat. Med.*, 2004, **10**, S122–S129.
- 52 J. Björkman, I. Nagaev, O. G. Berg, D. Hughes and D. I. Andersson, *Science.*, 2000, **287**, 1479–1482.
- 53 S. Maisnier-Patin, O. G. Berg, L. Liljas and D. I. Andersson, *Mol. Microbiol.*, 2002, **46**, 355–366.
- 54 L. S. Redgrave, S. B. Sutton, M. A. Webber and L. J. V Piddock, *Trends Microbiol.*, 2014, **22**, 438–445.
- 55 E. Harrison and M. A. Brockhurst, *Trends Microbiol.*, 2012, **20**, 262–267.
- 56 K. Nordstrom and S. J. Austin, *Annu. Rev. Genet.*, 1989, **23**, 37–69.

- 57 E. Gullberg, L. M. Albrecht, C. Karlsson, E. Gullberg, L. M. Albrecht, C. Karlsson, L. Sandegren and D. I. Andersson, *MBio*, 2014, **5**, 19–23.
- 58 L. Poirel, J.-M. Rodriguez-Martinez, H. Mammeri, A. Liard and P. Nordmann, *Antimicrob. Agents Chemother.*, 2005, **49**, 3523–3525.
- 59 M. F. Lartigue, L. Poirel, D. Aubert and P. Nordmann, *Antimicrob. Agents Chemother.*, 2006, **50**, 1282–1286.
- 60 C. Humeniuk, G. Arlet, V. Gautier, P. Grimont, R. Labia and A. Philippon, *Antimicrob. Agents Chemother.*, 2002, **46**, 3045–3049.
- 61 E. M. H. Wellington, A. B. A. Boxall, P. Cross, E. J. Feil, W. H. Gaze, P. M. Hawkey, A. S. Johnson-Rollings, D. L. Jones, N. M. Lee, W. Otten, C. M. Thomas and A. P. Williams, *Lancet Infect. Dis.*, 2013, **13**, 155–165.
- 62 N. J. Ashbolt, A. Amézquita, T. Backhaus, P. Borriello, K. K. Brandt, P. Collignon, A. Coors, R. Finley, W. H. Gaze, T. Heberer, J. R. Lawrence, D. G. J. Larsson, S. A. McEwen, J. J. Ryan, J. Schönfeld, P. Silley, J. R. Snape, C. Van den Eede and E. Topp, *Environ. Health Perspect.*, 2013, **121**, 993–1001.
- 63 R. L. Finley, P. Collignon, D. G. J. Larsson, S. A. Mcewen, X. Z. Li, W. H. Gaze, R. Reid-Smith, M. Timinouni, D. W. Graham and E. Topp, *Clin. Infect. Dis.*, 2013, **57**, 704–710.
- 64 K. Kümmerer, *Chemosphere*, 2009, **75**, 417–434.
- 65 K. Kümmerer, *Chemosphere*, 2009, **75**, 435–441.
- 66 L. B. Price, M. Stegger, H. Hasman, M. Aziz, J. Larsen, S. Andersen, T. Pearson, F. Laurent, P. Keim, R. Skov and F. M. Aarestrup, *MBio*, 2012, **3**, 1–7.
- 67 M. A. Cooper and D. Shlaes, *Nature*, 2011, **472**, 32.
- 68 J. O’Neill, (2015) *Securing New Drugs for Future Generations: The Pipeline of Antibiotics*, Review on Antimicrobial Resistance. Report number: 1.
- 69 M. Hay, D. W. Thomas, J. L. Craighead, C. Economides and J. Rosenthal, *Nat. Biotechnol.*, 2014, **32**, 40–51.
- 70 L. L. Silver, *Clin. Microbiol. Rev.*, 2011, **24**, 71–109.
- 71 D. J. Payne, M. N. Gwynn, D. J. Holmes and D. L. Pompliano, *Nat. Rev. Drug Discov.*, 2007, **6**, 29–40.
- 72 N. R. Pace, *Science.*, 1997, **276**, 734–740.
- 73 D. M. Livermore, *J. Antimicrob. Chemother.*, 2011, **66**, 1941–1944.
- 74 L. Silver and K. Bostian, *Eur. J. Clin. Microbiol. Infect. Dis. Off. Publ. Eur. Soc. Clin. Microbiol.*, 1990, **9**, 455–461.
- 75 L. L. Silver and K. A. Bostian, *Antimicrob. Agents Chemother.*, 1993, **37**, 377–383.
- 76 A. J. O’Neill and I. Chopra, *Expert Opin. Investig. Drugs*, 2004, **13**, 1045–1063.
- 77 K. Miller, *J. Antimicrob. Chemother.*, 2002, **49**, 925–934.
- 78 L. J. V. Piddock, *Lancet Infect. Dis.*, 2012, **12**, 249–253.
- 79 C. A. Lipinski, F. Lombardo, B. W. Dominy and P. J. Feeney, *Adv. Drug Deliv. Rev.*, 2012, **64**, 4–17.
- 80 L. L. Silver, *Expert Opin. Drug Discov.*, 2008, **3**, 487–500.
- 81 M. F. Richter, B. S. Drown, A. P. Riley, A. Garcia, T. Shirai, R. L. Svec and P. J. Hergenrother, *Nature*, 2017, **545**, 299–304.
- 82 P. F. Chan, D. J. Holmes and D. J. Payne, *Drug Discov. Today Ther. Strateg.*, 2004, **1**, 519–527.
- 83 W. Kim, Tracking the Pipeline of Antibiotics in Development, <https://www.pewtrusts.org/en/research-and-analysis/issue-briefs/2019/09/tracking-the-global-pipeline-of-antibiotics-in-development>, (accessed 4 February 2020).

- 84 K. J. Aldred, R. J. Kerns and N. Osheroff, *Biochemistry*, 2014, **53**, 1565–1574.
- 85 A. M. Emmerson and A. M. Jones, *J. Antimicrob. Chemother.*, 2003, **51**, 13–20.
- 86 G. Y. Leshner, E. J. Froelich, M. D. Gruett, J. H. Bailey and R. P. Brundage, *J. Med. Pharm. Chem.*, 1962, **5**, 1063–1065.
- 87 W. A. Goss, W. H. Deitz and T. M. Cook, *J. Bacteriol.*, 1964, **88**, 112–118.
- 88 A. Sugino, C. L. Peebles, K. N. Kreuzer and N. R. Cozzarelli, *Proc. Natl. Acad. Sci. U. S. A.*, 1977, **74**, 4767–4771.
- 89 M. Gellert, K. Mizuuchi, M. H. O’Dea, T. Itoh and J. I. Tomizawa, *Proc. Natl. Acad. Sci. U. S. A.*, 1977, **74**, 4772–4776.
- 90 S. R. Rohifing, J. F. Gerster and D. C. Kvam, *J. Antimicrob. Chemother.*, 1976, **10**, 20–24.
- 91 C. M. Oliphant and G. M. Green, *Am. Fam. Physician*, 2002, **65**, 455–464.
- 92 R. Wise, *J. Antimicrob. Chemother.*, 1984, **13**, 59–64.
- 93 W. Cullmann, A. M. Geddes, E. Weidekamm, H. Urwyler and A. Braunsteiner, *Int. J. Antimicrob. Agents*, 1993, **2**, 203–230.
- 94 V. T. Andriole, *Int. J. Antimicrob. Agents*, 1994, **4**, S1–S6.
- 95 J. A. Balfour, P. A. Todd and D. H. Peters, *Drugs*, 1995, **49**, 794–850.
- 96 WHO, (2019) *World Health Organization Model List of Essential Medicines*, WHO. Report number: 21.
- 97 R. Kishii, Y. Yamaguchi and M. Takei, *Antimicrob. Agents Chemother.*, 2017, **61**, 1–8.
- 98 H. Furuie, S. Tanioka, K. Shimizu, S. Manita, M. Nishimura and H. Yoshidab, *Antimicrob. Agents Chemother.*, 2018, **62**, 1–8.
- 99 R. Chavan, V. Zope, N. Chavan, J. Shaikh, K. Patil, R. Yeole, S. Bhagwat and M. Patel, *Xenobiotica*, 2020, **50**, 1149–1157.
- 100 G. Xue, D. M. Crabb, L. Xiao, Y. Liu and K. B. Waites, *Antimicrob. Agents Chemother.*, 2018, **62**, 1–5.
- 101 S. S. Bhagwat, M. Nandanwar, A. Kansagara, A. Patel, S. Takalkar, R. Chavan, H. Periasamy, R. Yeole, P. K. Deshpande, S. Bhavsar, A. Bhatia, J. Ahdal, R. Jain and M. Patel, *Drug Des. Devel. Ther.*, 2019, **13**, 4351–4365.
- 102 K. McKeage, *Drugs*, 2015, **75**, 687–693.
- 103 S. P. Chang, H. Z. Lee, C. C. Lai and H. J. Tang, *Infect. Drug Resist.*, 2019, **12**, 433–438.
- 104 J. G. Heddle, F. M. Barnard, L. M. Wentzell and A. Maxwell, *Nucleosides, Nucleotides and Nucleic Acids*, 2000, **19**, 1249–1264.
- 105 J. J. Champoux, *Ann Rev Biochem*, 2001, **70**, 369–413.
- 106 J. I. Kato, H. Suzuki and H. Ikeda, *J. Biol. Chem.*, 1992, **267**, 25676–25684.
- 107 A. B. Khodursky, E. L. Zechiedrich and N. R. Cozzarelli, *roc. Natl. Acad. Sci. USA*, 1995, **92**, 11801–11805.
- 108 K. Hoshino, A. Kitamura, I. Morrissey, K. Sato, J.-I. Kato and H. Ikeda, *Antimicrob. Agents Chemother.*, 1994, **38**, 2623–2627.
- 109 M. Gellert, K. Mizuuchi, M. H. O’dea and H. A. Nash, *Proc. Natl. Acad. Sci.*, 1976, **73**, 3872–3876.
- 110 J. A. Oates, A. J. j. Wood, D. C. Hooper and J. S. Wolfson, *N. Engl. J. Med.*, 1991, **324**, 384–394.
- 111 N. R. Cozzarelli, *Science.*, 1980, **207**, 953–960.
- 112 V. F. Holmes and N. R. Cozzarelli, *Proc. Natl. Acad. Sci. USA.*, 2000, **97**, 1322–1324.
- 113 J. ichi Kato, Y. Nishimura, R. Imamura, H. Niki, S. Hiraga and H. Suzuki, *Cell*, 1990, **63**, 393–404.

- 114 E. L. Zechiedrich, A. B. Khodursky and N. R. Cozzarelli, *Genes Dev.*, 1997, **11**, 2580–2592.
- 115 E. L. Zechiedrich, A. B. Khodursky, S. Bachellier, R. Schneider, D. Chen, D. M. J. Lilley and N. R. Cozzarelli, *J. Biol. Chem.*, 2000, **275**, 8103–8113.
- 116 L. Ferrero, B. Cameron, B. Manse, D. Lagneaux, J. Crouzet, A. Famechon and F. Blanche, *Mol. Microbiol.*, 1994, **13**, 641–653.
- 117 C. Levine, H. Hiasa and K. J. Mariani, *Biochim. Biophys. Acta - Gene Struct. Expr.*, 1998, **1400**, 29–43.
- 118 C. R. Chen, M. Malik, M. Snyder and K. Drlica, *J. Mol. Biol.*, 1996, **258**, 627–637.
- 119 F. Collin, S. Karkare and A. Maxwell, *Appl. Microbiol. Biotechnol.*, 2011, **92**, 479–497.
- 120 X. S. Pan and L. M. Fisher, *Antimicrob. Agents Chemother.*, 1997, **41**, 471–474.
- 121 A. Robicsek, J. Strahilevitz, G. A. Jacoby, M. Macielag, D. Abbanat, H. P. Chi, K. Bush and D. C. Hooper, *Nat. Med.*, 2006, **12**, 83–88.
- 122 M. W. Vetting, H. P. Chi, S. S. Hegde, G. A. Jacoby, D. C. Hooper and J. S. Blanchard, *Biochemistry*, 2008, **47**, 9825–9835.
- 123 H. Yoshida, M. Bogaki, M. Nakamura, L. M. Yamanaka, S. Nakamura, L. M. Yamanaka and S. Nakamura, *Antimicrob. Agents Chemother.*, 1991, **35**, 1647–1650.
- 124 J. Ruiz, *J. Antimicrob. Chemother.*, 2003, **51**, 1109–1117.
- 125 J. Vila, J. Ruiz, F. Marco, A. Barcelo, P. Goni, E. Giralt and T. J. De Anta, *Antimicrob. Agents Chemother.*, 1994, **38**, 2477–2479.
- 126 J. Ruiz, J. Gómez, M. M. Navia, A. Ribera, J. M. Sierra, F. Marco, J. Mensa and J. Vila, *Diagn. Microbiol. Infect. Dis.*, 2002, **42**, 257–261.
- 127 M. J. Everett, Y. F. Jin, V. Ricci and L. J. V. Piddock, *Antimicrob. Agents Chemother.*, 1996, **40**, 2380–2386.
- 128 M. Oram and L. M. Fisher, *Antimicrob. Agents Chemother.*, 1991, **35**, 387–389.
- 129 M. del M. Tavíoa, J. Vilab, J. Ruizb, J. Ruiza, A. M. Martín-Sánchez and M. T. J. de Anta, *J. Antimicrob. Chemother.*, 1999, **44**, 735–742.
- 130 M. E. Jones, D. F. Sahm, N. Martin, S. Scheuring, P. Heisig, C. Thornsberry, K. Köhrer and F. J. Schmitz, *Antimicrob. Agents Chemother.*, 2000, **44**, 462–466.
- 131 P. Heisig, *Antimicrob. Agents Chemother.*, 1996, **40**, 879–885.
- 132 Y. Kumagai, J. I. Kato, K. Hoshino, T. Akasaka, K. Sato and H. Ikeda, *Antimicrob. Agents Chemother.*, 1996, **40**, 710–714.
- 133 J. Strahilevitz and D. C. Hooper, *Antimicrob. Agents Chemother.*, 2005, **49**, 1949–1956.
- 134 J. S. Chapman and N. H. Georgopapdakou, *Antimicrob. Agents Chemother.*, 1988, **32**, 438–442.
- 135 K. Hirai, H. Aoyama, T. Irikura, S. Iyobe and S. Mitsunashi, *Antimicrob. Agents Chemother.*, 1986, **30**, 342–342.
- 136 H. Aoyama, K. Sato, T. Kato, K. Hirai and S. Mitsunashi, *Antimicrob. Agents Chemother.*, 1987, **31**, 1640–1641.
- 137 J. I. Mitsuyama, Y. Itoh, M. Takahata, S. Okamoto and T. Yasuda, *Antimicrob. Agents Chemother.*, 1992, **36**, 2030–2036.
- 138 G. Jacoby, V. Cattoir, D. Hooper, L. Martínez-Martínez, P. Nordmann, A. Pascual, L. Poirel and M. Wang, *Antimicrob. Agents Chemother.*, 2008, **52**, 2297–2299.
- 139 M. J. Ellington and N. Woodford, *J. Antimicrob. Chemother.*, 2006, **57**, 1026–1029.
- 140 J. Ruiz, M. J. Pons and C. Gomes, *Int. J. Antimicrob. Agents*, 2012, **40**, 196–203.
- 141 M. C. Garrido, M. Herrero, R. Kolter and F. Moreno, *EMBO J.*, 1988, **7**, 1853–1862.
- 142 D. B. Zamble, D. A. Miller, J. G. Heddle, A. Maxwell, C. T. Walsh and F. Hollfelder, *Proc.*

- Natl. Acad. Sci. USA*, 2001, **98**, 7712–7717.
- 143 J. G. Heddle, S. J. Blance, D. B. Zamble, F. Hollfelder, D. A. Miller, L. M. Wentzell, C. T. Walsh and A. Maxwell, *J. Mol. Biol.*, 2001, **307**, 1223–1234.
- 144 J. H. Tran, G. A. Jacoby and D. C. Hooper, *Antimicrob. Agents Chemother.*, 2005, **49**, 3050–3052.
- 145 M. W. Vetting, S. S. Hegde, M. Wang, G. A. Jacoby, D. C. Hooper and J. S. Blanchard, *J. Biol. Chem.*, 2011, **286**, 25265–25273.
- 146 D. Ince and D. C. Hooper, *J. Bacteriol.*, 2003, **185**, 6883–6892.
- 147 L. R. Peterson, *Clin. Infect. Dis.*, 2001, **33**, S180–S186.
- 148 J. M. Domagala, L. D. Hanna, C. L. Heifetz, M. Hutt, T. F. Mich, J. P. Sanchez and M. Solomon, *J. Med. Chem.*, 1986, **29**, 394–404.
- 149 I. Laponogov, M. K. Sohi, D. A. Veselkov, X. S. Pan, R. Sawhney, A. W. Thompson, K. E. McAuley, L. M. Fisher and M. R. Sanderson, *Nat. Struct. Mol. Biol.*, 2009, **16**, 667–669.
- 150 T. Lu, X. Zhao, X. Li, A. Drlica-Wagner, J. Y. Wang, J. Domagala and K. Drlica, *Antimicrob. Agents Chemother.*, 2001, **45**, 2703–2709.
- 151 P. C. Sharma, A. Jain and S. Jain, *Acta Pol. Pharm. - Drug Res.*, 2009, **66**, 587–604.
- 152 P. C. Appelbaum and P. A. Hunter, *Int. J. Antimicrob. Agents*, 2000, **16**, 5–15.
- 153 J. M. Domagala, *J. Antimicrob. Chemother.*, 1994, **33**, 685–706.
- 154 J. Marchant, *Nature*, 2018, **555**, 431–433.
- 155 N. L. Millar, S. Siebert and I. B. McInnes, *Nature*, 2019, **566**, 326–326.
- 156 C. J. Hackbarth, H. F. Chambers and M. A. Sande, *Antimicrob. Agents Chemother.*, 1986, **29**, 611–613.
- 157 R. M. Harrell, *South. Med. J.*, 1999, **92**, 622–625.
- 158 B. A. Lipsky and C. A. Baker, *Clin. Infect. Dis.*, 1999, **28**, 352–364.
- 159 R. Stahlmann and H. Lode, *Drugs*, 1999, **58**, 37–42.
- 160 J. O'Donnell, K. Lawrence, K. Vishwanathan, V. Hosagrahara and J. P. Mueller, *Antimicrob. Agents Chemother.*, 2019, **63**, 1–14.
- 161 M. D. Huband, P. A. Bradford, L. G. Otterson, G. S. Basarab, A. C. Kutschke, R. A. Giacobbe, S. A. Patey, R. A. Alm, M. R. Johnstone, M. E. Potter, P. F. Miller and J. P. Mueller, *Antimicrob. Agents Chemother.*, 2015, **59**, 467–474.
- 162 G. Kern, T. Palmer, D. E. Ehmann, A. B. Shapiro, B. Andrews, G. S. Basarab, P. Doig, J. Fan, N. Gao, S. D. Mills, J. Mueller, S. Sriram, J. Thresher and G. K. Walkup, *J. Biol. Chem.*, 2015, **290**, 20984–20994.
- 163 G. S. Basarab, G. H. Kern, J. McNulty, J. P. Mueller, K. Lawrence, K. Vishwanathan, R. A. Alm, K. Barvian, P. Doig, V. Galullo, H. Gardner, M. Gowravaram, M. Huband, A. Kimzey, M. Morningstar, A. Kutschke, S. D. Lahiri, M. Perros, R. Singh, V. J. A. A. Schuck, R. Tommasi, G. Walkup and J. V. Newman, *Sci. Rep.*, 2015, **5**, 1–14.
- 164 S. Foerster, D. Golparian, S. Jacobsson, L. J. Hathaway, N. Low, W. M. Shafer, C. L. Althaus and M. Unemo, *Front. Microbiol.*, 2015, **6**, 1–14.
- 165 J. R. Papp, K. Lawrence, S. Sharpe, J. Mueller and R. D. Kirkcaldy, *Int. J. Antimicrob. Agents*, 2016, **48**, 328–330.
- 166 B. D. Bax, P. F. Chan, D. S. Eggleston, A. Fosberry, D. R. Gentry, F. Gorrec, I. Giordano, M. M. Hann, A. Hennessy, M. Hibbs, J. Huang, E. Jones, J. Jones, K. K. Brown, C. J. Lewis, E. W. May, M. R. Saunders, O. Singh, C. E. Spitzfaden, C. Shen, A. Shillings, A. J. Theobald, A. Wohlkonig, N. D. Pearson and M. N. Gwynn, *Nature*, 2010, **466**, 935–940.
- 167 D. J. Biedenbach, S. K. Bouchillon, M. Hackel, L. A. Miller, N. E. Scangarella-Oman, C.

- Jakielaszek and D. F. Sahn, *Antimicrob. Agents Chemother.*, 2016, **60**, 1918–1923.
- 168 P. J. Hergenrother, E. I. Parkinson, J. S. Bair, (2015) *Compounds for Treatment of Fluoroquinolone-resistant Bacteria*. WO 2015/142952 A1 (patent).
- 169 O. A. Bardell-cox, A. J. P. White, L. Aragón and M. J. Fuchter, *Medchemcomm*, 2019, **10**, 1438–1444.
- 170 E. I. Parkinson, J. S. Bair, B. A. Nakamura, H. Y. Lee, H. I. Kuttub, E. H. Southgate, S. Lezmi, G. W. Lau and P. J. Hergenrother, *Nat. Commun.*, 2015, **6**, 1–9.
- 171 F. Strelitz, H. Flon and I. N. Asheshov, *Proc. Natl. Acad. Sci. USA*, 1955, **41**, 620–624.
- 172 K. L. Rinehart, G. Leadbetter, R. A. Larson and R. M. Forbis, 1970, **92**, 6995–6996.
- 173 R. M. Forbis and K. L. Rinehart Jr, *J. Antibiot.*, 1971, **24**, 326–327.
- 174 H. Naganawa, T. Wakashiro, A. Yagi, S. Kondo, T. Takita, M. Hamada, K. Maeda and H. Umezawa, *J. Antibiot.*, 1970, **23**, 365–368.
- 175 K. L. Rinehart and H. B. Renfroe, *J. Am. Chem. Soc.*, 1961, **83**, 3729–3731.
- 176 A. M. Nadzan and K. L. Rinehart, *J. Antibiot.*, 1977, **30**, 523–524.
- 177 S. C. Kampranis and A. Maxwell, *J. Bio. Chem.*, 1998, **273**, 22615–22626.
- 178 M. Arai, K. Kamiya, P. Pruksakorn, Y. Sumii, N. Kotoku, J.-P. P. Joubert, P. Moodley, C. Han, D. Shin and M. Kobayashi, *Bioorganic Med. Chem.*, 2015, **23**, 3534–3541.
- 179 S. Adelman, T. Baldhoff, B. Koepcke and G. Schembecker, *J. Chromatogr. A*, 2013, **1274**, 54–64.
- 180 J. A. Pope, R. A. Nelson, C. P. Schaffner, R. T. Rosen and R. C. Pandey, *J. Ind. Microbiol.*, 1990, **6**, 61–69.
- 181 R. M. Forbis and K. L. Rinehart, *J. Am. Chem. Soc.*, 1973, **95**, 5003–5013.
- 182 F. Nussbaum, A. Ebbinghaus, A. Mayer-Bartschmid, W. Zitzmann, W. Wiese, M. Stadler, S. Anlauf, (2009) *CDC25 Inhibitors*. EP 2 130 831 A1 (patent).
- 183 E. I. Parkinson, J. S. Bair, M. Cismesia and P. J. Hergenrother, *ACS Chem. Biol.*, 2013, **8**, 2173–2183.
- 184 J. S. Bair, R. Palchaudhuri and P. J. Hergenrother, *J. Am. Chem. Soc.*, 2010, **132**, 5469–5478.
- 185 C. L. Coon, W. G. Blucher and M. E. Hill, *J. Org. Chem.*, 1973, **38**, 4243–4248.
- 186 T. J. Heckrodt, Y. Chen and R. Singh, *Tetrahedron*, 2019, **75**, 2385–2399.
- 187 Boyer, F. E. Domagala, J. M. Ellsworth, L. E. Gajda, C. A. Hagen, S. E. Lovdahl, M. J. Lunney, E. A. Markoski, L. J. Josyula, V. P. Tait, B. D., (2000) *HIV Protease Inhibitors*. WO 00/15634 (patent).
- 188 R. N. Misra, B. R. Brown, W. Han, D. N. Harris, A. Hedberg, M. L. Webb and S. E. Hall, *J. Med. Chem.*, 1991, **34**, 2882–2891.
- 189 H. J. Gim, H. Li, S. R. Jung, Y. J. Park, J. H. Ryu, K. H. Chung and R. Jeon, *Eur. J. Med. Chem.*, 2014, **85**, 107–118.
- 190 J. Wu, S. Xiang, J. Zeng, M. Leow and X. W. Liu, *Org. Lett.*, 2015, **17**, 222–225.
- 191 P. Rocca, C. Cochennec, F. Marsais, L. Thomas-dit-Dumont, M. Mallet, A. Godard and G. Quéguiner, *J. Org. Chem.*, 1993, **58**, 7832–7838.
- 192 A. Hooper, A. Zambon and C. J. Springer, *Org. Biomol. Chem.*, 2016, **14**, 963–969.
- 193 H. Ji, L. Y. Wu, J. H. Cai, G. R. Li, N. N. Gan and Z. H. Wang, *RSC Adv.*, 2018, **8**, 13643–13648.
- 194 G. A. Molander, S. L. J. Trice and S. M. Kennedy, *J. Org. Chem.*, 2012, **77**, 8678–8688.
- 195 P. Boontiem and S. Kiatisevi, *Inorganica Chim. Acta*, 2020, **506**, 119538.
- 196 H. Y. Jung, X. Feng, H. Kim and J. Yun, *Tetrahedron*, 2012, **68**, 3444–3449.
- 197 A. P. Pulis, P. Fackler and V. K. Aggarwal, *Angew. Chem*, 2014, **53**, 4382–4385.

- 198 W. Zhou, M. Fan, J. Yin, Y. Jiang and D. Ma, *J. Am. Chem. Soc.*, 2015, **137**, 11942–11945.
- 199 K. Nagao, A. Yamazaki, H. Ohmiya and M. Sawamura, *Org. Lett.*, 2018, **20**, 1861–1865.
- 200 K. K. Park and J. J. Lee, *Tetrahedron*, 2004, **60**, 2993–2999.
- 201 V. V. Kravtsova, E. Y. Kovalenko, I. V. Ukrainets, A. A. Tkach and V. I. Mamchur, *Chem. Heterocycl. Compd.*, 2010, **46**, 850–855.
- 202 K. L. Hopkins, R. H. Davies and E. J. Threlfall, *Int. J. Antimicrob. Agents*, 2005, **25**, 358–373.
- 203 S. Ando, M. Tsuzaki and T. Ishizuka, *J. Org. Chem.*, 2020, **85**, 11181–11189.
- 204 X. Yang, L. Wang, F. Hu, L. Xu, S. Li and S. S. Li, *Org. Lett.*, 2021, **23**, 358–364.
- 205 W. A. Bauer, D. M. Perry and W. M. Kirby, *AMA. Arch. Intern. Med.*, 1959, **104**, 208–216.
- 206 N. Vineetha, R. A. Vignesh and D. Sridhar, *Int. J. Appl. Res.*, 2015, **1**, 624–631.
- 207 M. Vestergaard, B. Leng, J. Haaber, M. S. Bojer, C. S. Vegge and H. Ingmer, *Front. Microbiol.*, 2016, **7**, 1–10.
- 208 J. M. Stokes, C. R. Macnair, B. Ilyas, S. French, J. P. Côté, C. Bouwman, M. A. Farha, A. O. Sieron, C. Whitfield, B. K. Coombes and E. D. Brown, *Nat. Microbiol.*, 2017, **2**, 1–8.
- 209 S. French, M. Farha, M. J. Ellis, Z. Sameer, J. P. Côté, N. Cotroneo, T. Lister, A. Rubio and E. D. Brown, *ACS Infect. Dis.*, 2020, **6**, 1405–1412.
- 210 A. Daniel V. Zurawski, A. A. Reinhart, Y. A. Alamneh, M. J. Pucci, Y. Si, R. Abu-Taleb, J. P. Shearer, S. T. Demons, S. D. Tyner and T. Lister, *Am. Soc. Microbiol.*, 2017, **61**, 1–6.
- 211 C. R. MacNair, J. M. Stokes, L. A. Carfrae, A. A. Fiebig-Comyn, B. K. Coombes, M. R. Mulvey and E. D. Brown, *Nat. Commun.*, 2018, **9**, 1–8.
- 212 Y. V. Zakalyukina, M. V. Birykov, D. A. Lukianov, D. I. Shiriaev, E. S. Komarova, D. A. Skvortsov, Y. Kostyukevich, V. N. Tashlitsky, V. I. Polshakov, E. Nikolaev, P. V. Sergiev and I. A. Osterman, *Biochimie*, 2019, **160**, 93–99.
- 213 J. M. Blair and L. J. Piddock, *Curr. Opin. Microbiol.*, 2009, **12**, 512–519.
- 214 C. Alvarez-Ortega, J. Olivares and J. L. Martínez, *Front. Microbiol.*, 2013, **4**, 1–11.
- 215 N. Chowdhury, S. Suhani, A. Purkaystha, M. K. Begum, T. Raihan, M. J. Alam, K. Islam and A. K. Azad, *Microbiol. Insights*, 2019, **12**, 1–10.
- 216 R. Morona, P. A. Manning and P. Reeves, *J. Bacteriol.*, 1983, **153**, 693–699.
- 217 T. J. Opperman, S. M. Kwasny, H. S. Kim, S. T. Nguyen, C. Houseweart, S. D'Souza, G. C. Walker, N. P. Peet, H. Nikaido and T. L. Bowlin, *Antimicrob. Agents Chemother.*, 2014, **58**, 722–733.
- 218 I. T. Paulsen, J. H. Park, P. S. Choi and M. H. Saier, *FEMS Microbiol. Lett.*, 1997, **156**, 1–8.
- 219 X. Z. Li and H. Nikaido, *Drugs*, 2004, **64**, 159–204.
- 220 S. Murakami, R. Nakashima, E. Yamashita, T. Matsumoto and A. Yamaguchi, *Nature*, 2006, **443**, 173–179.
- 221 Y. Takatsuka, C. Chen and H. Nikaido, *Proc. Natl. Acad. Sci. USA*, 2010, **107**, 6559–6565.
- 222 H. I. Zgurskaya and H. Nikaido, *Proc. Natl. Acad. Sci. USA*, 1999, **96**, 7190–7195.
- 223 H. Nikaido, *J. Bacteriol.*, 1996, **178**, 5853–5859.
- 224 M. Martins, M. Viveiros, I. Couto, S. S. Costa, T. Pacheco, S. Fanning, J. M. Pagès and L. Amaral, *In Vivo*, 2011, **25**, 171–178.
- 225 M. Martins, M. P. McCusker, M. Viveiros, I. Couto, S. Fanning, J.-M. Pagès and L. Amaral, *Open Microbiol. J.*, 2013, **7**, 72–82.

- 226 J. P. Diamond, L. White, J. P. Leeming, H. B. Hoh and D. L. Easty, *Br. J. Ophthalmol.*, 1995, **79**, 606–609.
- 227 R. Kirk, A. Ratcliffe, G. Noonan, M. Uosis-Martin, D. Lyth, O. Bardell-Cox, J. Massam, P. Schofield, A. Lyons, D. Clare, J. Maclean, A. Smith, V. Savage, S. Mohmed, C. Charrier, A.-M. Salisbury, E. Moyo, N. Ooi, N. Chalam-Judge, J. Cheung, N. R. Stokes, S. Best, M. Craighead, R. Armer and A. Huxley, *RSC Med. Chem.*, 2020, **11**, 1379–1385.
- 228 R. Kirk, A. Ratcliffe, G. Noonan, M. Uosis-Martin, D. Lyth, O. Bardell-Cox, J. Massam, P. Schofield, S. Hindley, D. R. Jones, J. Maclean, A. Smith, V. Savage, S. Mohmed, C. Charrier, A.-M. Salisbury, E. Moyo, R. Metzger, N. Chalam-Judge, J. Cheung, N. R. Stokes, S. Best, M. Craighead, R. Armer and A. Huxley, *RSC Med. Chem.*, 2020, **11**, 1366–1378.
- 229 M. Cornbise, F. Reck, (2008) *Substituted Piperidines for use in the Treatment of Bacterial Infections*. WO 2008/120003 A1 (patent).
- 230 V. Pace, F. Martínez, M. Fernández, J. V. Sinisterra and A. R. Alcántara, *Org. Lett.*, 2007, **9**, 2661–2664.
- 231 J. Yamawaki and T. Ando, *Chem. Lett.*, 1979, **8**, 755–758.
- 232 S. Hayat, Atta-Ur-Rahman, M. Iqbal Choudhary, K. M. Khan, W. Schumann and E. Bayer, *Tetrahedron*, 2001, **57**, 9951–9957.
- 233 J. Derosa, M. L. O’Duill, M. Holcomb, M. N. Boulous, R. L. Patman, F. Wang, M. Tran-Dubé, I. McAlpine and K. M. Engle, *J. Org. Chem.*, 2018, **83**, 3417–3425.
- 234 L. E. Kiss, H. S. Ferreira, L. Torrão, M. J. Bonifácio, P. N. Palma, P. Soares-Da-Silva and D. A. Learmonth, *J. Med. Chem.*, 2010, **53**, 3396–3411.
- 235 R. Abramowitz and S. H. Yalkowsky, *Pharm. Res. An Off. J. Am. Assoc. Pharm. Sci.*, 1990, **7**, 942–947.
- 236 S. H. Yalkowsky and S. C. Valvani, *J. Pharm. Sci.*, 1980, **69**, 912–922.
- 237 Alan R. Katritzky, R. Jain, A. Lomaka, R. Petrukhin, U. Maran and M. Karelson, *Cryst. Growth Des.*, 2001, **1**, 261–265.
- 238 J. Dong, N. N. Wang, Z. J. Yao, L. Zhang, Y. Cheng, D. Ouyang, A. P. Lu and D. S. Cao, *J. Cheminform.*, 2018, **10**, 1–11.
- 239 M. Harfenist, *J. Am. Chem. Soc.*, 1954, **76**, 4991–4993.
- 240 G. R. Fulmer, A. J. M. Miller, N. H. Sherden, H. E. Gottlieb, A. Nudelman, B. M. Stoltz, J. E. Bercaw and K. I. Goldberg, *Organometallics*, 2010, **29**, 2176–2179.
- 241 M. R. Reithofer, G. E. Dobereiner, R. R. Schrock, P. Muller and P. Mu, *Organometallics*, 2013, **2**, 8–11.
- 242 G. Barker, S. Webster, D. G. Johnson, R. Curley, M. Andrews, P. C. Young, S. A. MacGregor and A. L. Lee, *J. Org. Chem.*, 2015, **80**, 9807–9816.
- 243 T. Oberhauser, *J. Org. Chem.*, 1997, **3263**, 4504–4506.
- 244 H. Aihara, (2016) *Nitrophenol Compounds and their Preparation by Coupling Reaction*. JP 2016147939 (patent).
- 245 J. Bos and T. W. Muir, *J. Am. Chem. Soc.*, 2018, **140**, 4757–4760.
- 246 A. Otaka, E. Mitsuyama, T. Kinoshita, H. Tamamura and N. Fujii, *J. Org. Chem.*, 2000, **65**, 4888–4899.
- 247 P. J. Hergenrother, D. A. Boothman, J. S. Bair, R. Palchaudhuri, (2013) *Compounds and Anti-Tumor NQO1 Substrates*. WO 2013/056073 A1 (patent).
- 248 P. J. Hergenrother, A. P. Ley, (2018) *Topoisomerase Inhibitors with Antibacterial and Anticancer Activity*. WO 2018/237140 A1 (patent).
- 249 L. T. Kliman, S. N. Mlynarski and J. P. Morken, *J. Am. Chem. Soc.*, 2009, **131**, 13210–

- 13211.
- 250 N. Saygili, R. J. Brown, P. Day, R. Hoelzl, P. Kathirgamanathan, E. R. Mageean, T. Ozturk, M. Pilkington, M. M. B. Qayyum, S. S. Turner, L. Vorwerk and J. D. Wallis, *Tetrahedron*, 2001, **57**, 5015–5026.
- 251 X. Lu, S. Wan, J. Jiang, X. Jiang, W. Yang, P. Yu, L. Xu, Z. Zhang, G. Zhang, L. Shan and Y. Wang, *Eur. J. Med. Chem.*, 2011, **46**, 2691–2698.
- 252 F. H. S. Gama, R. O. M. de Souza and S. J. Garden, *RSC Adv.*, 2015, **5**, 70915–70928.
- 253 A. Maiti, P. V. N. Reddy, M. Sturdy, L. Marler, S. D. Pegan, A. D. Mesecar, J. M. Pezzuto and M. Cushman, *J. Med. Chem.*, 2009, **52**, 1873–1884.
- 254 K. K. S. Sai, T. M. Gilbert and D. a Klumpp, *J. Org. Chem.*, 2007, **72**, 9761–9764.
- 255 V. Nadaraj and S. T. Selvi, *Indian J. Chem.*, 2007, **46B**, 1203–1207.
- 256 R. M. Moslin, D. S. Weinstein, S. T. Wroblewski, J. S. Tokarski, A. Kumar, (2014) *Amide-Substituent Heterocyclic Compounds Useful as Modulators of IL-12, IL-23 and/or IFN Alpha Responses*. WO 2014/074661 A1 (patent).
- 257 K. J. Duffy, C. Erickson-Miller, J. Jenkins, J. I. Luengo, (2011) *Thrombopoietin Mimetics*. US 2011/0212054 A1 (patent).
- 258 K. Hiramatsu, Y. Morimoto, T. Baba, I. Hayakawa, (2014) *Novel Compounds with Antibacterial Activity*. EP 2 987 787 A1 (patent).
- 259 Y. Yan, B. Qin, C. Ren, X. Chen, Y. K. Yip, R. Ye, D. Zhang, H. Su and H. Zeng, *J. Am. Chem. Soc.*, 2010, **132**, 5869–5879.
- 260 B. Qin, X. Chen, X. Fang, Y. Shu, Y. K. Yip, Y. Yan, S. Pan, W. Q. Ong, C. Ren, H. Su and H. Zeng, *Org. Lett.*, 2008, **10**, 5127–5130.
- 261 Q. Wang, E. Lucien, A. Hashimoto, G. C. G. Pais, D. M. Nelson, Y. Song, J. A. Thanassi, C. W. Marlor, C. L. Thoma, J. Cheng, S. D. Podos, Y. Ou, M. Deshpande, M. J. Pucci, D. D. Buechter, B. J. Bradbury and J. A. Wiles, *J. Med. Chem.*, 2007, **50**, 199–210.
- 262 A. W. Bauer, J. C. Sherris, M. Turck and W. M. M. Kirby, *Am. J. Clin. Pathol.*, 1966, **45**, 493–496.

7. Appendix

7.1 Failed Reaction Conditions

7.1.1 Table 1 - Scheme 5 Unsuccessful amide coupling of 2 to form 14.

Trial	Attempted Conditions
1	i) Crotonic acid, (COCl) ₂ , CH ₂ Cl ₂ , 0 °C to rt, 2 h, ii) 2 , NEt ₃ , CH ₂ Cl ₂ , 0 °C to rt to 50 °C, 18 h.
2	Crotonic anhydride, pyridine, 120 °C, 5 h.
3	EDCI, crotonic acid, DMAP, NEt ₃ , CH ₂ Cl ₂ , rt, 18 h.

7.1.2 Table 2 - Scheme 5 Unsuccessful acetylation of 2 to form 15.

Trial	Attempted Conditions
1	Acetyl chloride, NEt ₃ , THF, rt, 18 h.
2	Acetic anhydride, CH ₂ Cl ₂ , rt to 125 °C, 18 h.
3	Acetic anhydride, TFA, CH ₂ Cl ₂ , rt, 18 h.
4	Acetic anhydride, pyridine, THF, rt, 18 h.

7.1.3 Table 3 - Scheme 10 Unsuccessful Suzuki-Miyaura cross-coupling of 22 and 19 to form 26.

Trial	Attempted Conditions
1	Pd(dppf)Cl ₂ (10 mol%), K ₂ CO ₃ , DME: H ₂ O (9:1), 85 °C, 18 h.
2	Pd(dppf)Cl ₂ (10 mol%), K ₂ CO ₃ , DME: H ₂ O (4:1), 85 °C, 18 h.
3	Pd G2 Xphos (10 mol%), Xphos, Cs ₂ CO ₃ , DME: H ₂ O (4:1), 90 °C, 18 h.
4	Pd(dppf)Cl ₂ (10 mol%), K ₂ CO ₃ , Dioxane: H ₂ O (9:1), 90 °C, 18 h.
5	Pd(dppf)Cl ₂ (10 mol%), K ₃ PO ₄ , DME: H ₂ O (9:1), 90 °C, 18 h.
6	Pd(dppf)Cl ₂ (10 mol%), K ₂ CO ₃ , DME: H ₂ O (9:1), 87 °C, under microwave irradiation (1 h)

7.1.4 Table 4 - Scheme 11 - Unsuccessful hydrolysis of ester 28 to acid 29.

Trial	Attempted Conditions
1	NEt ₃ , H ₂ O, rt, 18 h
2	NaOH (1 M), THF, rt, 18 h
3	NaOH (2 M), EtOH, rt, 18 h
4	HCl (1M), H ₂ O, rt, 18 h

7.1.5 Table 5 - Scheme 13 - Unsuccessful cyclisation of 30 to form 34.

Trial	Attempted Conditions
1	Pd Xphos G2, Xphos, K ₂ CO ₃ , <i>i</i> -PrOH, 85 °C, 18 h
2	Pd Xphos G2, Xphos, K ₂ CO ₃ , <i>i</i> -PrOH, 100 °C, 18 h
3	Pd Xphos G2, Xphos, K ₂ PO ₃ , DME, 100 °C, 18 h
4	Pd Xphos G2, Xphos, Cs ₂ CO ₃ , Toluene, 100 °C, 18 h
5	Pd Xphos G2, Xphos, K ₂ CO ₃ , <i>i</i> -PrOH, 110 °C, 18 h
6	Pd(OAc) ₂ , Cs ₂ CO ₃ , ^t BuBrettPhos, ^t BuOH, H ₂ O, 110°C, 18 h
7	CuI, DMEDA, Cs ₂ CO ₃ , H ₂ O, 1,4-Dioxane, 100 °C, 8 h
8	NaH (60 % mineral oil), DMF, 80 °C, 3 h

7.1.6 Table 6 - Scheme 14 - Unsuccessful reduction of 30 to form 35.

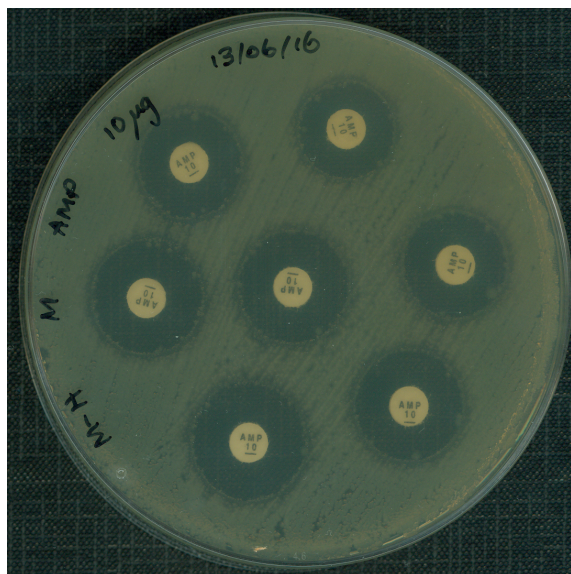
Trial	Attempted Conditions
1	NaBH ₄ , AcOH, Pd/C (10 %), Toluene, rt, 18 h
2	Pd/C (10 %), H ₂ , EtOAc, rt, 18 h
3	Pd/C (10 %), H ₂ , MeOH, CH ₂ Cl ₂ , rt, 18 h
4	PMHS, CuCl, IPr.HCl, NaO ^t Bu, ^t BuOH, Toluene, rt, 18 h
5	NaBH ₄ , MeOH, THF, 0 °C to rt, 2 h

7.1.7 Table 7 - Scheme 17 - Unsuccessful hydrolysis of ester 41 to acid 42.

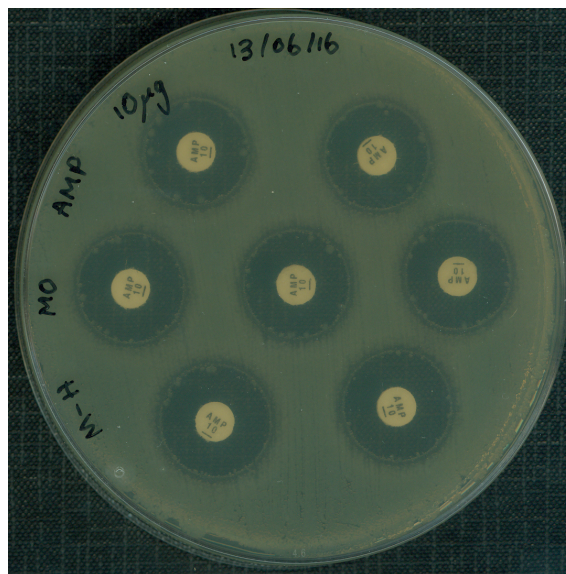
Trial	Attempted Conditions
1	NaOH (1 M), MeOH, rt
2	NaOH (1 M), THF, EtOH, rt, 18 h
3	NaOH (3 M), MeOH, THF, rt, 18 h
4	LiOH (1 M), THF, H ₂ O, 60 °C, 18 h
5	LiOH (1 M), EtOH, MeCN, rt, 18 h
6	K ₂ CO ₃ , MeOH, H ₂ O, 40 °C, 18 h
7	NEt ₃ , THF, H ₂ O, rt, 18 h
8	NEt ₃ , H ₂ O, rt, 18 h
9	HCl (1M), H ₂ O, rt - 110 °C, 18 h
10	HCl (conc), dioxane, rt - 110 °C, 18 h
11	TMSCl, NaI, MeCN, 85 °C, 18 h
12	TBAH, MeCN, rt, 18 h
13	KF, TBAF, THF, 70°C, 18 h
14	TMSOK, THF, rt, 18 h
15	NH ₄ OH, THF, H ₂ O, rt, 18 h

7.2 Controls for the Kirby–Bauer disc diffusion assay

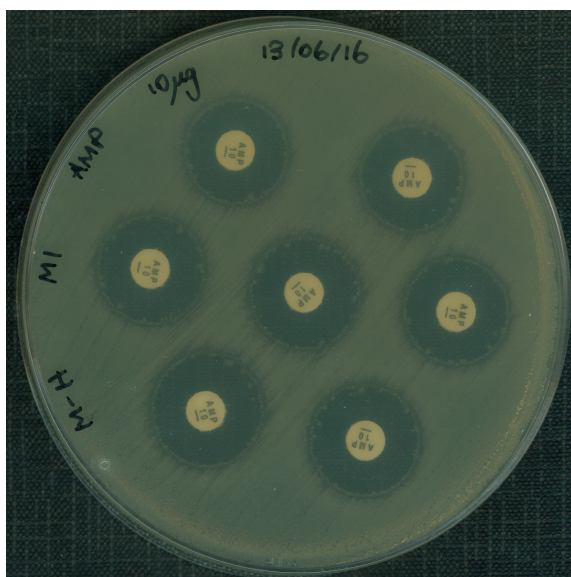
7.2.1 Kirby–Bauer disc diffusion with Amoxicillin (10 µg commercial disc)



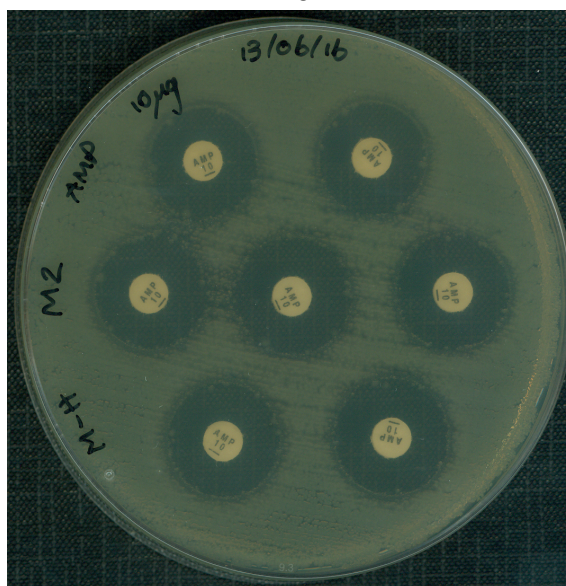
M



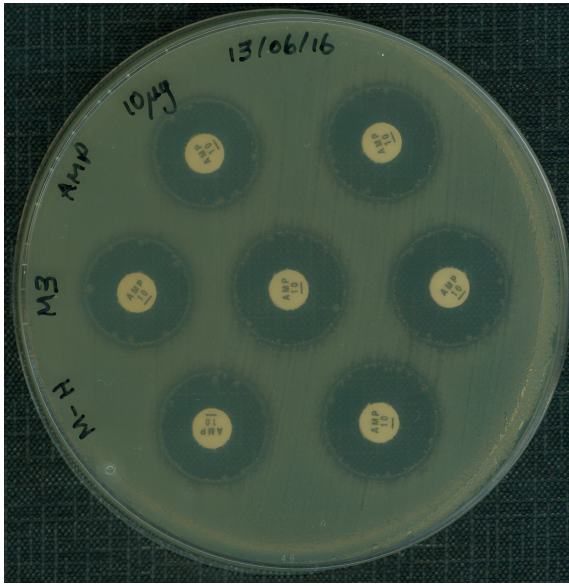
M0



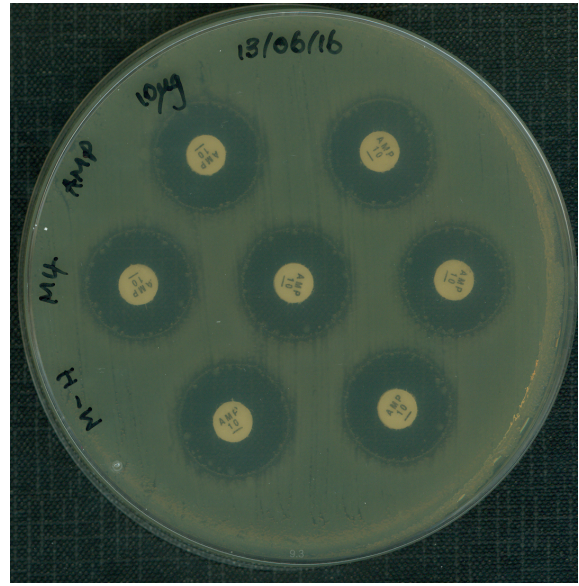
M1



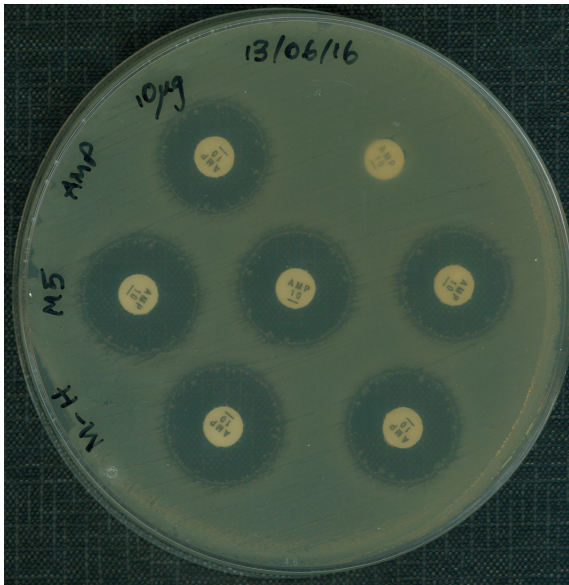
M2



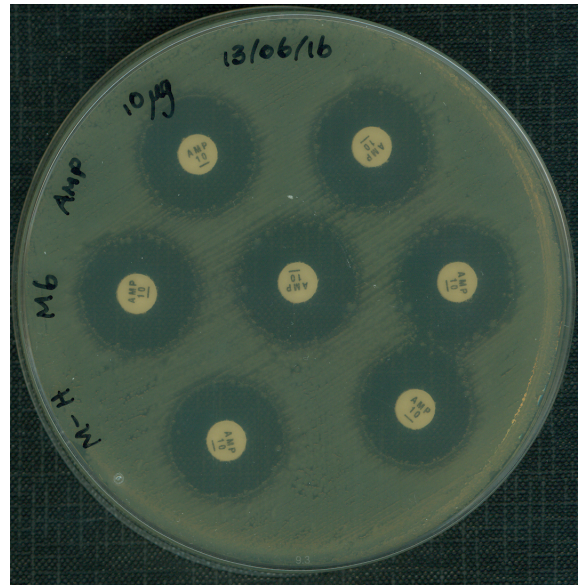
M3



M4

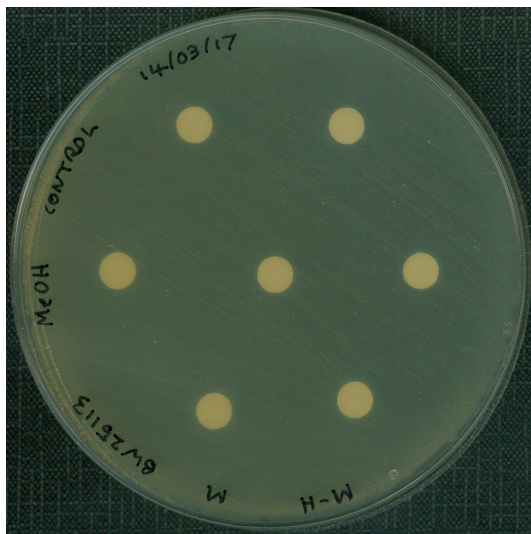


M5

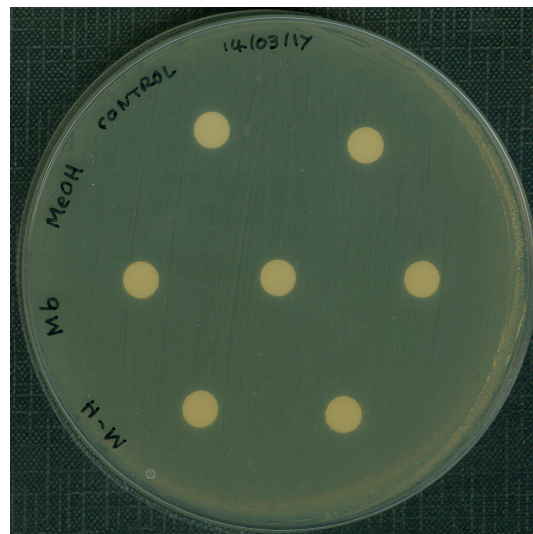


M6

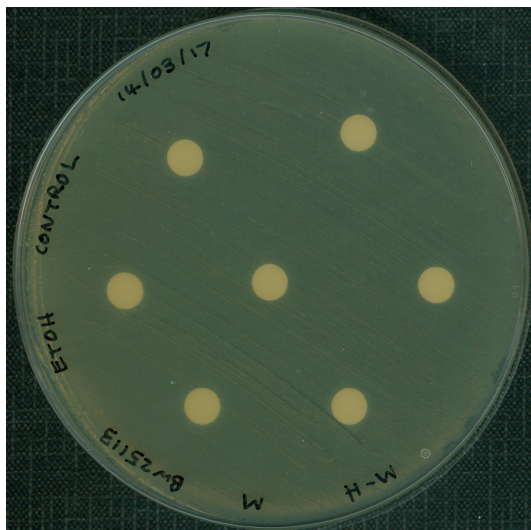
7.2.2 Kirby-Bauer disc diffusion solvent controls (MeOH, EtOH and CHCl₃)



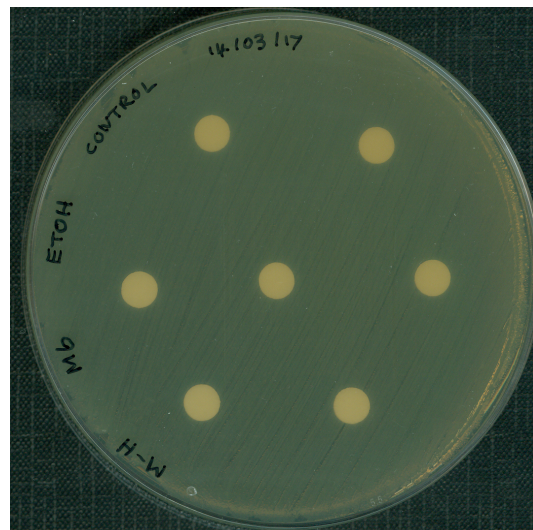
BW25113 – MeOH



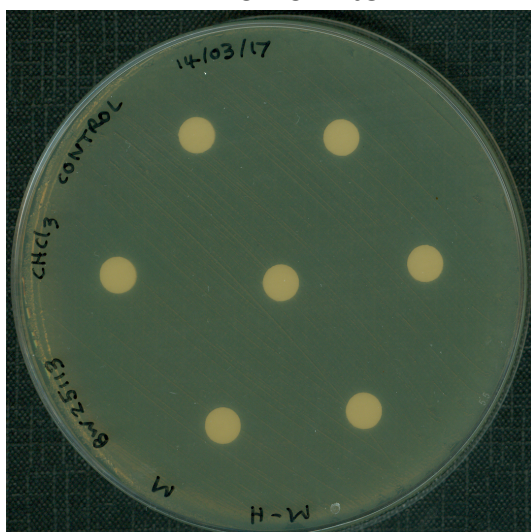
M6 - MeOH



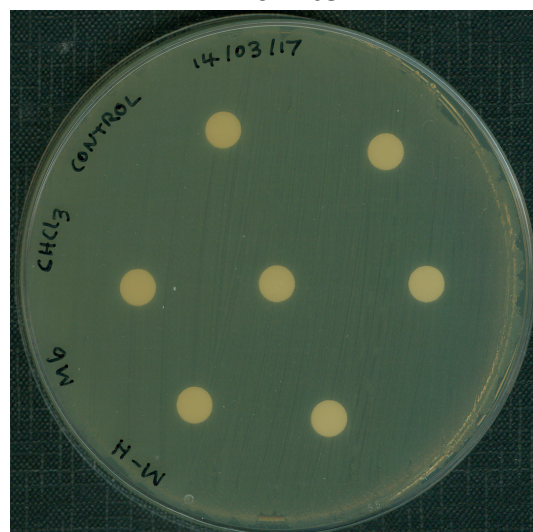
BW25113 – EtOH



M6 - EtOH



BW25113 – CHCl₃



M6 – CHCl₃